UNIVERSITY OF TECHNOLOGY
(INSTITUT NATIONAL POLYTECHNIQUE DE LORRAINE)

DOCTORAL SCHOOL: RP2E (Resources, Process, Products, Environment)
Reactions and Chemical Engineering Laboratory (LRGP)

POZNAN UNIVERSITY OF MEDICAL SCIENCES

Chair and Department of Pharmaceutical Technology

THESIS

Presented 28/10/2011
in order to obtain the grade of Doctor of INPL
(Speciality: Process and Product Engineering)
[Génie des Procédés et des Produits]
and the grade of Doctor in Pharmacy (Speciality: Pharmaceutical Technology)

BY

Małgorzata GESZKE-MORITZ

Synthesis of stable and non-cadmium containing quantum dots conjugated with folic acid for imaging of cancer cells

Thesis Supervisors:	Raphaël SCHNEIDER	Professor (Nancy)
	Janina LULEK	Professor (Poznan)

Jury Composition:

President of jury: Professor Edmund GRZEŚKOWIAK (Poznan)
Reviewers: Professor Jean-Jacques GAUMET (Metz), Professor Jerzy Aleksander PAŁKA (Bialystok)
Invited member: Doctor Lavinia BALAN (Mulhouse)

Poznan, October 2011

This PhD was financially supported by:

The scholarship from French Embassy in Poland

The “Scholarship for Ph.D. students specializing in majors strategic for Wielkopolska’s development”, sub-measure 8.2.2. Human Capital Operational Programme, co-financed by European Union under the European Social Fund

The scholarship from the Polpharma Scientific Foundation

and

Scientific project Nº 501-02-03314429-03439-50478
from Poznan University of Medical Sciences

I would like to thank my two PhD directors

Professor Raphaël Schneider and Professor Janina Lulek

for admitting me to their laboratories, for the gained knowledge
and for the helpful hand during experiments and redaction of the thesis

and all collaborators and colleagues from the laboratory

who contributed to the presented work.

I dedicate this PhD dissertation to my Parents, Husband and all Family without whom I would not be in this place of my life

Keywords: quantum dots, nanocrystals, semiconductors, nanotechnology, fluorescence, cadmium-free QDs, zinc sulfide, zinc selenide, manganese and copper doped QDs, folic acid, cancer, cytotoxicity, cellular imaging, biosensing

Table of contents

Abbreviations

5-FU	5-fluorouracil
A	acceptor
ADH	adipic acid
AMØ	alveolar macrophages cells
BSA	bovine serum albumin
CB	conduction band
CD	cyclodextrin
CL	chemiluminescence
CT	computed tomography
CTAB	cetyltrimethyl ammonium bromide
Cys	cysteine
D	donor
d-dots	doped quantum dots
DHLA	dihydrolipoic acid
DLI	drug light interval
DLS	dynamic light scattering
DMEM	Dulbecco's modified Eagle's medium
DMF	N,N-dimethylformamid
DMSO	dimethyl sulfoxide
DNA	deoxyribonucleic acid
Dox	doxorubicin
Eg	bandgap energy
Eg^{bulk}	bandgap energy of bulk material
EDC	1-ethyl-3-3(3-dimethylaminopropyl)carbodiimide
EDX	energy-dispersive X-ray spectroscopy
e^-/h^+	electron/hole pair
EGF	epidermal growth factor
EPR	electron paramagnetic resonance
FA	folic acid
FA-CMC-ZnS:Mn	folic acid conjugated carboxymethyl chitosan coordinated to manganese doped zinc sulfide quantum dot
FACS	fluorescence-acivated cell sorting
FOXO	ferrous oxidation-xylenol orange
FR	folate receptor
FRET	fluorescence (or Föster) resonance energy transfer
FT-IR	Fourier transform infrared spectroscopy
FWHM	full width at half maximum of the emission spectrum
GSH	glutathione
HDA	hexadecylamine
HOMO	highest occupied molecular orbital
HRP	horseradish peroxide
IgG	immunoglobulin G
K_d	dissociation constant
LADME	liberation, absorption, distribution, metabolism, excretion

LEDs	light-emitting diodes
LUMO	lowest unoccupied molecular orbital
MAA	mercaptoacetic acid
MBP	maltose binding protein
ME	2-mercaptoethanol
Meth	methionine
MPA	mercaptopropionic acid
MRI	magnetic resonance imaging
MTT	3-(4,5-dimethylthiazol-2-yl)-2,5-diphenyltetrazolium bromide
MUA	mercaptoundecanoic acid
NADH	reduced form of nicotinamide adenine dinucleotide
NaHSe	sodium hydrogen selenide
NCs	nanocrystals
NHS	*N*-hydroxysuccinimide
NIR	near infrared
NPs	nanoparticles
$\cdot^1O_2$	singlet oxygen free radical
·OH	hydroxyl free radical
ODA	octadecylamine
ODPA	octadecylphosphonic acid
PAA-$OA_{0.4}$	octylamine-grafted polyacrylic acid
PDT	photodynamic therapy
PEG	polyethylene glycol
PEG-$DSPE_{2000}$	1,2-distearoyl-*sn*-glycero-3-phosphoethanoloamine-*N*-[methoxy (polyethylene glycol)-2000
PET	positron emission tomography
PL	photoluminescence
PL QY	photoluminescence quantum yield
PMAT	hydrolyzed poly(maleic anhydride-alt-1-tetradecene)
PS	photosensitizer
q-dots	undoped quantum dots
QDs	quantum dots
QY	quantum yield
RES	reticuloendothelial system
Rluc	*Renilla* luciferase enzyme
RNA	ribonucleic acid
RNS	reactive nitrogen species
ROI	reactive oxygen intermediates
ROS	reactive oxygen species
rt	room temperature
SiO_2	silicon dioxide
Si-OH	silanol
SPECT	single photon emission computed tomography
Sulfo-SMCC	sulfosuccinimidyl-4-(*N*-maleimidomethyl)cyclohexane-1-carboxylate
TBP	tributylphosphine
TEOS	tetraethyl orthosilicate
TET	triplet energy transfer
TG	1-Thioglycerol
TGA	thioglycolic acid
TOA	tri-*n*-octylamine

TOP	tri-*n*-octylphosphine
TOPO	tri-*n*-octylphosphine oxide
TDPA	tetradecylphosphonic acid
THF	tetrahydrofuran
US	ultra-sonography
UV	ultra-violet
UV-vis	ultra-violet-visible
VB	valence band
W	wurzite
wl	wavelength
Z	zinc blende
XTT	2,3-bis (2-methoxy-4-nitro-5-sulfophenyl)-5-[(phenylamino)-carbonyl]-2H-tetrazolium hydroxide
α hFR	human α isoform folate receptor

General Introduction

Since a few decades nanotechnology plays a crucial role in our live. The development of technologies and people's ambition causes unbelievable progress in huge variety of disciplines. New technologies that can manipulate with such small units as atoms are called nanotechnologies. The usefulness of this new scientific field led to the explanation of many processes unknown before as well as to creation of very modern and more efficient tools for electronics, optoelectronics, plastics, energy, biology, chemistry, medicine, pharmacy, toxicology or even domestic field. However, there is still unanswered question concerning potential human adverse effects resulting from exposure to these new materials.

Recently discussed nanoscale materials are carbon nanotubes, fullerene derivatives, quantum wires or quantum dots. Nanoparticles (NPs) are very small particles in the size range between 2 and 100 nm. Due to their very small size, they possess unique properties and behave in different way than particles in macro scale or bigger. The specificity of NPs makes them widespread in many branches of human life. The disciplines that took recently huge advantage from the development of nanotechnology are medicine and pharmacy. The creation of particles of very tiny sizes allowed these two sciences to develop or revolutionize the techniques of diagnosis or drug delivery. The feature of NPs that make them useful for medical and pharmaceutical purposes is especially high surface to volume ratio and connected with that possibility of attaching many different ligands on particles surface. Other properties of great importance are dispersibility and water stability, high and not easy quenched fluorescence, biocompatibility, small and uniform sizes. All these unusual characteristics of NPs were an inspiration to focus in the following thesis more precisely on one specific kind of NPs which are fluorescent nanocrystals (NCs) called quantum dots (QDs).

QDs are fluorescent NPs (of semiconductors or metals) in the size range from 1-20 nm that possess specific structural, optical and electronic properties depending on their surface to volume ratio and on the phenomenon of so-called "quantum confinement" [1]. Since their first dispersion in water in 1998 and due to the specific photophysical properties depending on their dimensions, these NCs became a new class of fluorescent nanoprobes with much better characteristics than traditional organic dyes [2-5]. Surface

functionalization of these NCs makes possible modifying their physicochemical properties according to the ligand nature at the surface.

The following studies were realized in “co-tutelle” system of PhD in cooperation between French and Polish Universities, namely Laboratoire de Réactions et Génie de Procédés (LRGP) in Institut National Polytechnique de Lorraine (INPL) in Nancy and Chair and Department of Pharmaceutical Technology in Poznan University of Medical Sciences.

The purpose of this PhD was to develop a new class of low toxic QDs probes for bioimaging of cancer cells with essential attributes such as water dispersibility, photostability, biocompatibility, high luminescence and low toxicity using simple aqueous method. In my studies folic acid (FA) was attached at the QDs surface to facilitate the FR-mediated targeting of cancer cells.

The thesis is divided into four main chapters. Chapter 1 presents bibliographic studies concerning general information about QDs and potential applications of these NCs in medicine and pharmacy. Chapters 2 and 3 present the aim of performed studies and materials and methods used. Chapter 4 presents the obtained results and discussion. As the experimental studies were performed in few steps, paragraph 1 in chapter 4 describes the synthesis methods of four different types of QDs (ZnS:Mn/ZnS@MPA, ZnS:Mn@TG, ZnS:Cu/ZnS@MPA, ZnSe:Mn/ZnS@MPA) as well as size, shape, crystal structure and photoluminescence (PL) properties of synthesized NCs. QDs characterization was performed with the help of such analytical techniques as spectrophotometry UV-Vis, fluorymetry, X-ray diffraction (XRD), X-ray photoelectron spectroscopy (XPS), transmission electron microscopy (TEM), dynamic light scattering (DLS), thin layer chromatography (TLC), infrared analysis (FT-IR) and electron paramagnetic resonance (EPR). In the paragraph 2 of chapter 4 surface functionalization of ZnS:Mn MPA- and TG-capped QDs with folic acid (FA) playing a role of targeting agent is presented followed by description of size, shape, crystal structure and PL properties of these functionalized NCs. In paragraph 3 the cytotoxicity of synthesized bare and conjugated Mn-doped NCs was evaluated on cancer cell lines (MCF-7, T47D, PC-3) using MTT, XTT and ferrous oxidation-xylenol orange (FOXO) tests. Finally, in paragraph 4, two chosen types of as-prepared and characterized QDs were used for bioimaging of cancer cells. In this experiment NCs were excited biphotonically.

Chapter 1. Bibliographic studies

1.1. Quantum dots (QDs)

In this bibliographic chapter, the structure, the optical and electronic properties of quantum dots (QDs), the strategies of their dispersion in aqueous medium developed during the last years, the strategies of QDs synthesis by organometallic route and in aqueous medium, the functionalization of NCs' surface followed by QDs cytotoxicity concerns and the potential applications of these NPs in medicine and pharmacy are described.

1.1.1. Chemical composition of QDs

NPs are of great interest as they are a bridge between bulk and atomic or molecular structures [6]. Semiconductor QDs are tiny light-emitting crystals, and are emerging as a new class of fluorescent labels for medicine and biology [7]. QDs are NCs that are generally composed of a semiconductor core encased within the shell of a second semiconductor material. Average QDs diameter is in the range of 1-20 nm [8]. In comparison to corresponding bulk crystals/solids, colloidal NCs are metastable species and have to be kinetically stabilized usually by the chemical attaching of the monolayer of organic molecules to the atoms on the surface of NCs [9]. The advantage of working with QDs instead of bulk materials lies in the fact that, due to the quantum confinement effect, the luminescence spectrum is dependent on such factors as: the presence of defects, the presence of dopants and on the particle size and composition [10].

Each component of QDs is important and there is still many questions concerning their impact on human body what is listed below in Figure 1. These metalloid-crystal structures contain from 200-10,000 atoms [11]

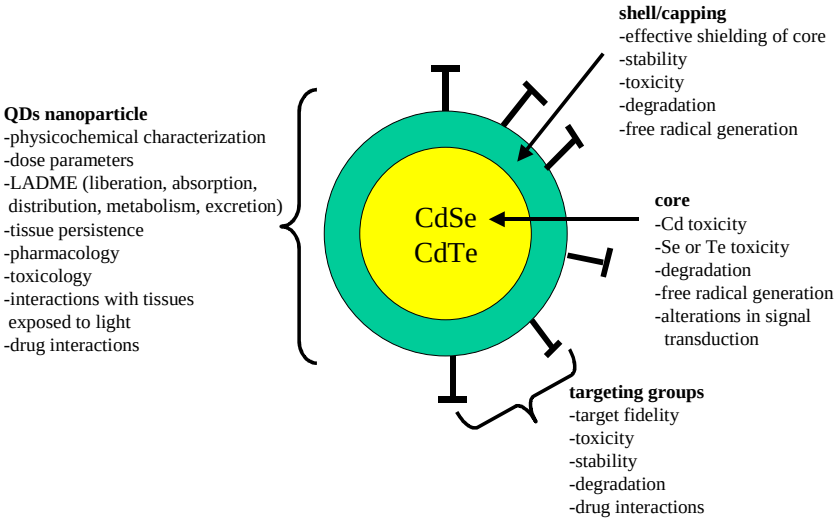

Figure 1. Components and characterization of a representative QD, the core, shell, and targeting ligands [12].

Structurally, QDs consist of a metalloid core and a "cap" or "shell" which covers the core. The core consists of a variety of metal complexes, namely semiconductors, noble metals, and magnetic transition metals. The QDs more often used for biological applications belong to the group II-IV elements in the periodic table (CdS, CdSe, CdTe, ZnO, ZnS, ZnSe) [13-18]. The NCs that belong to the group III-V (InP, InAs, GaN, GaP, GaAs), IV-VI (PbS, PbSe, PbTe), I-VII (CuCl), V-VI (Bi_2Te_3) and II-V (Cd_3As_2, Zn_3P_2, Zn_3As_2) can also be cited [19-26].

In the presented studies, I focus on ZnS and ZnSe QDs.

The increase of NPs size increases energy of the surface resulting in agglomeration of the particles [27]. To control the size of the semiconductor particles and to protect the QDs core and significantly decrease cytotoxicity, a shell (generally ZnS) showing much lower toxicity is introduced [28]. Other capping materials from which thin shell might be prepared are CdS, ZnO or ZnSe [29]. The shell around the particles of a wider band gap semiconductor protects them from photoinitiated surface degradation [30], it means it prevents surface quenching of excitons in the emissive core [29] and in this way improves the luminescence properties by elimination of surface defects [31]. In other words, surface passivation effect of the NCs inhibits the nonradiative recombination [32]. Typical physicochemical QDs characteristics is refereed as "core-shell-conjugate" [12].

1.1.2. Electronic structure of QDs

The bulk materials might be classified according to the ability of their electrical conductivity into three groups, the insulators, the semiconductors and the conductors (Figure 2).

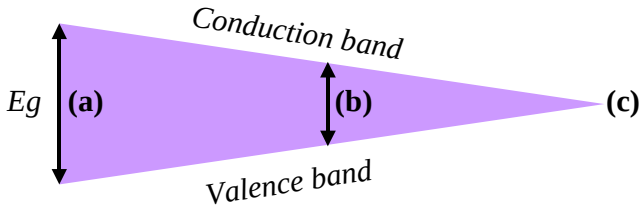

Figure 2. Energy bands of insulator (a), semiconductor (b) and conductor (c) materials [4].

The tree types of materials contain a band low in energy called the valence band (VB) and the band high in energy called the conduction band (CB). The distance that separates these two bands is called the bandgap and it is different for each mentioned material.

In the case of insulators, electrons completely fill the VB and the CB is empty. The distance separating the bands is very large and the energy needed for displacement of electron from the VB to the CB is very high and generally exceeds 9 eV.

In semiconductor materials, the distance between the VB and the CB is much smaller than in the case of insulators. To transfer the electron from the VB to the CB energy of only 1-2 eV has to be supplied.

In the case of conductors, the CB and the VB interpenetrate and there is no bandgap. The CB is partially filled and the conduction of the material is elevated. Electrons can easily move under the influence of an electric field.

QDs possess photophysical and physicochemical properties directly depending on their dimensions. During the last twenty five years the property of great interest is the possibility of changing the broadness of the bandgap (bandgap energy: *Eg*) by the simple changing of NP diameter (Figure 3) [1, 33].

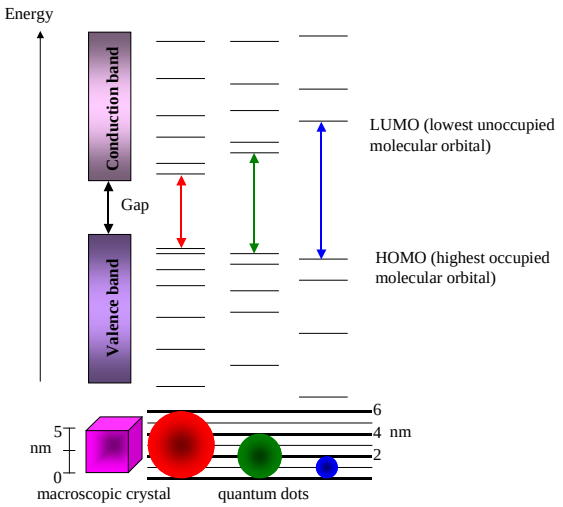

Figure 3. Evolution of the electronic structure from the bulk material to QDs of decreasing diameter (modified from [34]).

As mentioned above, bulk semiconductor material presents a VB (containing electrons of ground energy state, low in energy) and a conduction band (empty, high in energy), separated by the forbidden gap, the bandgap, the broadness *Eg*. By light excitation of photons with an energy $h\upsilon_{exc} \geq Eg$, it is possible to transfer an electron from the VB to the CB and to create a hole in the VB. The electron and the hole cannot be displaced independently due to the coulombic interaction. Together, they form an exciton.

The decrease of the particle size to few nanometers results in an unusual situation where the exciton is bigger than the crystal dimensions. In this case, QDs have to accept higher kinetic energy what leads to the increment of the gap and to confinement of the energetic levels in discrete values. This phenomenon is called "quantum confinement" [35]. Due to that decrease of diameter, the energetic structure transfers from the band structure to the discrete levels structure.

The correlation between the diameter and the bandgap energy (*Eg*) for semiconductor NCs was established by Brus in approximation to spherical particles (Equation 1),

$$Eg = Eg^{bulk} + \frac{\eta^2 \pi^2}{2r^2}\left(\frac{1}{m_e^*} + \frac{1}{m_h^*}\right) - \frac{1{,}786\, e^2}{\varepsilon_r \varepsilon_0}\frac{1}{r}$$

Equation 1. Equation that permit to calculate the first approximation of the bandgap of spherical nanocrystal [36].

where Eg^{bulk} corresponds to the gap of bulk crystal to which *Eg* tends when r increases indefinitely. The second term $1/r^2$ (with r in nm) is a term of "quantum confinement" calculated according to the hypothesis of spherical potential in which the electron and the hole of the effective masses m_e* and m_h*(without dimensions) are confined (m_e= 9,1.10 $^{-31}$ kg) and ħ is the Planck constant divided by 2π (ħ= 1,0546.10 $^{-34}$ J.s). The third term expresses the coulombic attraction between the electron and the hole, ε_r (without dimensions) is the dielectric constant of the material relative to that one of the vacuum (ε_0= 8,854.10^{-12} F/m).

The physical distance that separates the electron and the hole is equal to the Bohr radius (r_B) of an exciton. That distance is a function of material (Figure 4). Bohr radius can be calculated using the Bohr hydrogen atom model with the parameters of semiconductor NC material (Equation 2).

$$r_B = 0{,}053.\varepsilon_r \cdot m_e \left(\frac{1}{m_e^*} + \frac{1}{m_h} \right)$$

Equation 2. Equation for the Bohr radius of an exciton [37].

Therefore, the broadness of the bandgap is explained by introduction r_B from the equation 2 to equation 1 what gives us the equation 3.

$$Eg(eV) = Eg^{bulk}(eV) + \frac{2{,}6}{\varepsilon_r \times r(nm)} \left(2{,}74 \frac{r_B(nm)}{r(nm)} - 1 \right)$$

Equation 3. Formula used to calculate the gap as a function of Bohr radius of an exciton.

This formula permits to calculate the *Eg* of known radius made of different materials due to the parameters of bulk material. Table 1 shows the parameters at room temperature (rt) of some semiconductors II-VI and II-V and in Figure 4 the evolution of the gap as a function of the radius of QDs made from various materials is presented. Depending on the type of semiconductor material, different energies of the gap might be obtained what enables covering the wide spectral range from UV to the NIR.

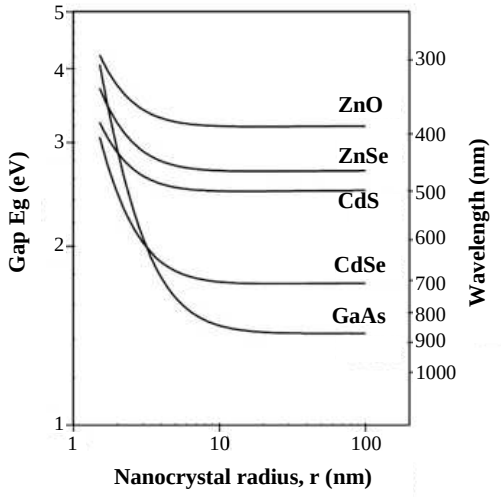

Figure 4. Theoretical variation of the gap calculated for QDs of different semiconductors using the Equation 3 and the parameters from the Table 1[34].

Table 1. Physical properties of certain semiconductors from groups II-VI and III-V [37, 38]

Material	Structure	Type	Eg bulk (eV) at 300 K	m_e*	m_h*	ε_r	r_B (nm)
ZnO	Wurzite	II-VI	3,30	0,26	0,6	8,2	2,4
ZnSe	zinc blende	II-VI	2,70	0,157	0,75	8,7	3,6
ZnS	zinc blende	II-VI	3,60	0,28	0,61	8,9	2,5
CdS	Wurzite	II-VI	2,52	0,2	0,7	8,8	3,0
CdSe	Wurzite	II-VI	1,76	0,12	0,45	9,5	5,3
CdTe	zinc blende	II-VI	1,45	0,1	0,4	7,2	4,8
GaAs	zinc blende	III-V	1,42	0,063	0,5	12,9	12,2
InP	zinc blende	III-V	1,34	0,075	0,64	12,56	9,9
InAs	zinc blende	III-V	0,35	0,027	0,41	14,9	31,2

Eg- bandgap energy, m_e*- effective mass of an electron, m_h*- effective mass of the hole, ε_r- dielectric constant, r_B- Bohr radius of an exciton

1.1.3. Photophysical properties of QDs

Considering the photophysical properties of QDs, they offer many advantages in comparison to conventional organic dyes such as bright photoluminescence (PL) [high quantum yield (QY) which is the ratio of the number of photons emitted to the number of photons absorbed], narrow emission, broad ultra-violet (UV) and visible excitation, and high photostability [39, 40].

As mentioned above semiconductor NCs are characterized by a band gap between their VB and CB. When a photon having an excitation energy exceeding the semiconductor band gap is absorbed by QDs, an electron is promoted from the VB to the high-energy CB. Such an excited electron may then relax to its ground state by the emission of another photon with an energy that is equal to the bandgap [41] (Figure 5).

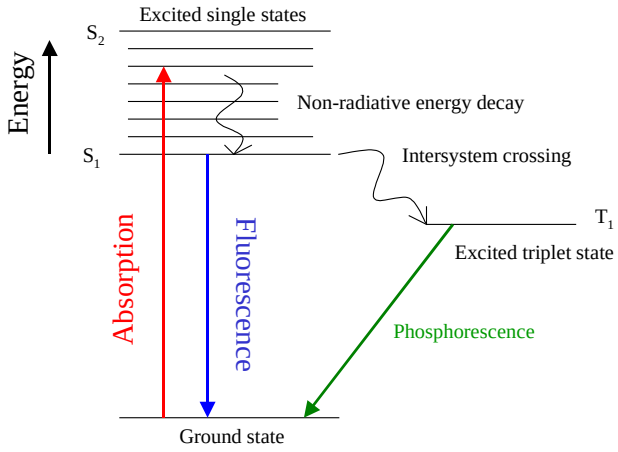

Figure 5. A simplified Jablonski diagram [42].

Recorded UV-vis spectrum reveals many energy states in QDs [43]. The characteristic electron-hole pair peak corresponding to the bandgap energy, called first excitonic peak, can be observed [44]. This peak (quantum-confinement peak) is the result of the lowest excited energy state [43]. The position of excitonic peak shifts to longer wavelength (wl) as NCs grows to larger diameters [44] (Figure 6).

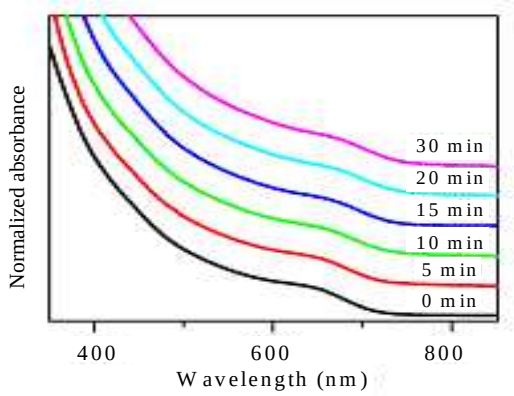

Figure 6. Temporal evolution of normalized UV-vis absorption spectra of CdTeSe growing at 220ºC with the feed ratio of 5Cd-0.5Te-0.5Se [45].

This effect is analogous to the quantum mechanical “particle in the box”- the particle energy increases as the box size decreases [41].

Photophysical properties of QDs depend on “quantum confinement” [46]. The results of quantum confinement are that the electron and hole energy states within the NCs are discrete, however the electron and hole energy levels (and therefore the bandgap) is a function of the QD diameter as well as of the composition [41] (Figure 7).

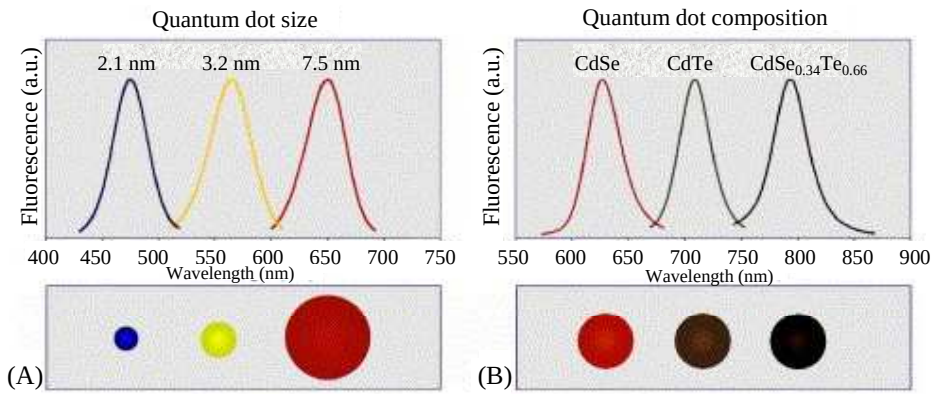

Figure 7. Tuning the QD emission wavelength by changing the nanoparticle size (A) or composition (B) [47].

The narrow PL bands are contributed by the carrier recombination in the band-edge states (full width at half maximum of the emission spectrum FWHM from 20 to 30 nm) [48, 49]. The range of the QDs fluorescence maxima is determined by their elemental composition, e.g. CdS and CdSe QDs emit fluorescence in visible range while CdTe up to near infrared (NIR). Due to the quantum confinement, the energy of the bandgap is inversely proportional to the wl of absorption of the first exciton. The decreasing of NC diameter brings in the hypsochrome displacement (it means directed to the wl weaker than that one of the absorption). Due to this fact the emission can be tuned precisely by adjusting the diameter of QDs. Smaller NCs emit light with shorter wl than larger ones [28] (Figure 8).

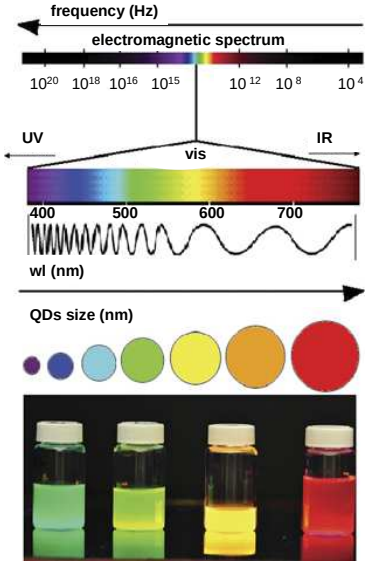

Figure 8. Influence of QDs diameter on their fluorescence emission [50].

QDs can be excited by a wide range of wavelengths, and have minimal interference from natural autofluorescent biomolecules [51]. Due to the broad absorption band and large two-photon absorption cross-section, these NCs might be photoactivated using one- or multi-photon excitation (Figure 9). The absorption spectra of QDs are broad due to a combined effect of electronic transitions distribution in the bulk semiconductor and discrete electronic transitions such as s-s, p-p and d-d transitions coming from quantum confinement effect [49]. Two-photon absorption (TPA) is a third-order non-linear optical process in which two photons are absorbed simultaneously, such that the energy necessary for the molecule excitation is equal to the sum of the energies of the photons [52]. The values of that non-linear optical cross-section are exprimed in GM (1GM = 10^{-50} cm^4 s $photon^{-1}$ $molecule^{-1}$). The highest is that value, the probability of exciting a molecule by simultaneous absorption of two photons increases [53]. The molecules characterized by large TPA cross-section are of interest in many applications. One of them is two-photon excitation microscopy. By an accessing of higher-energy excited states using relatively low-energy laser sources, the penetration depth in biological tissues might be markedly increased [53, 54].

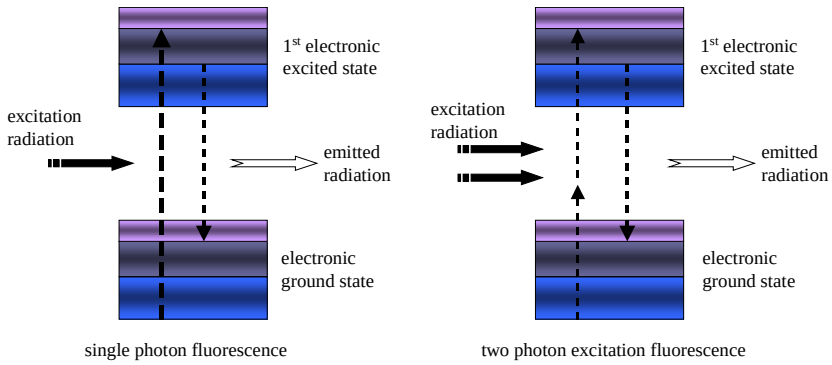

Figure 9. Mechanism of single photon and two photon excitation fluorescence [55].

1.1.4. Crystalline structure of QDs

The crystal is a solid material with arranged and periodical order of atoms in all three spatial dimensions. The crystalline structure is composed of one pattern and all of the atoms are arranged in a specific manner forming a crystal lattice. Six lattice constants are generally needed to define the form and the size of one unit cell. The axial lengths (the lengths between lattice points, the lengths of the principal axis) are

generally named as a, b and c and the interaxial angles are generally named as alpha (α), beta (β) and gamma (γ) [56]. In some crystalline structures, the lengths between the lattice points of all axis are equal (a = b = c), in such a way only one lattice constant for the dimension description is used (a).

The lattice parameters of the unit cell, thus also the crystalline structure, are necessary to calculate the distances between the neighboring atoms in the crystal and to determine the physical and electric properties of the crystalline structure. The main crystalline structure and the lattice constants of some semiconductors from group II-VI are listed in Table 2.

Table 2. Crystalline structures and the crystal lattice constants of some semiconductors from group II-VI [57]

QDs	Structure	Lattice parameters (Å)
CdS	zinc blende	5,83
CdS	wurzite	a= 4,16 ; c= 6,75
CdSe	zinc blende	6,08
CdSe	wurtzite	a= 4,31, c= 7,02
CdTe	zinc blende	6,48
ZnS	zinc blende	5,42
ZnS	wurtzite	a= 3,82 ; c= 6,26

The II-VI semiconductors generally crystallize in the zinc blende (ZB) cubic structure where a = b = c and wurzite (W) hexagonal structure where a = b # c (Figure 10). These two structures are quite similar (Table 2). The ZB structure is of ABCABC type whereas W structure is of ABABAB type. The differences in the energy between these two structures are very slight. The ZB structure is stable at low temperature whereas the W structure is more stable at higher temperature [58].

ZnS NCs usually obtained by the hydrothermal method [59] or by simple aqueous synthesis [60] are typically of ZB cubic structure. It is also the case of ZnSe NCs obtained via the organometallic [61] or the hydrothermal route [62].

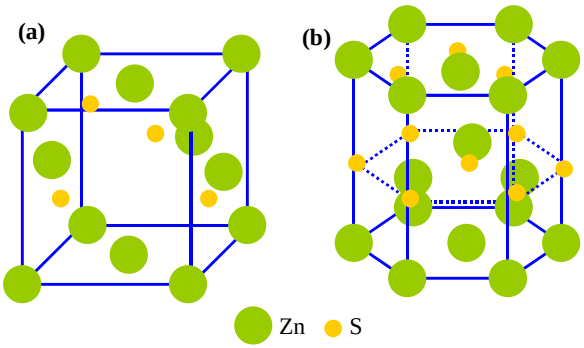

Figure 10. Unit cell of the zinc blende (a) and wurzite (b) ZnS crystal lattice (modified from [63]).

1.1.5. Core/shell structure

Frequently, the NC surface contains some imperfections and defects such as bonds between reagents or vacant sites in the unit cell. These imperfections cause the entrapment of electrons and decrease of optical efficacy of QDs, and notably alter the photoluminescence quantum yield (PL QY). If the QDs core is not covered, the disexcitation by the nonradiative pathway is more possible than the radiative recombination and therefore the fluorescence QY is considerably decreased. The appearance of the energetically weak fluorescence band at the higher wavelengths ("trap emissions") is observed as well (Figure 11) [64-68].

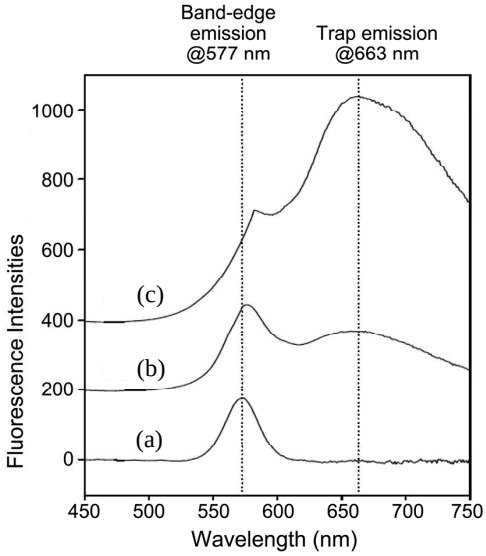

Figure 11. Fluorescence emission spectra of (a) $^{CTAB/TOPO}$CdSe/ZnSe QDs and (b, c) *Dapnia magna* exposed to these QDs. The second signal of fluorescence observed ca. 660 nm comes from surface defects. CTAB- cetyltrimethyl ammonium bromide, TOPO- trioctylphosphine oxide, *D. magna* is a freshwater crustacean frequently used as toxicity test organism [69].

To eliminate the surface defects, an inorganic shell of another semiconductor (generally of wider bandgap) is introduced around the core to correct the surface defects.

There are three configurations for the core/shell system due to the alignment of bands between the core and the shell (Figure 12) [70].

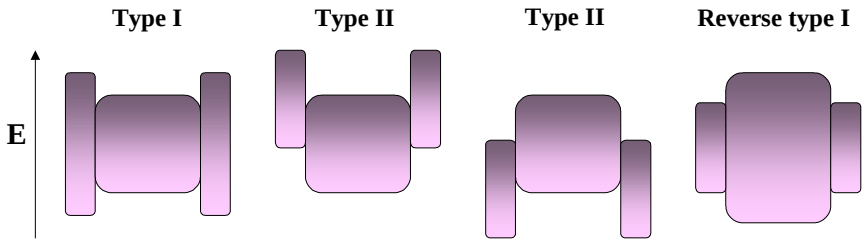

Figure 12. Alignment of bands in the core/shell structure of type I, type II and reverse type I. The upper and lower edges of the rectangles correspond to the positions of the conduction- and valence-band edge of the core (center) and shell materials, respectively. [70].

Type 1: the shell of other semiconductor that has a bandgap larger than the core is introduced. The CB of the shell has a higher energy than the core whereas the VB has the energy lower than the core (for example: CdSe/ZnS). The electrons and the holes are confined in the core. Accordingly, the emission wl of core/shell QDs is few nanometers redshifted in comparison with the core alone [71, 72]. That redshift is observable in the time of the shell growth as the result of the partial leakage of the exciton in the shell matrix, thus reducing the confinement. It is more pronounced for the small sizes NCs where the leakage of exciton in the shell is the effect more important on the confinement energy of charge carriers.

Type II: there are two structures of that system. In the first one, the VB and the CB of the core are lower than the ones of the shell. In the second structure, it is reverse. The QDs structures of type II usually seen are CdTe/CdSe and ZnTe/CdTe. These structures are currently often studied because it is possible to displace the fluorescence emission to the NIR. It is worth to mention that the exciton lifetime in the QDs type II is longer than in QDs type I for the reason that the electron and the hole might be relocated in the core and in the shell all at once [73, 74].

Reverse type 1: the shell has a bandgap lesser than the core. The CB of the shell has lower energy than the core whereas the VB has the energy higher than the core. Thus, the charge carriers are at least partially relocated in the shell. The emission wl is modulable by the thickness of the shell as well. The redshift of the fluorescence emission is observed (for example: CdS/CdSe).

The photophysical properties of that core/shell system are frequently very modest. To improve the photostability, the shell of the semiconductor of wider bandgap might be introduced, like in classical system of Type I (for example: CdS/CdSe/CdS).

The constraints of unit cell (or lattice mismatch) between the core and the shell are very important parameters to consider before the introduction of the shell at the NC surface. The constraint can be calculated using the lattice parameters. An example is demonstrated in Figure 13 presenting the scheme of the synthesis of CdTe/CdS/ZnS core/shell/shell QDs and corresponding relationship between band gap energy, lattice constant and lattice mismatch of bulk CdTe, CdS, and ZnS as well as absorption and PL spectra of core, core/shell and core/shell/shell QDs.

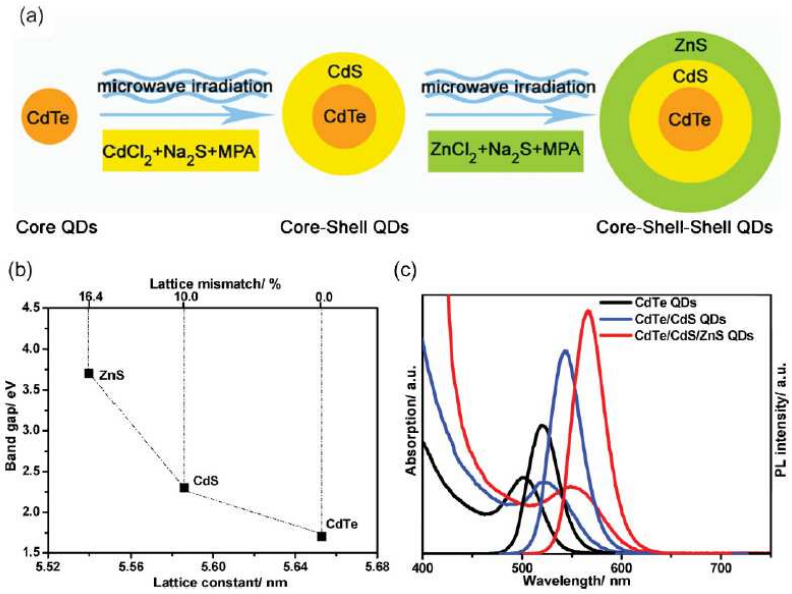

Figure 13. (a) Schematic synthesis of CdTe/CdS/ZnS core/shell/shell QDs, (b) relationship between band gap energy, lattice constant, and lattice mismatch of bulk CdTe, CdS, and ZnS-lattice mismatch refers to the mismatch compared to CdTe, and (c) corresponding absorption and PL spectra of CdTe, CdTe/CdS and CdTe/CdS/ZnS QDs [75].

1.1.6. Dispersion of QDs in aqueous medium

QDs prepared by the organometallic route are typically stabilized by the hydrophobic ligands such as trioctylphosphine oxide (TOPO), trioctylphosphine (TOP) or hexadecylamine (HDA). These QDs are soluble only in slightly polar organic solvents such as chloroform, toluene or hexane [5]. For the majority of biological applications, QDs water-dispersibility is needed in order to exploit them as fluorescent labels.

There are several strategies to make QDs obtained through the organometallic synthesis water-dispersible.

1.1.6.1. Exchange of the ligand at the QDs surface

This method is based on the replacement of the hydrophobic ligand at the QDs surface by hydrophilic molecules. The hydrophilic molecules are typically bi- or trifunctional (Table 3).

Table 3. Examples of hydrophilic molecules used for dispersion of hydrophobic QDs in aqueous medium

Hydrophilic molecule	Example
Thioacids	TGA, MPA and MUA
Thioamine	2-aminoethanothiol
Thioalcohols	1-thioglycerol, 2-mercaptoethanol
Thioacid-α-amines	L-cysteine, thiopronine

TGA- thioglycolic acid, MPA- 3-mercaptopropionic acid, MUA- mercaptoundecanoic acid

The hydrophylic molecules include the anchor function (typically a thiol) which interacts with the QDs surface and the hydrophilic head (acid, amine, alcohol) that enables not only the dispersion in water but also the subsequent coupling with biomolecules to guide the NPs to the specific biological targets [3, 9, 76-80]. In Figure 14 an example of such ligand exchange is presented. Ligands surrounding a TOPO-coated QD are replaced with TGA making QD readily dispersed in aqueous solvents [47].

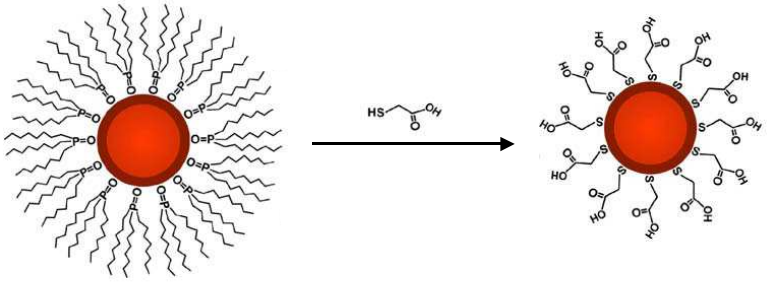

Figure 14. Schematic representation of ligand exchange at the QDs surface [47].

The improvement of the exchange and the NCs stability has led to the development of bidentate ligands. One of such ligand is dihydrolipoic acid (DHLA) (Figure 15).

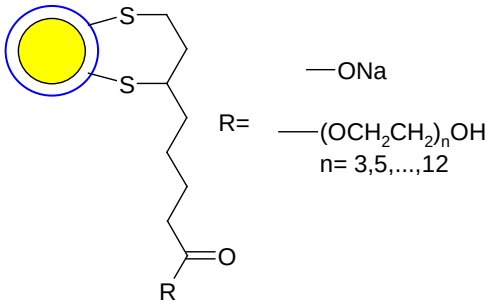

Figure 15. Schematic representation of QDs stabilized by dihydrolipoic acid (DHLA) and its PEGylated derivatives (modified from [5, 81]).

QDs functionalized by dihydrolipoic acid (DHLA) were stable during months whereas the stability of QDs substituted by the simple thioacids is described as lower [82]. The strategy frequently used to improve the biocompatibility of QDs stabilized by DHLA is the pegylation at the surface of these QDs [82, 83]. The addition of PEG decreases the possibility of the non-specific interactions between the carboxylate function of DHLA and the biological system at the time of labeling [84].

Another possibility of the exchange strategy is the silanization of the QDs surface. This method uses thiosilanes such as mercaptotrimethoxysilane. Methoxysilanes are subsequently hydrolized to silanol (Si-OH). The siloxane bonds are formed and the stable shell around the QDs is created enabling their dispersion in aqueous medium (Figure 16).

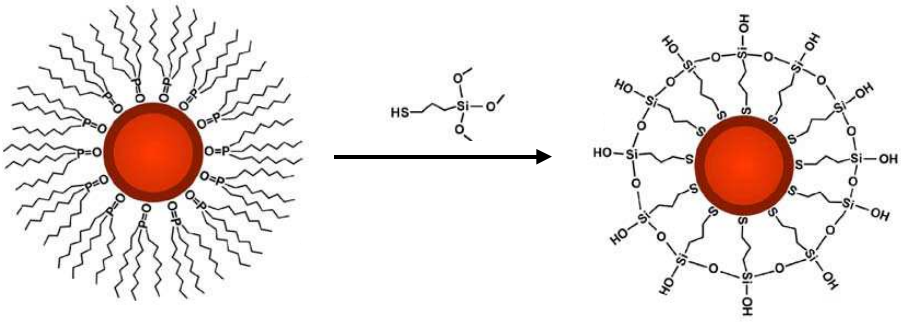

Figure 16. Schematic representation of silanization of the QDs surface [47].

Other polyfunctional hydrophilic molecules have been evaluated to stabilize QDs. The use of coordinating oligomers (for example phosphine oligomers) (Figure 17) can be mentioned. These oligomers form a dense organic layer at the QDs' surface after the replacement of TOP and TOPO ligands [85].

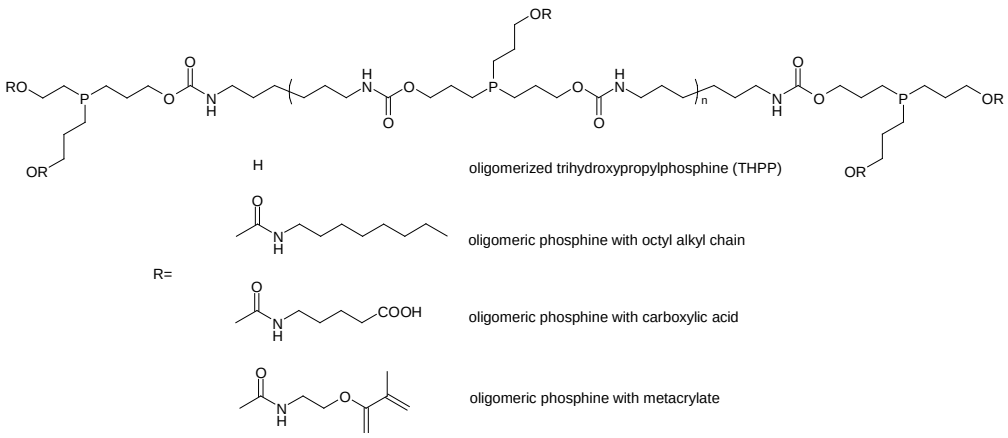

Figure 17. Chemical structures of representative oligomeric phosphines [85].

The stabilization of QDs by dendrons has been recently discussed. Organic dendron ligands are regularly hyperbranched organic molecules with a central thiol point (–SH) which is used as the binding site for the cationic/metallic elements on the surface of QDs [86]. The number of the branching points along one chain from the focal point to the outer terminal group is the generation number of the dendrons (Figure 18). It is worth to mention that from the structural point of view, a dendrimer is a compound with 2-4 dendrons attached to a center core.

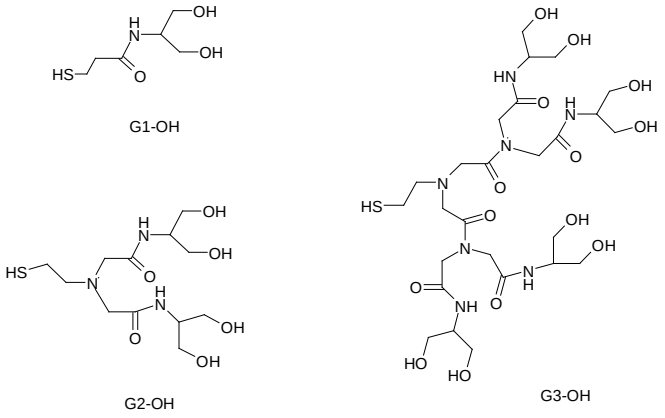

Figure 18. Molecular structures of dendrons [86].

The modification of QDs with dendrons can markedly increase QDs photochemical stability due to the strong protection of the photoactive core [87]. It was observed that dendrons with generation-2 (G2) and 3 (G3) are the most stable photochemically [86]. Usually, the groups at the end of dendrons are amines, carboxylic acids, alcohols and esters that enable the coupling of NCs with the biomolecules used as the specific labels [86] (Figure 19).

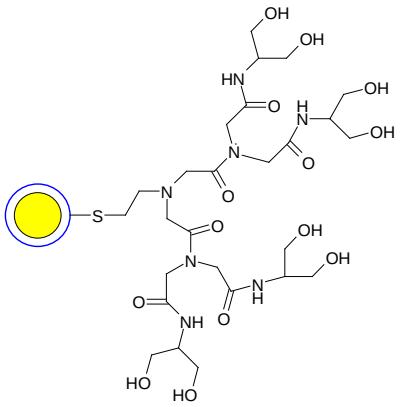

Figure 19. Schematic representation of QDs stabilized by the 3rd generation dendron [86, 87].

Most of the ligand exchange reactions lead to significant decreases of PL QY. This decrease is related to the strong polarity of the aqueous solvent and to the fragility of the NCs surface hence the displacement of the TOP/TOPO ligands [76]. It is worth to mention that the hydrodynamic diameter of the NCs obtained after such kind of exchange is smaller than of QDs water-dispersed via the micelle strategy (*vide infra*) [88].

1.1.6.2. New strategies of QDs encapsulation

In that procedure, the hydrophobic ligand stays linked to the QD's surface. This method consists of the addition of amphiphilic molecules in order to disperse QDs in aqueous medium. The alkyl chains of amphiphilic compounds interact with the *n*-octyl groups of TOP and/or TOPO groups through Van der Walls bonds. The hydrophilic endpoints of the amphiphilic molecules enable the dispersion in aqueous medium [89].

1.1.6.2.1. Encapsulation of QDs by surfactants. Micelle formation

Amphiphilic compounds can encapsulate QDs stabilized by TOPO and form micelles by hydrophobic/hydrophobic interaction.

The polar head of surfactants is generally an ammonium function (case of CTAB (cetyltrimethyl ammonium bromide), tetradecyltrimethyl ammonium bromide, or of Gemini 12-4-12 [$C_{12}H_{25}N^{+}(CH_3)_2(CH_2)_4(CH_3)_2N^{+}C_{12}H_{25}$].

$2Br^-$). In Figure 20 the chemical structures of CTAB and Gemini 12-4-12 are presented.

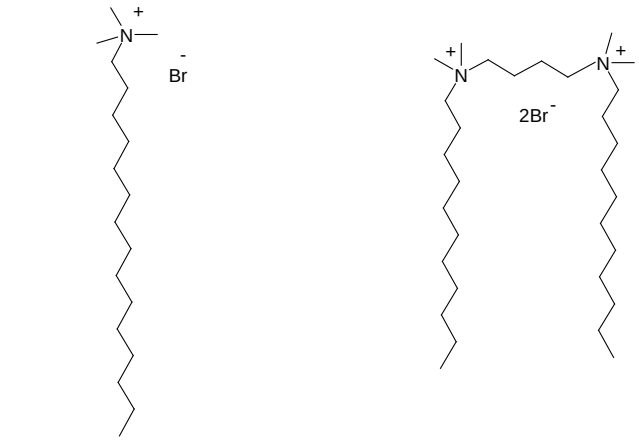

Figure 20. Chemical structures of cetyltrimethyl ammonium bromide (CTAB) and Gemini surfactant 12-4-12 [90].

The surfactant of Gemini type ensures the best stabilization of QDs and enables the perfect preservation of their optical properties (Figure 21). The fluorescence QYs are often improved after the encapsulation. It is finally worth to mention that the use of simple surfactants such as CTAB can lead to a marked increase of QDs' diameter (up to the 100 nm) [90, 91].

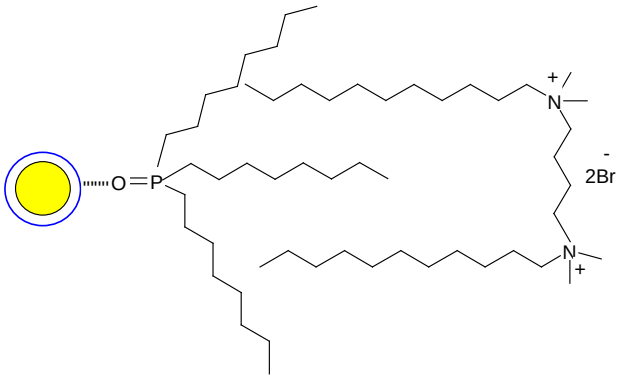

Figure 21. Water-dispersion of TOPO-stabilized QDs by use of a Gemini type surfactant (modified from [91]).

During the last years, these simple surfactants have been replaced by more sophisticated amphiphilic molecules that ensure better protection of QDs and/or do not lead to a marked increase of the NP's diameter (the micelle diameter is usually between 20-25 nm). The headlight compounds in that group are gallates [92, 93] or the PEGylated phosphoglicerolipids (Figure 22) [94, 95]. Gallates are salts and esters of gallic acid (trihydroxybenzoic acid).

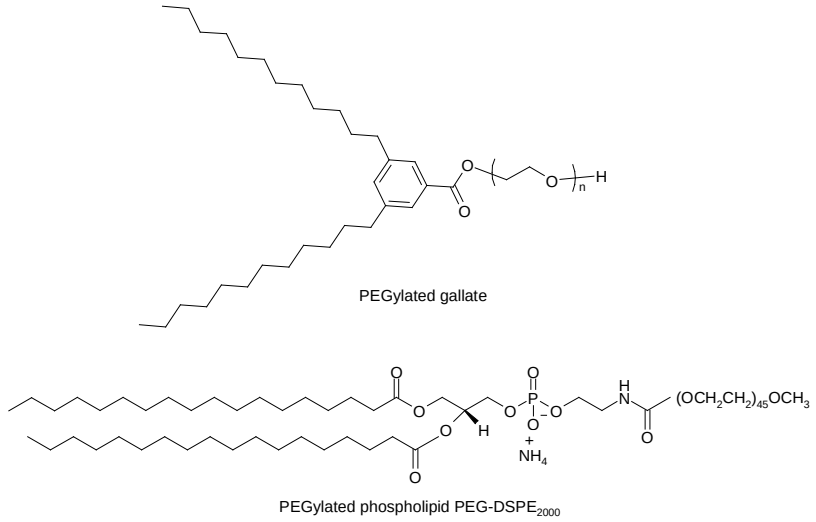

Figure 22. Chemical structure of PEGylated gallate and PEGylated phospholipid $DSPE_{2000}$ [93, 95].

In the case of phospholipids, the polar hydrophilic head generally consists of a polyethylene glycol function having at the endpoints the ether function (case of PEG-$DSPE_{2000}$ (1,2-distearoyl-*sn*-glycero-3-phosphoethanoloamine-*N*-[methoxy (polyethylene glycol)-2000]) or primary amine (case of 1,2-distearoyl-*sn*-glycero-3-phosphoethanolamine-*N*-amino (polyethylene glycol)). Encapsulation of QDs by phospholipids receives much attention because such functionalization does not change the QDs surface and the photophysical properties of QDs stay not changed. Moreover, the density of PEG chains at the QDs surface limits the probability of non-specific interactions. Additionally, the hydrodynamic diameter obtained by dynamic light scattering (DLS) of QDs dispersed by encapsulation can be modulated by varying the QD/phospholipid ratio (between 25 and 190).

1.1.6.2.2. Encapsulation of QDs by use of amphiphilic oligomers

This strategy consists of the covering of QDs with the amphiphilic polymers. In Figure 23 the use of polymeric compounds of tri-block polymer constituted from three fragments is presented [96]. Amphiphilic multidentate ligands used for preparation of QDs render them soluble in organic solvents. Interestingly, upon exposure to water, these QDs are spontaneously dispersed by a second layer of the excess multidentate polymer.

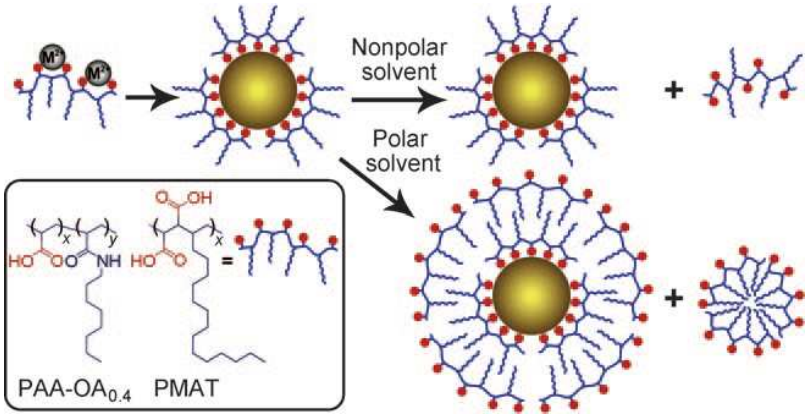

Figure 23. Schematic representation of the use of amphiphilic multidentate ligands to prepare QDs instantly dispersible in both polar and non-polar solvent. PAA-$OA_{0.4}$- octylamine-grafted polyacrylic acid, PMAT- hydrolyzed poly(maleic anhydride-alt-1-tetradecene, M-metal)[96].

Other possible modifications include the use of polyacrylic acid modifed by alkylamines [97] (Figure 24), polymaleic acids modifed by aliphatic alcohols [98] and methacrylate/methacrylic acids copolymers [99].

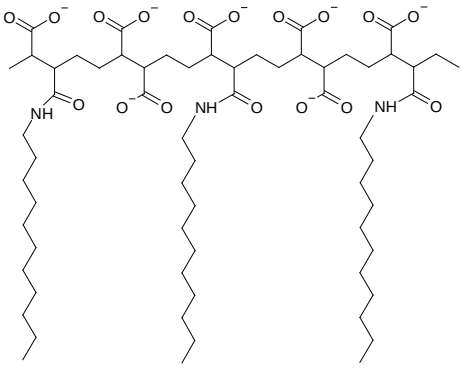

Figure 24. Chemical structure of polyacrylic acid modified by alkylamine [97].

The advantages of this encapsulation strategy are almost the same that these obtained with amphiphilic molecules, namely the encapsulation does not change the QDs surface and their photophysical properties are preserved. Moreover, the thickness of the organic shell enables an excellent passivation of the QDs surface as the polymeric envelope is often highly netted. The QDs stabilized by the polymers are generally stable in a pH range wider that the ones prepared by the ligand exchange. The serious inconvenience of this water-dispersion strategy is that the polymeric shell causes a significant increase of the QDs' diameters (usually from 5 to 30 nm).

1.1.6.3. Incorporation of QDs in silica nanospheres

In this method, QDs are exposed to tetraethyl orthosilicate (TEOS). TEOS is then gently hydrolyzed under controlled conditions to form the silica nanospheres encapsulating the QDs [100]. QDs incorporated in these nanospheres are well isolated from the environmental medium and generally possess better photophysical properties that the starting QDs [101, 102]. There are usually 3-10 QDs in the silica nanosphere, however that number can be adjusted by the QDs/TEOS ratio and by the kinetic of TEOS hydrolysis. It was observed that if TEOS concentration is too high, larger silica particles with multiple QDs were synthesized, while if the TEOS concentration was too low, the QDs are not covered by a silica shell. Moreover, water catalyzes the hydrolysis and therefore, increases the nucleation rate of silica particles. It was observed that the amount of spontaneous nucleation increased and the size of resulting silica particles decreased as the water content increased [103]. It is worth to mention that the silica nanospheres have the diameter typically over 25 nm and it is the limiting factor for their use in imaging (Figure 25) [104].

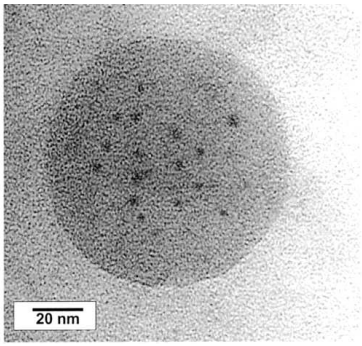

Figure 25. TEM image illustrating silica nanosphere with inclusions of CdTe nanocrystals [65].

1.1.7. Nucleation, growth, synthesis and photophysical characterization of semiconductor nanocrystals from group II-VI

In the following paragraph, the photophysical properties of bare and doped ZnS and ZnSe QDs are described, demonstrating advantages coming from NCs doping, especially in improvement of PL properties. Furthermore, nucleation and growth strategy of NCs are described, followed by different methods of QDs preparation.

1.1.7.1.Photoluminescence properties of bare and doped ZnS and ZnSe QDs

During the last ten years, and especially for bio-labeling applications, there has been a great interest in the cadmium chalcogenide (CdS, CdSe and CdTe) NCs, mainly due to their optical advantages over the commonly used organic fluorophores [105]. Because of the ultimate elimination of highly toxic class A elements like Cd, Hg and Pb, numerous researches are currently conducted to develop QDs without any heavy metal [61, 105].

In this study, I focus on two non-heavy metal containing core QDs, namely ZnS and ZnSe. These NCs can be doped with metal transition ions such as Mn^{2+} and Cu^{2+} and their surface can be passivated with a ZnS shell. All these steps are applied to improve PL properties of resulting QDs.

The photophysical properties of pure ZnS and ZnSe QDs are described followed by the demonstration of the changes, especially in PL emission properties, caused by doping with such metal transition ions as Mn^{2+} in the case of ZnS and ZnSe QDs, and Cu^{2+} in the case of ZnS QDs. It is shown that transition element-doped NCs (d-dots) can be an alternative to Cd-based ones for numerous applications [105-107]. Recently, it was reported that doped quantum dots (d-dots) (e.g. Mn:ZnSe d-dots) can overcome some disadvantages of non-doped quantum dots (q-dots) emitters, which might be, self-quenching caused by their small ensemble Stokes shifts (energy differences between absorption spectrum and emission band) and sensivity to thermal, chemical, and photochemical disturbances [108].

1.1.7.1.1. ZnS and ZnSe host materials

ZnS is an important type of II-VI group semiconductor with wide band gap energy of 3.67 eV at rt and probably the most important material used as a luminescent host material for a very large variety of dopants [27, 32]. ZnS has been extensively studied for a variety of applications, such as electroluminescent devices, optical coatings, photocatalysts, photoconductors, and solid state solar window layers [31, 32].

Room-temperature PL spectra of the nanocrystalline undoped ZnS show a small broad peak which appears at about 450 nm. PL in this region is due to the presence of sulfur vacancies in the lattice [109] or in other words so-called

trap state's emission [31]. The surface states are likely to trap electrons and/or holes, inducing nonradiative recombination [110]. The energy-level diagram of ZnS NPs is shown in Figure 26.

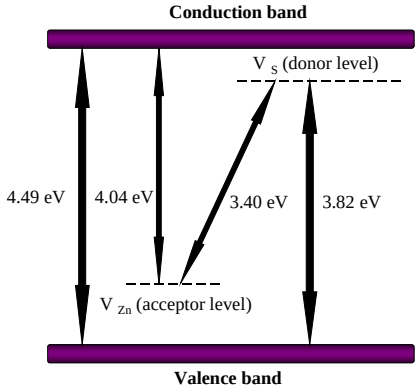

Figure 26. The energy-level diagram of ZnS nanoparticles. Modified from [111].

Over the various non-cadmium II-VI semiconductors that constitute hosts for dopants, zinc selenide ZnSe with a room temperature bulk band gap of 2.80 eV is another interesting material because it is widely used for various applications like light-emitting diodes (LEDs), photovoltaic solar cells, photocatalysts, and biological sensors [112-115]. ZnSe based QDs can satisfy the need of current trends of safe handling nanotechnology as ZnSe is an environmentally friendly material. ZnSe QDs could be useful for biological imaging or clinical and therapeutic diagnostics [61]. ZnSe QDs are excellent UV-blue emitters [105, 116]. The typical absorption and emission spectra are presented in Figure 27, the exact shape and value of peaks maxima may differ.

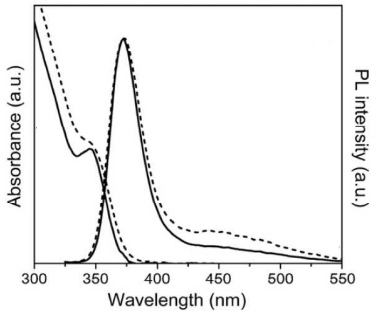

Figure 27. Absorption and PL spectra of ZnSe QDs [116].

Absorption edges of ZnSe NCs are shifted to higher energies compared to the bulk band gap of ZnSe (460 nm). Analyzing the emission band profile, two main bands might be observed. Depending on parameters used during the

synthesis procedures, the PL intensity of these two bands may be different. The band in the range from 400-600 nm is related to emission from surface traps. The contribution in blue region (ca. 400 nm) is related to band-edge emission [18, 105].

1.1.7.1.2. Doping of ZnS and ZnSe QDs by Mn^{2+} and Cu^{2+} ions

Recently, much interest has been focused on the synthesis of semiconductor NCs doped with optically active substances [10, 31, 117]. Such doped NCs with high luminescence efficiencies are expected to be a new class of fluorescent labels for biological imaging and detection [117]. Transition metals or rare earth ions could be doped into II-VI semiconductor NC hosts such as ZnS, CdS, ZnSe, and CdSe. However, the doping efficiency into a specific host depends on the similarities of chemical properties (e.g. ionic radius, valence state) between host and dopant as well as on the synthesis conditions [118].

Doped ZnS NCs have attracted more attention since 1994, when Bhargava et *al.* [119] reported for the first time that ZnS:Mn semiconductor could yield high quantum luminescence efficiency. In Figure 28 the model of incorporation of Mn^{2+} ions within the crystal ZnS lattice is presented.

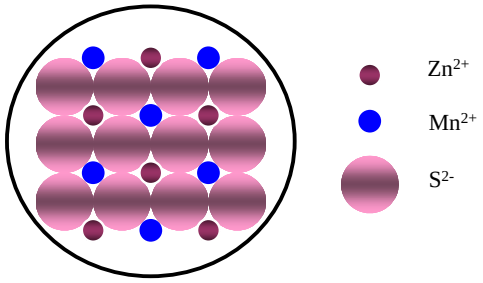

Figure 28. The model of ZnS host lattice doped with Mn^{2+} ions. Modified from [120].

The dopant luminescence mechanism in QDs is related to its position in the host lattice. The dopant should incorporate in the NCs and take the place of the host metallic ions on the host lattice site [107]. The Mn^{2+} ions are the most commonly used as the QDs dopant. The PL properties of modified NCs are improved. It can come from the fact that Mn^{2+} has the same charge as Zn^{2+} and the size and chemical properties of these two ions are similar [107]. Other reasons of common use of Mn^{2+} as doping ions for many II-VI semiconductors

is its location inside the crystal lattice of the host material, which can be confirmed by electron paramagnetic resonance (EPR), additionally, Mn^{2+}-doped NCs exhibit a typical PL from the Mn ions centered at ca. 595 nm [121]. Manganese-doped ZnS NCs focused much attention in recent years also due to their radiative lifetime increasing and enhanced emission efficiencies [108, 122-125]. ZnS NCs might be doped by wide range of other dopants like commonly used copper [126, 127], silver [128], europium [129], terbium [130], samarium [131], and cadmium [132].

The addition of well chosen dopants is a useful technique to change the optical and electric properties of NCs [11] as the luminescence characteristics of dopant-activated ZnS NCs differ markedly from those of the bulk ZnS [107]. In Figure 29 the mechanism of fluorescence emission from Mn-doped ZnS QDs is shown. The mechanism is similar in ZnSe NCs [133, 134]. Mn-doped ZnS and ZnSe NCs belong together with CdS NCs to the most commonly studied group of Mn^{2+}- doped semiconductor NCs in which the Mn^{2+} ligand-field excited states reside within the optical gap of the host semiconductor [124]. The ground state of Mn^{2+} is $^6A_1$ and the first ligand-field excited state is $^4T_1$. The large $^4T_1$-$^6A_1$ energy gap combined with the low phonon energies provided by most II-VI semiconductor lattices allows for $^4T_1$-$^6A_1$ PL with high quantum efficiencies. This is a transition most commonly described in PL studies of Mn-doped NCs [124].

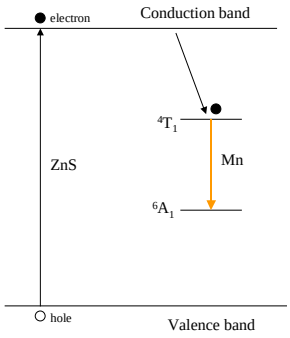

Figure 29. Fluorescence emission of ZnS QDs doped by Mn^{2+} ions [122].

In the fluorescence emission spectrum of Mn-doped ZnS NCs, in addition to blue fluorescence centered ca. 460 nm (characteristic for pure ZnS NCs), much stronger band of orange fluorescence centered ca. 590 nm is observed (Figure

30). The influence of doping ions concentration on PL properties is further described.

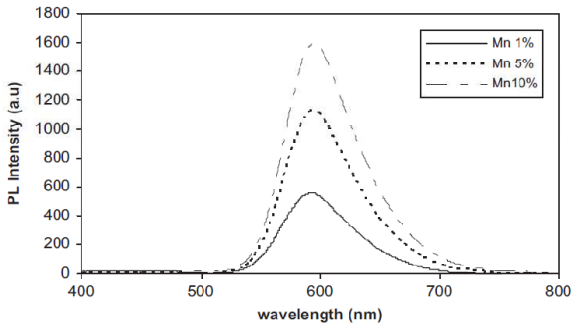

Figure 30. Photoluminescence spectra of ZnS:Mn^{2+} nanoparticles with different concentrations of Mn^{2+} [135].

Contrary to Mn-doped NCs, in which the dopant emission is generally restricted to the yellow-orange spectral window [119], for Cu-doping, a wide range of emission has been observed due to the tunability of the size of the hosts [136]. However, the study of Cu-doping is in a very nascent stage and many questions are still unanswered. The problems encountered are:

- the oxidation state of Cu ions in doped semiconductors (Cu^{+} or Cu^{2+}),
- the exact position of the Cu d energy levels between the VB and the CB,
- the nature of Cu-dopant emission,
- and the selective adsorption of the Cu dopant at different facets of the host nanocrystal.

Very recently, Pradhan's group resolved some of these problems [137]. To understand the exciton recombination process, the oxidation state of Cu in the NC is very important. Cu^{+} d^{10} and Cu^{2+} d^{9} have different electronic configurations. Using electron paramagnetic resonance (EPR) studies, Srivastava *et al.* demonstrated that even when Cu^{2+}-precursors are used for doping, no signal is observed suggesting the absence of Cu^{2+} and supporting the presence of Cu^{+}, which is formed by reduction of Cu^{2+} with Na_2S in the reaction system [137]. These results are supported by the earlier report of Isarov *et al.* who suggested such a reduction of Cu^{2+} by sulfides present in the NCs [138]. Additionally, it has been shown that the Cu energetic position, which is close to the VB, varies from one semiconductor to another and can be clearly distinguished from surface states emission (Figure 31). Moreover, it has been proven that the adsorption of

the Cu dopant is facilitated in the ZB crystal phase and that the dopant-related broadening is associated with the composition distribution of the NCs [137].

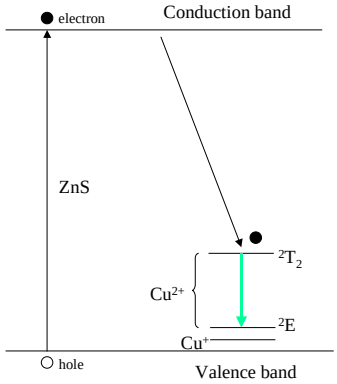

Figure 31. Schematic energy level diagram showing the emission mechanism in the ZnS:Cu nanoparticles [137].

It is worth to discuss the phenomenon of fluorescence emission quenching caused by increasing concentration of dopant ions in the crystal host lattice. The mechanism of this concentration quenching effect is different in Mn^{2+} and Cu^{2+}-doped NCs. First, the effect is described for Mn-doped QDs.

The occupancy of Zn^{2+} sites by Mn^{2+} in the ZnS lattice produces localized levels in the energy gap of the semiconductor ZnS NP due to crystal field effects similar to that in the bulk ZnS:Mn. At higher Mn concentration, the isolated Mn ion may stay at the surface or interstitial positions of the crystallites with octahedral symmetry and do not favour radiative transitions [109]. There are few possible doping states of Mn^{2+} in the ZnS lattice. They might be isolated in the core of NCs, isolated around the NCs surface, segregate to form Mn clusters [139]. The irradiation combination occurs on the isolated Mn ions in the tetrahedral site of ZnS lattice, while the luminescence is mainly attributed to the isolated Mn ions near the NCs surface. The luminescence quenching, especially in high doping concentrations, is the result of different reactivity between Mn^{2+} and Zn^{2+} and a tendency of nanocluster formation by Mn ions [139].

In the case of Cu-doped ZnS NCs, the quenching of fluorescence emission observed with increasing of doping ions concentration is the result of differences in solubility product constant values for the corresponding ZnS and CuS metal sulfides [140] and, as a result, formation of CuS NCs. CuS particles act as nonradiative recombination centers and, additionally, reduce the number of Cu^{2+} ions that are optically active luminescence centers in ZnS NCs [141].

Different concentrations of dopant ions were reported as the ones from which the quenching of fluorescence emission is observed. For Mn-doped NCs, the reported values varied, however in the most of works, the highest PL intensity was found with a molar fraction of 4-5% [110], while for Cu-doped QDs cited values were of 2% [141] or lower [140-142]. Such different values might come from different synthesis procedures used. It was noticed that careful control of synthesis conditions must be employed in the synthesis of doped semiconductor NCs in order to obtain materials with optimized properties [140].

Another important factor that can markedly change the PL properties of core NCs that was already described in previous paragraph is the introduction of the shell, usually from the material of wider energy bandgap. It is worth to mention that the surface passivation is essential for the improvement of the luminescence properties in pure and doped NCs [117]. It was reported by many groups that such surface modification and preparation of core/shell NCs, resulting in effective passivation of quenching core NCs states by a pure ZnS shell, enhances the PL in different range. After the introduction of the ZnS shell, the 30% increase of PL [31] to even 7-fold stronger PL [143] in the case of ZnS:Mn/ZnS QDs in comparison with core structures was observed. Song *et al.* [144] reported that the core/shell ZnSe/ZnS NCs showed 20 times greatly enhanced PL QY as those of bare ZnSe NCs. An inorganic shell passivation not only leads to a significant reduction of surface-related states, but also leads to the confinement of charge carriers in the core region [110].

1.1.7.2. Nucleation and growth of nanocrystals

There exist two main methods of the QDs synthesis. The first is called “organometallic synthesis” and the second one is called “hydrothermal synthesis”. The principle of the synthesis is the temporal separation of the nucleation process and the growth [145]. Experimentally, the separation of the nucleation and the growth might be realized by quick injection, for example in the case of CdSe, the selenium (Se) precursor in the solvent of high boiling point containing the cadmium precursor. The formation of QDs evolves in several steps successively (Figure 32).

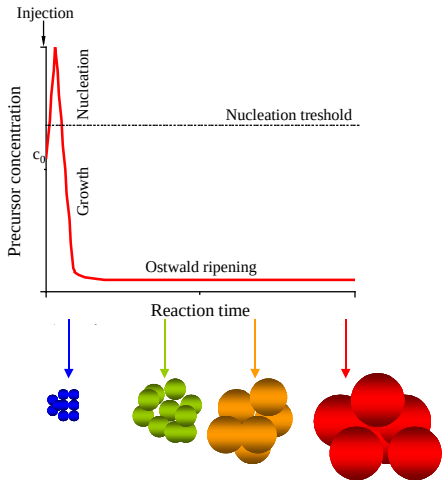

Figure 32. Different steps of QDs synthesis: homogenic nucleation by quick injection of the precursor, growth of germs by the consumption of the precursor in solution, followed by dissolution of the smaller germs to form the bigger ones [146].

Initially, the cadmium precursor is at the concentration of c_o in the solution. The injection of the selenium precursor causes the increase of concentration in "monomers" CdSe above the nucleation threshold and hence, the germs are formed. It leads to the fast decrease of concentration. When the threshold is reached, the formation of germs stops immediately. Thus, the injection of selenium precursor has to be fast in order to have quasi-instantaneous nucleation, what is the key to obtain the monodisperse QDs. Afterwards, the germs growth rapidly in homogeneous manner by consumption of the precursor that remains in the solution. When there is not enough of the precursor in the solution to enable the homogene growth, the phase of Ostwald ripening begin [147]. During that phase, the small particles having higher energy of the surface are going to dissolve forming bigger particles to certain equilibrium. Accordingly, the number of particles diminished when their medium sizes increase.

1.1.7.3.Synthesis of ZnS and ZnSe QDs

Pure and doped ZnS and ZnSe QDs might be fabricated by different methods such as reverse micelle, high-temperature organometallic, ion-implantation techniques [117], chemical precipitation method, microemulsion method, and nucleation-doping strategy [108]. However, the two main synthesis procedures are organometallic synthesis and the synthesis in aqueous medium. The later one, might be distinguished into hydrothermal synthesis, when during the reaction the

temperature exceeds 100ºC or/and the reaction takes place in the high pressure. Otherwise, the reaction is simply called aqueous synthesis. Organometallic synthesis takes place at high temperature, often exceeding 250ºC, using expensive and toxic reagents.

1.1.7.3.1. Organometallic synthesis

To the best of my knowledge, there are only two available reports dealing with the organometallic synthesis of ZnS/ZnS core/shell NPs doped with manganese [148]. In the synthesis procedure of the first one, zinc precursor, oleic acid and manganese aliquot (in N,N-dimethylformamide (DMF)) were dissolved in tri-*n*-octylamine- (TOA)) at 80ºC and DMF was removed *in vacuum*. After the complete dissolving and degassing, 1-hexadecanethiol was added at 80ºC and the reaction mixture was heated to 300ºC under nitrogen. It was observed that the reaction time influenced the particle growth. As-synthesized QDs were then transferred into water by means of surface ligand exchange with different thiol containing molecules, e.g. 2-mercaptoethanol (ME) or 3-mercaptopropionic acid (MPA). However, due to the degradation and dissociation processes, the colloidal stability of obtained QDs was not satisfying for further bioapplication. To improve the stability of as-prepared NCs they were coated with Bovine Serum Albumin (BSA). From transmission electron microscopy (TEM) analysis of as-obtained NPs, a diameter of 5 nm was found. This result was confirmed by X-ray diffraction (XRD) analysis, additionally indicating cubic sphalerite phase of obtained NCs. The authors did not report the value of PL QY, however they mentioned successful introduction of the shell indicating that the fluorescence emission spectrum of core/shell QDs was comparable with the spectrum of the core, with the peak maximum ca. 580 nm, but much narrower.

In the second report, the authors synthesized high-quality core and core/shell Mn-doped ZnS QDs by high-boiling solvent process in hexane. For that, they mixed zinc chloride with TOPO and oleylamine at 170ºC and then elevated the temperature to 290ºC for 1 h. The obtained NCs were of 6 and 8 nm in diameter for core and core/shell nanostructures, respectively, and

possessed cubic zinc blende structure. Once again, the authors did not mention the value of PL QY, however indicated the improvement of 30% in fluorescence emission after introduction of the ZnS shell.

Over the last ten years, a few groups have reported the synthesis of ZnSe [149-154] and of the related Mn-doped ZnSe NCs [133, 136, 155-160] via organometallic synthesis. This approach generally utilizes pyrolysis of organometallic complexes in coordinating solvents such as TOP or TOPO. In 2001, Norris *et al.* [161] presented organometallic synthesis route for the preparation of good-quality Mn:ZnSe QDs which, since now, was often used by many researchers [162, 163]. Later on, the group of Peng [136] introduced nucleation-doping and growth-doping strategy, two new synthesis strategies in high-temperature organometallic synthesis. In a typical procedure of manganese doped ZnSe NPs synthesis proposed by Norris *et al.*, dimethylmanganese ($MnMe_2$) is freshly prepared by reacting manganese chloride ($MnCl_2$) with methylmagnesium chloride in anhydrous tetrahydrofuran (THF) (Equation 4):

$$MnCl_2 + 2CH_3MgCl \rightarrow MnMe_2$$

Equation 4. Schematic representation of $MnMe_2$ preparation.

The Se precursor is prepared by dissolving Se powder in TOP (Equation 5):

$$Se + TOP \rightarrow TOPSe$$

Equation 5. Schematic representation of Se precursor preparation.

The $MnMe_2$ solution is added to the TOPSe and diethylzinc (Et_2Zn).
The as-prepared solution is then rapidly injected into a vigorously stirred HDA at 310ºC. The ZnSe:Mn^{2+} NCs growth at 240-280ºC about 3 h.
Obtained NCs prepared by such organometallic route possess high PL QY (22% at 295 K (rt) and 75% below 50 K [161]), high crystallinity and monodispersity.

However, it was always a challenge to dope all NCs simultaneously, even with the vigorous organometallic approaches which provide the extremely small volume of QDs and dynamic nature in growth process. Due to this fact, Peng's group proposed two methods to decouple the doping process from nucleation and/or growth, which enable to dope almost all NCs in a given sample. Two different strategies nucleation-doping and growth-doping are presented in Figure 33.

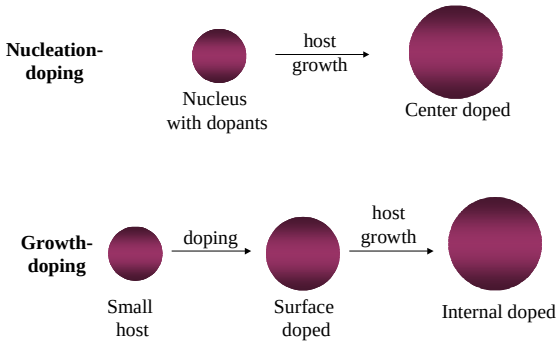

Figure 33. Schematic representation of nucleation- and growth-doping strategy [136].

In growth-doping strategy, the formation of small host ZnSe NCs occurred, while nucleation-doping is realized by a mixed dopant and host precursors during the nucleation. After nucleation, the reaction conditions are tuned to be sufficiently mild to make the dopant precursors inactive, and the growth of the host becomes the only procedure, which overcoats the dopants [164]

By using such synthesis methods to prepare Mn:ZnSe d-dots, the resulting samples have very high dopant emission, tunable wavelength (565-610 nm), and high PL QY of about 40-70% [156].

Unfortunately, the existing protocols of "non-class A" d-dots organometallic synthesis always involve pyrophoric and dangerous chemical reagents. In most cases organo-phosphines have been used as the ligands for introducing Se precursor (starting as Se powder) into the reaction system. Very recently, the synthesis of high-quality Mn:ZnSe QDs synthesized without use of pyrophoric, highly toxic, and expensive organophosphines was reported [159]. During this synthesis air-stable starting materials such as zinc (manganese) fatty acid salts with corresponding free fatty acids, Se powder, fatty amine, and octadecene were used. The synthesis strategy was nucleation-doping in which Mn^{2+} were introduced into the d-dots in the initial stage. The temperatures of MnSe formation as well as of overcoating by the host ZnSe were both reduced in

comparison with traditional organometallic synthesis earlier reported. Multiple injection techniques were employed to realize balanced diffusion on the Mn ions in the QDs. The resulting NCs were found to have zinc blende structure, spherical shape and were nearly monodisperse, they possess high optical quality and pure dopant emission (PL QY 40-60%) [159].

However, NCs obtained with all these approaches are only dispersible in nonpolar organic solvents and must be prepared at relatively high temperature. The exchange of the hydrophobic TOP or TOPO ligands with hydrophilic ligands, such as thioacids, and subsequent transfer of QDs from oil to aqueous solution can significantly reduce the PL efficiency of the NCs [3]. That is why it is desirable to prepare directly water-dispersible NCs by a cheaper and easiest route.

1.1.7.3.2. Synthesis in aqueous medium or hydrothermal synthesis

The synthesis in aqueous medium has been developed by Weller *et al.* in 1996 [165]. During the last years, the synthesis of QDs such as CdS [166], CdSe [167], CdTe [168], ZnS [169], ZnSe [116], and HgTe [170] in aqueous medium was successfully developed.

Direct synthesis of thiol-capped QDs in water is a promising alternative route to organometallic reactions and offers the following advantages: (1) it uses less toxic reagents, (2) it is cheaper and simpler, (3) it uses lower reaction temperatures (100°C) to obtain QDs with comparable PL QY and size-tunable fluorescence, (4) the surface functionalization with water-soluble ligands occurs during the synthesis, and (5) the QDs obtained have a small diameter, which is suitable for biological applications.

As before, I focus on the preparation of doped ZnS and ZnSe QDs in the aqueous medium.

Doped ZnS QDs are usually obtained by chemical precipitation method. The processing parameters of materials, reaction temperature, solution pH, titration rate, even stirring rate [107, 171], have strong effects on the properties of final nanomaterials, such as particle size, particle size distribution, particle shape and particle PL properties. Starting materials can be either oxides or salts

and the precipitation temperature can be in the range from 0 to 100ºC and pH from 2-11 [107]. In a typical reaction, the precipitation from homogenous solutions of various zinc and manganese or copper salts compounds with S^{2-} as precipitating anion, formed by thermal decomposition of sulfur source like thioacetamide [172, 173] and thiourea [174] or coming from sodium sulfide (Na_2S) [107, 175] under specific pH conditions takes place. The capping molecules commonly used are thioglycolic acid (TGA) [176], 3-mercaptopropionic acid (MPA) or/and (3-mercaptopropyl)trimethoxysilane (MPS) [169] or L-cysteine (Cys) [177]). It was reported that doped ZnS NCs prepared via such aqueous methods possess usually zinc blende crystalline structure, have few nm in diameter, and their fluorescence emission is centered at ca. 590 nm in the case of Mn^{2+}-doped, and at ca. 500 nm in the case of Cu^{2+}-doped QDs [174, 178], with usually few percent of PL QY.

It was reported that hydrothermal preparation has been successfully used to prepare ZnS:Mn NCs [179]. The authors observed that PL spectra were influenced by $[S^{2-}]/[Zn^{2+}]$ ratio, Mn^{2+} ions concentration (1-20%), and the temperature (70-110ºC). The reactants were zinc and manganese sulfates and sodium sulfate. The reaction lasted 10 h. The obtained NCs possessed a zinc blende structure and diameter of ca. 3 nm. The strongest brightness was observed with the $[S^{2-}]/[Zn^{2+}]$ ratio equal to 0.7, a synthesis temperature of 90ºC and 20% molar ratio of Mn^{2+} relative to Zn^{2+}. In 2010, Rashad *et al.* [180] reported on the successful synthesis of Mn-doped ZnS NCs by hydrothermal method using thiourea as a source of sulfur. In the synthesis protocol, zinc and manganese chloride were mixed with thiourea and the reaction lasted 24 h and was performed at 150-200ºC. The crystal size decreased with Mn^{2+} concentration increase from 7.5 to 3.8 nm for 0 and 40% of molar Mn^{2+} doping, respectively. The obtained NCs were of wurzite hexagonal structure and were spherical in shape. In both hydrothermal reports, the PL QY of the dots is not mentioned.

The nucleation-doping strategy was also applied in the preparation of ZnSe:Mn d-dots in aqueous media. However, usually the optical properties of these QDs prepared in aqueous media were not as good as their counterparts prepared in an oil phase. To the best of my knowledge, there are very few

reports on the synthesis of ZnSe:Mn d-dots prepared via aqueous route. Recent studies have demonstrated that good quality ZnSe QDs can be prepared in water either under hydrothermal conditions [105, 181-185] or under microwave irradiation [186] by reaction of a Zn^{2+} salt with sodium hydroselenide (NaHSe), generally in the presence of a thioalkyl acid stabilizer. Sodium hydroselenide is prepared by mixing sodium borohydride and selenium powder in water (Equation 6):

$$Se + NaBH_4 \rightarrow NaHSe.$$

Equation 6. Preparation of sodium hydroselenide.

After the complete reduction of selenium powder, the NaHSe solution is added to the solution containing zinc precursor and the ligand at basic pH [18]. Using a mixture of the dopant and of the host precursor during the nucleation step, Wang *et al.* in 2009 succeeded in the preparation of Mn^{2+}-doped ZnSe QDs with a PL QY of 2.4%, which represents the first direct synthesis of fluorescent Mn^{2+}-doped ZnSe QDs in aqueous solution [187]. One year later, Fang *et al.* reported on the synthesis of much better quality water-dispersible ZnSe:Mn/ZnS core/shell NCs prepared in aqueous media with the possible PL QY up to 35 ± 5%. The reported synthesis was based on two-step approaches, firstly on the synthesis of ZnSe:Mn d-dots and secondly, on the overcoating of ZnS shell around prepared cores. The synthesis route followed the standard methods for synthesis of II-VI semiconductor NCs in aqueous media, in which zinc and acetate salts together with MPA, playing the role of the stabilizing ligand, were mixed together and then, a freshly prepared NaHSe solution was added. The reaction mixture was heated for 90 min. at 90ºC [188]. Finally, in 2011, Shao *et al.* [189] reported on similar aqueous method of the preparation of ZnSe:Mn QDs via nucleation-doping. By controlling the injection volume of precursors in each step, the ideal core and shell were obtained. By varying the ZnSe shell epitaxial-growth time, the size of prepared d-dots was controllable. Obtained QDs were stable and color-tunable (PL peak position could be tuned from 572 to 602 nm) and possessed cubic zinc blende structure. The authors indicated that the highest PL QY of the resulting QDs could approach 4.8%.

1.1.8. Anchorage of biomolecules at the QDs surface

As it was shown in the previous paragraph, the modification of the QDs surface is a key step for their hydrodispersion. However, a second functionalization is needed to provide selective interaction between the fluorescent probe and the cellular target. One of the most exciting applications of nanotechnology in medicine is the use of QDs for bio-imaging. Luminescent QDs can be made very effective for targeted imaging by attaching them with disease specific ligands such as vitamins, proteins, peptides or monoclonal antibodies [16]. Surface chemistry is also a critically important consideration in developing various types of bioassays based on QDs. Different biorecognition agents such as enzymes, antibodies, small molecule binding protein, and oligonucleotides can be conjugated to QDs [190]. In Figure 34 some selected surface chemistries described in previous subsection and conjugation strategies applied to QDs are demonstrated.

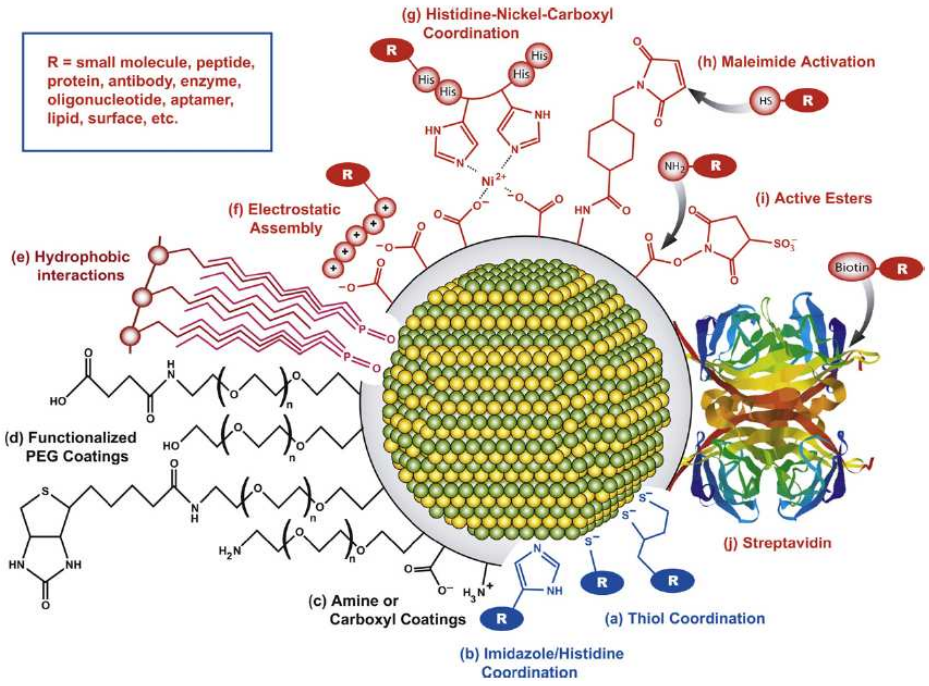

Figure 34. An illustration of some selected surface chemistries and conjugation strategies that are applied to QDs. The grey periphery around the QD represents a general coating. This coating can be associated with the surface of the QD via (e) hydrophobic intractions, or ligand coordination. Examples of the latter includes: (a) monodendate or bidendate thiols, (b) imidazole, polyimidazole (e.g. histidine). The exterior of the coating mediates aqueous solubility by the display of (c) amine or carboxyl groups, or (d) functionalized PEG. Common strategies for bioconjugation include: (a) thiol modifications or (b) polyhistidine tags that penetrate the coating and interact with the surface of the QD; (f) electrostatic association with the coating; (g) nickel mediated assembly of polyhistidine to carboxyl coating; (h) maleimide activation and coupling; (i) active ester formation and coupling; (j) biotin-labeling and streptavidin-QD conjugates [190].

The conjugation strategies with the biomolecules require the link of the biomolecules with QDs without any change of their activity or/and recognition by certain targets. There are two main procedures enabling the anchorage of the biomolecules at the QDs' surface.

1.1.8.1.Non-covalent conjugation

QDs can be conjugated with the charged biomolecules via a non-covalent strategy involving electrostatic interactions [191]. In this case, the QDs are synthesized in the way that they carry a charge complementary to that one of the biomolecule. The two entities are simply mixed and self-associate. This simple approach has been successfully used for the preparation of QDs functionalized with the antibodies and proteins via the streptavidin/biotin interaction [192].

The conjugation can also involve the interaction between the molecules and the metals (Cd, Zn) that are at the QDs surface. The proteins or peptides possess the aminoacid sequences that have the affinity to the metals or the metallic cations [104, 193]. Then, the biomolecules adsorb at the QDs surface via interactions between the carboxylate function (COO^-) of the ligand and Cd or Zn being at the QDs surface and/or by the hydrogen bond between the amine function (NH_2) or alcohol function –OH of the biomolecule aminoacids and the carboxylate function present at the QDs' surface [194]. Schematic representation of CdTe QDs surface stabilized by TGA and phenylalanine is shown in Figure 35.

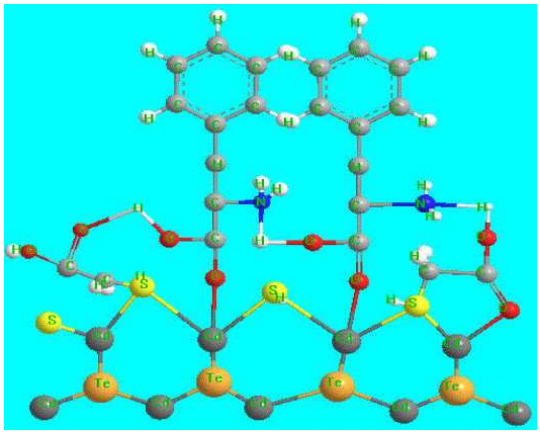

Figure 35. Schematic representation of the surface of CdTe QDs modified with thioglycolic acid and phenylalanine [194].

1.1.8.2.Covalent conjugation

The anchorage of the biomolecules by the covalent bond is more often based on the reaction of the amine function of the biomolecule and the carboxylic acid (or carboxylate) belonging to the QD ligand. The coupling is usually performed by means of a carbodiimide playing the role of the coupling agent such as *N*-(3-dimethylaminopropyl)-*N*-ethylcarbodiimide (EDC) chlorohydrate associated to *N*-hydroxysuccinimide (NHS) as activator. The activated ester formed with NHS facilitates the coupling of the biomolecule by the nucleophilic attack of the amine function at the electrophilic center of the carbonyl function. The conjugation between the ligand at the QDs surface and the desired biomolecule leads to the formation of an amide bond (Figure 36) [5, 195].

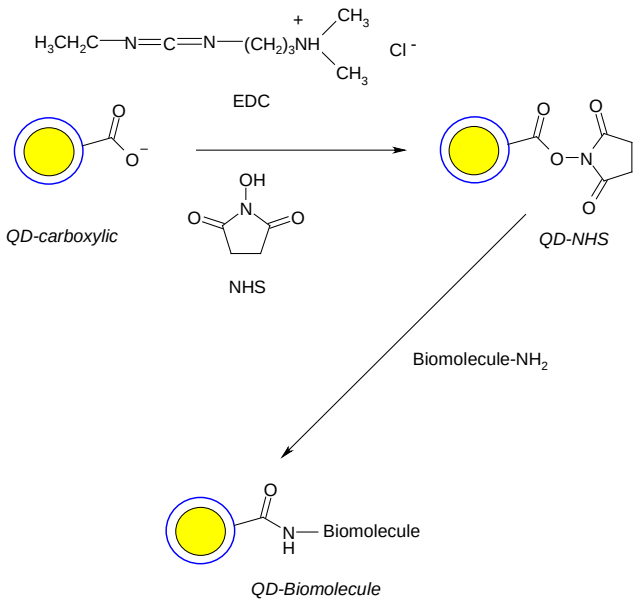

Figure 36. Coupling between carboxylic QDs and an aminated biomolecule by use of EDC and/or NHS (modified from [196]).

The covalent coupling can also be done between the carboxylic acid function and the hydrazid such as the hydrazid of adipic acid (ADH) by use of EDC. As obtained QDs-hydrazid enable the coupling between the biomolecule having the acid function [5, 195].

In the case of biomolecules that contain a thiol function or are modified by a thiol function, there are two methods of covalent coupling for conjugation with QDs. The first method uses the heterobifunctional networking agent sulfosuccinimidyl-

4-(*N*-maleimidomethyl)cyclohexane-1-carboxylate (sulfo-SMCC) (Figure 37). The quantum dots capped with nitrogen containing ligand (QD-NH_2) react with the sulfo-SMCC and form QDs-maleimide. Then, the maleimide function forms a stable thioether bond with the thiol function of the biomolecule by addition involving a radical intermediate [5, 195].

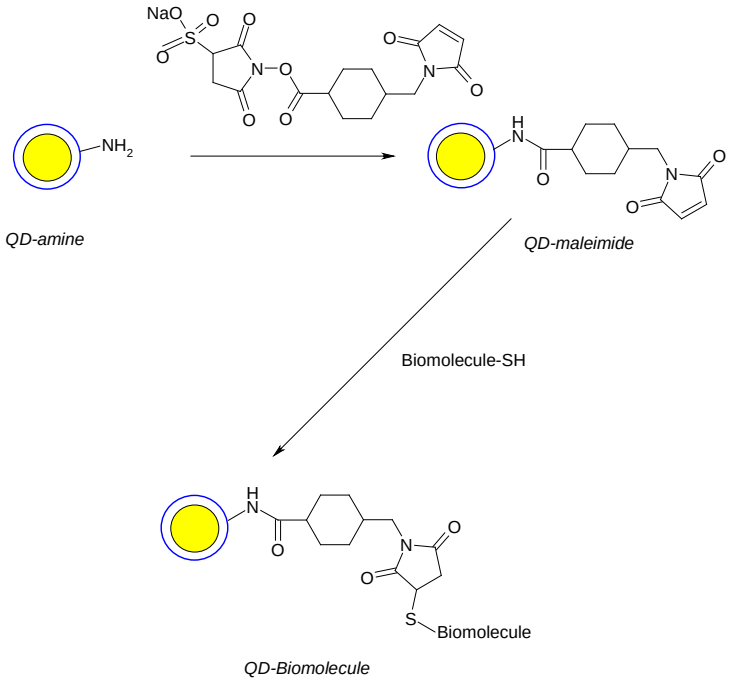

Figure 37. Coupling between nitrogen QDs and the biomolecule containing a thiol function using sulfo-SMCC (modified from [196]).

The second method based on coupling of QDs-NH_2 with succinimidyl 3[3′-(2-pyridyldithio) propanoate. The new disulfide bond is formed between the biomolecule containing sulfur and the thiol at the QD surface [5, 195].

1.2. QDs cytotoxicity

The rapidly expanding field of nanotechnology with the development of various NPs has the potential to revolutionize the medical treatment. However, the information on toxicology of these materials is little to date and needs much development making difficult to assess all the risks associated with these new tools. There exist many works on toxicology of QDs, however many question remain still unanswered and the hypothesis on toxicity mechanism evoluated with time. Recently, Rzigalinski et Strobl [12] published a very interesting review summarizing all existing work on cadmium-containing QDs, not forgetting about critical gaps in our knowledge concerning the toxicity of these NCs. Although the toxicity of QDs has not been throughly examined, there are some ideas of its sources. Up to 2005, QDs toxicity was mainly attributed to the toxic effects of heavy metals leaching from the NPs core and QDs surface-covering molecules. Later on, other mechanism of QDs toxicity were proposed such as NPs aggregation on the cell surface [197]. Most importantly, since QDs are efficient energy donors, they can transfer energy to the nearby oxygen molecules, inducing the generation of reactive oxygen species (ROS), in turn leading to cell damage and death [198]. Additionally, the pharmalogy of QDs should be considered to indicate additional aspects of NCs toxicity. All of these points are discussed in the following paragraph.

1.2.1. QDs pharmacology

QDs toxicity is associated with traditional pharmacological parameters such as liberation, absorption, distribution, metabolism and elimination (LADME) and these QDs parameters in biological systems require investigation. It should be considered that QDs, in comparison with an organic drug molecule that is delivered, are characterized by quantum effect and electronic interactions, and for that reason, all pharmacological parameters should be adapted to these nanostructures. As the chemical structure of an organic molecule is considered in pharmacological studies, in the case of QDs such physicochemical characterization as the size, coating, atomic composition and purity should be described. This is difficult due to the lack of particle consistency across experiments. It should also be taken into account that QDs of

different composition are compared in different studies, while their photophysics range diametrary.

Considering dose metrics of QDs, different units have been reported by scientific groups in terms of mg/kg, mg/mL or on a molar basis. These engineered entities dose exprimation via mass or molar number may be inappropriate descriptor. As the surface area is critical to NPs function, dose description by surface area proposed by Oberdörster *et al.* [199] or by the number of cadmium atoms exposed at the QDs surface [200] seems to be much correct.

The extent of QDs tissue retention is important for dosing consideration, since repeated doses may induce systemic accumulation. Moreover, NCs containing toxic atoms might be very toxic when persisting in biological systems due to limited metabolism and excretion. That is the reason of description of traditional pharmacological parameters as LADME.

Absorption into the system depends of the delivery route. Possible routes of QDs exposure are environmental, workplace, and therapeutic or diagnostic administration [201]. NPs may enter the organism via skin absorption, inhalation, oral delivery and parenteral administration. Functionalized-QDs delivered to the organism via parenteral *iv* route can be accumulated is selected tissues. It was shown that dermal QDs absorption depends on shape, size and surface coating [202]. Considering inhalation of NPs, it was reported that QDs < 2.5 nm can penetrate in the lung and interact with the alveolar epithelium, while larger aerosolized QDs can deposit in bronchial spaces [201].

Most of examined QDs absorbed readily at the cellular level, primarily via endocytic mechanism [203]. Cells internalize QDs in different ways depending on cell type, QDs concentration, their sizes, charges or ligands [204]. Some reports indicate selective incorporation of ligand-targeted QDs via specific receptor [205]. Such pathway for active and selective transport on NPs is called the receptor-mediated endocytosis. Interestingly, the specific uptake of ligands allows for a 1000-fold increase of the intracellular concentration of macromolecules [28]. QDs might be eventually taken up by the reticuloendothelial system (RES), including the liver, spleen and lymphatic system [7, 206]. Maysinger *et al.* [204] suggested that the extent of poorly internalized QDs can be enhanced by electroporation or microinjection, other possible mechanism of cellular internalization may be by inducement of plasma membrane damage (Figure 38).

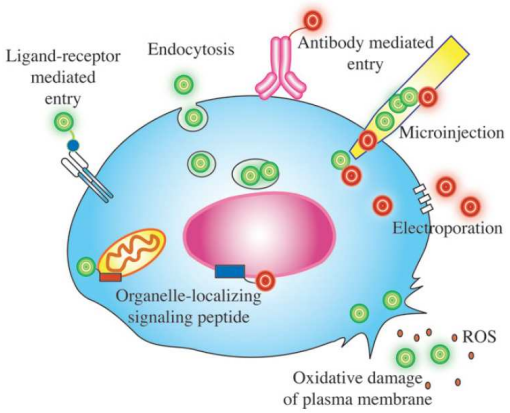

Figure 38. Internalization of QDs by cells [204].

The process of phagocytosis can be divided into phagocytosis characteristic only to mammalian cells (uptake of large particles) and pinocytosis that can be found in every cell (uptake of fluids and solutes) [28]. There are four mechanisms of pinocytosis: macropinocytosis, clathrin-mediated endocytosis, caveolae-mediated endocytosis and clathrin- and caveolae-independent endocytosis.

Lovrić *et al.* [207] found subcellular localization dependent on NCs size, larger QDs accumulated in the cytoplasm, smaller in the nucleus.

Regarding distribution, there is not much information about blood/QDs interaction considering parenteral route of delivery. Surface coating, addition of biological targeting ligands influence plasma half-lives. Such parameters as QDs size and agglomeration as well as immune responses should be considered at that level [208].

Metabolism of QDs is another studied aspect of cadmium-containing QDs. It seems that the core is not enzymatically metabolized, but shells and coating are. It might be a critical factor as they shield the more toxic CdTe and CdSe cores from the intracellular environment. The outer QDs elements appear to degrade under photolytic and oxidative conditions. The degradation products such as CdO, TeO_2, SeO_2 and SeO_4^{2-} might be formed what is described more precisely in the following paragraph concerning mechanisms of QDs toxicity.

Elimination of QDs is undoubtedly regulated by the size, coating and physicochemistry. It was reported that QDs smaller than 5 nm can be removed by the kidneys. However, these studies suggested that only a fraction of injected dose of QDs was found in the kidney and liver and observed fluorescence indicated that at least some QDs remained in their original form [209]. Other reports suggested that a part of

administered QDs persist in the tissues and since QDs are photoactive, the persistence in the skin may have unknown consequences when exposed to light. Derfus *et al.* [203] suggested three fates for QDs circulating in the body- clearance intact through the kidney, breakdown into smaller particles, or sequestering of the particles. However, since QDs conjugates are usually spherical, greater that 7 nm in diameter, and negatively charged, clearance through the kidney is very rare, unless they are first broken down into smaller particles.

As we can see, there is a need for a comprehensive study on QDs pharmacology.

1.2.2. Mechanisms of QDs toxicity. Role of reactive oxygen species (ROS)

As it was mentioned above the core of II-VI QDs is generally composed of CdSe and CdTe, being the most commonly used for biological applications [7]. Due to this fact, the potential mechanisms of cadmium-containing NCs are discussed.

The toxicity of cadmium element was extensively studied during last decades. Its toxicity is mainly associated with liver and kidney injury, osteoporosis and neurological deformations at the level of living organism. At the cellular level, cadmium induces oxidative stress by depletion of endogenous antioxidants such as glutathione and is associated with mitochondrial damage, apoptosis induction and disruption of intracellular calcium signaling. Cadmium-containing QDs may raise the ROS level through a several pathways, namely (i) upon excitation, QDs can form electron-hole pairs to transfer electron to oxygen (generation of H_2O_2, $OH^{\cdot}$, $O_2^{\cdot-}$), (ii) intracellular antioxidant system may be directly damaged via interaction with QDs and/or (iii) Cd^{2+} released from QDs can cause intracellular ROS elevation [197]. As mentioned in the introduction to this paragraph, other multiple parameters such as size, shape, concentration, charge, redox acitivity, surface coating and mechanical stability influence QDs toxicity. All that is discussed in the following section.

A main source of QDs toxicity may result from cadmium residing in the core. The toxicity of uncoated cadmium-containing QDs is associated with free cadmium present in the particle suspension or released from the particle core intracellularly [203, 210]. It was reported that cadmium-containing QDs induced apoptotic-like cell

death including chromatin condensation and membrane fragmentation [198]. Potentially generated by cadmium-based QDs, Cd^{2+} ions are known to bind to sulfhydryl groups of mitochondrial proteins and cause hepatic injury [211, 212]. It was found that from uncoated QDs cadmium might be released via surface oxidation [203] suggesting that the core could degrade in biological environment. It this process O_2 molecules oxidize chalcogenide atoms (Se, S) which are located on the QDs surface to oxidized forms (SeO_2, SO_4^{2-}) and for example in the case of CdSe NCs, these SeO_2 molecules desorb from the surface, leaving behind reduced Cd atoms. That is the reason why prolonged exposure of QDs to the oxidation conditions can cause the decomposition of the CdSe NCs and lead to desorption of Cd ions from the QDs core [203] and/or formation of QD-biomolecules complexes [204]. It is worth to mention that other QDs core components may also be toxic. For example, it is suggested that the cytotoxicity of selenium is associated with oxidative stress and inorganic compound, sodium selenite, induce DNA damage, particularly DNA strand breaks and base damage. [213].

Due to the reactivity of QDs that contain cadmium, they might be photo- and air-oxidized. Therefore, free radical formation is another possible mechanism of QDs toxicity. Free cadmium does not directly generate free radicals (it does increase oxidative stress), however active QD core participates in radical formation. There are many different mechanisms of ROS production and there exist different forms of ROS. Free radicals might be generated from photoexcited NPs by reductive or oxidative pathway. The reductive pathway involves the electron transfer to an acceptor (A) while oxidative pathway involves the hole transfer to a donor (D) what is presented in the equation 7:

$$A + e^-_{CB} \longrightarrow A^{\cdot -}$$

$$D + h^+_{VB} \longrightarrow D^{\cdot +}$$

Equation 7. Possible mechanism of free radicals generation by QDs (CB- conduction band, VB- valence band) [14].

ROS are generated when as-formed free radicals interact with water or oxygen. When NPs are excited by the light more energetic than the bandgap ($h\upsilon$), an exciton (electron-hole pair) is formed. The electron can interact with A, and/or the hole with a D (Figure 39). An electron wave function penetrates significantly into the surrounding

solution while that of the hole does not. It is the reason why the donors must be strongly adsorbed to the NPs for reaction to occur [14].

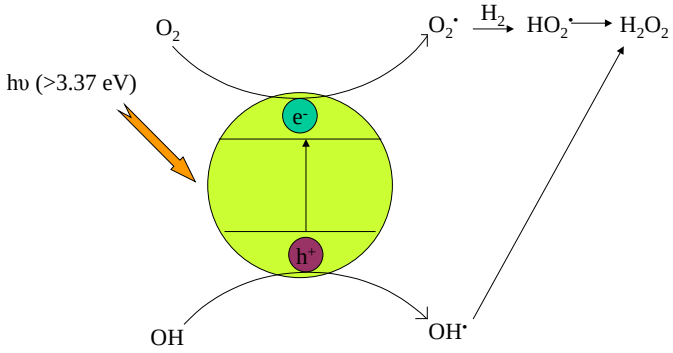

Figure 39. Mechanisms of possible energy transfer involving QDs (modified from [14]).

The complex antioxidant system that includes antioxidants (glutathione, NADH, thioredoxin) and antioxidant enzymes (superoxide dismutase, catalase, glutathione reductase, glutathione peroxidase) create specific redox microenvironment for the subcellular organelles [214]. However, cells are sensitive to ROS and once the production of ROS overcomes the antioxidant defense, cellular redox balance is shifted and the cells are in the state of oxidative stress. The sensitivity of the cells to ROS depends on the cell type, the level and the duration of oxidant production, the species of ROS generated and the specific site of ROS production. ROS can react with many types of cellular biomolecules, resulting in their damage, degradation and finally, loss of function [198, 204]. The oxidation of aromatic DNA basis is the main source of DNA damage. The oxidation of aromatic and sulfur-based aminoacids is the main source of protein damage. The oxidation of polyunsaturated fatty acids in lipids leads to the loss of compartmentalization and plasma-membrane integrity [204, 215]. Lipid peroxydation can also generate harmful and relatively stable aldehyde products which add to the oxidative stress [216]. QDs toxicity seems to be also dependent on the charge of the NPs and their ability to form complexes with various biomolecules. The possible interactions between QDs and cells are presented in Figure 40.

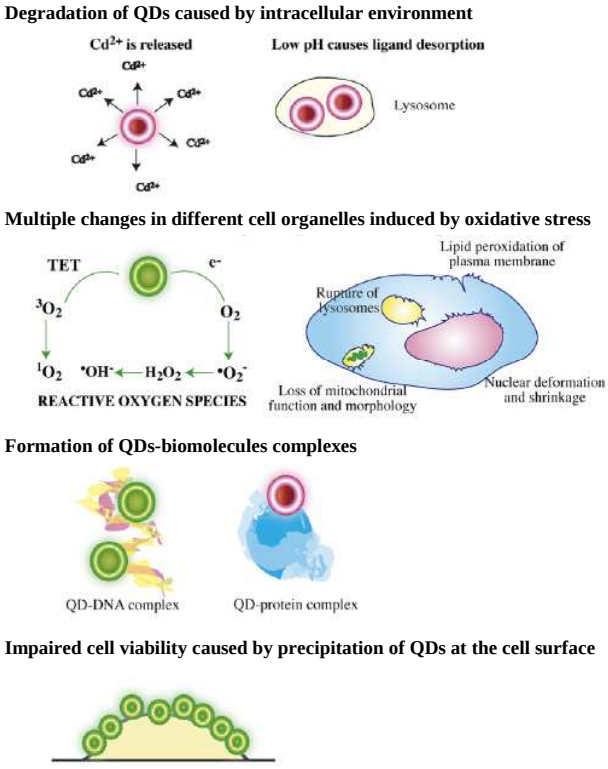

Figure 40. Possible interactions between QDs and cells (TET- triplet energy transfer) [200, 204].

ROS can be formed in an aqueous medium (cell culture medium) particularly in the presence of exogenous oxygen, since the medium is supplied by CO_2/O_2 [198]. As it was mentioned before, it is possible that a photon of light excites the QD generating an excited electron which transfers to molecular oxygen, producing singlet oxygen. Singlet oxygen in turn initiates free radical formation upon reaction with water or other biological molecules [13]. This is the basis of photodynamic therapy (PDT) in cancer application of QDs that is further discussed, but must also be considered when assessing toxicity of QDs in normal tissues. Uncoated QDs caused other cytotoxic effects similar to those resulting from cadmium toxicity and/or oxidative stress. It was reported that depending on the cell type, the cell death was associated with upregulation of Fas expression possibly through an increase of oxidative stress (neuroblastoma cells) [217] or activation of p53 and hypoacetylation (human breast cancer cells) [218].

Core Cd atom accessibility is linked to the permeability to oxygen and protons of the different extra layers of materials that are added to the core (shell and ligands) [212]. It has been shown that encapsulation of the core with a ZnS shell or other capping material reduce toxicity [203]. In addition to reduction in release of free cadmium, the shell was also found to reduce free radical generation due to air

oxidation of QDs. Protons (in low pH environment) may lead to protonation of the coordination groups of the ligands and their subsequent detachment from the QDs surface. A shell will reduce QDs toxicity by delaying the oxidation of the core [212]. Other capping materials can be used to insulate the QD core and reduce toxicity in many cases. It was found that QDs coated with MPA and cysteamine required higher concentration to produce toxicity in PC12 cells in comparison to uncoated QDs [207]. N-acetylcysteine (NAC) or dihydrolipoic acid (DHLA) were also reported to reduce the toxicity of QDs [217, 219]. Interestingly, all these capping materials appear to be good antioxidants, further supporting a role for oxidative stress in cadmium QD toxicity. However, toxicity of capping materials must also be considered, coating layer or functional groups per se might be cytotoxic [201]. It was observed that thioglycolic acid (TGA) and tri-*n*-octylphosphine oxide (TOPO) increased QDs toxicity [7].

Also functionalizing groups targeting specific cells and attached to the QDs surface can contribute to the toxicity since distribution to non-targeted tissue may produce toxicity, especially when QDs are used as a photosensitizing agents or drug carrier.

Toxicity might be used as the biomedical advantage, particularly in targeted delivery to tumors [220]. Photoactivated toxicity can be directed to a specific location followed by application of light. The light photon excites the QD, and an excited electron can transfer to nearby molecular oxygen initiating a chain of radical generation ultimately inducing cell death. Whereas this is a principle for PDT in oncology, the distribution of QDs to non-cancerous tissue such as skin and retina, which are normally exposed to light, must be considered.

The interpretation of the data concerning QDs cytotoxicity is difficult as a result of differences in cellular handling of QDs and possible contribution of unexpected factors. Handling has been shown to be affected by many factors such as size, coating, charge, composition or redox potential. With the limited data accumulated since now, it is not easy to estimate the true extent of QDs cytotoxicity, which factors contribute, and the effect they may have [221]. The most of data concerning QDs toxicity comes from *in vitro* experiments, usually MTT or XTT assays [13, 197, 207]. Animal studies are decidedly lacking for both pharmacology and toxicology of QDs. The results of *in vivo* experiments indicated that the NPs seem to be non toxic, but they are not cleared from the system either [222]. These cytotoxicity studies underscore the need for short

and long term toxicity evaluation that examines multiple organ systems before QD risk can be adequately assessed or a shift to safer and more reliable materials will be required for QD applications. Of potential materials, ZnS and ZnSe should be the ideal candidates.

1.3. Potential biomedical QDs applications

Semiconductor QDs are of considerable interest as a potential tool in bio-applications due to the dimensional similarities with biological macromolecules, like nucleic acids, proteins or peptides [221]. Recent developments in chemistry and material physics have allowed optical, electrical and magnetic detection of different states of biological systems where the characteristic biokinetic behavior of NPs is an attractive quality for applications in diagnosis and therapy (e.g. use of fluorescent or magnetic particles as contrast agents, in magnetic separation, fluorescent labeling of cellular compartments or targeted drug delivery). NPs can also serve as new tools to investigate and to understand molecular processes in living cells [6]. The potential applications of QDs in medicine and pharmacy are presented in Figure 41.

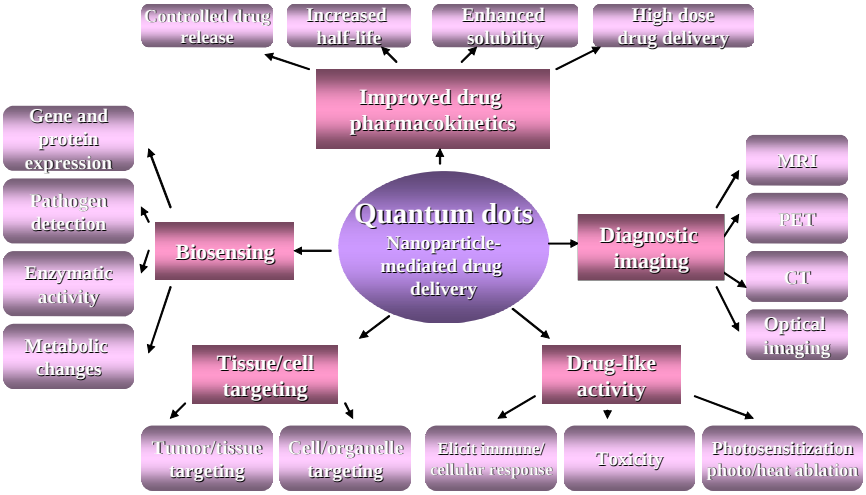

Figure 41. Potential applications of QDs in medicine and pharmacy [223].

In the following paragraph QDs application in cell imaging, drug delivery and biosensing is described demonstrating great potential of these fluorescent NCs in future development of medicine and pharmacy.

1.3.1. QDs-based cell imaging and drug delivery

The technique of fluorescence microscopy with its recently improved resolution and sensitivity together with the development of fluorescent sensors and labeling of proteins in live cells enabled clearer understanding of the dynamics of

intracellular networks. However, there are some problems associated with fluorescence microscopy such as cell autofluorescence in the visible spectrum and the requirement of long observation times [81].

Due to the light emitting properties of QDs, which include increased photostability and narrow and symmetric emission spectra, these NCs have been increasingly used as an alternative to organic dyes for bioimaging. The increased photostability is especially useful for three-dimensional (3-D) optical sectioning, where a major issue is bleaching of fluorophores during acquisition of succesive *z*-sections needed for the correct reconstruction of 3-D structures [81]. The broad absorption band of QDs is beneficial for selecting NIR wl for two/multi-photon excitation [49, 224]. By use of such probes, a signal from deeper placed tissue (e.g. skin cancer) could be detected non-invasively [30, 225]. QDs might be also ideal probes to improve real-time fluorescence detection in living cells and live animals. The great advantage of QDs for imaging in living subjects is the possibility of their emission tuning from visible light to the NIR spectrum by adjusting their composition and size. Larson *et al.* [226] have used two-photon excitation confocal microscopy to image blood vessels in live mice after *iv* injection, showing that higher contrast and imaging depth can be obtained at a lower excitation power than with organic dyes.

However, to act as useful biological probes, QDs have to be surface functionalized. QDs have the ability to conjugate with various bio-recognition molecules such as peptides, nucleic acids, antibodies and small-molecule ligands for application as targeted fluorescence probes. Targeting is usually achieved by conjugating a high-affinity ligand that provides preferential accumulation of the QD-ligand complexes. Over-expressed receptors on the surface of many cancer cells are ideal targets for bioimaging. Therefore, an important aspect of developing QDs in biomedical research is to use them as tumor diagnosis probes when they bind with tumor-targeting ligands. Tumor targeting for both therapeutic and diagnostic applications has been focused on some candidate ligands whose receptors are over-expressed in tumor cells. One of such receptors is folate receptor (FR) [98]. Folic acid (FA) has been recognized as a marker for a variety of tumors (detailed information concerning FA characteristics is further described) [227]. The idea to employ QDs as cell markers was based not only on their superior optical properties but also on the discovery that they can be internalized by cells via receptor-mediated or by non-specific endocytosis (Figure 42) [228].

In the passive mode of imaging, QDs accumulate in tumor sites through an enhanced permeability and retention effect. For active tumor targeting, QDs are conjugated to molecular ligands (antibodies, peptides, …) to recognize protein targets that are over-expressed on the tumor cells surface.

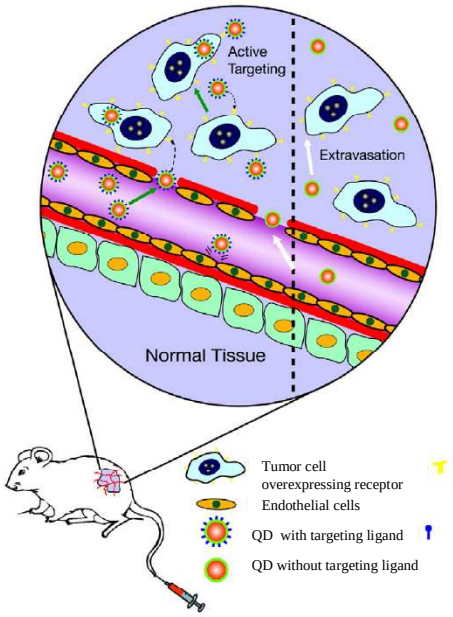

Figure 42. Scheme illustrating active and passive bioimaging of cancer cells using QDs [7].

Especially in recent years, there has been much interest in application of FA-conjugated QDs in tumor cell imaging, diagnosis and drug delivery. Some examples are listed in Table 4 and other are discussed more detailed further in the work.

Table 4. Examples of FA-conjugated QDs application in drug delivery and bioimaging of FR-positive cell lines

QDs core	Purpose	Cells	Technique	Ref.
CdTe/ZnS coated with BSA (bovine serum albumin)	Diagnosis of cancer	Human nasopharyngeal carcinoma cells (KB cells)	Confocal fluorescence microscopy under single-photon and two-photon excitation	[227]
ZnO coated with chitosan and loaded with anti-cancer agent-doxorubicin-DOX)	Anti-cancer drug therapy (tumor-targeted drug delivery), documentation of the delivery process	Cell imaging by confocal microscopy is planned	Drug release studies in a dialysis membrane tube by use of fluorescence analysis	[229]
CdSeS were used as templates to obtain core/shell silica nanocomposites	Tumor cell imaging	Hela cancer cells	Fluorescence microscopy	[230]
CdSe/ZnS	Cancer cells imaging	Human epidermal carcinoma (KB cells)	Fluorescence microscopy	[228]
CdHgTe	Cancer cells targeting fluorescence probes (early tumor diagnosis)	Hela cells for imaging, S180 carcinosarcoma tumors for in vivo studies	NIR fluorescence imaging system	[98]
InP-ZnS	Bioimaging (luminescent probes for cell imaging)	Human nasopharyngeal carcinoma cells (KB cells)	Confocal and two-photon microscopy	[231]
CdSe entrapped in lipid shells (DSPE) and post-loaded with a folate-lipid conjugate forming so-called lipidots	Targeting to mouse and human tumor cells	Mouse J6456 lymphoma cells, human KB cancer cells	Confocal microscopy and in vivo observation after injection into tumors based on FACS analysis and confocal imaging	[224]
CdSeS	Tumor cell labeling	Hela cells	Fluorescence microscopy	[232]

FACS- fluorescence-activated cell sorting

The development of multifunctional QDs and their potential applications in oncology, with the particular emphasis on the diagnosis, prognosis, and treatment of cancer, is very promising [233]. Multi-functional NPs became alternative system for drug delivery. They show a great potential for example in cancer therapy (see Table 4). Multi-functionalization of NPs allows for the targeted delivery of drugs with imaging agents. Such nanocarriers can provide versatile platforms for the delivery of different pharmacological agents. That enables enhancement of therapeutic effect and overcomes drug resistance in cancer [234]. Yuan *et al.* [229] recently reported on a new approach of combining QD technology with anti-cancer drug therapy that facilitates the distribution of drug-loaded carrier in cells to be visualized during drug therapy. In these preliminary studies, chitosan, a natural copolymer of *N*-acetylglucosamine and *D*-glucosamine was used as an encapsulating agent, while FA was used as a tumor recognition moiety. Blue-emitting ZnO QDs were encapsulated in

folate-conjugated chitosan and loaded with doxorubicin (Dox) (Figure 43). The drug release response of DOX-loaded nanocarrier was characterized and obtained results point toward the application of QDs in the design of new drug release carrier [229].

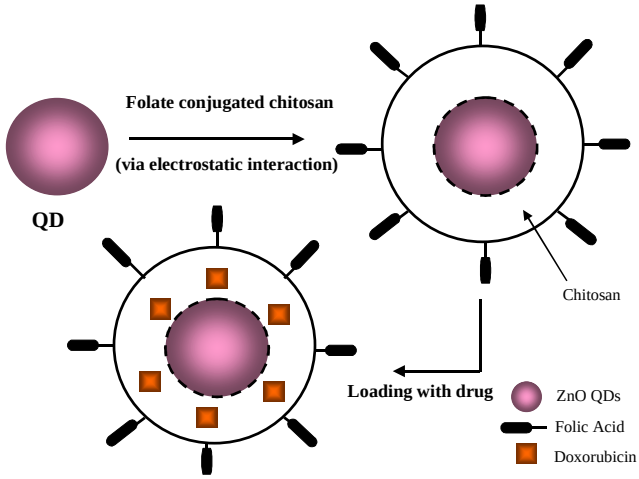

Figure 43. Schematic representation of the encapsulation of ZnO QDs with folate-conjugated chitosan and the drug-loading step, where biofunctionalized chitosan loaded with doxorubicin is used to encapsulate QDs [229].

The ability of nanoconjugates of CdSe/CdS/ZnS QDs and mentioned before doxorubicin (Dox) to target alveolar macrophages cells (aMØ), which play a critical role in the pathogenesis of inflammatory lung injuries was recently reported [235]. The ability to provide targeted therapeutic delivery in the lung would be a huge progress in pharmacological treatments for many pulmonary diseases. The results demonstrated that NP platforms can provide targeted macrophage-selective therapy for the treatment of pulmonary disease [235].

Another group reported that other anticancer drug well established for chemotherapy in colorectal, pancreatic, breast, head and neck cancer 5-Fluorouracil (5-FU) was encapsulated in FA-conjugated carboxymethyl chitosan coordinated to manganese-doped zinc sulfide quantum dot (FA-CMC-ZnS:Mn) NPs [234]. Targeting of tumor cells enhances the therapeutic potential of chemotherapy agents, while FR is a potential molecular target for tumor-selective drug delivery [234]. In this study the polymeric carrier, CMC as well as imaging agent QDs enabled controlled drug delivery and, at the same time, imaging the path of 5-FU carrier system [234].

It should be kept in mind that before NCs could be widely used as biolabels and/or drug delivery agents, they must maintain three properties in biological environment: efficient fluorescence, colloidal stability and low nonspecific adsorption [89].

1.3.1.1. Folate receptor (FR)

The folate receptor (FR) represents a target for intracellular NPs delivery because it is overexpressed in many cancer cell lines [28]. High levels of the human α isoform folate receptor (αhFR) expression with a very high affinity for FA and reduced folates (dissociation constant K_d =0.1-20 nmol/L) can be detected in some cancer cells, namely ovarian, breast, lung, brain, and colorectal cancers, but cannot be detected in most normal tissues [236]. FR is a glycosylphosphatidylinositol-linked membrane glycoprotein of 38 kDa located in the caveolae. In the process of folate accumulation (through the process of potocytosis) ligand-bound receptor is sequestered in caveolae, followed by internalization into postcaveolar plasma vehicles, released from the receptor via an intravesicular reduction in pH, and subsequently transported into the cytoplasm for polyglutamation. Ligand-free receptor is recycled to the cell surface by the caveolae reopening [237].

The folates are required for many biological processes like transmethylation or deoxyribonucleic acid (DNA) and ribonucleic acid (RNA) synthesis. High overexpression of αhFR in cancer cells is unclear, however it is supposed that elevated levels of it promote cell proliferation and possibly generate some other regulatory signals [236]. It can be explained by increased need of cancer cells for FA as a coenzyme for the synthesis of amino acids and nucleic acids.

FA might be used as a targeting ligand to functionalize for example QDs against tumor cells because of the ease of the reaction procedure and the small size of the folate molecule (Figure 44). FA can be easily connected to functionalized QDs by (EDC/NHS) chemistry [28]. That enables a stable binding with QDs surface coating and permits folate receptor-mediated endocytosis [238].

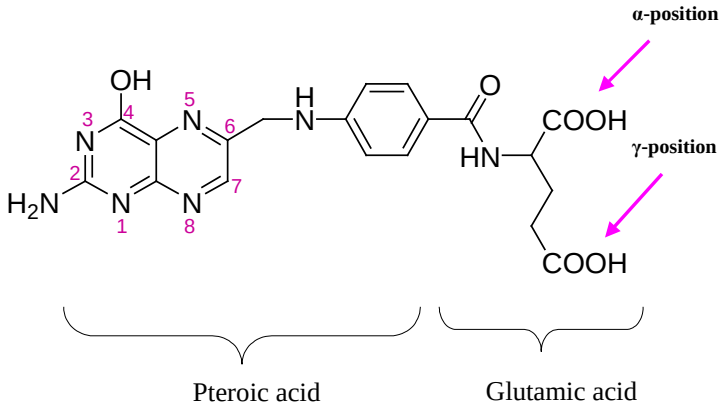

Figure 44. Schematic representation of FA structure [239].

In FA molecule two carboxyl groups, α and γ, in its glutamate moiety can be distinguished. It is known that only the γ-conjugate is capable of binding to the FR. Gabizon *et al.* [237] reported on the relative amounts of each α- and γ-carboxyl conjugate of folic acid-poly(ethylene glycol)-distearoylphosphatidylethanolamine (FA-PEG-DSPE), indicating that 80% and 20% conjugates were γ- and α-linked, respectively. Even though the modification of the α-carboxylic acid group in FA might disrupt the binding recognition by FR, it is not a concern because the γ-functionalized FA is the main product due to the steric hindrance resulting in its higher reactivity.

Surface functionalization can be applied to link NCs to DNA, antibodies or proteins, to achieve selective binding or targeting properties. The selective targeting is an important aspect for developing QDs in biomedical applications [224]. In recent years, tumor cell targeting for both therapeutic and diagnostic applications has focused on a small number of candidate ligands whose receptors are overexpressed in tumor cells. Apart from FA, other ligands whose receptors are overexpressed in cancer cells are transferrin, HER2, and growth factors that may also target angiogenesis, with various degrees of successful application [224].

1.3.2. Biosensing

In the introduction to this paragraph at first some general information about the biosensors applied from the review of Mohanty and Kougianos is given [240]. Then, the application of QDs as biosensors based on PL intensity variations is shown, and

finally more sophisticated biosensing entities based on QDs resonance energy transfer are described.

For the first time, it was heard about biosensors in 1962 due to the development by Leland C. Clark of enzyme electrode to sense the glucose in the blood. Since that time, more sophisticated and reliable biosensing devices for application in medicine, biotechnology, military and agriculture have been developed. There are many definitions of biosensor. One of them says that a biosensor is a chemical sensing device in which a biologically derived recognition entity is coupled to a transducer which allows the quantitative development of some biochemical parameter. Other definition says that a biosensor is an analytical device being a combination of a specific biological element (that creates a recognition event) and a physical element (that transduces the recognition event). The concept of biosensor and its elements are illustrated in the Figure 45.

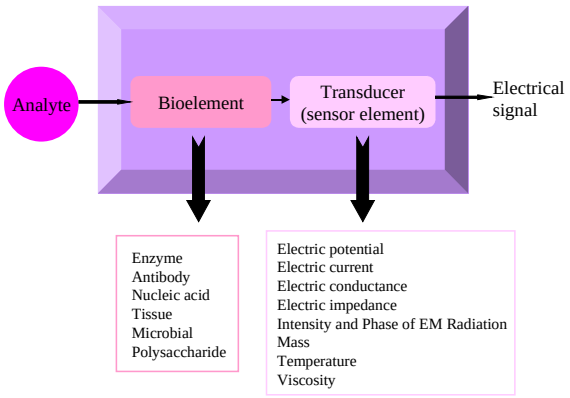

Figure 45. A schematic representation and elements of biosensors (modified from [240]).

As it can be seen, the biosensor is a combination of two parts: a bio-element and a sensor-element. A bio-element recognizes a specific analyte and the sensor-element transduces the change in the biomolecule into, for example, an electrical signal. It is important that the bio-element is very specific to the analyte to which it is sensitive and does not recognize other analytes. The “bio” and “sensor” elements can be coupled together in a few possible ways such as membrane entrapment (semi permeable membrane separates the analyte and the bioelement, the sensor is attached to the bioelement), physical adsorption (dependent on the combination of van der Waals forces, hydrophobic forces, hydrogen bounds, ionic forces to attach the biomaterial to the surface of the sensor), matrix entrapment (porous encapsulation matrix is formed around the biological material that helps in binding it to the sensor)

and covalent bonding (the sensor surface is treated as a reactive group to which biological materials can bind). Different types of biosensors depending on the transducing mechanism used can be listed such as resonant biosensors, optical-detection biosensors, thermal-detection biosensors, ion-sensitive biosensors, electrochemical biosensors (conductimetric, amperometric, potentiometric), glucose biosensors or biosensors for DNA detection.

Due to the fact that the most common method of detecting and quantitating biomolecules still remains the use of fluorescence, the fluorescent probes have found widespread biosensing applications in immunoassays, nucleic acid detection, ions detection, clinical/diagnostic assays or cellular labeling [241]. Luminescent semiconductor NCs are a recently developed class of nanomaterial whose unique photophysical properties are helping to create a new generation of fluorescent biosensors. QDs properties of interest include high QY, broad absorption spectra coupled to narrow size-tunable PL emissions. In the area of biosensors, QDs are particularly attractive due to their long-term photostability, allowing continuous and real-time monitoring [47]. That enables emerging practical applications of QDs in biochemistry and medicine [41]. Numerous advantages of QDs over organic/protein fluorophores are listed in Table 5.

Table 5. Comparison of QDs and organic/protein fluorophores properties (adapted from [241])

Property	*QDs*	*Fluorophores*
Photophysical		
Absorption spectra	Broad	Variable/narrow (generally a mirror of the emission spectra)
Molar extinction coefficient	High	Variable (generally < 200,000 $M^{-1}cm^{-1}$)
Emission spectra	Narrow (FWHM 25-40 nm)	Broad, asymmetric
Effective Stokes shifts	> 200 nm possible	Generally < 100nm
Quantum yield	Generally high	Variable, low to high
Fluorescence lifetime	Long ~10-20 ns or greater	Short < 5 ns
Photostability	Excellent	Variable to poor
Multiphoton cross section	Excellent	Variable to poor
FRET capabilities	Excellent donors	Variable
Chemical		
Chemical resistance	Excellent	Variable
Reactivity	Limited conjugation chemistry available	Multiple reactivities commercially available
Mono-valent attachment	Difficult	Easy
Multi-valent attachment	Good possibilities	Rare
Other		
Physical size	1-20 nm	< 0.5 nm
Cost effectiveness	Poor/ 2 commercial suppliers	Very good/ multiple suppliers

The application of QDs as biological labels was first reported in 1998 by two groups [2, 3]. It has been demonstrated that highly luminescent QDs can be made

water-dispersible and biocompatible by appropriate surface chemistry and bioconjugation.

As the luminescence of QDs is very sensitive to the QDs surface states, it was expected that the interactions between a given chemical species and the QDs surface will result in the changes in the efficiency of the core electron-hole recombination. That gave the basis to the increased development of the QD-based optical sensors [41]. QDs have been used in optical sensing of small molecules and ions what is listed in Table 6.

Table 6. QD-based fluorescent probes for chemical determination of small molecules and ions

QD material	QD coating	Analyte	Ref.
ZnS	L-cysteine	Cu(II)	[177]
CdTe	Thioglycolic acid	ATP, folic acid, L-cysteine	[242]
CdSe	TOPO	spironolactone	[243]
(CdSe)ZnS	2-mercaptoacetic acid + organophosphorous hydrolase	paraoxon	[244]
CdS	polyphosphate	Cu(II)	[245]
	L-cysteine	Fe(III)	
	Thioglycerol	Zn(II)	
CdS	L-cysteine	Ag(I)	[246]
CdTe	Mercaptopropionic acid-capped QDs in nanocomposite films	glucose	[247]

Using QD-based optical biosensors, the measured signal is fluorescence enhancement or quenching. The PL activation effect is a result of the passivation of surface traps sites that are either being “filled” or energetically moved closer to the band edges. Such simple chemical process was observed after addition of Cd, Zn or Mn ions to the colloidal solutions of CdS or ZnS QDs and this behavior provided the basis of such metallic cations optical sensing. The principle of QD-based optical sensing quenching strategies is the quenching by the analyte affecting the PL emission of QDs. The quenching mechanisms include inner filter effects, non-radiative recombination pathways, electron-transfer processes and ion-binding interactions.

It was demonstrated that conjugation of the QDs with appropriate immunomolecules can be used for recognition of specific antibodies or antigens by measuring the luminescence emission of NCs.

New generation luminescent sensors based on energy transfer mechanisms are photochemically-induced fluorescence (or Förster) resonance energy transfer (FRET) [41], BRET (bioluminescence resonance energy transfer), and CRET (chemiluminescence resonance energy transfer) mechanisms [190]. The energy

transfer mechanisms involved in FRET, BRET and CRET are schematically presented in Figure 46.

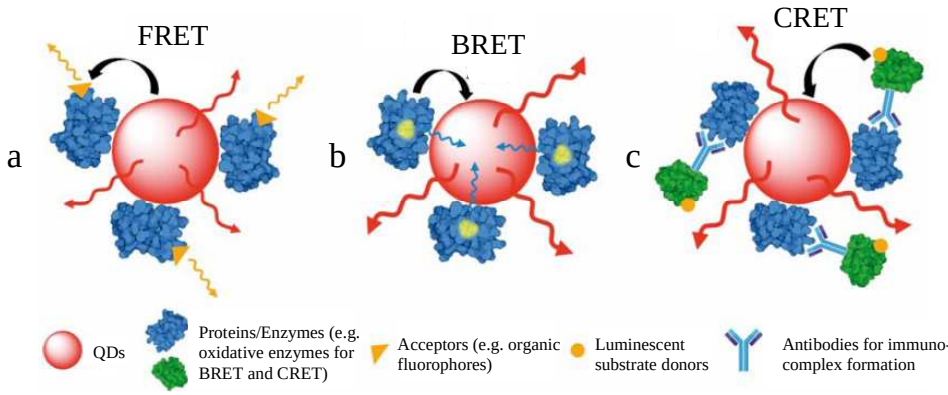

Figure 46. QD-based fluorescence resonance energy transfer (FRET), bioluminescence resonance energy transfer (BRET), and chemiluminescence resonance energy transfer (CRET) nanosensors. (a) QD donor conjugated with dye-acceptor-labeled proteins, with an efficient FRET ensured by site-specific protein labeling and controlled orientation of the protein on the QD providing homogenous donor-acceptor separation distances. (b) QDs conjugated with a BRET donor and transfer of bioluminescence energy to the QDs. (c) Immunoassay-based transfer of chemiluminescence energy from the CRET donor to the QD acceptor [248].

FRET involves the transfer of fluorescence energy from a donor particle to an acceptor particle when the distance between the donor and the acceptor is smaller than the critical radius (Förster radius) [221]. This leads to the reduction in the donor's emission and excited state lifetime, and an increase in the emission intensity of acceptor [221]. Generally, QDs serve as energy donors, and biomolecules are labeled with an acceptor dye. Biorecognition events at the surface of QDs are used to drive the association or dissociation of acceptors, or alter the QD-acceptor separation distance. An analytical signal is provided by the resulting modulation of FRET efficiency. A conventional FRET experiment uses optical excitation to create an excited state donor [190].

The capability of tailoring (via size) photoemission properties of QDs should allow efficient energy transfer with a number of organic fluorophores suggesting the use of the NPs in sensor or chemical assay applications [41]. As QDs emission spectrum is narrower and more symmetric than the emission from conventional organic dyes, it should be much easier to distinguish the emission of the donor from that of the acceptor. It is worth to mention that the high QY of QDs make energy transfer very efficient [41]. FRET is suited to measuring changes in distance, making it appropriate for measuring conformational changes, monitoring protein interactions and assaying of enzyme activity [221]. Several groups have already confirmed the

usefulness of QDs in the design of novel FRET-based strategies [41]. For example, a method for the detection of monosaccharides or dopamine was developed using QDs [249]. Figure 47 shows the use of CdSe QDs for sensing maltose in solution [249].

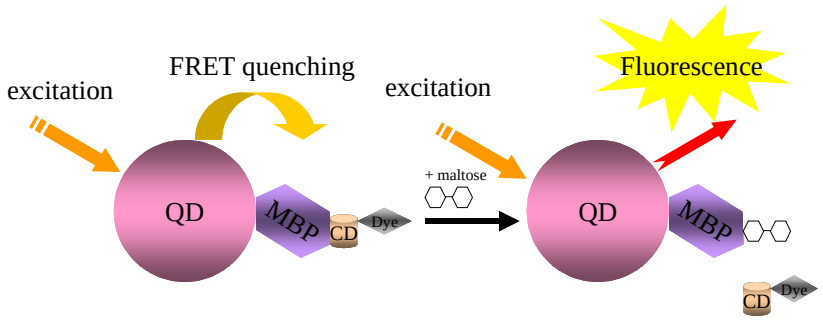

Figure 47. Schematic diagram of the QD-based FRET maltose sensor (adapted from [250]). QDs conjugated to maltose-binding proteins (MBP) play the role of FRET donors. Non-fluorescent dye bound to a cyclodextrin (CD) serves as an acceptor and in the absence of maltose is filling the protein binding sites resulting in the luminescence quenching. In the presence of maltose, the complex cyclodextrin-dye is removed and the fluorescence is recovered.

In contrast to FRET, BRET and CRET generate an excited state donor through a chemical reaction. More precisely, the biochemical reaction is the basis of BRET. QDs are ideal energy acceptors in BRET and CRET due to their strong broad absorption that enables potentially large spectral overlap integrals and excellent spectral separation between donor and acceptor emission. An advantage of BRET and CRET over FRET is very low background. Moreover, the absence of optical excitation avoids sample autofluorescence [190].

It was demonstrated that QDs can serve as an energy acceptor for a light-emitting protein (for example, the bioluminescent protein *Renilla* luciferase (Rluc)) in BRET. When the QD conjugates are exposed to the luciferase substrate, the energy released in the oxidation of the substrate is transferred to the QDs through BRET, thus generating light emission from the QDs [251]. The design of a BRET-based QD biosensor for detection of the activity of proteases (matrix metalloproteinases (MMPs)) was reported and the principle of BRET taking place is presented in Figure 48.

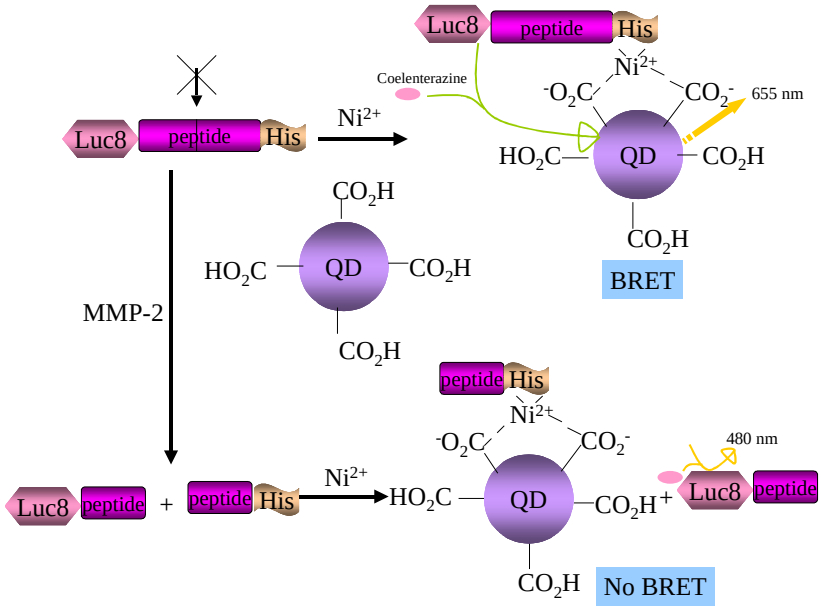

Figure 48. BRET-based detection of MMP-2 with assembled QD nanosensor (adapted from [252]). MMP-2 together with six-histidine tag is genetically fused to the BRET donor (*Renilla* luciferase (Luc8)). In the presence of Ni^{2+}, the carboxylic acids on the QDs bind the metal ions and form complexes with the His tag on the Luc8 fusion protein. BRET takes place and produce light emission from QDs. MMP-2 hydrolyzes peptide substrate. The cleavage of the amide bond by MMP-2 release the His tag from the fusion Luc8 and no BRET occurs.

In recent years, some groups have been reported on resonance energy transfer between chemiluminescent donors and luminescent QDs as acceptors. CRET involves non-radiative transfer of energy from a chemiluminescent donor to a suitable acceptor molecule. In contrast to FRET, CRET occurs by the oxidation of a luminescent substrate without an excitation source. The simple system choosing the luminol/hydrogen peroxide chemiluminescence (CL) reaction catalysed by horseradish peroxide (HRP) was reported [253]. The principle of the efficient CRET due to the continuous catalysis of CL reaction by HRP directly linked to QD is illustrated in Figure 49.

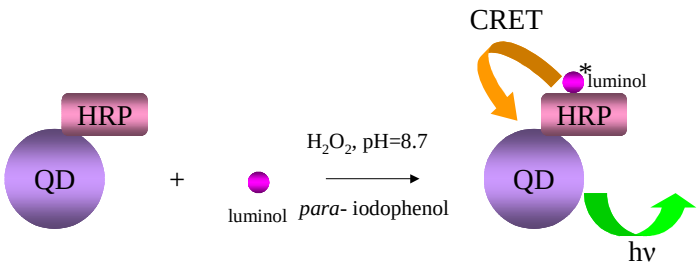

Figure 49. Schematic presentation of CRET based on luminol donor and HRP-labeled QD acceptor (adapted from [253]). The CL donor- luminol, is not directly linked with QD and catalyst- HRP is conjugated to QD. HRP can continuously catalyze the luminol/hydrogen peroxide CL reaction. The QD-HRP conjugates can be used as probes in cell and tissue imaging in such a system. *Para*-iodophenol plays a role of an enhancer.

Recently, Li *et al.* [254] reported a CRET process with QD as acceptor and the CL of luminol as donor without use of QD-HRP conjugates. QDs were directly linked with luminol that excites QDs through the luminol/hydrogen peroxide CL reaction in the presence of NaClO.

Since their first description in a biological context, luminescent QDs have elicited great interest in the biosensing due to their unique photophysical properties. These fluorescent NCs may overcome some liabilities of conventional fluorophores to help create a new generation of biosensors. As it can be seen, the progress have been made in adaptation of QDs for various biosensing application [241]. Apart from simple optical sensing including fluorescence-based transduction, these nanoprobes may be used in methods based on luminescence-based resonance energy transfer and can improved biotechnological techniques such as nucleic acid, proteins and enzymes detection. QD-based pH probes, ion sensors and organic compounds sensors were reported. However, chemical-surface modifications of QDs have still to be perfected in order to enhance the selectivity of the probes and to favorable their emission features. It can be said that the future use of QDs for sensing is promising and that field needs further development.

1.3.3. Photodynamic therapy (PDT)

Photodynamic therapy (PDT) has emerged over the last few years as a promising alternative or substitute to chemo- and radiotherapy for the treatment of cancer [255, 256]. PDT is a local, non-invasive, repeatable technique with potential to be also an effective alternative to antibiotic therapy in the treatment of local infections [257].

PDT involves a photoactivable agent, known as photosensitizer (PS), light and molecular oxygen [256]. After PS injection and an appropriate drug-light interval (DLI), the area to be treated is illuminated with light of convenient wl. Principle stages of PDT are presented in Figure 50.

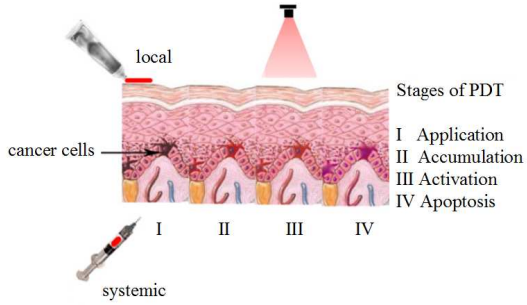

Figure 50. Principle stages of photodynamic therapy [55].

In a photodynamic reaction, the PS irradiated by light is promoted to a higher energy/electronic level, an excited singlet state (Figure 51). The singlet excited PS either decays back to the ground state, resulting in the fluorescence or undergoes intersystem crossover to the longer lived triplet excited state. The interaction of the triplet sensitizer with surrounding molecules results in two types of photo-oxidative reaction. Type I pathway involves electron or hydrogen atom transfer, producing radical forms of the PS or the substrate. These intermediates may react with oxygen to form peroxides, superoxides ions, and hydroxyl radicals indicating free radical chain reactions. Type II pathway is mediated by the energy transfer process with ground state oxygen ($1O_2$) and to the return of the sensitizer to its ground state. The *in situ* generation of singlet oxygen via this mechanism appears to play a crucial role in photodynamic cytotoxicity because of the highly efficient interaction of the $1O_2$ species with the biomolecules [258].

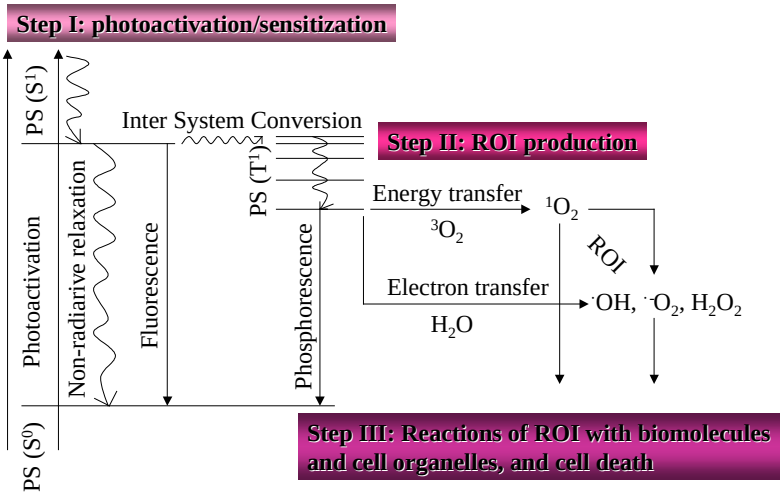

Figure 51. Photophysical and photochemical processes involved in PDT [49].

One essential element in PDT is the PS ability to generate reactive oxygen intermediates (ROI) and its selectivity for the target tissues of great importance for a good photodynamic effect. Various types of photosensitizers have been developed over the past decade in order to improve their light absorption and diseased tissues selectivity in comparison with the first-generation photosensitizers [259] Second-generation photosensitizers, such as chlorin and phthalocyanine, present better absorption in the red side of the visible light spectrum, which commonly represent the therapeutic window because of the slightest absorption of endogenous tissues compounds in this area (mainly hemoglobin and water) [260].

Recently, the potential of using QDs and QDs conjugates as sensitizers for PDT was described. As mentioned above QDs are characterized by large absorption spectra, narrow and symmetric emission bands, and a very high molar extinction coefficient (up to 5 x 10^5 $cm^{-1}.M^{-1}$) [2, 81], which can be great advantages over conventional PS for a PDT strategy. They also possess a better photostability than conventional organic fluorophores [89, 261, 262] and their fluorescence quantum yield can be up to 100% [263]. Recent studies have demonstrated that the efficiency of QDs to exchange energy after photoexcitation with $^3O_2$ surrounding molecules is low because of the relatively large hydrodynamic diameters of QDs and of the ultrafast carrier relaxation in QDs that compete with slow energy transfer process to $^3O_2$ that require the formation of collision-complexes [210].

As a result, QDs are generally associated to classical organic PS for PDT. Several QD-PS conjugates have emerged in the last years in which the excited singlet ($^1PS^*$) and triplet ($^3PS^*$) states of the PS are indirectly generated by non-radiative energy transfer, also called fluorescence (or Förster) resonance energy transfer (FRET), from photoactivated QDs.

Following photoexcitation, the QD conduction-band electron can also be transferred to surrounding O_2 or water molecules, thus producing ROS like hydrogen peroxide (H_2O_2), superoxide ($O_2^{\cdot-}$) or hydroxyl radicals ($OH^{\cdot}$), the latter being thought to be the most harmful among all ROS. A few studies have demonstrated that ROS generated by CdSe or CdTe-core QDs upon photoactivation cause irreversible damages to DNA, mitochondrial impairment and cell death [13, 264, 265]. ROS and reactive nitrogen species (RNS) like peroxynitrite ($ONOO^-$) were also found to be produced by core/shell CdSe/ZnS or InGaP/ZnS QDs upon NIR photoactivation [220].

Chapter 2. Aim of the work

A widespread application of fluorescent NCs in various areas, especially in medicine and pharmacy where they can be used as bioimaging, biosensing or drug-delivery agents is hindered by the inherent cytotoxicity of the elements such as Cd^{2+}, Se^{2-} or Te^{2-} that the QDs are composed of. To reduce QDs toxicity, NCs technology is moving toward the development of Cd-free fluorescent NCs. However, many of the Cd-free QDs obtained so far do not possess optical properties comparable to those of more classical type II/VI NCs.

Considering the above, the aim of this work is to develop a new class of non-toxic QDs probes with essential attributes such as water-dispersibility, photostability, biocompatibility, high luminescence and possible excitation with low-energy visible light, using simple processing method. Such nanoprobes could be used in various bioapplications including bioimaging of cancer cells. In my studies folic acid (FA) will be used to facilitate the folate receptor (FR)-mediated targeting of the malignant cells. In the performed studies I will focus on ZnS and ZnSe QDs as they are cadmium-free and might be excited bifotonically.

Firstly, the synthetic protocols of zinc sulfide (ZnS) and zinc selenide (ZnSe) QDs doped with two ions such as manganese (Mn) or copper (Cu) and stabilized by 3-mercaptopropionic acid (MPA) or 1-thioglycerol (TG) will be established, followed by NCs characterization (diameter, surface charge, photophysical properties, …) using analytical techniques such as spectrophotometry UV-vis, fluorimetry, X-ray diffraction (XRD), X-ray photoelectron spectroscopy (XPS), transmission electron microscopy (TEM), dynamic light scattering (DLS), infra-red analysis (FT-IR), thin layer chromatography (TLC) and electron paramagnetic resonance (EPR).

Secondly, the protocols of functionalization of as-prepared QDs with FA will be developed and QDs fluorescence emission quenching by FA will be examined.

Thirdly, the cytotoxicity of synthesized bare and conjugated NPs will be evaluated on cancer cell lines (MCF-7, T47D, PC-3) using MTT, XTT and ferrous oxidation-xylenol orange (FOXO) tests.

Finally, chosen well fluorescent and weakly toxic types of as-prepared and characterized QDs will be used for bioimaging of cancer cells. In these experiments, FA-functionalized NCs will be excited biphotonically (excitation wl > 700 nm).

Chapter 3. Materials and methods

3.1. Reagents and chemicals

Zinc sulfate heptahydrate ($ZnSO_4 \cdot 7H_2O$, 99.99%), zinc acetate dihydrate ($Zn(OAc)_2 \cdot 2H_2O$, 98+%), zinc nitrate hexahydrate ($Zn(NO_3)_2 \cdot 6H_2O$, 98%) manganese acetate tetrahydrate ($Mn(OAc)_2 \cdot 4H_2O$, 99%), 3-mercaptopropionic acid (MPA, 99%), copper (II) sulfate pentahydrate ($CuSO_4 \cdot 5H_2O$, 98%), 1-thioglycerol (98%), selenium powder (99.5%, 100 mesh), sodium borohydride ($NaBH_4$, 98%), sodium sulfide ($Na_2S \cdot 9H_2O$) (98+%), 2,2'-(ethylenedioxy)-*bis*-ethylamine (98%), folic acid (FA, >97%), 1-ethyl-3-(3-dimethylaminopropyl)carbodiimide hydrochloride (EDC, >98%) and ethanol (HPLC grade) were used as received without additional purification.

All solutions were prepared using Milli-Q water (18.2 $M\Omega.cm^{-1}$, Millipore) as the solvent. Sodium borate buffer (0.1 M) was prepared from Na_3BO_3 and the pH adjusted to 8.8 using 0.1 M H_3BO_3. All reactions were conducted in a three-neck flask under nitrogen flow.

3.2. Instruments

All the optical measurements were performed at rt (20 ± 2°C) under ambient conditions.

- Absorption spectra were recorded on a Perkin-Elmer (Lambda 2, France) UV-visible spectrophotometer.
- Fluorescence spectra were recorded on a Fluorolog-3 spectrofluorimeter F222 (Jobin Yvon, France) equipped with a thermostated cell compartment (25°C), using a 450 W Xenon source. The QY values were determined by the Equation 8,

$$QY\ (sample) = (F_{sample}/F_{ref})(A_{ref}/A_{sample})(n_{sample}^2/n_{ref}^2)QY_{(ref)}$$

Equation 8. Equation for calculation of QY of the sample.

where F, A and n are the measured fluorescence (area under the emission peak), the absorbance at the excitation wl, and the refractive index of the solvent, respectively. PL spectra were spectrally corrected and quantum yields were determined relative to Rhodamine 6G in water (QY = 95%) [266].

- The fluorescence lifetimes of ZnSe:Mn@MPA core and core/shell QDs were measured by a FluoroMax-4 spectrofluorometer (Jobin Yvon) using a NanoLED emitting at 372 nm as an excitation source with a nanoled controller module, Fluorohub from IBH, operating at 1 MHz. The detection was based on an R928P type photomultiplier from Hamamatsu.
- Luminescence decays of core/shell ZnS Mn- and Cu-doped QDs were obtained on a Fluorolog-3 spectrofluorimeter equipped with a pulsed xenon lamp using the decay by delay method with a 5 ms window and increments of 0.05ms. Excitation was set at 300 nm and detection at 590 nm.
- Fourier transform infrared spectroscopy (FT-IR) was performed using a Brucker Vector 22 spectrometer in case of ZnSe QDs. In case of ZnS:Mn@TG QDs, FT-IR spectroscopic studies were performed using transmission technique on a Varian 640 FT-IR.

- Powder samples (1 mg) were rubbed in agate mortar with potassium bromide (Sigma-Aldrich) in the amount of 300 mg, dried in temperature of 120°C during 24 h. Pastilles of 12 mm diameter were formed.
- Liquid substance (1-Thioglycerol) was placed in the form of thin film between two pastilles (300 mg) made from KBr.

Spectra measurements were performed with resolution equal to 2 cm^{-1}, using 32-times repetition of measurement (scanning).

- TEM images were taken by placing a drop of the particles in water onto a carbon film supported copper grid. The excess solvent was wicked away with a paper tip and the grid completely dried at rt. Samples were studied using a Philips CM20 instrument with LaB_6 cathode operating at 200 kV equipped with Energy Dispersive X-ray Spectrometer (EDX). Average diameters and their standard deviations were determined by measuring ca. 100 NPs in a given field on TEM images.
- Dynamic light scattering (DLS) was performed at rt using a Malvern zetasizer HsA instrument with a He-Ne laser (4 10^{-3} W) at a wl of 633 nm. The QDs aqueous solutions were filtered through Millipore membranes (0.2 μm pore size). The data were analyzed by the CONTIN method to obtain the hydrodynamic diameter (d_H) and the size distribution in each aqueous dispersion of NPs.
- Powder (XRD) analysis was carried out using a Panalytical X'Pert Pro MPD diffractometer using Cu Kα radiation (λ = 1.5405 Å). The crystalline grain sizes were obtained using the size broadening models built into FullProf and using an instrumental resolution function obtained with LaB_6 standard sample.
- XPS measurements were performed at a residual pressure of 10^{-9} mbar, using a KRATOS Axis Ultra electron energy analyzer operating with an Al Kα monochromatic source.
- Electron Paramagnetic Resonance (EPR) signals were observed with a Bruker EPR Spectrometer, EMX type, working at 9 GHz frequency. The microwave power of 8 mW, a modulation frequency of 100 KHz and second modulation amplitude of 1 G (0.1 mT) were used. Two scans ranges of magnetic field, 6500 and 100 G (650 and 10 mT) were used. EPR studies were performed at ambient temperature.

3.3. Preparation and purification of QDs

3.3.1. MPA-capped ZnS:Mn/ZnS core/shell nanocrystals

The preparation of the core ZnS:Mn@MPA QDs was performed according to Zhuang *et al.* [267] with some adaptations. Briefly, solutions of 1M $ZnSO_4 \cdot 7H_2O$ (5 mL), 0.1M $Mn(OAc)_2 \cdot 4H_2O$ (2.0 mL) for a Mn doping of 4 at.%, and 1M MPA (20 mL) were mixed, titrated to pH 10.3 with 2M NaOH and saturated with N_2 for 30 min. An aqueous solution of $Na_2S \cdot 9H_2O$ (1M, 4.5 mL) was then quickly injected in the reaction flask and the mixture was refluxed for 20 h at 100ºC. After cooling to rt, the ZnS:Mn@MPA NCs were precipitated by ethanol, centrifuged, washed with ethanol and dried under vacuum at rt.

The introduction of the ZnS shell on the as-obtained ZnS:Mn@MPA core was prepared according to a protocol of the literature with minor revisions [139]. 10 mL of a 0.1 M $Zn(OAc)_2 \cdot 2H_2O$ aqueous solution and 0.35 mL MPA were mixed in a flask. This solution was diluted to 98 mL with water, the pH was adjusted to 10.3 with 4 M NaOH and saturated with N_2 by bubbling for 30 min. Besides this, ZnS:Mn@MPA NCs were dispersed in water to obtain a Zn concentration of 0.01 mol/L. 30 mL of the ZnS:Mn@MPA QDs solution were diluted to 130 mL with water and purged by N_2 for 30 min. Then, 20 mL of the solution of the Zn^{2+}-MPA complex was added dropwise to the diluted ZnS:Mn QDs solution and the mixture was heated to reflux for 7 h. After cooling to rt, the reaction mixture was concentrated to the half using a rotating evaporator (50°C, 15 mm Hg), QDs were precipitated with ethanol and centrifuged. The NCs were further washed with ethanol and finally dried in vacuum at rt.

3.3.2. TG-capped ZnS:Mn core nanocrystals

For the preparation of ZnS:Mn@TG QDs solutions of 1M $ZnSO_4 \cdot 7\ H_2O$ (5 mL), 0.1M $Mn(OAc)_2 \cdot 4\ H_2O$ (1.5 mL) for a Mn doping of 4 at.%, and 1M 1-thioglycerol (TG)

(20 mL) were mixed, titrated to pH 10.3 with 2M NaOH and saturated with N_2 for 30 min. An aqueous solution of $Na_2S \cdot 9H_2O$ (1M, 4.5 mL) was then quickly injected in the reaction flask and the mixture refluxed for 20 h. After cooling to rt, the ZnS:Mn@TG NCs were precipitated by ethanol, centrifuged, washed with ethanol and dried under vacuum at rt.

3.3.3. MPA-capped ZnS:Cu /ZnS core/shell nanocrystals

Synthesis of ZnS:Cu@MPA core QDs was preformed according to Zheng *et al.* [268] with some modifications. In a three-necked flask of 100 mL equipped with a cooler and under Ar flow, 19.65 mL of ultra-pure water were introduced and deareated for 30 min. After that period, aqueous solutions of: 0.1M MPA (20 mL), 0.1M $Zn(NO_3)_2 \cdot 6H_2O$ (8.8 mL) and 31 mM $CuSO_4 \cdot 5H_2O$ (0.85 mL) for 3% doping were added. The pH of the as-prepared solution was adjusted to 11.3 using 2M NaOH and the solution was deareated for another half-an-hour. In the meantime, 5 mL of a 0.1M aqueous solution of $Na_2S \cdot 9\ H_2O$ was prepared and deareated. 4.5 mL of as-prepared solution was quickly injected into the reaction mixture. The mixture was stirred for 15 min and then heated to reflux for 2 h at 100ºC. The solution was allowed to cool, then it was concentrated using a rotavapor. Afterwards, QDs were precipitated and washed three times with EtOH and dried under the vacuum.

The introduction of the ZnS shell was performed according to Corrado *et al.* [269] with some modifications. The crude reaction mixture was placed in the 100 mL tricol equipped with the cooler and Ar flow. The reaction mixture was brought to reflux and then solutions of 0.15 M $Zn(NO_3)_2 \cdot 6H_2O$ and 0.1 M $Na_2S \cdot 9H_2O$/0.04M MPA/0.08M NaOH were added to the reaction flask in 200 μL-injections with a 30 s intervals between each injection. Twenty five injections of Zn and S solutions were supplied in the experiment. To obtain the optimal PL QY, 10 injections were applied (further injections caused marked decrease of PL QY). Aliquots were taken from the reaction mixture after two injections of each 200 μL for spectroscopic analysis.

3.3.4. MPA-capped ZnSe:Mn/ZnS core/shell nanocrystals

The preparation of NaHSe was performed according to Klayman *et al*. [270] with some modifications. Under an argon atmosphere, 76 mg (2.009 mmol) of $NaBH_4$ was added to a small flask containing 1 mL of ultrapure water cooled with ice. 79 mg (1.004 mmol) of selenium powder was then added and a small outlet was connected to the flask to discharge the hydrogen pressure generated by the reduction of Se into NaHSe. After 3 h at 4°C, the black selenium powder disappeared and a white NaHSe solution was obtained. The solution was diluted with 20 mL of argon-saturated water and the concentration of the final NaHSe solution was 0.05 M.

Typical procedure for the preparation of MPA-capped ZnSe:Mn QDs was as follows: Solutions of 0.1 M $ZnSO_4$. $7H_2O$ (5 mL), 0.01 M $Mn(OAc)_2$. $4H_2O$ (2 mL) for a Mn^{2+} doping of 4% relative to Zn^{2+} and 0.5 M MPA (20 mL) were mixed and the pH of the mixture was adjusted to 10.3 by dropwise addition of a 2 M NaOH solution. Obtained solution was placed in a three-necked flask fitted with a septum and valves, and further stirred under argon for 1 h. 9 mL of a freshly prepared NaHSe solution (0.05 M) were then injected through a syringe into the mixture at rt. The molar ratio Zn^{2+}/Se^{2-}/MPA in the solution was 1/0.9/20. The growth of the MPA-capped ZnSe:Mn NCs proceeded on refluxing at 100°C for 24 h under argon flow with a condenser attached. After cooling to room temperature, the MPA-capped ZnSe:Mn NCs were precipitated by ethanol, the precipitate was centrifuged, washed 3 times with ethanol, and then dried under vacuum (30 mmHg, 2 h, rt).

For the ZnS shell growth, 10 mL of 0.2 M $Zn(OAc)_2 \cdot 2H_2O$ solution and 0.7 mL of MPA were mixed together and the solution was diluted to 88 mL with water. The pH was adjusted to 10.3 with 4 M NaOH and the solution was saturated with Ar by bubbling for 1 h. The ZnSe:Mn core solution was prepared by dispersing 20 mg of ZnSe:Mn QDs in 130 mL of water, transferred into a three-necked flask fitted with a septum and valves and purged by argon bubbling for 1 h. Then, 20 mL of the Zn^{2+}-MPA complex were added dropwise to the ZnSe:Mn solution and the mixture was heated at 100°C for 10 h. After cooling to rt, the reaction mixture was concentrated down to approximately 15 mL, NCs were precipitated with ethanol and dried under vacuum at rt for 12 h before measurements.

3.3.5. Anchoring of QDs with FA (optionally by use of 2,2'-(ethylenedioxy)-*bis*-ethylamine)

In the case of MPA-capped ZnS:Mn and ZnSe:Mn core/shell NCs functionalization with the spacer 2,2'-(ethylenedioxy)-*bis*-ethylamine was applied before the conjugation with FA. For that, ZnS (5 mg) or ZnSe (14.5 mg) manganese-doped and MPA-capped core/shell QDs were dispersed in 6 and 12 mL of sodium borate buffer (0.1 M, pH 8.8), respectively. Then, 2,2'-(ethylenedioxy)-*bis*-ethylamine (0.1 mmol, 15 mg), 1-ethyl-3-[3-dimethylaminopropyl]carbodiimide hydrochloride (0.1 mmol, 19.7 mg) and *N*-hydroxysuccinimide (0.1 mmol, 11.9 mg) were added. As-prepared 2,2'-(ethylenedioxy)-*bis*-ethylamine modified ZnS (12.5 mg) and ZnSe (1.8 mg) QDs were dispersed in 15 and 1.5 mL of sodium borate buffer, respectively. 100 μL of a 12.8 mM solution of FA in sodium borate buffer, 100 μL of a 25.6 μM solution of EDC in sodium borate buffer and 100 μL of a 25.6 mM NHS solution in sodium borate buffer were added. The resulting solutions were allowed to stir for 3 h under inert atmosphere and in the dark. QDs were precipitated by adding ethanol to the reaction mixture, then washed twice with ethanol and dried in vacuum.

1-Thioglycerol-capped ZnS:Mn QDs were conjugated with FA without use of the linker. In that experiment, QDs (5 mg) were dispersed in 6 mL of borate buffer to which 40 μL of a solution of FA in borate buffer (0.256 μmol, 0.11 mg), 40 μL of a solution of EDC in borate buffer (0.516 μmol, 0.095 mg) and 40 μL of a NHS solution in borate buffer (0.516 μmol, 0.06 mg) were added.

3.4. QDs cytotoxicity evaluation

3.4.1. Cell culture and treatment with QDs

MCF-7 and T47D breast cancer cells and PC-3 prostate cancer cells were purchased from the European Collection of Cell Cultures (ECACC, Porton Down Salisbury UK). All cell lines were grown in phenol red-free DMEM (Dulbecco's modified Eagle's medium) tissue culture medium (Sigma-Aldrich, St Luis MO, USA), supplemented with 10% fetal bovine serum (FBS) and 1% penicillin-streptomycin (Gibco Invitrogen Corp., Grand Island, NY, USA) under standard conditions at 37°C and humidified atmosphere containing 5% CO_2 and 95% air. 24 h before treatment, cells were transferred to a DMEM medium supplemented with 2.5% FBS or to folate-deficient DMEM (Sigma-Aldrich, St Luis MO, USA) supplemented with 2.5% dialyzed FBS (PAA Pasching Austria) (in the case of ZnS:Mn@MPA QDs). For experiment, logarithmically growing cells (2.10^4 cells) were subcultured in 96-well microtiter plates (BD Biosciences) in a volume of 200 µl. Cells were allowed to attach overnight and were then exposed to various concentrations of QDs in different tests. Medium supplemented with 2.5% FBS or 2.5% dialyzed FBS was used in the experiments with ZnS:Mn@MPA QDs and with 10% FBS in other experiments.

3.4.2. MTT cell viability assay

The MTT assay is a colorimetric assay based on the ability of viable cells to reduce a soluble yellow tetrazolium salt, (3-(4,5-dimethylthiazol-2-yl)-2,5-diphenyltetrazolium bromide) (MTT), to blue formazan crystals [271]. MTT assay was employed to assess the cells viability after treatment with QDs. Following the incubation of cells with different types and concentrations of QDs, the supernatant was removed and 200 µL of MTT solution (0.5 mg/mL in serum-free DMEM) was added. After 4 h, the medium was aspirated and the precipitated formazan was dissolved in 200 µL of dimethylsulfoxide (DMSO). Cell viability was determined by measuring the absorbance at 570 nm using a BioTek microplate reader (Winooski, VT USA). In this study, the NCs concentration required to inhibit cell growth by 50% (IC_{50}) was

determined from a plot of percent cell viability of control untreated cells versus logarithm of concentration. The experimental plate included wells without cells, wells with cells treated with QDs and wells of untreated cells. Each treatment was performed in triplicate.

3.4.3. XTT cell proliferation assay

Cayman's XTT cell proliferation assay kit (Catalog No. 10010200) was used to study cell proliferation. The assay is based on the extracellular reduction of 2,3-*bis*-(2-methoxy-4-nitro-5-sulfophenyl)-5-[(phenylamino)-carbonyl]-2*H*-tetrazolium hydroxide (XTT) by reduced form of nicotinamide adenine dinucleotide (NADH) produced in the mitochondria *via trans*-plasma membrane electron transport and an electron mediator. Reduction of XTT produces a water-soluble formazan which dissolves directly into the culture medium, eliminating the need for an additional solubilization step. Immediately before use, the Electron Mediator Solution (Catalog No. 10008977) was used to reconstitute the entire vial of XTT Reagent (powder, Catalog No. 10010353) and mixed well. The experimental plate included wells without cells, wells with cells treated with QDs and wells of untreated cells. Each treatment was performed in triplicate.

T47D human breast cancer cells and PC-3 human prostate cancer cells in DMEM medium were seeded in 96-well microtiter plates at a density of $2 \cdot 10^4$ cells/well and let to grow for 24 h in a CO_2 atmosphere at 37ºC. After this time, different concentrations (0.08-5 mM) of ZnS:Mn@TG and ZnS:Mn@TG-FA QDs in culture medium were added. After 72 h, 10 μL of the reconstituted XTT mixture were added to each well. The microtiter plates were gently shaken and then incubated for 2 h at 37ºC in a CO_2 atmosphere. The plate was gently shaken for 1 min and absorption of each sample using a microplate reader at a wavelength of 450 nm was measured.

3.4.4. Ferrous oxidation-xylenol orange (FOXO) assay

T47D cells grown 24 h in a 96-well plate at a density of 2.10^4 cells/well were used to measure the concentration of H_2O_2 after exposition to ZnS:Mn@TG and ZnS:Mn@TG-FA QDs (0.08-5 mM) in the DMEM culture medium over time. After

the maintenance medium was removed, the cells were washed twice with DMEM (37ºC). 150 μL of medium containing QDs was added to the wells, and the cells were incubated in a humified atmosphere of 10% CO_2/90% air at 37ºC. The experiment was performed in triplicate. As a control, cells incubated only in medium were used. After various incubation times (1-24 h), 15-μL samples of culture medium were collected for the measurement of the peroxide concentration.

The peroxide concentrations were measured by a modification of the ferrous oxidation-xylenol orange (FOXO) assay [272] adapted to microtiter plate by Dringen *et al.* [273] and with some modification in comparison to Gülden *et al.* [274]. This assay is based on the ability of peroxides to oxidize the ferrous Fe^{2+} ions to ferric Fe^{3+} ions, which reacts with xylenol orange to give a colored complex. When the samples of culture medium were transferred to the microtiter plate wells, 140 μL of the reaction solution (0.5 mM $(NH_4)_2Fe(SO_4)_2$, 200 μM xylenol orange, 200 mM sorbitol in 20 mM H_2SO_4) were added to each well. The microtiter plate was incubated for 45 min. in the darkness and the absorption at 570 nm was measured with a microtiter plate reader. The concentrations of peroxides were determined using standard peroxide solutions in the same microtiter plate. Standard peroxide solutions (3.125-50 μM) were always freshly prepared using solutions of hydrogen peroxide (30%, Sigma-Aldrich) in the same culture medium that was used to incubate the cells with QDs.

3.5. Confocal fluorescent cell imaging by use of ZnS:Mn QDs

MCF-7, T47D and PC-3 cell lines were cultured as previously described. Subconfluent stock cultures were trypsinized and seeded in 8-well chamber slides (BD Biosciences) at a density of 2.10^4 and 4.10^4 cells per well in growth medium for experiments with ZnS:Mn@MPA and ZnS:Mn@TG QDs, respectively. Cells were allowed to attach for 24 h before treating with QDs. Then, the supernatant was discarded, followed by replacement of the media supplemented with 2.5% FBS containing QDs (500 μM). After 72 h of incubation at 37 °C, the incubation medium was removed, and cells were fixed using 4% formaldehyde (500 μL/well) in the case of ZnS:Mn@MPA core QDs.

In the case of ZnS:Mn@TG QDs after the removal of incubation medium, mixed solutions of Mitochondria Staining Kit (Sigma-Aldrich, CS0390) and Hoechst (Bisbenzimid H33258, Sigma-Aldrich) were added. Hoechst dye was used as DNA stain while Mitochondria Staining Mix was used for detection of changes in mitochondrial inner-membrane electrochemical potential. The Mitochondrial Staining Kit contains 5,5',6,6'-tetrachloro-1,1',3,3'-tetraethylbenzimidazolocarbocyanine iodide (JC-1, Catalog Number T4069), dimethyl sulfoxide (DMSO) (Catalog Number D8418), JC-1 Staining Buffer (Catalog Number J3645) and Valinomycin Ready Made Solution (Catalog Number V3639) and was prepared according to the procedure joined by the producer. Mixed solution of the two dyes was a combination of 7.5 μL of Hoechst stock solution (1.5 mg of Hoechst in 1.5 mL of ultra-pure water) and 1.5 mL of Mitochondria Staining Mix. After 10 min of incubation, dyes solution was discarded, cells were washed with culture medium and fixed using 4% formaldehyde (500 μL/well). At the end of the treatment with ZnS:Mn@MPA core QDs or with ZnS:Mn@TG QDs and organic dyes, the cells were washed twice with PBS and mounted with the mounting medium (Dako Faramount Aqueous Mounting Medium). To study the FR-targeted delivery of ZnS:Mn@MPA QDs, folic acid was first added to the medium at the concentration of 3.5 mM and cells were incubated for 30 min before addition of FA-QDs.

QDs and Hoechst-labeled cells were imaged on Leica TCS SP5 confocal microscope equipped with Ti:Sapphire MaiTai biphotonic laser (Spectra Physics) and HCX PL APO CS 63x 1.40 OIL objective. ZnS:Mn@MPA QDs fluorescence was detected using excitation 720 nm (effective excitation 360 nm) and emission filters 550-640 nm. Fluorescence of ZnS:Mn@TG QDs and Hoechst was detected using excitation 800 nm

(effective excitation 400 nm) and emission filters 500-650 nm and 400-500 nm, respectively. Fluorescence of JC-1 was detected using Argon laser excitation of 488 nm and emission filters 500-550 nm.

Chapter 4. Results and discussion

A part of that chapter demonstrates the results that have been already published by Aboulaich and Geszke et al. [275] and Geszke et al. [276].

4.1. Synthesis, photoluminescence properties, size, shape and crystal structure of nanocrystals

4.1.1. MPA-capped ZnS:Mn/ZnS core/shell nanocrystals

Water-dispersible Mn^{2+}-doped ZnS QDs with Mn^{2+} concentrations ranging from 2 to 5% were prepared in aqueous solution by reaction of $ZnSO_4$ and $Mn(OAc)_2$ with Na_2S in the presence of MPA [267]. Because of the high surface-to-volume ratio of the NPs prepared, elimination of surface defects which act as luminescence quenching centers plays a crucial role on photoluminescence quantum yields (PL QY) of ZnS:Mn QDs. Over recent years, introduction of shells such as ZnS [110, 132, 139, 277], $Zn(OH)_2$ [32, 278], SiO_2 [279, 280], polymers [281] or encapsulation into zeolites [282, 283] have been developed to modify the surface of ZnS:Mn QDs and thus improve the PL efficiency and their stability. A ZnS shell was introduced at the surface of ZnS:Mn core QDs by the decomposition of Zn^{2+}-MPA complexes at pH = 10.3 using a synthesis procedure adapted from Jian *et al.* except that the growth of the shell was performed in water at 100°C instead of under microwave irradiation [139]. The evolution of emission spectra of ZnS:Mn QDs doped with 4 at.% Mn recorded after excitation at 330 nm measured for aliquots taken from the reaction solution during the overgrowth of the ZnS shell on ZnS:Mn cores is presented in Figure 52.

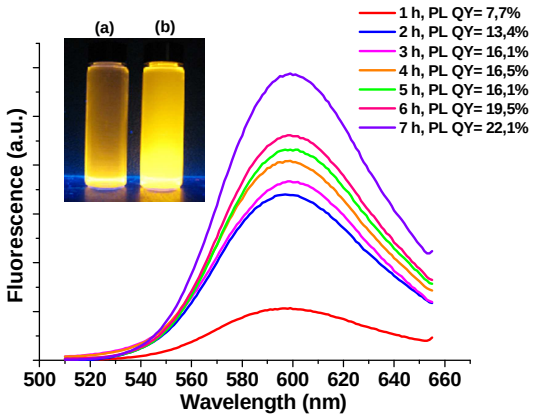

Figure 52. Temporal evolution of the photoluminescence spectra of ZnS:Mn QDs during the growth of ZnS shell. The inset shows a photography of (a) initial ZnS:Mn QDs and (b) core/shell ZnS:Mn/ZnS QDs dispersed in water and illuminated with an ultraviolet lamp.

The PL QYs of the core/shell QDs increase steadily with increasing the shell thickness, from ca. 2.7% for the original core particles to approximately 22% after 7 h heating at 100°C. PL QYs remain stable (ca. 22%) with increasing heating time and could not be improved even by attempting a hydrothermal growth of the ZnS shell (1 or 2 h at 150°C in a Teflon-lined stainless autoclave). The single PL emission peak observed in PL spectra rules out the separate homogeneous nucleation of ZnS NCs. The inset of Figure 52 shows a photograph under a 300 nm UV lamp of MPA-stabilized ZnS:Mn QDs before and after introduction of the ZnS shell. The bright orange fluorescence observed illustrates the improvement of PL QY after capping.

The effect of Mn^{2+} ion concentration on the PL properties of Mn^{2+}-doped ZnS QDs has been studied by many groups who have demonstrated a so-called “concentration quenching effect” [120, 284-286]. When the concentration of Mn^{2+} becomes higher than a certain threshold, the non-radiative energy transfers between neighbouring Mn^{2+} dopant ions reduce and even annihilate the fluorescence. Under our synthetic conditions, the formation of such pairs of Mn^{2+} dopant ions is probably observed when the amount of Mn^{2+} ions in QDs is higher than 4 at.%. The variations in PL efficiency of core/shell ZnS:Mn/ZnS QDs at different Mn^{2+} doping ratios are reported in Figure 53.

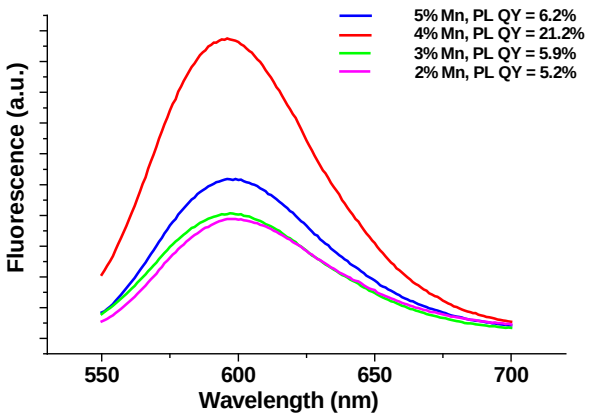

Figure 53. Room temperature PL spectra of core/shell ZnS:Mn/ZnS@MPA QDs with different initial concentrations of Mn^{2+} and the related PL QYs illustrating the quenching effect observed with 5% doping in Mn^{2+}. Spectra were recorded after excitation at 270 nm.

UV-vis absorption spectrum of the doped core/shell ZnS:Mn/ZnS@MPA QDs in water solution, together with the excitation and the PL spectra after excitation at 350 nm are shown in Figure 54.

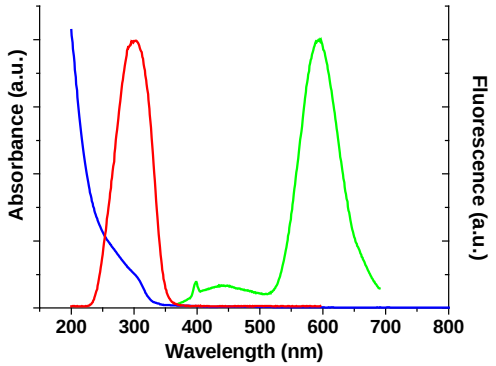

Figure 54. Room temperature absorption (blue line), excitation (red), and photoluminescence (green) spectra after excitation at 350 nm of core/shell ZnS:Mn/ZnS@MPA QDs dispersed in water.

It should first be noted that the Mn^{2+} emission in ZnS particles may shift to higher or lower energies compared to bulk ZnS:Mn, depending on both the diameter and surface effects. The blue-shift in the emission maxima (596 nm) compared to 600 nm for bulk ZnS:Mn, is a strong indication for the formation of particles with small diameters. The sharp absorption edge in the absorption spectrum is also a good indication of the high dispersion of QDs in aqueous solution. The absorption onset at 314 nm (3.94 eV) of the core/shell ZnS:Mn/ZnS QDs confirms that the bandgap of NPs shifts by 0.27 eV, as compared to bulk ZnS (Eg = 3.67 eV) [120]. Considering a cubic zinc blende

structure for ZnS (*vide infra*) having an effective electron mass ~ 0.25 m_e and hole mass ~ 0.59 m_e, an average diameter of 5.4 ± 0.4 nm was calculated using the Brus equation that has already appeared in the chapter 1 (Equation 1).

$$Eg = Eg^{bulk} + \frac{\eta^2 \pi^2}{2r^2}\left(\frac{1}{m_e^*} + \frac{1}{m_h^*}\right) - \frac{1{,}786 e^2}{\varepsilon_r \varepsilon_0}\frac{1}{r}$$

Equation 1. Equation that permit to calculate the first approximation of the bandgap of spherical nanocrystal.

where r is the radius of the NPs, ε the bulk optical dielectric constant, and ħ the Planck constant divided by 2π. The deviation of 0.4 nm in particle diameter corresponds to ± 10 nm change of wl for the determination of the onset of absorption.

Finally, the emission spectra of core/shell ZnS:Mn/ZnS QDs is quite entirely dominated by the orange Mn d-d transition. Only weak emissions centered at ca. 445 nm and originating from defect-state recombinations of the ZnS material were observed.

The effect of various thiol-stabilizers including thioglycolic acid (TGA), 3-mercaptopropionic acid (MPA), 6-mercaptohexanoic acid (MHA), and L-cysteine (Cys) on the optical properties of Mn-doped ZnS QDs was also investigated. Table 7 lists the PL QYs of ZnS:Mn cores and of core/shell QDs obtained after thermal decomposition of Zn^{2+}-MPA complexes.

Table 7. Influence of ligands on the PL QYs of Mn-doped ZnS nanocrystals and of core/shell ZnS:Mn/ZnS nanocrystals

Ligand	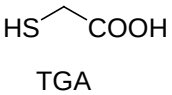 TGA	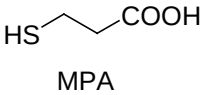 MPA	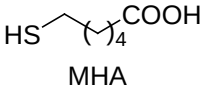 MHA	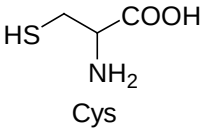 Cys
PL QY of the core (%)[a,b,c]	0.1	2.3	8.0	1.0
PL QY after introduction of the shell (%)[a,b]	2.7	22.1	1.2	0.5

[a.] PL QYs were measured in water at room temperature using Rhodamine 6G as the reference
[b.] PL QYs were measured on purified nanocrystals obtained after precipitation with ethanol, drying, and redispersion in water.
[c.] 4 at.% Mn^{2+} was used in all syntheses

After synthesis, the emission from surface-related defects at ca. 450 nm was found to be weak for all QDs that mainly exhibit the strong Mn^{2+} $^4T_1 \rightarrow {}^6A_1$ transition at ca. 600 nm. The highest PL QY for the doped-cores was obtained for NCs stabilized with MHA (8.0%). The PL intensity of QDs prepared in the presence of MPA or Cys is lower (ca. 3.5 and 8-fold, respectively). QDs prepared with TGA exhibit the lowest PL QY (0.1%) despite the ability of this thioacid to form stable hexagonal complexes with Zn atoms at the surface of NCs. After heating at 100°C with Zn^{2+}-MPA complexes for 7 h, the PL QY of MPA-stabilized Mn-doped ZnS QDs markedly increased from 2.3 to 22.1%. A strong increase of PL QY was also observed for TGA-capped cores but the PL QY of the core/shell QDs reminds modest (2.7%). Finally, as previously observed with CdTe and CdSe QDs [287], attempts to introducing a ZnS shell on QDs stabilized by long alkyl chain carboxylates like MHA failed probably due to the weak water-dispersibility of NCs and the poor secondary coordination of the carboxylate function to surface Zn sites (formation of polygonal loops).

The XRD patterns of the as-prepared ZnS:Mn@MPA QDs, and of the core/shell ZnS:Mn/ZnS@MPA QDs are shown in Figure 55.

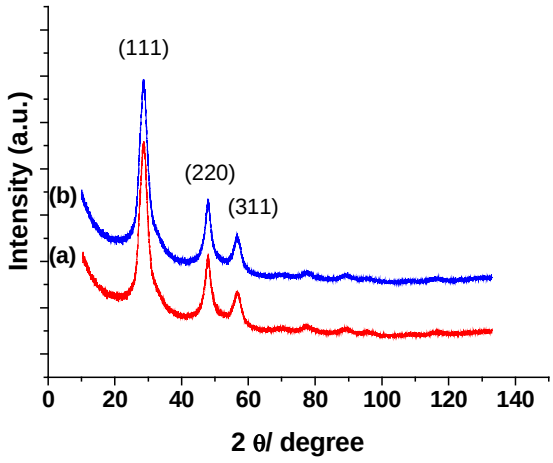

Figure 55. XRD peak patterns for (a) ZnS:Mn@MPA and (b) ZnS:Mn@MPA/ZnS QDs.

All of the XRD peaks can be indexed to the cubic zinc blende structure of ZnS and are consistent with the standard cubic bulk ZnS peak position from JCPDS file N°. 77-2100. The three main peaks correspond to the (111), (220), and (311) planes. It can be observed that these peaks are broadened compared to bulk ZnS, thus confirming the nanocrystalline nature of all the samples. A crystallite size of 4.2 ± 1.0 nm was deduced from XRD data (Figure 56).

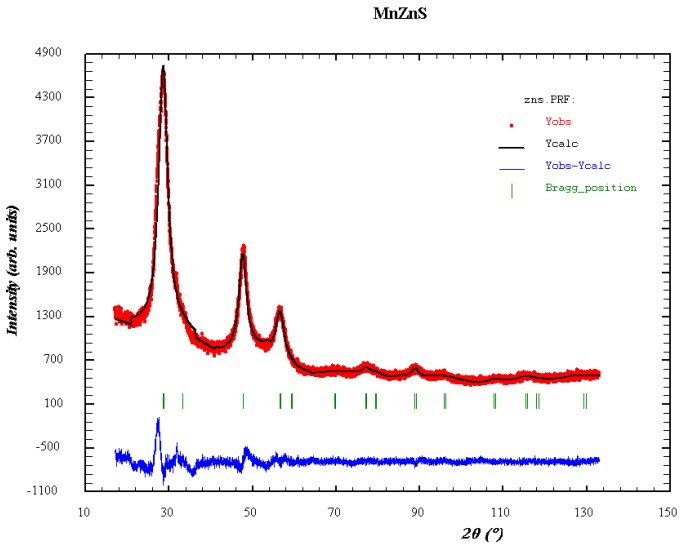

Figure 56. A Rietveld refinement result (red curve) of the powder XRD data of ZnS:Mn QDs (black curve), using the cubic phase of ZnS. The blue curve below illustrates the difference between data and simulation.

The calculated lattice constant a for Mn-doped ZnS QDs was determined to be 0.5388 ± 0.0003 nm, slightly different from pure ZnS NCs (a = 0.5386 nm measured with a internal standard Diamond). The deviation in the lattice constant observed for ZnS:Mn QDs probably originates from substitution of Zn^{2+} by Mn^{2+} ions in the crystal structure since the diameter of the Mn^{2+} ion (0.083 nm) is larger than that of the Zn^{2+} ion (0.074 nm) [288].

Transmission electron microscopy (TEM) image of ZnS:Mn/ZnS QDs is shown in Figure 57a.

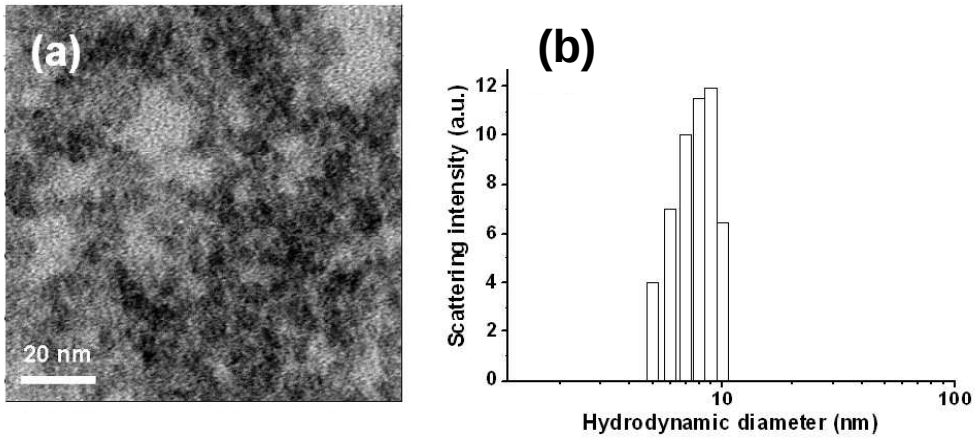

Figure 57. (a) Bright field TEM micrograph and average diameter D of ZnS:Mn/ZnS@MPA QDs, D = 4.4 ± 0.7 nm and (b) the corresponding intensity-hydrodynamic size distribution graph of QDs in water at 25°C measured by DLS.

The particles appear spherical in shape (*vide infra*). The average diameter of ZnS:Mn/ZnS QDs is 4.4 ± 0.7 nm. The diameter estimated from TEM image is in good agreement with that calculated from the absorption edge (ca. 5.4 ± 0.4 nm) and X-ray diffraction studies (4.2 ± 1.0 nm). The size and size-distribution of ZnS:Mn/ZnS@MPA QDs was also examined by Dynamic Light Scattering (DLS). Figure 57b shows the scattering intensity distributions of these NCs dispersed in water at rt. Analyzed sample was found to be quite aggregate-free. The average hydrodynamic size determined from DLS data was 8.7 nm, thus suggesting that NPs dispersed well in water. The hydrodynamic diameter was larger than that of the core due to the solvatation layer around QDs in aqueous solution.

The X-ray photoelectron spectroscopy (XPS) scan survey of the core/shell ZnS:Mn/ZnS@MPA sample shows only the peaks of Zn, S, Mn, O, C and Na elements and no peaks of any other elements were observed (Figure 58a).

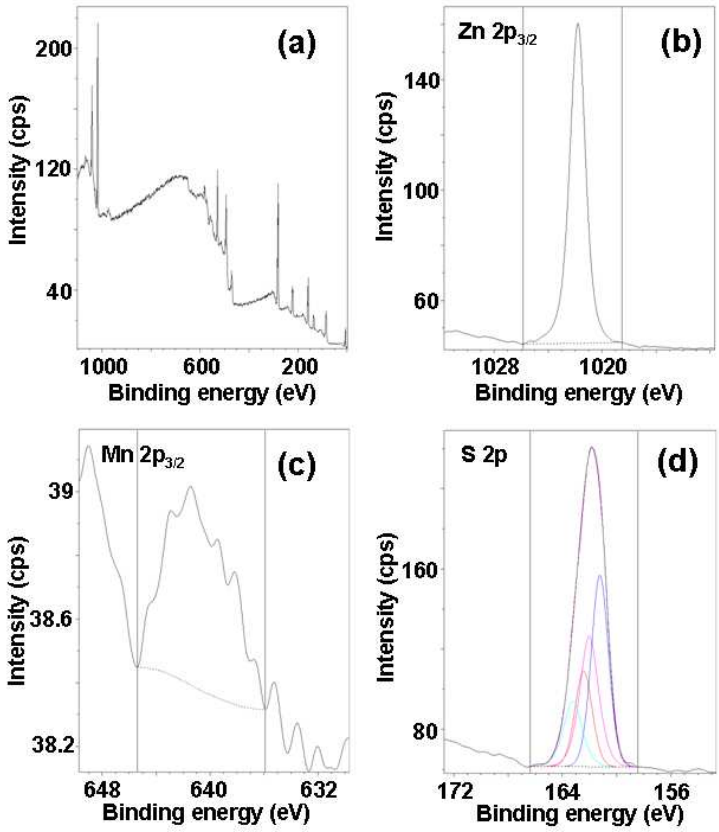

Figure 58. (a) XPS survey scan of core/shell ZnS:Mn/ZnS@MPA QDs. The Zn 2p (b), Mn 2p (c) and S 2p (d) emissions are presented.

As seen on Figure 58b, the peak of Zn $2p_{3/2}$ appears at 1021.7 eV confirming that the Zn element exists only in the form of Zn^{2+} linked to a sulfur atom. The Mn $2p_{3/2}$ peak centered at 641.0 eV is very weak due to the low concentration of this element at the

surface of NPs (Figure 58c). A similar phenomenon was observed for other types of Mn-doped NCs, especially after introduction of a shell around the doped-core [31, 289, 290]. The atomic Mn/Zn ratio was found to be 0.045. Figure 58d shows the peak of S 2p centered at 161.5 eV. The deconvoluted peaks at 161.2, 162.0, 162.4 and 163.2 eV originate from the different kinds of sulfur species in the sample (S from the core linked either to Zn or to Mn, S from the shell and S from the stabilizing ligand).

The electric potential, referred to as zeta potential ζ, which controls the colloidal stability and interparticles interactions, was also determined by DLS method. At pH = 7.0, the ζ value measured for ZnS:Mn/ZnS@MPA QDs (-45 ± 5 mV) confirmed the presence of negative charges on the surfaces of the QDs due to the carboxylate end group of the MPA ligand.

4.1.2. TG-capped ZnS:Mn core nanocrystals

Water-dispersible Mn^{2+}- doped ZnS QDs with Mn^{2+} concentrations ranging from 2 to 6% were prepared in aqueous solution by reaction of Zn precursor and $Mn(OAc)_2$ with Na_2S in the presence of 1-thioglycerol (TG). The evolution of PL emission intensity with the increase of Mn^{2+} concentration from 2 to 6% relative to Zn^{2+} which proves the successful incorporation of Mn^{2+} into ZnS QDs is presented in Figure 59.

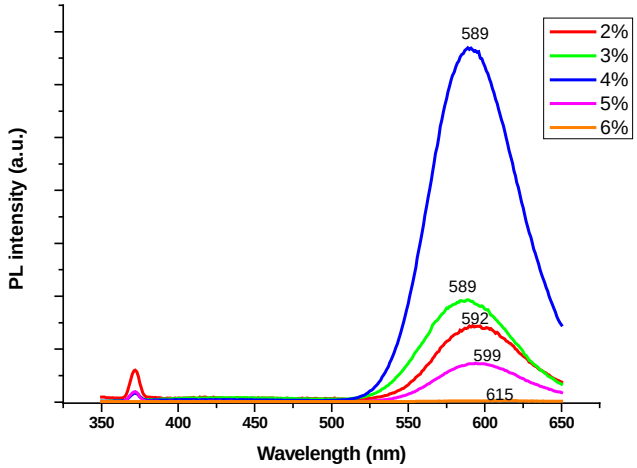

Figure 59. Influence of the concentration of Mn^{2+} relative to Zn^{2+} on PL spectra of ZnS:Mn@TG nanocrystals prepared using zinc acetate as a source of zinc. Spectra were recorded after excitation at 330 nm.

The PL QY increased from 4.5% in the case of 2 and 3% doping of Mn^{2+} to optimal 9.1% PL QY for 4% Mn^{2+} doping, then dropped rapidly to 2.8% for 5% doping, and finally fluorescence nearly totally disappeared at the concentration of 6% of Mn^{2+}. The fluorescence emission quenching is due to the mentioned before "concentration quenching effect" [120, 284-286]. Simultaneously, the changes in the fluorescence emission peak maximum were observed. The wl of the emission maximum peak changes from 592 nm in the case of 2% Mn^{2+} doping and 589 nm for 3 and 4% doping to 599 nm for 5% doping and finally reached 615 nm for 6% of Mn^{2+} doping.

Figure 60 shows the UV-vis absorption spectrum of the doped ZnS:Mn@TG NCs in water solution, together with the excitation and the PL spectra after excitation at 350 nm.

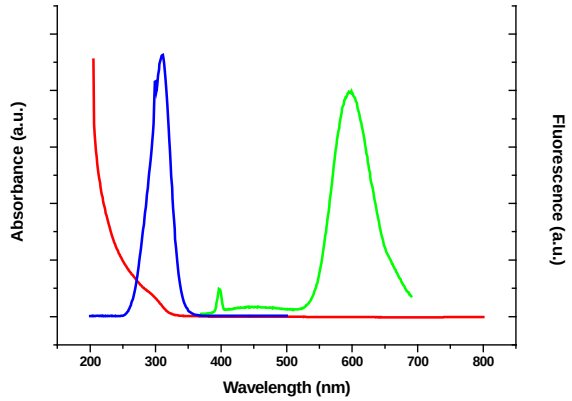

Figure 60. Room temperature absorption (red line), excitation (blue), and photoluminescence (green) spectra after excitation at 350 nm of ZnS:Mn@TG QDs dispersed in water.

The blue shift in the emission maxima (595 nm) compared to 600 nm for bulk ZnS:Mn is observed which is an indication of the formation of particles with small diameters. The emission spectrum of synthesized QDs is dominated by the orange Mn d-d transition with only weak emission at about 450 nm originating from defect-state recombinations.

To establish the optimal heating time of the synthesis, the temporal evolution of the PL spectra of ZnS:Mn@TG QDs was monitored (Figure 61).

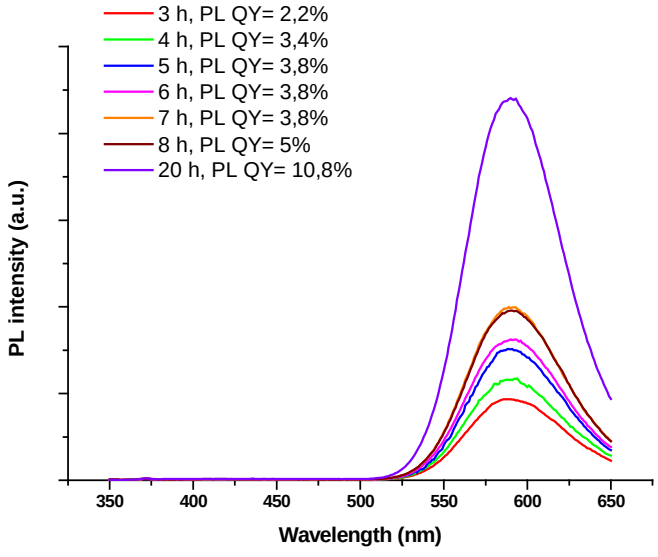

Figure 61. Temporal evolution of the photoluminescence spectra of ZnS:Mn@TG QDs during the time. Spectra were recorded after excitation at 330 nm.

The PL QYs of QDs increase steadily with increasing the reaction time, from ca. 2.2% after 3 h heating to ca. 10.8% after 20 h heating. The maximum of fluorescence

emission peak is always centered at 590 nm. The increase of the refluxing time over 20 h does not result in the further increase of the PL QY.

The effect of various zinc precursors including $ZnSO_4$, $Zn(OAc)_2$ and $Zn(NO_3)_2$ on the optical properties of Mn-doped ZnS QDs was also investigated and the obtained results are shown in Figure 62.

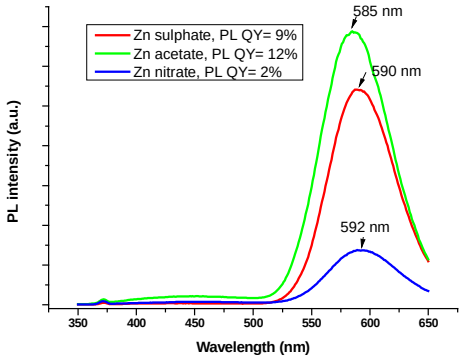

Figure 62. Room temperature PL spectra of ZnS:Mn@TG QDs synthesized using different zinc precursor: $ZnSO_4$ (red line), $Zn(OAc)_2$ (green) and $Zn(NO_3)_2$ (blue). Spectra were recorded with 330 nm excitation.

The use of various zinc salts resulted in different PL properties of synthesized QDs. The differences in the maximum value of the emission peaks as well as different values of PL QY were observed. The best results of PL QY of 9 and 12% were obtained using the sulfate and the acetate zinc salt, respectively. The choice of the zinc acetate in further experiments was justified due to the results obtained in XRD studies (Figure 63a). It was observed that using zinc sulfate, some impurities rest in the final QDs powder. XRD patterns of ZnS:Mn@TG QDs depending on the type of zinc precursor applied during the NCs synthesis are shown in Figure 63.

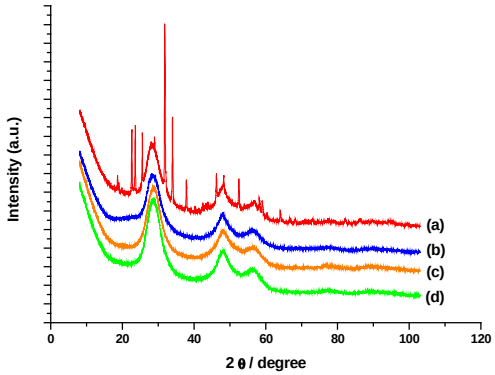

Figure 63. XRD peak patterns for ZnS:Mn@TG QDs obtained using (a) zinc sulfate (red line), (b) zinc sulfate followed by QDs purification by dialysis (blue), (c) zinc nitrate (orange) and (d) zinc acetate (green) as a zinc precursor in QDs synthesis.

The average diameter of ZnS:Mn NCs calculated from TEM was found to be 3.9 ±0.5 nm (Figure 64).

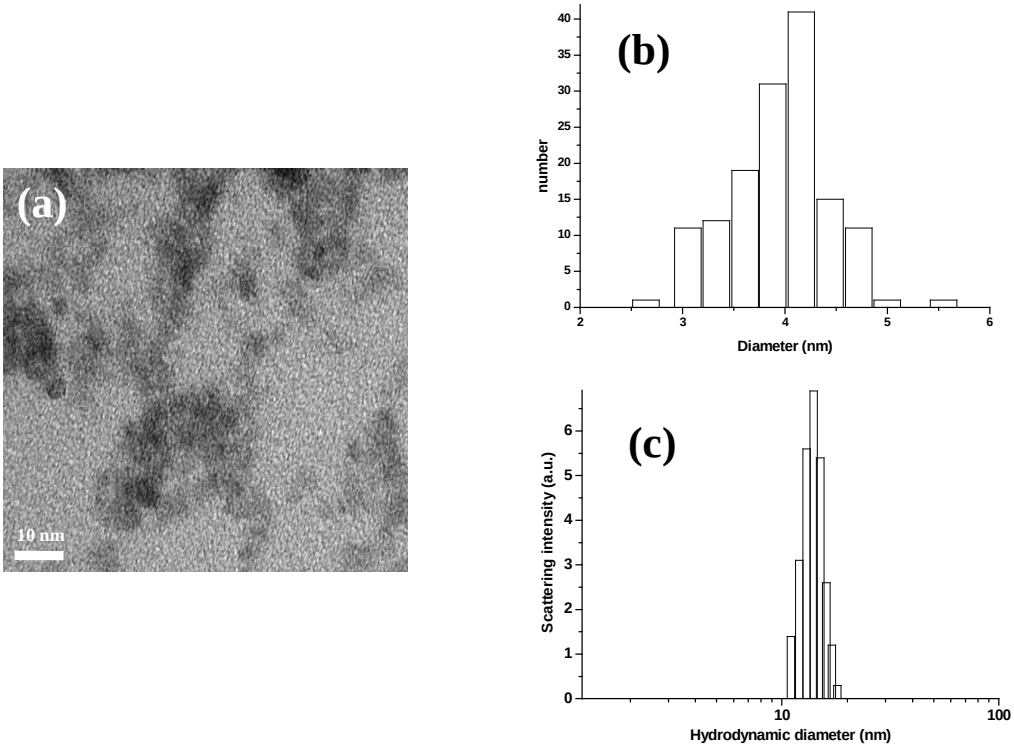

Figure 64. (a) TEM micrograph, (b) the corresponding particle size distribution, and (c) hydrodynamic size of ZnS:Mn@TG d-dots d-dots measured by DLS.

The use of semiconductor NCs, especially in biological applications, needs the evaluation of the external factors that may affect the optical properties of QDs. As shown in Figure 65, TG-capped ZnS:Mn QDs are sensitive to the changes of pH with greater fluorescence at basic pH (8-12). A rapid decay of PL of examined QDs was observed when the pH was below 5. Under pH= 4, the QDs became unstable, they precipitated and the PL nearly disappeared.

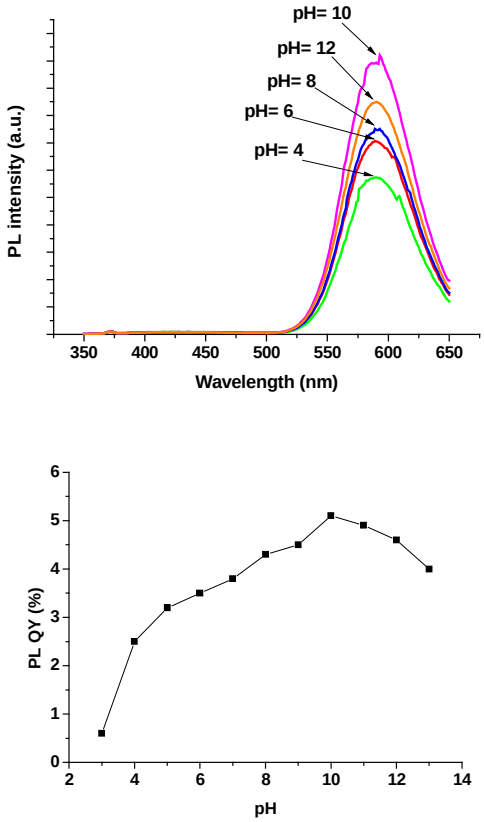

Figure 65. Influence of aqueous solution pH on (a) fluorescence spectra and (b) PL QY of ZnS:Mn@TG QDs.

The X-ray photoelectron spectroscopy (XPS) scan survey of the ZnS:Mn@TG QDs sample shows only the peaks of Zn, S, O, C and Na elements and no peaks of any other element was observed (Figure 66a).

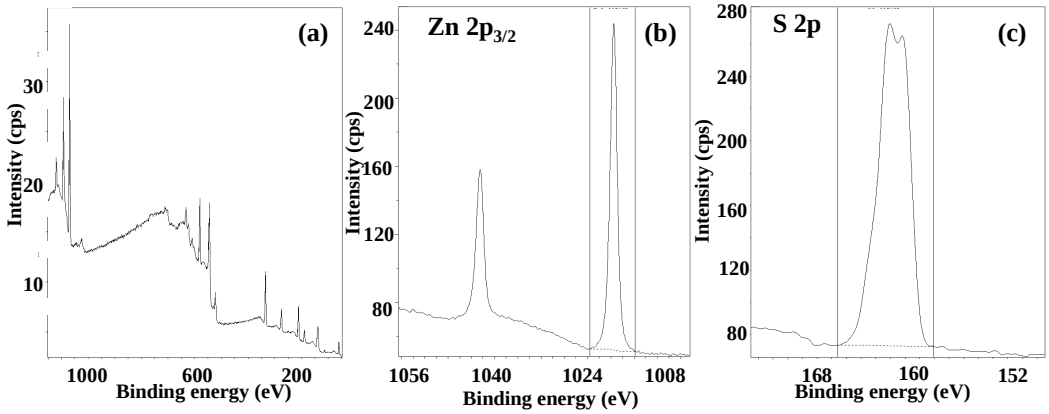

Figure 66. (a) XPS survey scan of ZnS:Mn@TG QDs. The Zn 2p (b) and S 2p (c) emissions are presented.

As seen on Figure 66b, the peak of Zn $2p_{3/2}$ appears at 1021 eV confirming that the Zn element exists only in the form of Zn^{2+} linked to a sulfur atom. Figure 66c shows the peak of S 2p centered at 162 eV that can come from the S core linked either to Zn or to Mn and S from the stabilizing ligand.

Fourier transform infrared (FT-IR) spectra of neutral 1-thioglycerol ligand and the purified and dried ZnS:Mn@TG QDs are given in Figure 67.

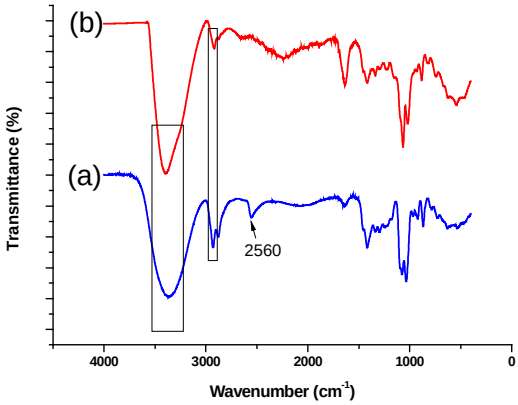

Figure 67. FT-IR spectra of (a) 1-Thioglycerol and (b) ZnS:Mn@TG QDs.

Thioglycerol (Figure 67a) has characteristic peak at ~2560 cm^{-1} which is assigned to the –SH stretching vibrations. The disappearance of the –SH vibration of 1-TG clearly indicates that this reagent is coordinated onto the QDs surface [291]. The bands at 2930 and 3350 cm^{-1} can respectively be assigned to C-H and –OH stretching vibrations of 1-TG [291, 292].

The electronic structure of Mn-doped ZnS:@TG QDs was studied with electron paramagnetic resonance (EPR) technique. The EPR spectrum of the QDs sample, recorded using 100 KHz field modulation is shown in Figure 68. The EPR spectrum shows six-line pattern. The lines represent the six allowed transitions for Mn^{2+} corresponding to $\Delta M_s = \pm 1$ and $\Delta M_I = \pm 0$. In the ZnS lattice containing substitutional Mn^{2+}, hyperfine transitions are possible due to $\Delta M_s = \pm 1$ and $\Delta M_I = \pm 0$, that is, $\pm 5/2 \leftrightarrow \pm 3/2$, $\pm 3/2 \leftrightarrow \pm 1/2$ and $+1/2 \leftrightarrow -1/2$ transitions. But the random orientations cancel out the anisotropic contributions from $\pm 5/2 \leftrightarrow \pm 3/2$ and $\pm 3/2 \leftrightarrow \pm 1/2$ transitions. Thus only $+1/2 \leftrightarrow -1/2$ transition shows six line spectrum what was also concluded by Gripal and Gupta [293].

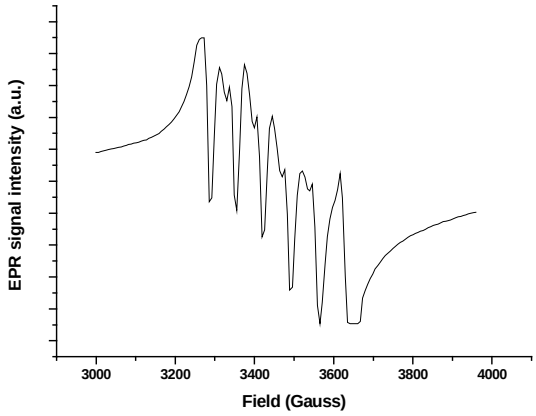

Figure 68. EPR spectrum of ZnS:Mn@TG QDs at room temperature.

The six-line pattern in EPR spectrum of the ZnS:Mn@TG sample confirmed the incorporation of Mn^{2+} in ZnS NCs.

4.1.3. MPA-capped ZnS:Cu/ZnS core/shell nanocrystals

Water-dispersible Cu^{2+}-doped ZnS QDs with Cu^{2+} concentrations ranging from 2 to 5% were prepared in aqueous solution by reaction of $Zn(NO_3)_2$ and $CuSO_4$ with Na_2S in the presence of MPA [268]. The effect of Cu^{2+} ion concentration of Cu^{2+}-doped ZnS QDs photoluminescence has been studied. The variations in PL efficiency of core ZnS:Cu QDs at different Cu^{2+} doping ratios are reported in Figure 69.

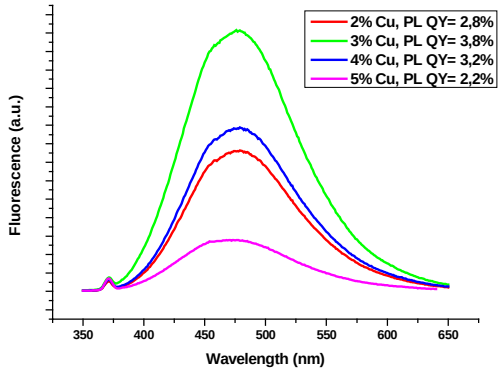

Figure 69. Room temperature PL spectra of core ZnS:Cu@MPA QDs with different initial concentrations of Cu^{2+} and the related PL QYs illustrating the quenching effect observed above 4% doping in Cu^{2+}. Spectra were recorded after excitation at 330 nm.

In a typical synthetic protocol the $Zn^{2+}/S^{2-}/Cu^{2+}$/MPA ratio was established to 1/0.52/0.03/2.27. The effect of various ratios on the optical properties of 3 at.% Cu-doped ZnS QDs was investigated. Table 8 lists the PL QYs of ZnS:Cu cores.

Table 8. Influence of the $Zn^{2+}/S^{2-}/Cu^{2+}$/MPA ratio on the PL QYs of Cu-doped nanocrystals

$Zn^{2+}/S^{2-}/Cu^{2+}$/MPA ratio	**PL QY (%)**
1/0.52/0.03/2.27	3.8
1/0.25/0.03/2.27	1.6
1/0.75/0.03/2.27	0.7
1.2/0.52/0.03/2.27	2.6
1/0.52/0.03/1	0

The effect of various thiol-stabilizers including thioglycolic acid (TGA), 3-mercaptopropionic acid (MPA), thioglycerol (TG) and L-cysteine (Cys) on the optical properties of Cu-doped ZnS QDs was also investigated, however using mentioned

synthesis protocol very modest PL QYs of NCs was obtained for the ligands other than MPA.

The influence of heating time on the PL properties of QDs was also checked (Figure 70). The results show that after 16 h of heating PL QY of QDs drops to 2.8% comparing with 3.8% after 2 h of heating time. The red shift of 8 nm (from 479 to 487 nm) was also observed with the increase of heating time.

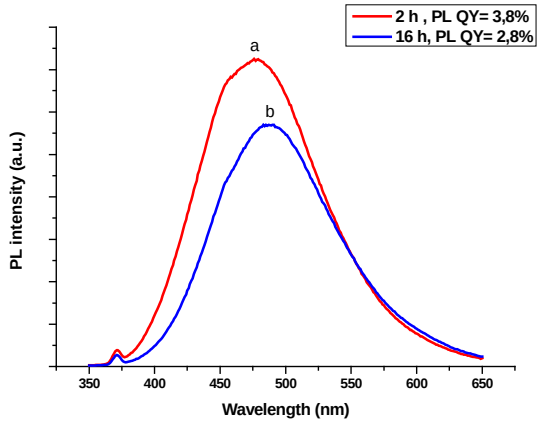

Figure 70. Evolution of PL spectra obtained after (a) 2 h and (b) 16 h of heating. Spectra were recorded after excitation at 330 nm.

The PL QY of as-prepared NCs was improved by introduction of the ZnS shell which eliminates the surface defects acting as luminescence quenching centers. A ZnS shell was introduced at the surface of ZnS:Cu core QDs by addition of small portions of $Zn(NO_3)_2$ solution and Na_2S, MPA and NaOH solution according to Corrado *et al.*, 2010 [269]. Figure 71 shows the evolution of the emission spectra of ZnS:Cu QDs doped with 3 at.% Cu recorded after excitation at 330 nm measured for aliquots taken from the reaction solution during the overgrowth of the ZnS shell on ZnS:Cu cores.

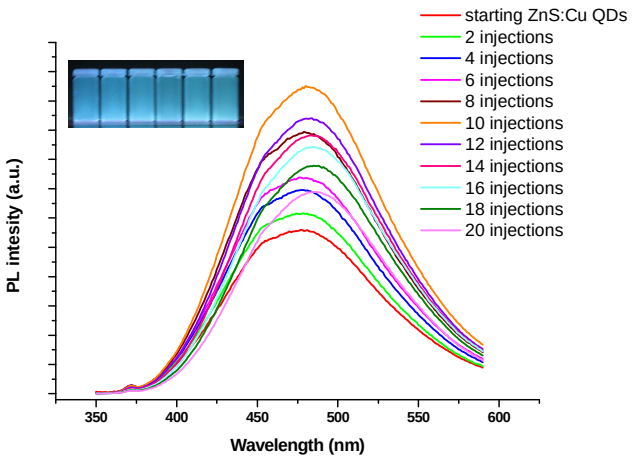

Figure 71. Temporal evolution of the photoluminescence spectra of ZnS:Cu QDs during the growth of ZnS shell. Spectra were recorded after excitation at 300 nm. The inset shows a photography of initial ZnS:Cu QDs and core/shell ZnS:Cu/ZnS QDs after each two-200 µL injections illuminated with an ultraviolet lamp.

The PL QYs of examined core/shell QDs did not increase markedly with the following injections of Zn and Na_2S, MPA and NaOH solutions. Starting from 3.4% of PL QY of the core ZnS:Cu, the increment of 0.5% in PL QY was observed after ten-200 µL injections of both solutions and then up to 20 injections the PL QY dropped slowly to starting value. However, the red shift of 10 nm (from 476 to 486 nm) in maximum of fluorescence emission peak was observed resulting in change of fluorescence emission color from green-blue to green-blue sky.

UV-vis absorption spectrum of the doped core/shell ZnS:Cu/ZnS@MPA NCs in water solution, together with the excitation and the PL spectra after excitation at 350 nm is shown in Figure 72.

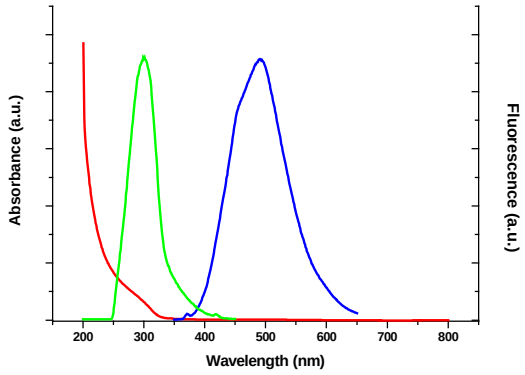

Figure 72. Room temperature absorption (red line), excitation (green), and photoluminescence (blue) spectra after excitation at 330 nm of core/shell ZnS:Cu/ZnS@MPA QDs dispersed in water.

Figure 73 shows the XRD patterns of the as-prepared ZnS:Cu@MPA QDs and of core/shell ZnS:Cu/ZnS@MPA QDs.

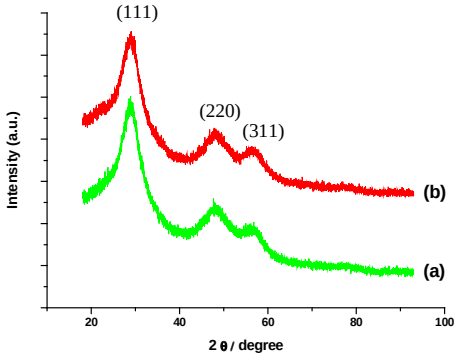

Figure 73. XRD peak patterns for (a) core ZnS:Cu@MPA, and (b) core/shell ZnS:Cu/ZnS@MPA.

All of the XRD peaks can be indexed to the cubic zinc blende structure of ZnS. The three main peak correspond to the (111), (220), and (311) planes and are consistent with the standard cubic bulk ZnS peak position from JCPDS file Nº 77-2100. It can be observed that these peaks are broadened compared to bulk ZnS, thus confirming the nanocrystalline nature of both samples.

Using TEM, the average diameters of the core and core/shell NCs obtained were found to be 2.7 and 3.2 nm, respectively (average hydrodynamic diameter = 5.9 ± 0.1 and 11.7 nm, respectively) (Figure 74).

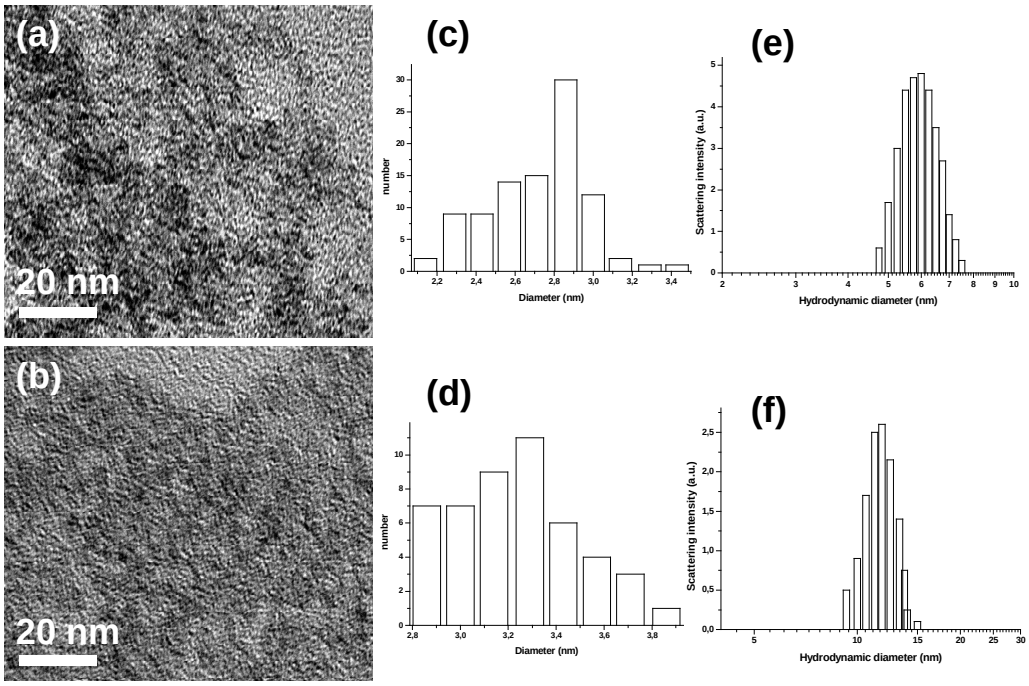

Figure 74. Bright field TEM micrographs, (c, d) the corresponding particle size distribution, and (e, f) hydrodynamic size of (a) core ZnS:Cu@MPA and (b) core/shell ZnS:Cu@MPA/ZnS d-dots measured by DLS.

The electric potential, referred to as zeta potential ζ, which controls the colloidal stability and interparticles interactions, was also determined. The ζ value measured for ZnS:Cu@MPA QDs (-21.9 mV) confirmed the presence of negative charges on the surfaces of QDs, due to the carboxylate end group of the MPA ligand. After the introduction of the ZnS shell, the value of ζ (-26.6 ± 0.1 mV) of ZnS:Cu/ZnS@MPA QDs slightly increases.

The X-ray photoelectron spectroscopy (XPS) scan survey of the core ZnS:Cu@MPA sample shows the peaks of Zn, S, Cu, O, C and Na (Figure 75a).

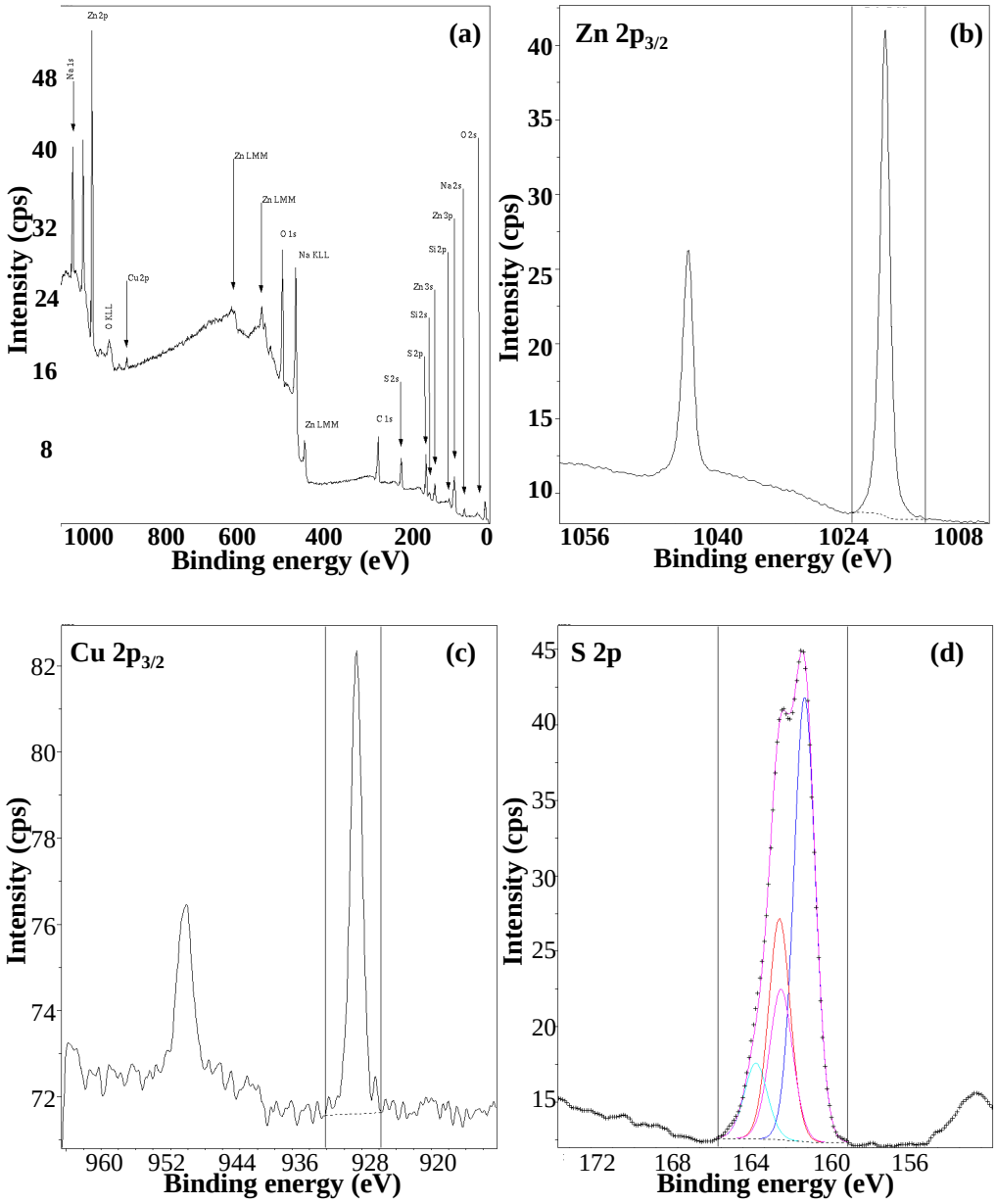

Figure 75. (a) XPS survey scan of the core ZnS:Cu@MPA QDs. The Zn 2p (b), Cu 2p (c) and S 2p (d) emissions are presented.

As seen on Figure 75b, the peak of Zn $2p_{3/2}$ appears at 1021 eV confirming that the Zn element exists only in the form of Zn^{2+} linked to a sulfur atom. The Cu $2p_{3/2}$ peak is centered at 932.0 eV (Figure 75c). Figure 75d shows the peak of S 2p centered at 161.5 eV. The deconvoluted peaks at 161.2, 162.0, 162.4 and 163.2 eV originate from the different kinds of sulfur species in the sample (S from the core linked either to Zn or to Cu, S from the shell and S from the stabilizing ligand). The presence of silica (Figure 75a) may originate from a contamination of the samples by the glassware.

The effect of the concentration of the QDs on their PL properties was studied (Figure 76). The PL intensity increased with the increase of both QDs concentration and no self-quenching of QDs fluorescence was observed.

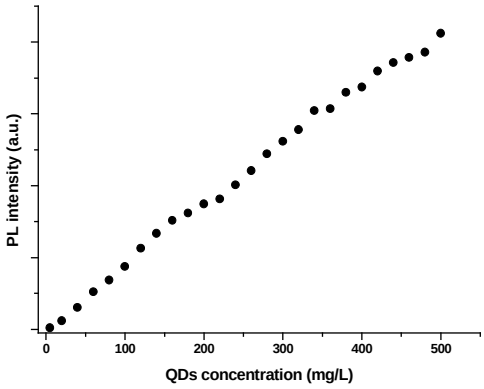

Figure 76. Evolution of PL intensity of ZnS:Cu@MPA/ZnS QDs (5-500 mg/L in 2 mL of borate buffer) upon stepwise addition (with an increment of 20 µL) of the QDs stock solution (10 mg of QDs in 5 mL of borate buffer).

The effect of pH in the range 2-13 was also studied. The optimum net fluorescence intensity was obtained in the pH range between 8 and 10. Typical evolution of PL intensity versus pH for ZnS:Cu/ZnS@MPA QDs is presented in Figure 77a.

The effect of the temperature on PL intensity of ZnS:Cu/ZnS@MPA QDs was also evaluated. Indeed, at temperature above 25°C, the kinetic energy of the dots increases, which causes increase in the dissociation rate of the MPA ligand stabilizing the QDs. Thermal quenching may also decrease the PL intensity as the temperature increases. The PL intensity of the dots was found to be stable between 10 and 45 °C (see Figure 77b). Above 45°C, a decrease (by ca. 30%) of the PL intensity was observed.

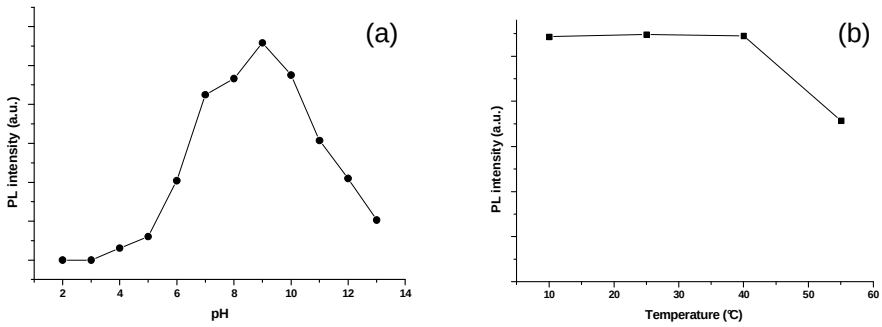

Figure 77. Effect of (a) pH and (b) temperature on the PL intensity of ZnS:Cu@MPA/ZnS QDs.

4.1.4. MPA-capped ZnSe:Mn/ZnS core/shell nanocrystals

A series of ZnSe:Mn QDs were synthesized in aqueous solution containing thioalkylacids [thioglycolic acid (TGA), 3-mercaptopropionic acid (MPA), 6-thiohexanoic acid (MHA), mercaptosuccinic acid (MSA) or cysteine (Cys)]. Thioalkyl acids contain two functional groups possessing lone pair electrons that might influence the nucleation, the growth and the stabilization of ZnSe:Mn QDs and hence affect their physical and optical properties. Since the synthesis of the d-dots is conducted at basic pH, the negative charges of thioalkyl acids will also impose a kinetic barrier for the growth due to Coulombic repulsions between the ligand shells of neighboring QDs and thus favor stable and small NCs.

The synthesis and the optical properties of 3-MPA acid-capped ZnSe NCs were first studied.

Initial experiments performed with 4% doping in Mn^{2+} and a 2.7 mM $ZnSO_4$ solution demonstrated that good quality QDs (PL QY = 3.5%) were obtained when using NaHSe in short supply (by ca. 0.9-fold) relative to the mole amount of the Zn^{2+} precursor. A decrease (0.4 or 0.6) or an increase of the Zn/Se ratio (1.2 or 2.0) yielded ZnSe:Mn QDs with poor PL efficiency. It is well-known that Zn^{2+} precursors have a low reactivity towards NaHSe [294]. Increasing the concentration of $ZnSO_4$ (5.0 or 10.0 mM) while maintaining a Zn/Se molar ratio of 1/0.9 did not effectively improve the PL properties of ZnSe:Mn QDs (PL QY < 2%).

To improve the PL properties of the Mn-doped ZnSe QDs, that is, improvement of the Mn^{2+}-related $^4T_1 \rightarrow {}^6A_1$ emission and suppression of the trap emission, the influence of the pH of the Zn^{2+}-MPA precursors solution using 4% doping in Mn^{2+} and a Zn^{2+}/Se^{2-}/MPA molar ratio of 1/0.9/20 was also investigated. It was found that when the pH of the Zn^{2+}/MPA precursors solution was set at 10.3 (the pH increased to 10.4 after the injection of the NaHSe solution), the as-prepared NCs obtained after 24 h heating showed a strong orange emission at ca. 595 nm and a very weak trap emission. When the pH value of the Zn^{2+}/MPA precursors was decreased below 10.0 (9.0 or 8.0), the trap emission increased and the PL QY decreased (<1%). The pH value of the Zn^{2+}/MPA precursors solution was fixed at 10.3 in latter experiments.

After the injection of NaHSe, small aliquots were removed from the reaction solution with a syringe to monitor the growth of NCs via optical absorption. Using a Zn^{2+}/Se^{2-}/MPA molar ratio of 1/0.9/20 and 4% Mn^{2+} relative to Zn^{2+}, a well-resolved peak at 343 nm was observed after 15 min heating at 100°C indicating the homogeneous nucleation of small crystallites (Figure 78). The absorption peak attenuated sharply for longer growth times becoming a shoulder due to the Ostwald ripening process (formation of larger NCs at the expense of smaller ones) and gradually red-shifted to 378 nm, which was consistent with the growth of the ZnSe host. The subtle blue-shift in absorption spectra observed after 24 h reflux (375 nm) may be a consequence of the partial decomposition of the MPA ligand surrounding the ZnSe:Mn core, leading to a sulfur-enriched shell.

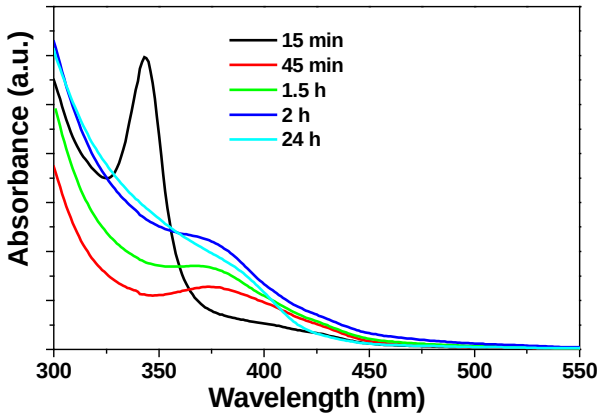

Figure 78. Temporal evolution of the UV-vis spectra of ZnSe:Mn@MPA nanocrystals grown at 100°C with a Zn^{2+}/Se^{2-}/MPA molar ratio of 1/0.9/20 and 4% doping in Mn^{2+}.

The photoluminescence of the clear pale yellow solution was also monitored in the course of the NCs growth. All aliquots taken during the first 5 h of growth exhibited at first no PL. Upon resting at rt, a strong orange-red emission evolved over a matter of hours (in some cases, minutes) (Figure 79). PL QYs measured from NCs obtained after 30 min or 2 h of growth at 100°C and respectively 6 and 21 h storage at rt were high (23 and 19%, respectively, without any post-preparative treatment and the absence of the broad trap-emission centered at ca. 480 nm) (Figure 79). The PL decreased however gradually and disappeared after 24 h for the dots synthesized during 30 min at 100°C (Figure 79a). It should also be pointed out that the stability of the d-dots obtained after short heating times (< 3 h) was found to be modest. A deterioration of these NCs accompanied by precipitation was generally observed after 48 h storage at rt. Good quality powder X-ray diffraction (XRD) patterns could also

not be obtained for MPA-capped ZnSe:Mn QDs prepared during short reaction times (< 3 h). As the reaction prolonged, widths of the diffraction peaks were found to decrease and were more resolved (*vide infra*). The stability of ZnSe:Mn d-dots was markedly increased by extending the heating time at 100°C. No sign of macroscopic aggregation or loss of fluorescence were observed for the dots obtained after 24 h heating upon storage at rt for up to 3 months.

One interesting feature during the early stages of growth (15 min to 2 h) is the significant blue-shift of the maximum wl of the Mn^{2+} $^4T_1 \rightarrow {}^6A_1$ emission from 609 to 595 nm after excitation at 350 nm. Negatively-charged MPA ligands strongly interact with surface zinc atoms of small doped-ZnSe NCs formed at the beginning of the growth stage. As a consequence, the d-orbitals of the Mn center will experience a high electric field difference along different directions, which results in a higher splitting of the energy levels [156]. Once the thickness of the ZnSe shell increases around the doped-ZnSe cores, the lattice field around Mn^{2+} ions becomes more symmetric leading to smaller splitting of the energy levels and a change of the PL color from orange-red to orange.

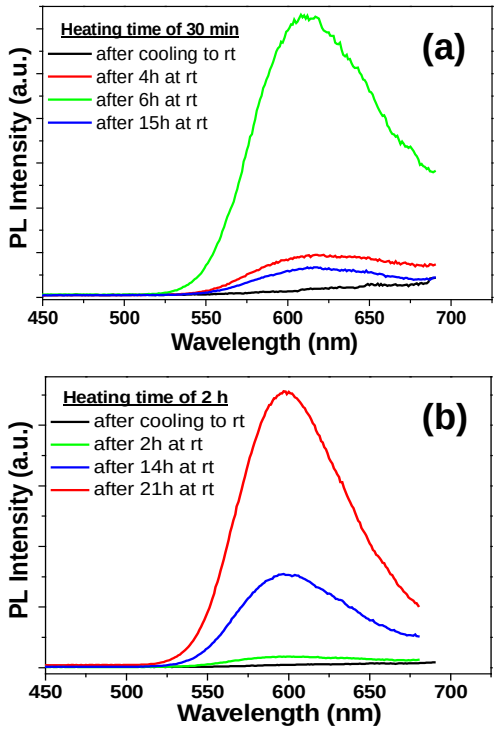

Figure 79. Temporal evolution of the PL spectra of ZnSe:Mn@MPA nanocrystals prepared with a Zn^{2+}/Se^{2-}/MPA molar ratio of 1/0.9/20 and 4% doping in Mn^{2+} and grown at 100°C (a) during 30 min, (b) during 2 h. Excitation wavelength is 350 nm.

I also tested the impact of various thiols (TGA, MHA, MSA and Cys) on the PL properties of ZnSe:Mn QDs when the Zn^{2+}/Se^{2-}/ligand molar ratio and the doping percentage were fixed at 1/0.9/20 and 4, respectively. All reactions were conducted at 100°C for 24 h. It was found that TGA-, MHA-, MSA-, and Cys-capped ZnSe:Mn QDs exhibited the Mn^{2+} $^4T_1$ □ $^6A_1$ transition at ca. 595 nm but the emissions were found to be broad (fwhm increased up to 94 nm while it was of ca. 60 nm for MPA-capped QDs). The PL QYs were also found to be weaker (< 1%) compared to NCs prepared with MPA. The NC growth with TGA, MHA, MSA, and Cys ligands occurred finally with higher defect densities (increase of the ZnSe band-edge transition at ca. 460 nm). Compared to the other thiols used in this study, I suggest that MPA provides the better surface passivation of the QD crystalline lattice under used synthesis conditions.

The ratio of Mn^{2+} relative to Zn^{2+} was varied from 1 to 6% to evaluate the effects of Mn^{2+} on the optical properties of the d-dots under the same experimental conditions (Zn^{2+}/NaHSe/MPA = 1/0.9/20, heating time of 24 h). While the dopant PL peak position and spectral contour were found to be independent of the Mn^{2+} concentration in the solution (PL emission at 596 nm and fwhm of ca. 60 nm), an increase of the Mn^{2+} concentration from 1 to 4% relative to Zn^{2+} leads to an increase in the PL emission intensity, which also proves the successful incorporation of Mn^{2+} into ZnSe QDs (Figure 80). Further increasing of the concentration of Mn^{2+} to 5 or 6% leads to a decrease of the PL QYs. The effect of Mn^{2+} ion concentration on the PL properties of Mn^{2+}-doped II-VI semiconductors QDs has been extensively studied in recent years and a so-called “concentration quenching effect” has been demonstrated [120, 284, 285, 295]. When the concentration of Mn^{2+} becomes higher than a certain threshold, the non-radiative energy transfers between neighbouring Mn^{2+} dopant ions reduce and even annihilate the fluorescence. Under used synthesis conditions, the formation of such pairs of Mn^{2+} dopant ions is probably observed when the amount of Mn^{2+} ions in QDs is higher than 4%. Energy Dispersive X-ray (EDX) spectroscopy experiments (*vide infra*) conducted on ZnSe:Mn@MPA QDs after purification indicated that the Mn^{2+} at.% was ca. 3%. This value is slightly higher than those used in organometallic syntheses (0.5-3% in growth solutions leading to NCs doped with ca. 0.02-2.0% Mn^{2+} ions).

It was also surprising to observe that the $^4T_1 \rightarrow {}^6A_1$ transition of Mn^{2+} ions is red-shifted by ca. 25 nm compared to the MPA-capped ZnSe:Mn QDs prepared by

Wang *et al*. [187] using an aqueous route. As demonstrated by several groups [296-298], the position of Mn^{2+} emission peak is sensitive to the electric field imposed by the organic capping layer, to the Mn^{2+} radial positions, to the heating time, and to the Mn^{2+} concentration inside the NCs. Wang and coworkers [187] used a theoretical concentration of Mn^{2+} twice lower than mine (4 versus 2) and heated the reaction mixture for 5 h, while the growth of my NCs was performed during 24 h. A possible explanation for the red-shift observed with Mn-doped ZnSe dots prepared under used synthesis conditions is that the crystal field for each dopant ion became more symmetric in long range due to the thicker ZnSe shell formed. As a result, the crystal field splitting of Mn^{2+} d-orbitals became smaller, which resulted in a PL red-shift.

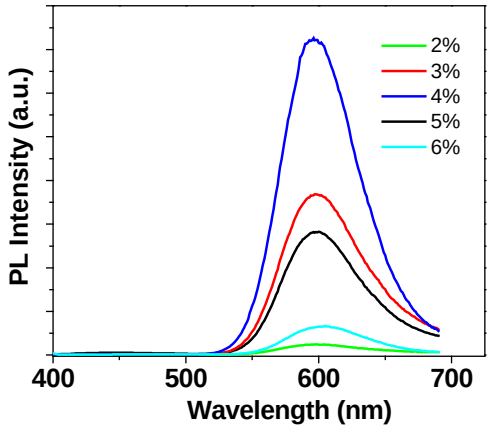

Figure 80. Influence of the concentration of Mn^{2+} relative to Zn^{2+} on PL spectra of ZnSe:Mn@MPA nanocrystals prepared with a Zn^{2+}/Se^{2-}/MPA molar ratio of 1/0.9/20 and grown at 100°C for 24 h. Excitation wavelength is 350 nm.

The dopants might also change the lattice structure of the ZnSe host material because the diameter of the Mn^{2+} ion (0.83 nm) is larger than that of the Zn^{2+} ion (0.74 nm) [288]. To confirm that the crystal lattice of the ZnSe host NCs was intact, powder XRD pattern of the MPA-capped ZnSe:Mn QDs was recorded (Figure 81a). The XRD pattern of the NCs exhibited characteristic peaks at ca. 27.5, 45.6, and 54.3° corresponding to the (111), (220) and (311) reflecting planes of cubic zinc blende ZnSe (JCPDS Card N° 80-0021). The peaks are broadened due to the finite crystalline size. These results prove that the ZnSe:Mn d-dots have a cubic zinc blende structure similar to undoped ZnSe QDs and confirm that the crystal lattice of the ZnSe host material is intact after doping with Mn^{2+} ions. A crystallite size of 3.5 ± 1.0 nm was estimated from the diffraction line broadening, value which correlated well with the results obtained from TEM analysis (*vide infra*). Finally, it is worth noting that the

XRD patterns of the ZnSe:Mn QDs are located on higher angle compared to that of the pure ZnSe material probably because the MPA ligand partially decomposed by heating leading to a sulfur-enriched ZnS shell with smaller lattice parameters compared to ZnSe. The formation of alloyed doped-ZnSe(S) QDs is likely after 24 h heating at 100°C.

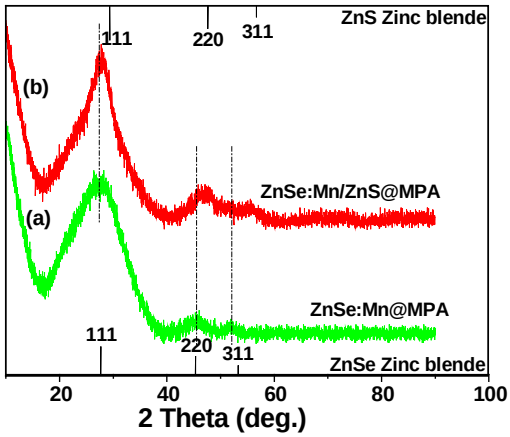

Figure 81. XRD patterns of ZnSe:Mn@MPA QDs (a) before and (b) after introduction of the ZnS shell.

Figure 82 presents UV-vis, PL, and PL excitation (PLE) spectra of ZnSe:Mn dots d-dots (~ 3 nm in size). The quantum confinement of an electron-hole pair caused a marked blue-shift in the absorption peak of ZnSe:Mn QDs obtained after 24 h heating at 100°C in comparison to the 442 nm (2.80 eV) band gap of the bulk ZnSe material. The NC radius was calculated using the equation of quantum confinement (see Equation 1). Using the absorption peak for MPA-capped Mn-doped ZnSe QDs after 24 h of growth yields a NC diameter of 2.7 ± 0.4 nm. The deviation of 0.4 nm corresponds to ± 10 nm for the determination of the onset of absorption. The PLE spectrum corresponding to the 600 nm emission exhibits maximum at about 345 nm corresponding to the band gap excitation of host ZnSe NCs.

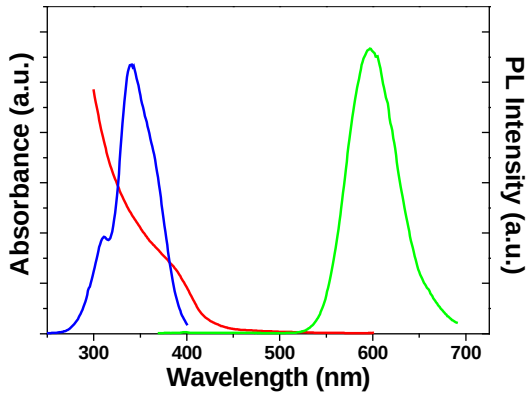

Figure 82. Optical absorption (red line), PL excitation (blue) and PL emission (green) after excitation at 365 nm of MPA-capped ZnSe:Mn d-dots.

FT-IR spectra of the neutral MPA ligand and of the purified and dried ZnSe:Mn@MPA QDs are given in Figure 83. The acid function of MPA can clearly be identified on Figure 83a both through the very broad 3150 cm^{-1} O-H stretching vibration and through the 1718 cm^{-1} C=O stretching vibration. The strong vibration of the carbonyl group of MPA vanished upon surface functionalization of QDs. The symmetric and asymmetric stretching vibrations of the carboxylate group of the charged MPA appear at 1438 and 1575 cm^{-1}, respectively. The absence of SH stretch band between 2680-2560 cm^{-1} supports the attachment of the MPA ligand through covalent bonds between thiols and surface Zn atoms of ZnSe:Mn QDs. The spectrum of ZnSe:Mn QDs also displayed the bands assigned to the hydroxyl group of the acid function at 3432 cm^{-1} and of C-H stretching at 2921 cm^{-1}.

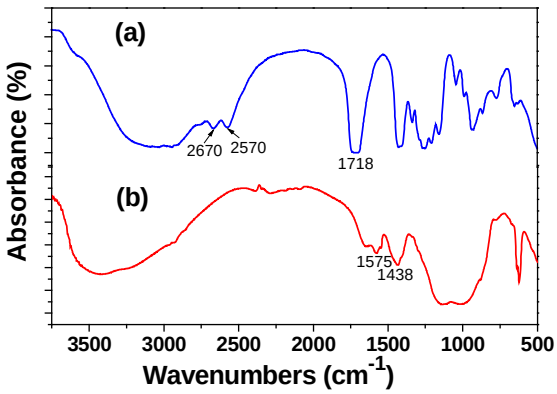

Figure 83. FT-IR spectra of (a) MPA and (b) ZnSe:Mn@MPA QDs.

Figure 84 shows a transmission electron microscopy (TEM) micrograph of 3.1 ± 0.3 nm diameter Mn-doped ZnSe QDs, corresponding to the final spectrum of Figure 79 with 3.5% PL QY (blue line), which is in good accordance with the value calculated from the quantum confinement equation. Dynamic light-scattering (DLS) measurements indicate that the QDs are well-dispersed in water and that their hydrodynamic diameters range from 5 to 11 nm (average hydrodynamic diameter of 7.6 nm). The hydrodynamic diameter is larger than the diameter of the inorganic core due to the solvatation layer around the QDs in aqueous solution. Energy dispersive spectroscopy (EDS) measurements revealed that the atomic composition of the d-dots had a value similar to that of the ratios of precursors (see details in the core/shell subsection). An average diameter of 3.1 nm represents ca. 88 ZnSe structural units in each monocrystal (using a theoretical lattice parameter a of 0.56 nm, JCPDS Card N° 80-0021). Using 4% Mn^{2+} dopant means ca. 14 Mn^{2+} ions per NC.

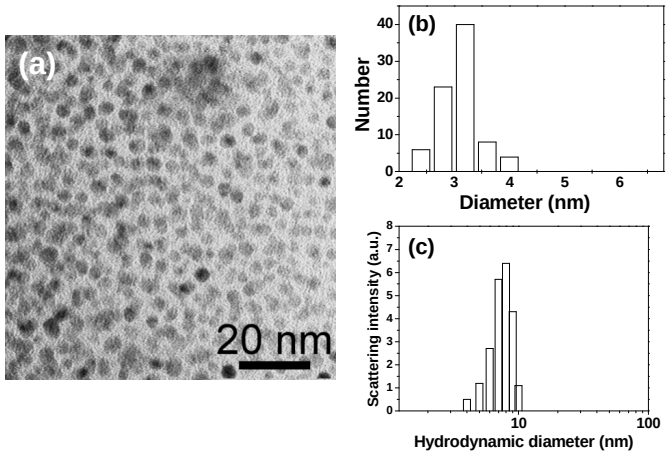

Figure 84. (a) TEM micrograph of ZnSe:Mn@MPA d-dots, (b) the corresponding particle size distribution, and (c) hydrodynamic size of ZnSe:Mn@MPA d-dots measured by DLS.

A synthesis of core/shell ZnSe:Mn/ZnS QDs was also developed with the goal to improve the chemical, PL stabilities and QY of the QDs but also with the hope that the higher band gap ZnS shell with a small lattice mismatch with ZnSe (ca. 5%) will provide a diffusion barrier by stabilizing the Mn^{2+} doping ions. Although, there is no report on the preparation of ZnSe:Mn/ZnS d-dots, the preparation of ZnSe/ZnS d-dots in organic [144, 158, 299-301] or aqueous [302, 303] solution has already been investigated by a few research groups. The ZnS shell was successfully introduced at the periphery of ZnSe:Mn cores by thermal decomposition at basic pH of Zn^{2+}/MPA complexes. The PL intensity of Mn^{2+} that corresponds to the $^4T_1 \rightarrow {}^6A_1$ transition

within the $3d^5$ configuration of Mn^{2+} increased gradually upon heating at 100°C and reached its maximum value (PL QY = 9%) after 10 h (Figure 85a). No improvement was observed by further heating. For ZnSe:Mn@MPA NCs under the same heating conditions but in the absence of the Zn^{2+}/MPA complex, there is almost no change of PL QY. This suggests that the enhancement of PL QY is related to the growth of the ZnS shell. The enhanced QY of ZnS-capped ZnSe:Mn d-dots is direct consequences of an effective surface passivation by which nonradiative recombination that compete with the regular luminescence are reduced significantly. A visual comparison of non-capped and of the ZnS-capped QDs is shown as inset in Figure 85b. Both samples are fluorescent under a handheld UV lamp providing 366 nm multiband irradiation, and it is obvious that the ZnS-passivated d-dots are much brighter. As shown in Figure 85b, the PL is shifted at 610 nm while it is located at 600 nm for the ZnSe:Mn core. Since Mn^{2+} had a higher affinity for ZnS than for ZnSe [157], we suppose that surface Mn^{2+} ions of the ZnSe:Mn core diffuse into the ZnS lattice in which they are subjected to the electric field of the deprotonated MPA ligand. In the XRD pattern (see Figure 81b), the peak positions shift to higher angles towards the position of ZnS, with peak widths and shapes being nearly unchanged, which proves the formation of core/shell ZnSe:Mn/ZnS QDs. This deviation could also result from the compression of the ZnS shell on the lattice planes of the doped-ZnSe core. Using TEM, the average diameter of core/shell NCs obtained was found to be 4.3 ± 0.5 nm (average hydrodynamic diameter = 8.0 nm) (Figure 86). Energy-dispersive X-ray spectroscopy (EDX) measurements of the core ZnSe:Mn and of the core/shell ZnSe:Mn/ZnS QDs confirmed the nature of the materials (Figure 87). Zn, Se, and Mn peaks arise from the doped core while the detected S mainly comes from the capping MPA ligand. The presence of silica (peak at ca. 1.7 keV) may originate from a contamination of the samples by glassware during their storage. The growth of the ZnS shell around the ZnSe cores was clearly demonstrated by EDX experiments. With the deposition of the ZnS shell, the Zn/Se ratio increased from 1.02 in the ZnSe:Mn cores to 9.88 in the core/shell NCs. In the meantime, the Zn/S atomic percentage decreased from 5.17 to 1.03.

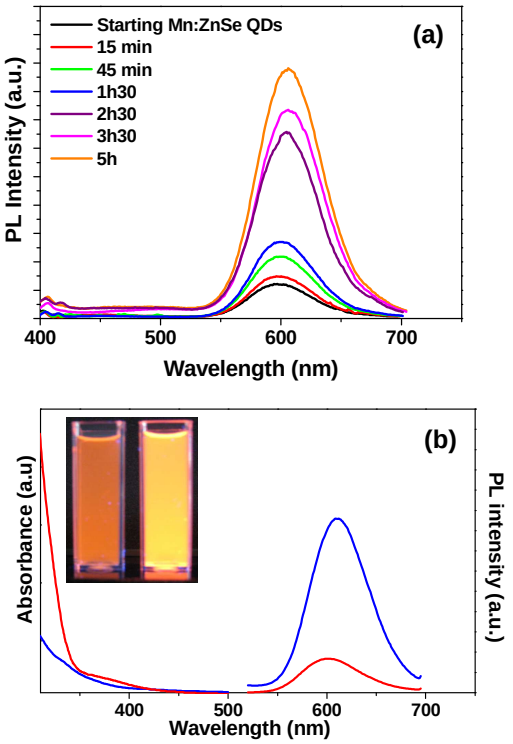

Figure 85. (a) Evolution of PL spectra during the overcoating of ZnSe:Mn QDs with the ZnS shell. (b) Absorption and PL spectra of ZnSe:Mn@MPA QDs before (red line) and after (blue) the introduction of the ZnS shell. Excitation wavelength is 350 nm. Inset shows digital pictures of the QDs before (left) and after (right) the overcoating with ZnS.

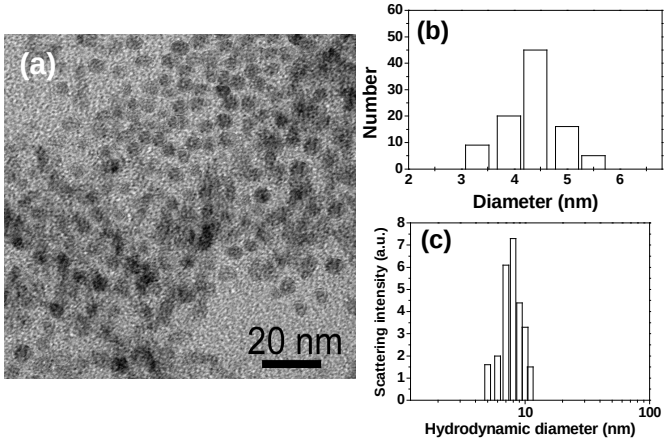

Figure 86. (a) TEM micrograph of core/shell ZnSe:Mn/ZnS@MPA d-dots, (b) the corresponding particle size distribution, and (c) hydrodynamic size of ZnSe:Mn/ZnS@MPA d-dots measured by DLS.

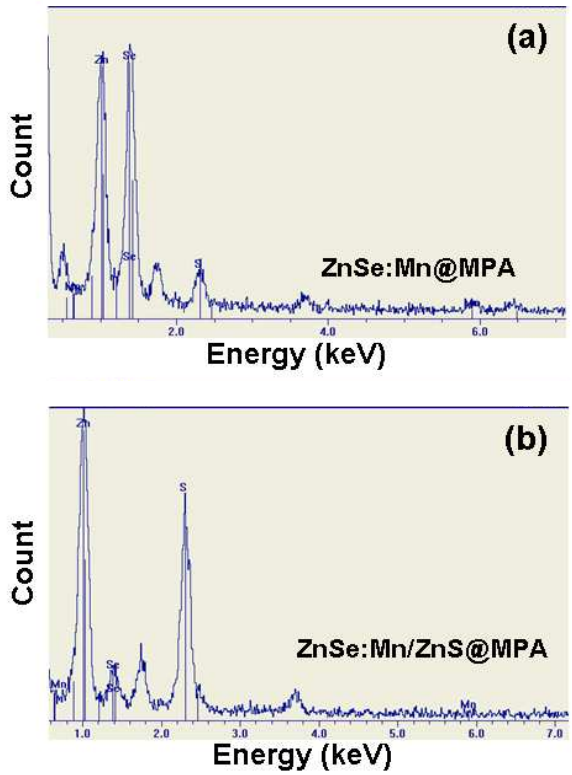

Figure 87. EDX spectra of ZnSe:Mn@MPA QDs (a) before and (b) after the introduction of the ZnS shell.

The overcoating of ZnSe:Mn d-dots with ZnS was further confirmed by measuring the slow PL decay of the NCs before and after surface modification. Indeed, Mn^{2+} ion emission lifetime is dependent on the diameter of the NCs and is longer for QDs with thicker overcoating layer or thicker diffusion region [304]. The slow PL decay curves of Mn^{2+} ions for the core ZnSe:Mn and the core/shell ZnSe:Mn/ZnS QDs are shown in Figure 88. The slow decay times, attributed to the emission of the single isolated Mn^{2+} ions in a cubic site [268, 305, 306], were 0.62 and 1.39 ms for the core and core/shell QDs, respectively. Interestingly, the shell dependence of the PL lifetime is related to the PL QY. After introduction of the shell, the PL QY increased by 257% (from 3.5 to 9%) while the PL lifetime was found to increase by 224%.

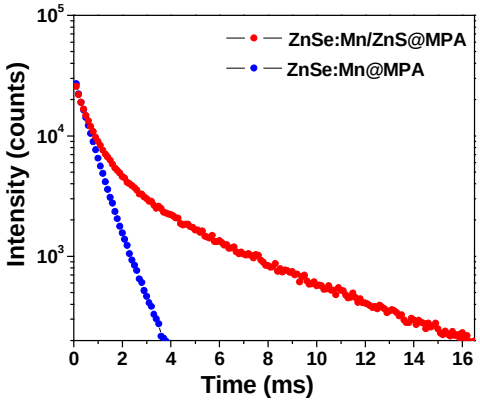

Figure 88. PL decay curves recorded at room temperature of ZnSe:Mn and ZnSe:Mn/ZnS QDs at a wavelength near 605 nm.

For the efficient and reliable use of semiconductor NC technology especially in biological applications, it is important to evaluate the external factors that may affect the optical properties of the QDs. As shown in Figure 89, MPA-capped ZnSe:Mn/ZnS QDs are sensitive to changes of pH with greater fluorescence at higher pH (PL QY = 12.5% at pH = 12). The PL QY at neutral pH is 8.9%. A rapid decay of PL was observed when the pH was below 6.0 (PL QY = 2.5% at pH = 4). Under pH = 4.0, the QDs became unstable in the acidic aqueous environment, they precipitated and the PL disappeared.

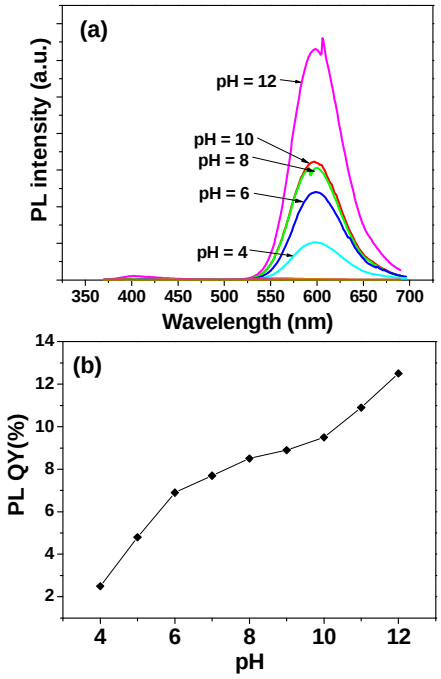

Figure 89. Aqueous solution pH influence on (a) fluorescence spectra and (b) PL QY of ZnSe:Mn/ZnS@MPA QDs.

In the conclusion of that paragraph I can say that I have reached to develop the synthesis methods to prepare highly luminescent, monodisperse and water-dispersible Mn- or Cu-doped ZnS d-dots stabilized by MPA and TG and Mn-doped ZnSe QDs stabilized by MPA.

I have demonstrated that the molar ratios of precursors, Mn^{2+} or Cu^{2+} concentration, pH value, heating time and the type of stabilizer play an important role in final stability and optical properties of these NPs. The PL properties were markedly improved by overcoating the MPA-capped Mn- and Cu-doped ZnS and Mn-doped ZnSe core QDs with a ZnS shell. The synthesized NCs possess high QY and good crystallinity.

The orange emission fluorescence of Mn- doped QDs is more interesting for the bioimaging experiments than the blue-green one of Cu- doped QDs. In the following paragraph I describe the preparation of functionalized Mn-doped NCs for bioimaging of cancer cells. QDs are functionalized with folic acid (FA) that is a targeting agent able to recognize the folate receptors (FRs) that are overexpressed in many types of cancer cells. The toxicity of as-prepared NCs is evaluated.

4.2. Surface functionalization of QDs with a targeting ligand (folic acid)

In this part of my thesis concerning functionalization of QDs by FA, primarily I focus on the studies of the influence of FA on PL properties of earlier-synthesized NCs.

4.2.1. Folic acid (FA) as a quencher of QDs fluorescence emission

QDs are sensitive to chemicals in their surrounding environment such as acids, bases, metallic ions and biomolecules like proteins. As recently observed by other groups [16, 242], small biomolecules like folic acid (FA) can markedly alter and even annihilate the luminescence of NPs like QDs that are extremely sensitive to their surface states. It was reported that QDs PL intensity can be directly correlated with pH values because QDs fluorescence is, in general, enhanced in basic medium and quenched in acidic one [307]. Taking into account findings from previous paragraphs concerning PL QY of QDs in different environmental conditions, borate buffer and room temperature were adopted in all experiments. The changes of PL properties of ZnS:Mn/ZnS@MPA, ZnS:Cu/ZnS@MPA, ZnS:Mn@TG and ZnSe:Mn/ZnS@MPA to FA was checked. Additionally, the mechanisms of PL quenching of MPA-capped Mn- and Cu-doped core/shell ZnS QDs by FA were examined.

Fluorescence quenching refers to any process that decreases the fluorescence intensity of the sample. There are two basic types of quenching: dynamic (collisional) and static. Both types require an interaction between the fluorophore and the quencher. In the case of dynamic quenching the quencher must diffuse to the fluorophore during the lifetime of the excited state. Upon contact the fluorophore returns to the ground state without emission of the photon. The static quenching implies either the existence of a sphere of effective quenching (of volume Vq surrounding the fluorophore) or the formation of a ground-state non-fluorescent complex [308]. The decrease in fluorescence intensity is usually described by the Stern-Volmer plot.

FA is a weakly fluorescent molecule due to the presence of the pterin moiety [309]. After excitation at 330 nm, a weak emission peak centered at ca. 453 nm is observed (Figure 90a).

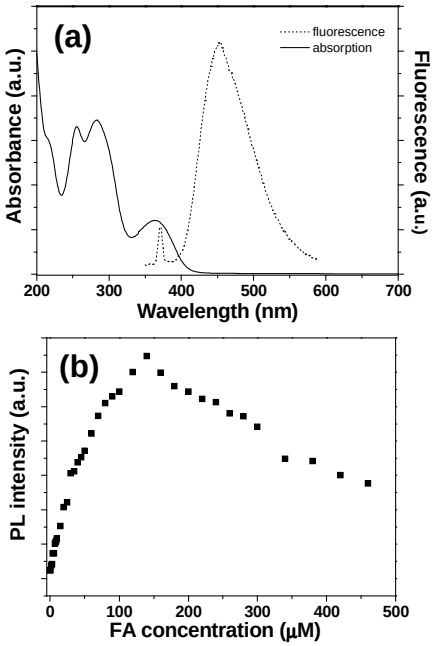

Figure 90. (a) Absorption and PL spectra (after excitation at 330 nm) of folic acid in borate buffer, and (b) effect of the concentration of FA on the PL intensity.

FA possess both H-bond donor and acceptor groups and has the potential for self-recognition and self-assembly [310, 311]. It was observed that at pH = 7.4 in phosphate buffer [311], the PL intensity of FA in borate buffer increased with FA concentration up to ca. 140 μM (Figure 90b), beyond which the PL intensity decreased probably due to intermolecular quenching by self-association. Quenching experiments were conducted with FA concentrations below and above that 140 μM concentration of FA (*vide infra*). At pH = 9, FA must be considered in the phenolate form (Figure 91).

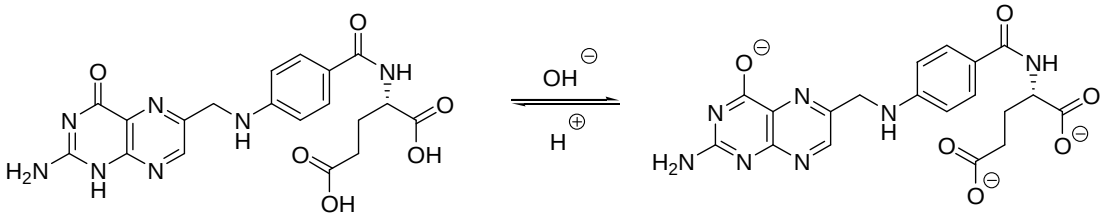

Figure 91. Molecular structures of folic acid in acid or basic medium.

As mentioned in chapter 1 PL of QDs originates from the recombination of electron-hole pair upon excitation. Once the radiative recombination is suppressed, PL quenching is usually observed. This phenomenon can be attributed to interactions of molecules or ions with the surface atoms of QDs [312, 313]. It was noticed that earlier-prepared water-dispersible NPs exhibit high fluorescence sensitivity to folic acid due to the high affinity of the carboxylate groups and nitrogen atoms of folic acid towards the Zn surface atoms of the doped dots. The changes in the PL intensities of the dots upon stepwise addition of aliquots of the 2.26 mM FA stock solution in borate buffer are shown for ZnS:Mn/ZnS@MPA (Figure 92a, b), ZnS:Cu/ZnS@MPA (Figure 92c, d), ZnS:Mn@TG (Figure 93a, b) and ZnSe:Mn/ZnS@MPA (Figure 93c, d) QDs.

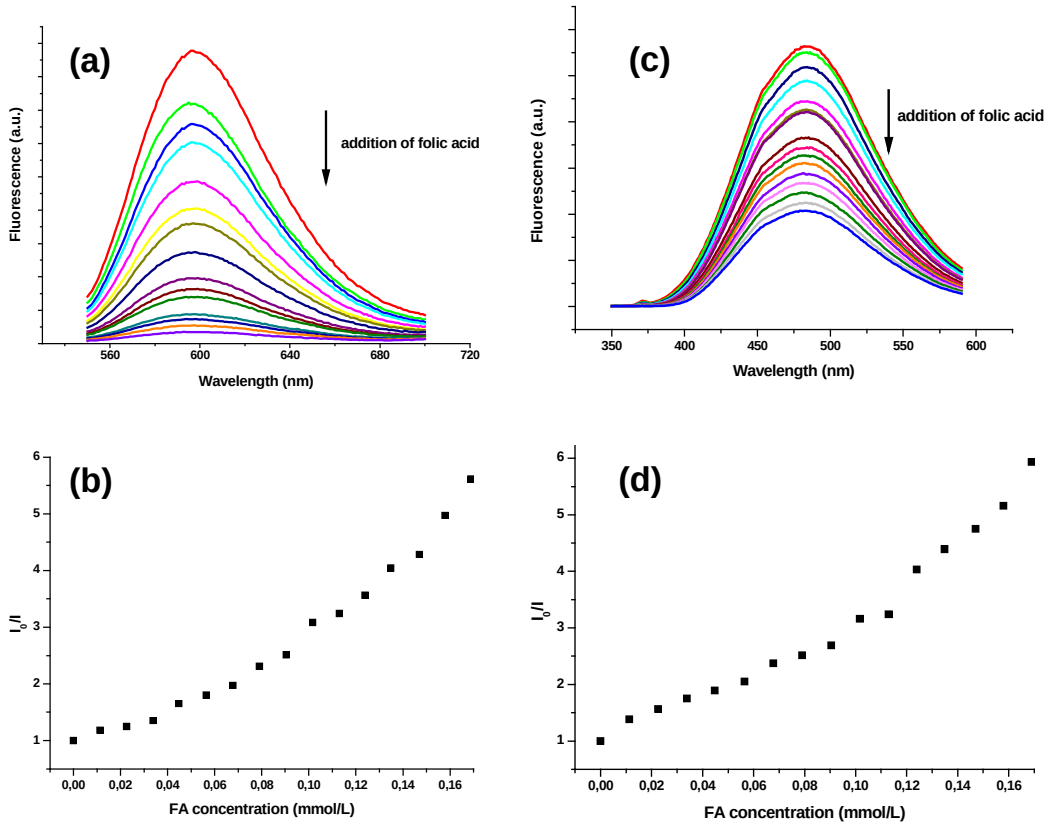

Figure 92. Evolution of photoluminescence spectra of (a) ZnS:Mn/ZnS@MPA and (b) ZnS:Cu/ZnS@MPA QDs (1 mg in 2 mL borate buffer) upon stepwise addition (with an increment of 10 µL) of a 2.26 mM folic acid solution in sodium borate buffer. A decrease of PL QY (a) from 12.0% (red line, starting ZnS:Mn/ZnS QDs) to 1.4% (violet, 150 µL of the folic acid solution added) and (b) from 4.2% (red line, starting ZnS:Cu/ZnS QDs) to 0.2% (blue, 150 µL of the folic acid solution added) was observed after the addition of the folic acid solution. Stern-Volmer plot of the photoluminescence intensity of (c) ZnS:Mn/ZnS@MPA and (d) ZnS:Cu/ZnS@MPA QDs as a function of the concentration of folic acid.

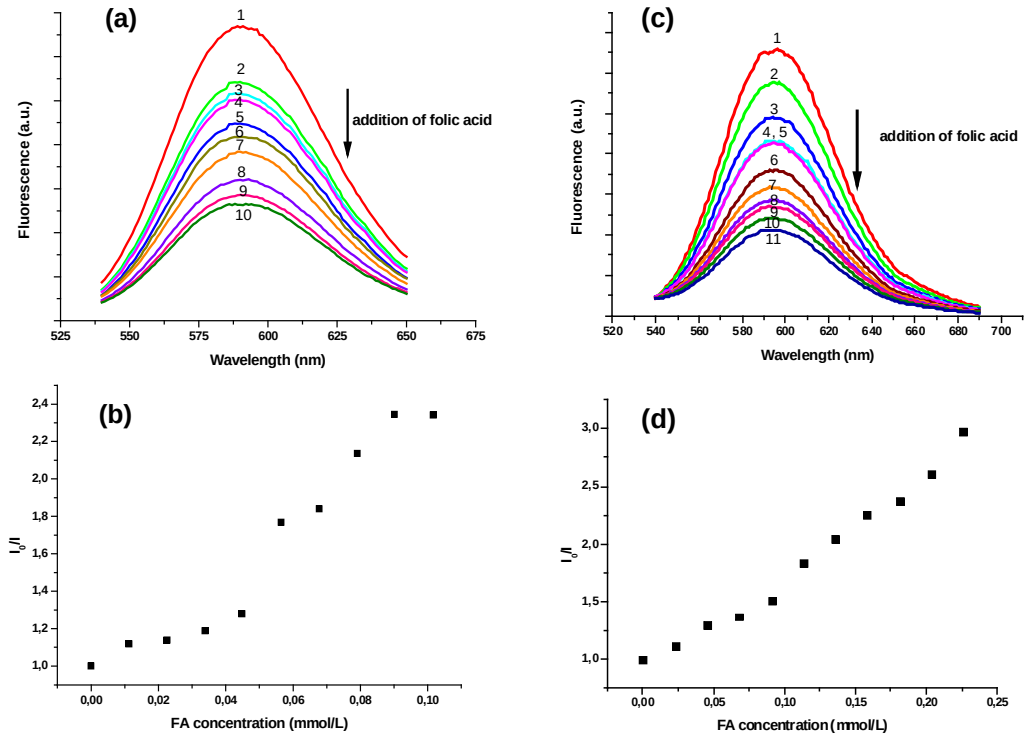

Figure 93. Evolution of photoluminescence spectra of (a) ZnS:Mn@TG QDs (2.5 mg in 2 mL of borate buffer) and (b) ZnSe:Mn/ZnS@MPA QDs (0.25 mg in 2 mL of borate buffer) upon stepwise addition (with an increment of (a) 10 µL or (b) 20 µL) of a 0.26 mM folic acid solution in sodium borate buffer. A decrease of PL QY from (a) 9.0 (spectrum 1, starting ZnS:Mn@TG QDs) to 3.8% (spectrum 10, 90 µL of the folic acid solution added) and (b) from 5.1% (spectrum 1, starting ZnSe:Mn/ZnS QDs) to 1.7% (spectrum 11, 200 µL of the folic acid solution added) was observed after the addition of the folic acid solution. Stern-Volmer plot of the photoluminescence intensity of (c) ZnS:Mn@TG and (d) ZnSe:Mn/ZnS@MPA QDs as a function of the concentration of FA.

It was observed that upon gradual addition of FA solution to QDs dispersed in borate buffer (pH = 9.0), the PL related to Mn^{2+} or Cu^{2+} ions was reduced. In the case of Mn- and Cu-doped MPA-capped core/shell ZnS QDs (Figure 92), FA was found to significantly quench the fluorescence intensity of the QDs and the points calculated for Stern-Volmer plots for concentrations of FA below 100 µM are nearly linear (see Figure 95). That is the reason why with greater attention, I investigated the possibility of use of water-dispersible Cu- or Mn-doped ZnS d-dots stabilized by MPA as the fluorescent nanoprobes for FA detection. Obtained results were additionally confirmed through fluorescence lifetimes measurements of these QDs. Discussing first the PL quenching of Mn- and Cu-doped core/shell ZnS QDs capped with MPA (Figure 92), it was found that FA quenches the PL of both QDs with a concentration dependence, but without discernible changes in the profile of PL spectra (peak shape and position). In addition, the extent of PL quenching by FA was quite independent on incubation time and a constant value was attained less than 1 min after the addition of FA. Under 265

nm irradiation, the PL quenching can even be recognized by naked eyes. The color of the solutions, upon addition of FA, changed rapidly from orange or blue-green for Mn- and Cu-doped QDs respectively, to colorless.

The time resolved luminescence decays of the Mn-doped ZnS QDs capped with MPA have been recorded in the presence of increasing amounts of FA. Without added FA, the decay of the QDs can be fitted by a biexponential function:

$$I_{lum} = A_1 \times e^{-\frac{t}{\tau_1}} + A_2 \times e^{-\frac{t}{\tau_2}}$$

Equation 9. Biexponential function illustrating the decay of QDs without folic acid.

where I_{lum} is the photoluminescence intensity, τ_1 and τ_2 are the time constants of fast and slow decays, respectively, and A_1 and A_2 the weights of each process. The values for τ_1 and τ_2 were found to be 0.14 and 0.65 ms, respectively, with relative weights of 67 and 33%. Interestingly, when FA was added, no variation of the decay profiles could be detected and τ_1 and τ_2 remained constant (standard deviation of 0.01 and 0.03 ms, respectively) (Figure 94a). However, the luminescence intensity decreased with increasing amounts of added FA (Figure 94b).

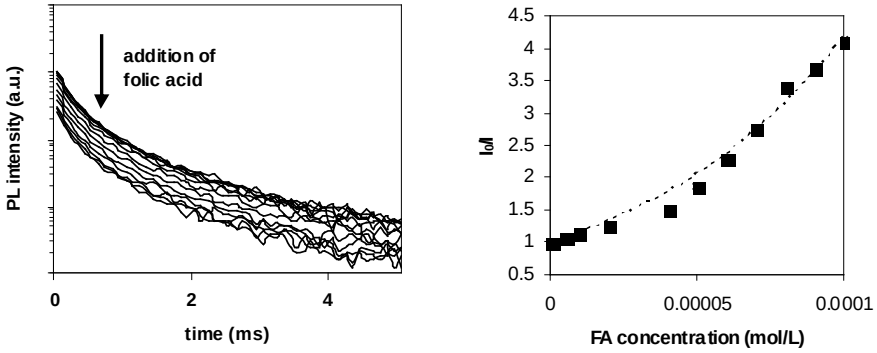

Figure 94. (a) PL decay and (b) corresponding plot of the FA concentration dependence of the PL intensities for ZnS:Mn/ZnS@MPA QDs. The broken line corresponds to an exponential fit following Perrin's model.

This situation is concordant with a static quenching mechanism [308], which implies the formation of a non-luminescent ground state complex. The corresponding Stern-Volmer plot up to 100 μM fits poorly with a linear function (correlation coefficient R = 0.975) (Figure 95a).

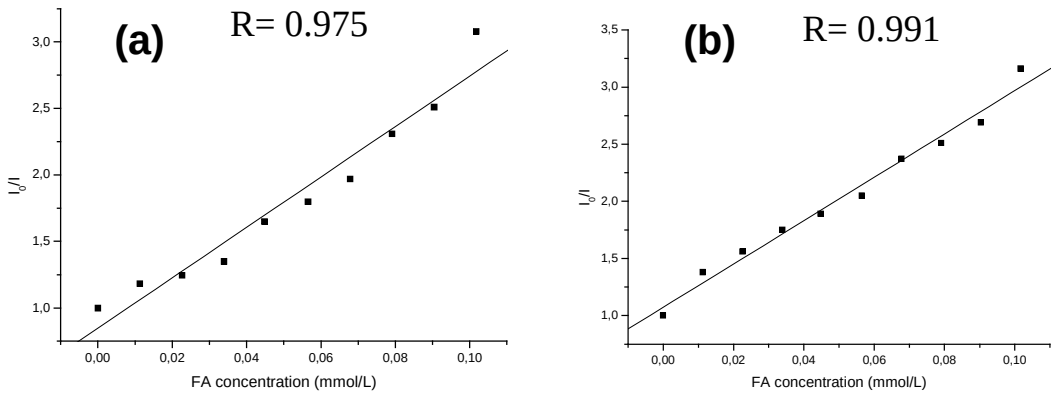

Figure 95. Stern-Volmer plots of the FA concentration dependence of the the PL intensities for (a) ZnS:Mn/ZnS@MPA and (b) ZnS:Cu/ZnS@MPA QDs up to 100 μM.

However, given the presence of multiple binding sites on the surface of the QDs and the probable non-specific nature of the complex, each QD probably interacts with more than one FA molecule to form $QD^*.FA_n$ complexes. The probability that one QD can be interacting with n FA molecules is better described by the Perrin's model:

$$I_0/I = \exp(Vq \times N_a \times [FA])$$

Equation 10. Perrin's model function describing the probability that the one QD interacts with n FA molecules [308].

where I_0 and I are the emission intensity in the absence and presence of the quencher, V_q is the volume of effective quenching, N_a is Avogadro's number, and [FA] is the concentration of FA. In contrast to Stern-Volmer equation, the ratio I_0/I is not linear [308]. This relation gives better results when applied to the variation of the initial intensity observed on the luminescence decays (Figure 94b) and yields a volume $V_q = 2.38\times10^{-23}$ m^3, corresponding to a sphere of ca. 18 nm radius, in which the excited state of Mn-doped ZnS QDs is instantaneously deactivated without emitting light.

The interference of FA with ZnS:Cu/ZnS@MPA QDs was found to be by ca. 30% less pronounced at low concentrations in FA (ca. 45 μM) in comparison to ZnS:Mn/ZnS@MPA QDs. Contrary to Mn-doped ZnS QDs, FA quenches the fluorescence of Cu-doped ZnS QDs with a concentration dependence that is best described by a Stern-Volmer equation [308]. This relation is given by the following equation:

$$I_0/I = 1 + K_{SV} \times [FA]$$

Equation 11. Formula illustrating Stern-Volmer relation [308].

where I_0 is the fluorescence intensity without FA, I is the fluorescence intensity observed in the presence of FA, K_{SV} is the Stern-Volmer constant and [FA] is the FA concentration. Generally, the ratio I_0/I is plotted against the quencher concentration (Stern-Volmer plot) [308]. As shown in Figure 95b, a good linearity (R = 0.991) between examined parameters is observed. K_{sv} is found to be 2.24×10^3 M^{-1}, the linear range was from 10 to 100 μM and the detection limit of FA was 1.13×10^{-6} $mol.L^{-1}$.
It should be considered that in Perrin's model at low concentrations the concentration dependance is almost linear (as in the case of the Stern-Volmer plot):

$$I_0/I = \exp(V_q \times N_a \times [FA]) \approx 1 + V_q \times N_a \times [FA]$$

Equation 12. Formula illustrating Perrin's model relation when $V_q \times N_a \times [FA]$ is small [308].

which could explain why in the case of the Cu-doped ZnS QDs, for which the quenching is less efficient, a linear relationship is observed.

The changes of PL intensity upon gradual addition of FA solution were also observed for ZnS:Mn@TG (Figure 93a) and ZnSe:Mn/ZnS@MPA (Figure 93b) QDs. The dependence of the PL intensity of these QDs vs the concentration of FA is also demonstrated as the points calculated for Stern-Volmer plot (Figures 93 b and d for ZnS:Mn@TG and ZnSe:Mn/ZnS@MPA QDs, respectively). Thus, the PL quenching appears also as a process driven by collisions between FA and the QDs and by the strong affinity of the two carboxylate groups and the nitrogen atoms of FA towards zinc atoms at the surface of QDs. The different behaviour of used QDs is the sign that the quenching mechanisms are quite complicated and differ one from another. Optimization experiments showed that the PL QY of various QDs is altered at different molar ratios of QDs to FA, namely 50% quenching of PL was observed for the ratio of QDs to FA of 1/0.013; 1/0.011, 1/0.007 and 1/0.16 for ZnS:Mn/ZnS@MPA, ZnS:Cu/ZnS@MPA (QDs not used in further conjugation with FA), ZnS:Mn@TG and ZnSe:Mn/ZnS@MPA QDs, respectively. Therefore, all the

coupling experiments were carried out with QD/FA/EDC/NHS molar ratios equal to 1/0.01/0.02/0.02; 1/0.005/0.01/0.01 and 1/0.1/0.2/0.2 for ZnS:Mn/ZnS@MPA, ZnS:Mn@TG, ZnSe:Mn/ZnS@MPA, respectively.

All QDs, namely ZnS:Mn/ZnS@MPA, ZnS:Cu/ZnS@MPA, ZnS:Mn@TG, ZnSe:Mn/ZnS@MPA prepared by aqueous route exhibit high fluorescence sensitivity to FA due to the high affinity of the carboxylate groups and nitrogen atoms of FA towards the Zn surface atoms of the doped dots.

The fluorescence sensor for FA is based on the fluorescence quenching of the doped dots. The Perrin's model and fluorescence lifetimes of ZnS:Mn@MPA QDs demonstrate a static quenching mechanism through the formation of non specific $QD.FA_n$ complexes until FA self-associate through H-bond donor and acceptor groups interactions at concentrations above 100 μM. Quenching efficiency of FA towards ZnS:Cu core QDs was found to be less pronounced and correlated with the classical Stern-Volmer model.

4.2.2. Surface functionalization of QDs with FA

The covalent anchorage of FA to the surface of core/shell ZnS:Mn/ZnS@MPA QDs was realized using 2,2'-(ethylenedioxy)-*bis*-ethylamine as a linker. One of the two amine groups was first reacted with an acid group present at the surface of QDs. This was achieved using 1-ethyl-3-(3-dimethylaminopropyl)carbodiimide hydrochloride (EDC) as crosslinking agent [314]. *N*-hydroxysuccinimide (NHS) was introduced in the reaction mixture to improve the efficiency of the EDC-mediated amide-forming reaction by producing hydrolysis-resistant active ester reaction intermediates [315]. After reaction, QDs were precipitated by adding ethanol. PEGamine-linked QDs were then redispersed in water and purified by successive precipitation-solubilisation rounds using ethanol as a bad-solvent. The fluorescence emission spectra of these QDs displayed the strong orange luminescence centered at 595 nm originating from Mn^{2+} ions on Zn^{2+} sites. A weak luminescence centered at 440 nm originating from ZnS defects could also be detected. The amine groups at the surface of QDs were in turn used to link FA through an additional amide bond formation mediated by EDC (Figure 96).

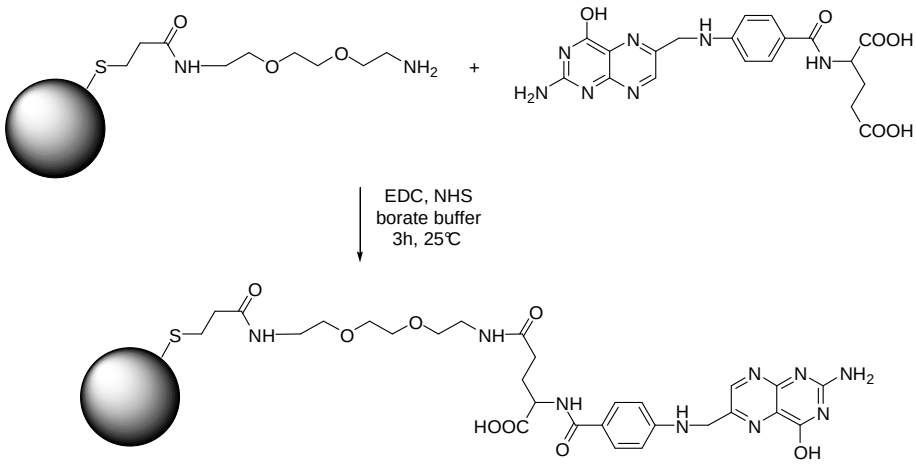

Figure 96. Synthesis of ZnS:Mn/ZnS@MPA QD-folic acid conjugate using a PEGamine linker.

Upon excitation at 270 nm, FA exhibits two fluorescence emissions at ca. 347 and 457 nm. These two peaks and the orange fluorescence originating from Mn^{2+} doping were detected after covalent anchorage of FA on ZnS:Mn/ZnS QDs (Figure 97).

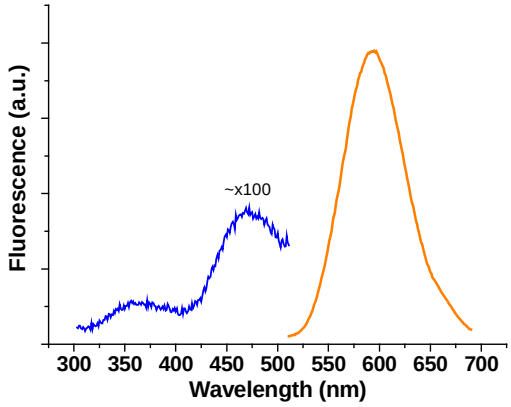

Figure 97. Room temperature photoluminescence spectrum of folic acid-conjugated ZnS:Mn/ZnS QDs after excitation at 270 nm. Two typical features can be distinguished, the strong orange emission of QDs at ca. 590 nm and the much weaker emissions of folic acid at 357 and 470 nm.

FA-conjugated ZnSe:Mn@MPA QDs were prepared in the similar manner.

The covalent anchorage of folic acid to the surface of ZnS:Mn@TG QDs was realized by direct reaction of NCs with FA. Similarly like in the case of ZnS:Mn/ZnS@MPA QDs, this was achieved by use of EDC and NHS (Figure 98). After reaction, QDs were precipitated by adding ethanol. FA-linked QDs were then redispersed in water and purified by successive precipitation-solubilisation rounds using ethanol as a bad-solvent.

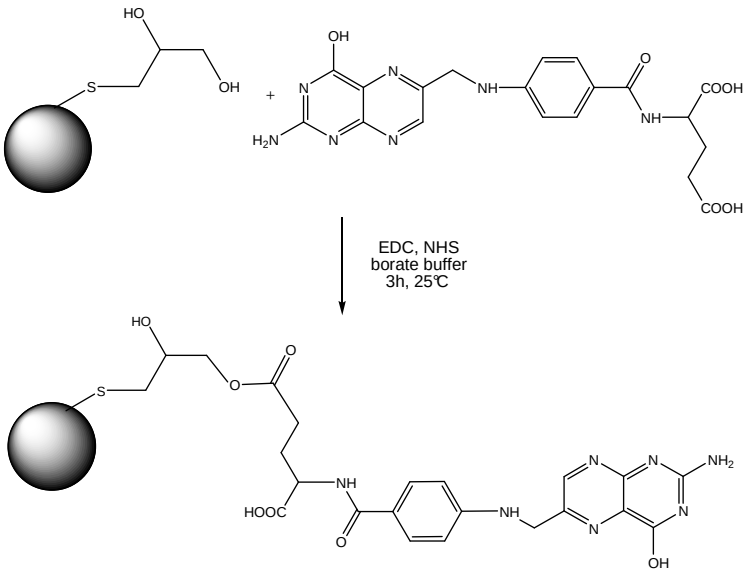

Figure 98. Synthesis of ZnS:Mn@TG QD-folic acid conjugate.

4.2.3. Size, shape, crystal structure and PL properties of FA-functionalized ZnS:Mn QDs

4.2.3.1.FA-functionalized ZnS:Mn/ZnS@MPA core/shell QDs

The optical characteristics of the PEGamine and FA-linked QDs resemble those of core/shell ZnS:Mn/ZnS@MPA QDs and are presented in Figure 99.

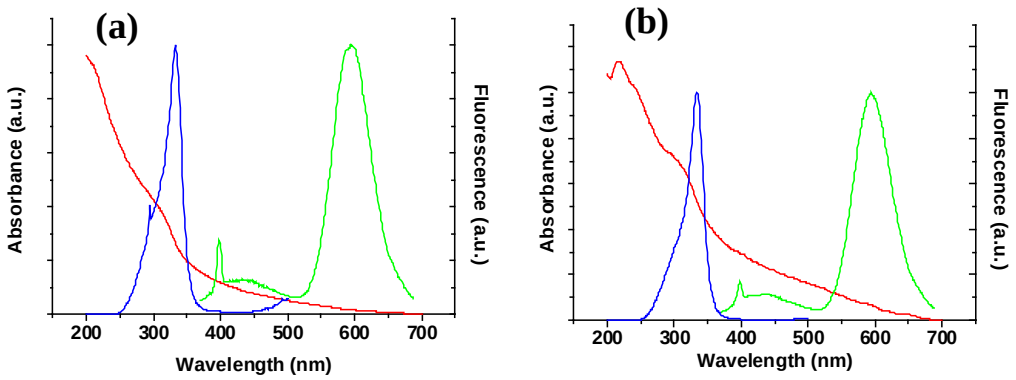

Figure 99. Room temperature absorption (red line), excitation (blue), and photoluminescence (green) spectra after excitation at 320 nm of (a) PEGamine-linked and (b) FA-conjugated ZnS:Mn/ZnS@MPA QDs dispersed in water.

Figure 100 shows the XRD patterns of FA-functionalized ZnS:Mn/ZnS@MPA QDs.

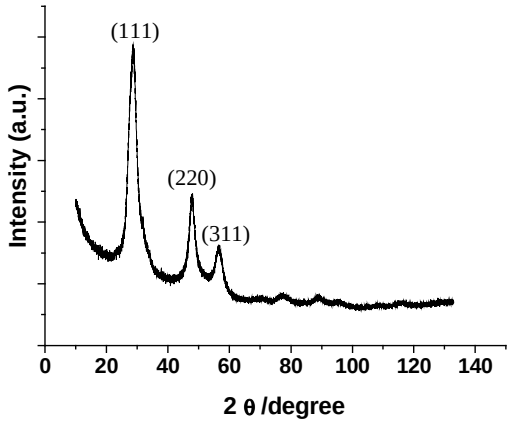

Figure 100. XRD peak patterns for folic acid-functionalized ZnS:Mn/ZnS@MPA QDs using 2,2'-(ethylenedioxy)-*bis*-ethylamine as the linker.

All of the XRD peaks can be indexed to the cubic zinc blende structure of ZnS and are consistent with the standard cubic bulk ZnS peak position from JCPDS file N°. 77-2100. The three main peaks correspond to the (111), (220), and (311) planes. It

can be observed that these peaks are broadened compared to bulk ZnS, thus confirming the nanocrystalline nature of all the samples. A crystallite size of 4.2 ± 1.0 nm was deduced from XRD data (see Figure 56). The calculated lattice constant a for Mn-doped ZnS QDs was determined to be 0.5388 ± 0.0003 nm, slightly different from pure ZnS NCs (a = 0.5386 nm measured with a internal standard Diamond). The deviation in the lattice constant observed for ZnS:Mn QDs probably originates from substitution of Zn^{2+} by Mn^{2+} ions in the crystal structure since the diameter of the Mn^{2+} ion (0.083 nm) is larger than that of the Zn^{2+} ion (0.074 nm) [288].

Transmission electron microscopy (TEM) images of 2,2'-(ethylenedioxy)-*bis*-ethylamine functionalized ZnS:Mn/ZnS QDs and FA-conjugated ZnS:Mn/ZnS QDs are shown on Figure 101.

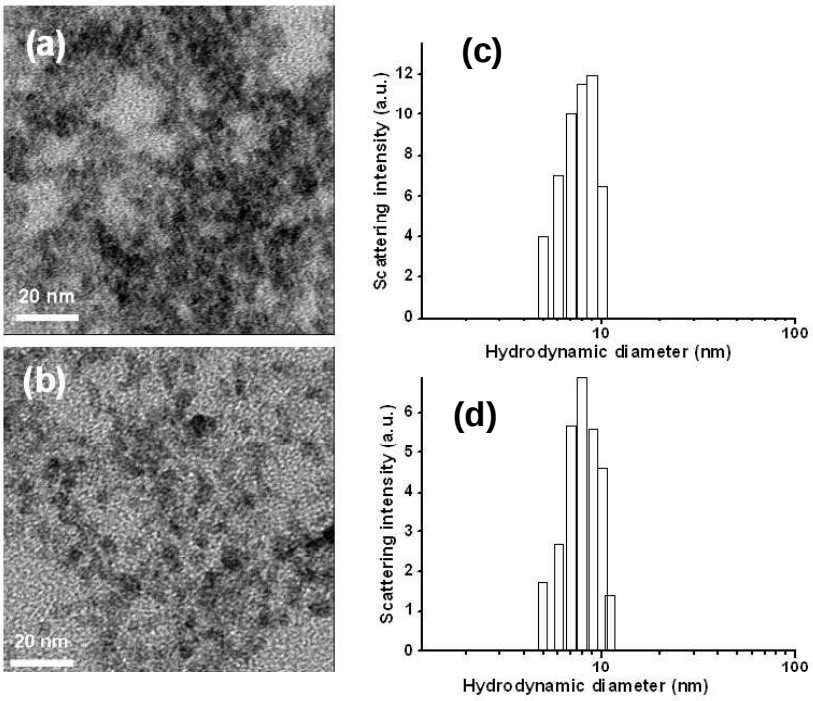

Figure 101. Bright field TEM micrographs and average diameters D of (a) PEGamine-linked ZnS:Mn/ZnS@MPA QDs, D = 4.6 ± 0.5 nm, and (b) folic acid-functionalized ZnS:Mn/ZnS@MPA QDs, D = 5.2 ± 1.0 nm. (c) and (d), the corresponding intensity-hydrodynamic size distribution graphs of QDs in water at 25°C.

All particles appear spherical in shape and surface functionalization with the diaminoPEG and FA did not induce aggregation (*vide infra*). The average diameters and the standard deviations of diaminoPEGs functionalized ZnS:Mn/ZnS QDs and FA-conjugated ZnS:Mn/ZnS QDs are 4.6 ± 0.5, and 5.2 ± 1.0 nm, respectively. For all QDs, the diameters estimated from TEM images are

in good agreement with those calculated from the absorption edge (ca. 5.4 ± 0.4 nm) and X-ray diffraction studies (4.2 ± 1.0 nm). The size and size-distribution of pegylated ZnS:Mn/ZnS@MPA and FA-functionalized ZnS:Mn/ZnS@MPA QDs were also examined by Dynamic Light Scattering (DLS). Figure 101c and d show the scattering intensity distributions of these NCs dispersed in water at rt. The two batches were found to be quite aggregate-free. The average hydrodynamic sizes determined from DLS data were 9.1 and 9.5 nm, for the 2 QDs samples respectively, thus suggesting that NPs dispersed well in water. The hydrodynamic diameters were larger than those of the cores due to the solvatation layer around QDs in aqueous solution.

The X-ray photoelectron spectroscopy (XPS) scan survey of the FA-functionalized core/shell ZnS:Mn/ZnS@MPA sample shows the peaks of Zn, S, Mn, O, C, Na elements and comparing with not modified ZnS:Mn@MPA/ZnS QDs (see Figure 58) additional signal of N 1s is observed (Figure 102b). The binding energies of Zn $2p_{3/2}$ and S 2p were only weakly affected by the covalent anchorage of 2,2'-(ethylenedioxy)-*bis*-ethylamine and FA at the surface of NCs and appeared respectively at 1021.8 and 161.8 eV. A broad signal was observed for Mn 2p at 640.6 eV (Figure 102a).

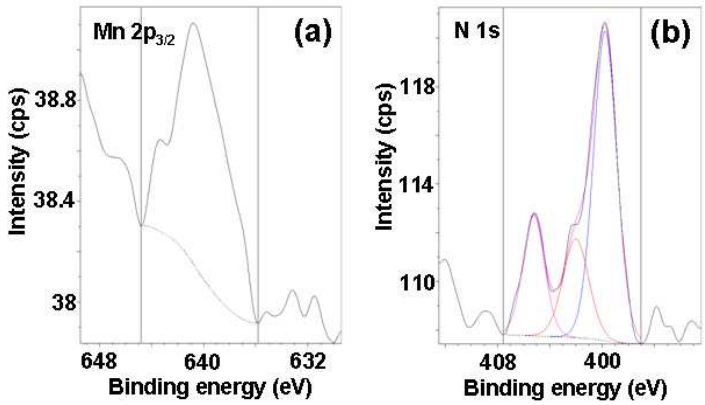

Figure 102. XPS spectra of folic acid functionalized ZnS:Mn/ZnS@MPA QDs using 2,2'-(ethylenedioxy)-*bis*-ethylamine as linker. The Mn 2p3/2 and N 1s emissions are presented.

The Mn/Zn atomic ratio dropped to 0.036, which can be explained by the formation of the organic shell around the ZnS:Mn/ZnS QDs. The deconvoluted peaks at 399.7 and 402.0 eV correspond respectively to the primary and secondary nitrogen atoms and to the amide nitrogens. The peak at 405.2 eV can be attributed to oxidized nitrogen species that might be formed during air exposure of the sample. Using a cubic blende crystal structure for ZnS with a lattice parameter a =

0.5388 nm, a 4.7 nm wide core/shell ZnS:Mn/ZnS nanocrystal should contain ca. 350 ZnS elemental lattices (ca. 1400 Zn atoms). Assuming a spherical geometry for doped-ZnS QDs and an interplanar distance d (thickness of one monolayer of surface atoms in each NC) of 0.31 nm, the volume occupied by surface atoms V_{SA} per QD can be determined by Equation 13, where r is the QD radius.

$$V_{SA} = 4/3\ \pi\ [r^3 - (r\text{-}d)^3]$$

Equation 13. Formula for calculation of the volume occupied by surface atoms V_{SA} per QD.

It was assumed that this spherical shell of surface atoms has the same density as bulk ZnS, and therefore the number of surface atoms per NC could be calculated using Equation 14:

$$n_{SA} = 2\ \frac{V_{SA} \times D \times N_A}{MW_{ZnS}}$$

Equation 14. Formula for the calculation of the number of surface atoms per nanocrystal.

where n_{SA} is the number of surface atoms per QD, D is the bulk density of zinc blende ZnS (4.1 g/cm^3), N_A is Avogadro's number, MW is the molecular weight of ZnS, and 2 is a factor accounting for 2 atoms per molecule of ZnS. The number of Zn^{2+} atoms at the surface was found to be 433. The N/Zn atomic ratios obtained from XPS analyses showed that one QD is covered by ca. 45 2,2'-(ethylenedioxy)-*bis*-ethylamine units and ca. 11 folic acid molecules.

The electric potential, referred to as zeta potential ζ, which controls the colloidal stability and interparticles interactions, was also determined. The NCs show a strong decrease of the ζ potential (-26 ± 4 mV) after the covalent anchorage of the diaminoPEG comparing with ZnS:Mn/ZnS@MPA QDs (-45 ± 5 mV), suggesting that a part of the MPA ligand on particles surface have been coupled with the diaminoPEG linker. Note also that a positive charge will appear on the primary amine end group of the linker at neutral pH. After coupling with FA, the ζ potential of the QDs increases slightly (-34 ± 5 mV) because FA ligands will bear a negative charge due to the ionization of its α-carboxylic group.

The covalent anchorage of FA at the surface of QDs was also qualitatively demonstrated by thin layer chromatography (TLC). MPA, PEGamine and FA-functionalized QDs were completely hydrolyzed by heating at 100°C for 24 h in a 5.5 M HCl solution. After evaporation of the solvents, the dry residues were redissolved in water for TLC analysis. Figure 103 shows a photograph of the TLC plate on which the ligands (PEGamine and FA), their acid hydrolysis products, compounds arising from the hydrolysis of QDs and reference compounds have been deposed.

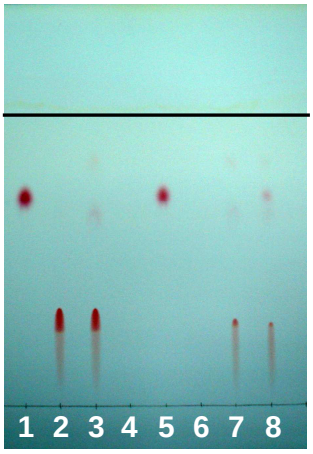

Figure 103. Photograph of the silica gel TLC plate used to demonstrate the presence of FA at the periphery of QDs. The samples were loaded on the bottom part of the plate, eluted using a 3:1:1 (v/v/v) n-butanol/acetic acid/water, and revealed with nihydrin. The 8 lanes correspond to (1) commercial glutamic acid, (2) commercial PEGamine, (3) PEGamine after acid hydrolysis, (4) commercial folic acid, (5) folic acid after acid hydrolysis, (6) ZnS:Mn/ZnS@MPA QDs after acid hydrolysis, (7) PEGamine-functionalized ZnS:Mn/ZnS QDs after acid hydrolysis, and (8) folic acid-functionalized ZnS:Mn/ZnS QDs after acid hydrolysis.

Using a *n*-butanol/acetic acid/water mixture as the eluent (3:1:1 v/v/v) and nihydrin as a revelator, γ-glutamic acid, resulting from the hydrolysis of FA, and PEGamine were clearly observed as a pink spot on the TLC plate after decomposition of FA-conjugated QDs.

4.2.3.2.FA-functionalized ZnS:Mn@TG core QDs

Figure 104 presents UV-vis, PL and PL excitation (PLE) spectra of ZnS:Mn@TG d-dots.

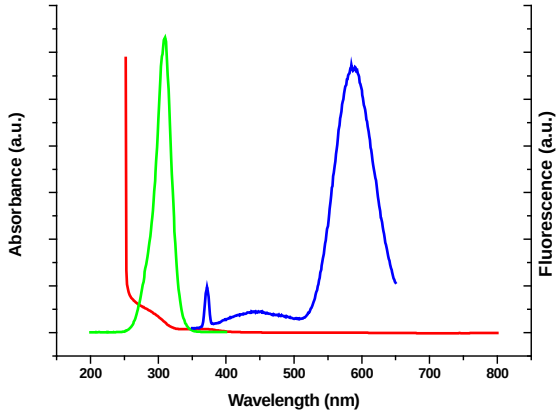

Figure 104. Optical absorption (red line), PL excitation (green) and PL emission (blue) after excitation at 330 nm of TG-capped ZnS:Mn d-dots.

The quantum confinement of an electron-hole pair caused a blue-shift in the absorption peak of ZnS:Mn@TG QDs obtained after 20 h of heating at 100 ºC in comparison to the 336 nm (3.67 eV) band gap of the bulk ZnS material.

Figure 105 shows the XRD patterns of the FA-functionalized ZnS:Mn@TG QDs.

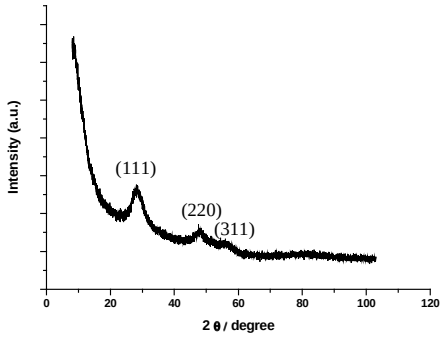

Figure 105. XRD peak patterns for folic acid- functionalized ZnS:Mn@TG QDs.

The XRD peaks can be indexed to the cubic zinc blende structure of ZnS and are consistent with the standard cubic bulk ZnS peak position from JCPDS file Nº 77-2100. The three main peaks corresponds to the (111), (220), and (311) planes.

Transmission electron microscopy (TEM) image of folic acid-functionalized ZnS:Mn@TG QDs is shown in Figure 106.

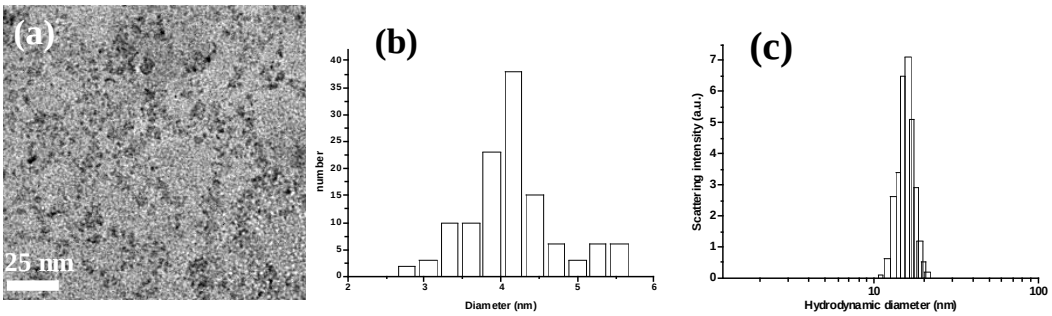

Figure 106. (a) Bright filed TEM micrograph, (b) the corresponding average diameter, and (c) hydrodynamic size of folic acid-functionalized ZnS:Mn@TG d-dots measured by DLS.

All particles appear spherical in shape and surface functionalization with the FA did not induce aggregation (*vide infra*). The average diameter and the standard deviation of FA- conjugated ZnS:Mn@TG is 4.2 ± 0.7 nm.

The X-ray photoelectron spectroscopy (XPS) scan survey of the FA-conjugated ZnS:Mn@TG sample shows the peaks of Zn, S, C, O, Na and additional signal from N compared to non-modified ZnS:Mn@TG QDs which proves the successful conjugation of FA (Figure 107).

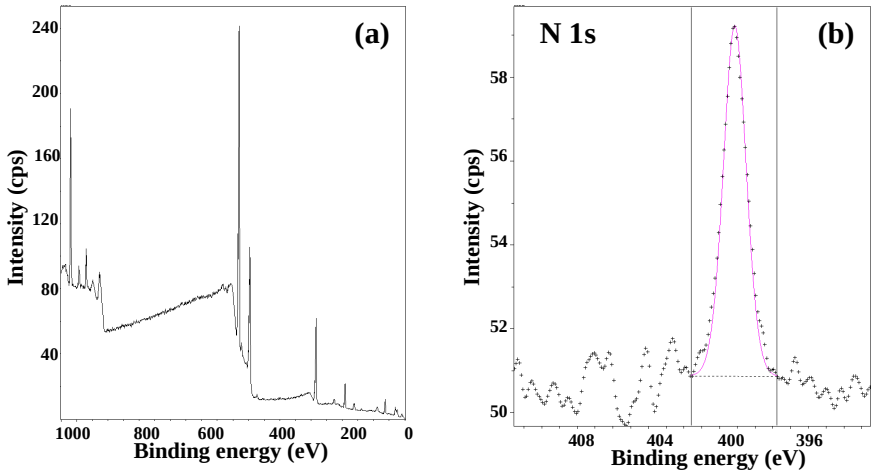

Figure 107. (a) XPS survey scan of folic acid-conjugated ZnS:Mn@TG QDs. (b) The N 1s emission is presented.

The covalent anchorage of FA at the surface of QDs was also qualitatively demonstrated by thin layer chromatography (TLC). TG-capped and FA-functionalized QDs were completely hydrolyzed by heating at 100°C for 24 h in a 5.5 M HCl solution. After evaporation of the solvents, the dry residues were redissolved in water for TLC analysis. Figure 108 shows a photograph of the TLC plate on which FA, its acid hydrolysis products, compounds arising from the

hydrolysis of TG-capped and FA- functionalized QDs and reference compound have been deposed.

Figure 108. Photograph of the silica gel TLC plate used to demonstrate the presence of FA at the periphery of QDs. The samples were loaded on the bottom part of the plate, eluted using a 2.5:1:1:1.5 (v/v/v/v) methanol/acetic acid/water/acetonitrile, and revealed with nihydrin. The 5 lanes correspond to (1) TG-capped ZnS:Mn QDs after acid hydrolysis, (2) commercial glutamic acid, (3) commercial folic acid after acid hydrolysis, (4) commercial folic acid, (5) FA-functionalized ZnS:Mn@TG QDs after acid hydrolysis.

Using a methanol/acetic acid/water/acetonitrile mixture as the eluent (2.5:1:1:1.5 v/v/v/v) and nihydrin as a revelator, γ-glutamic acid, resulting from the hydrolysis of FA was clearly observed as a pink spot on the TLC plate after decomposition of FA-conjugated QDs.

As-prepared FA-functionalized ZnS:Mn/ZnS@MPA and ZnS:Mn@TG QDs are used as bioimaging probes for the detection of cancer cells in further work. However, due to the fact that all kinds of such new nanoprobes must be safe to the biological environment, the cytotoxicity of prepared NCs was evaluated, including ZnSe:Mn@MPA QDs, which are expected to be more toxic due to the inherent selenium element.

4.3. Evaluation of the cytotoxicity of Mn-doped QDs

As the toxicity concerns are very important for the future biological applications of new nanoprobes such as semiconductor QDs, in this paragraph the results demonstrating QDs cytotoxicity to different human cancer cells are described. The cytotoxicity of three types of earlier-synthesized Mn-doped QDs was examined. The cell lines used as the targets were T47D cells (as the ones that express folate receptor (FR)) [316], and MCF-7 and PC-3 cells (that only weakly express the FR) as references [317, 318]. T47D and MCF-7 cells are human breast cancer cells, and PC-3 are prostate cancer cells.
The paragraph is divided into 3 subsections schematically shown in Tabel 9.

Tabel 9. Scheme of cytotoxicity tests performed with different types of synthesized QDs

Steps of cytotoxicity evaluation	Material	Examined cells	Test
1	Bare and modified ZnS:Mn@MPA	T47D and MCF-7	MTT
2	Bare and modified MPA-capped ZnSe:Mn@MPA QDs	T47D	MTT
3	Bare and FA-conjugated ZnS:Mn@TG QDs	T47D	MTT
		T47D and PC-3	XTT
		T47D	FOXO

The MTT assay is a colorimetric assay based on the ability of viable cells to reduce a soluble yellow tetrazolium salt, (3-(4,5-dimethylthiazol-2-yl)-2,5-diphenyltetrazolium bromide (MTT)), to blue formazan crystals [271].

Recently, the MTT alternatives were developed by introducing positive or negative charges and hydroxyl or sulfonate groups to the phenyl ring of the tetrazolium salt. In XTT test, one of such compounds is used, namely XTT (2-methoxy-4-nitro-5-sulfophenyl)-5-[(phenylamino)-carbonyl]-2H-tetrazolium hydroxide) yielding higher sensitivity. Additionally, the formed formazan dye is water-soluble, avoiding a final solubilisation step.

Another assay applied in this work for evaluation of QDs cytotoxicity is the test in which H_2O_2 concentration is measured in medium of cells after exposition to QDs. The peroxide concentrations were measured by a modification of the ferrous oxidation-xylenol orange (FOXO) assay [272] adapted to microtiter plated by Dringen *et al.* [273] and with some modification in comparison to Gülden *et al.* [274]. This assay is based on the ability

of peroxides to oxidize the ferrous Fe^{2+} ions to ferric Fe^{3+} ions, which react with xylenol orange to a colored complex.

QD-induced cytotoxicity was investigated in a chronic exposure paradigm at concentrations above and below the optimal level for confocal microscopy (ca. 500 μM).

4.3.1. Cytotoxicity of MPA-capped ZnS:Mn QDs evaluated by MTT test

In the MTT assay, the FR+ T47D cells were grown for up to 72 h with the medium containing core, core/shell, PEG-modified, and FA-conjugated Mn-doped ZnS@MPA QDs with the final concentration ranging from 0 to 5000 μM (Figure 109). All MTT assays demonstrated that the cytotoxicity of QDs correlated with their concentration, the viability of cell growth was decreased with the increasing QD concentration.

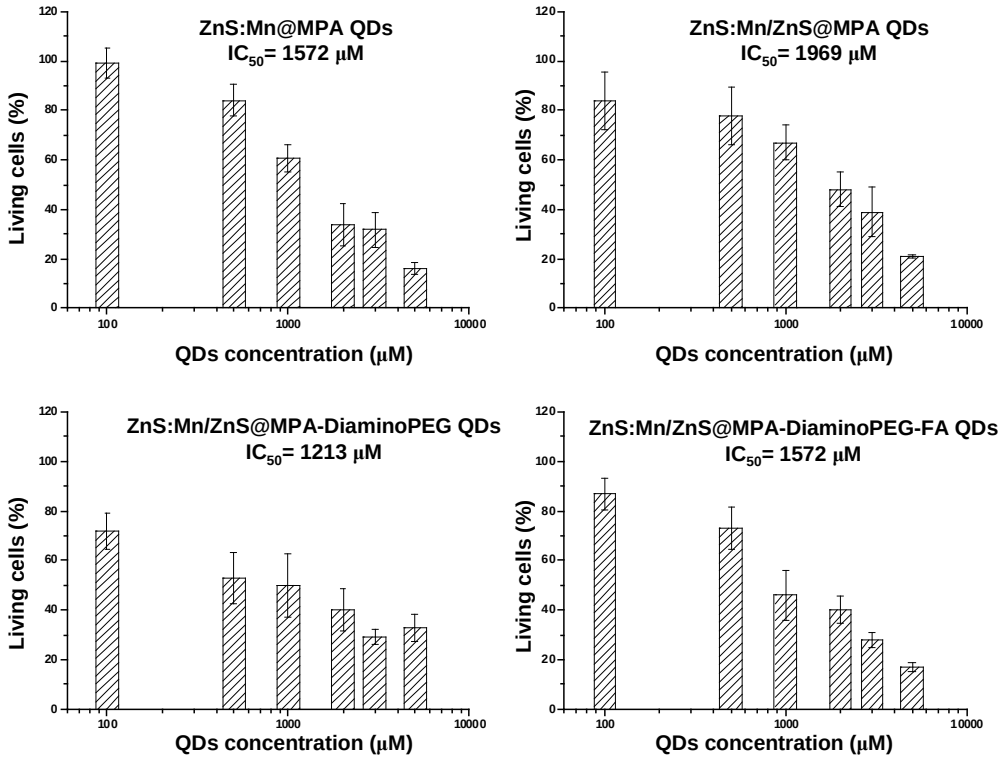

Figure 109. Cytotoxicity of ZnS:Mn@MPA core QDs toward FR+ T47D cells for 72 h at 37°C measured by MTT assay. Each value is averaged on a series of 3 experiments.

At concentration of 100 μM, QDs had little influence on cell growth and development. Thus, when used at low dose, these QDs did not exhibit discernable adverse effects on the targeted cells *in vitro* compared with the same cells not exposed

to QDs. IC_{50} values determined for core, core/shell, PEGamine-linked QDs and FA-conjugated ZnS:Mn@MPA QDs after 72 h incubation are 1.57, 1.96, 1.21 and 1.57 mM, respectively. From the obtained results two things can be concluded. Primarily, IC_{50} values obtained for core and core/shell MPA-capped ZnS demonstrate that the ZnS shell is important for lowering the toxicity and protect the cells from QDs. Secondly, it should be noticed that these QDs are toxic at high concentration close to 5 mM causing nearly 60-80% decrease of cell viability.

Results obtained with MPA-capped ZnS QDs covered by diaminoPEG ligand indicate that as-modified QDs are more toxic that unmodified-ones. It is not surprising since cationic QDs are known to be significantly more cytotoxic than anionic ones [207, 319]. As recently observed with FA-conjugated CdS QDs [320], FA-linked ZnS:Mn/ZnS QDs were found to be more toxic than the parent non-conjugated QDs. This observation highlights the critical role played by the surface chemistry and the enhanced interaction of FA-conjugated QDs towards T47D cells. It is assumed that the concentration of dissolved elements originating from QDs and the production of reactive oxygen species (ROS) is enhanced in the intracellular compartments of T47D with FA-linked QDs, leading to the difference in toxicity levels observed.

To compare the cytotoxic behaviour of ZnS:Mn@MPA QDs on different cell lines, the MTT test was also performed using MCF-7 cells. The cells were grown for up to 72 h with the medium containing Mn-doped ZnS@MPA core QDs (Figure 110), with the final concentration ranging from 0 to 3000 μM. In this way the critical role of the intracellular concentration of ZnS:Mn@MPA QDs on their cytotoxicity was confirmed.

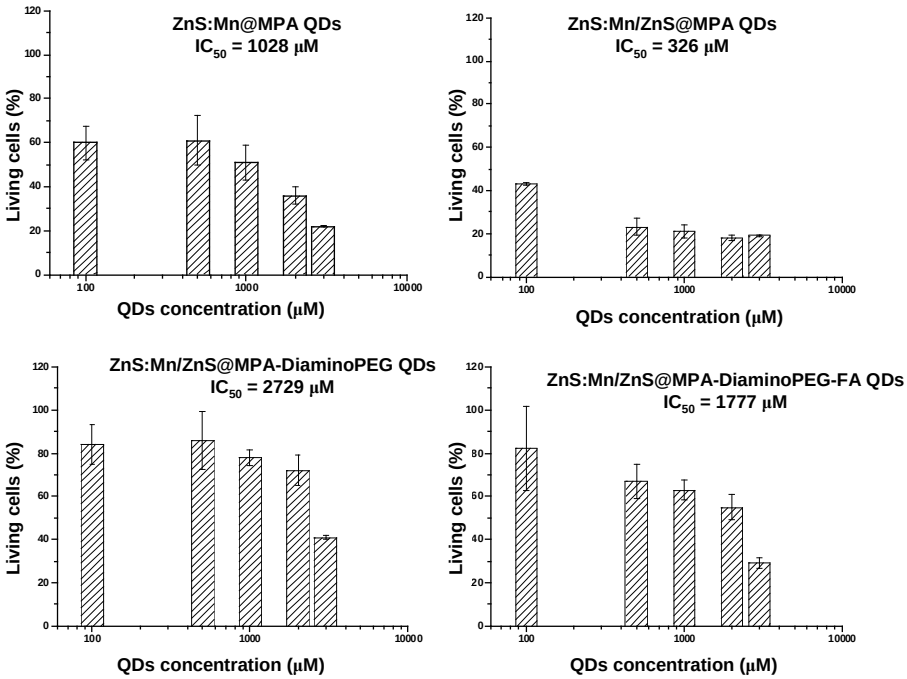

Figure 110. Cytotoxicity of ZnS:Mn core QDs toward MCF-7 cells for 72 h at 37°C measured by MTT assay. Each value is the average of a series of three experiments.

Uncapped ZnS:Mn/ZnS@MPA were found to be the most toxic to cells (IC_{50} = 0.326), while PEGamine- and FA-conjugated core/shell ZnS:Mn/ZnS QDs did not significantly alter cell growth at concentrations below 500 μM (the IC_{50} values are 2.729 and 1.777 mM after 72 h incubation, respectively). These results clearly point out the changes in nature of the interaction between QDs and the two cells lines, thus inducing marked differences in their cytotoxicity levels.

4.3.2. Cytotoxicity of MPA-capped ZnSe:Mn QDs evaluated by MTT test

In the MTT assay, the FR+ T47D cells were grown for up to 72 h with the medium containing core, core/shell, PEG-modified, and FA-conjugated Mn-doped ZnSe@MPA QDs at the final concentration ranging from 0 to 5000 μM (Figure 111). All MTT assays demonstrated that the cytotoxicity of QDs correlated with their concentration, the viability of cell growth was decreased with the increasing QD concentration.

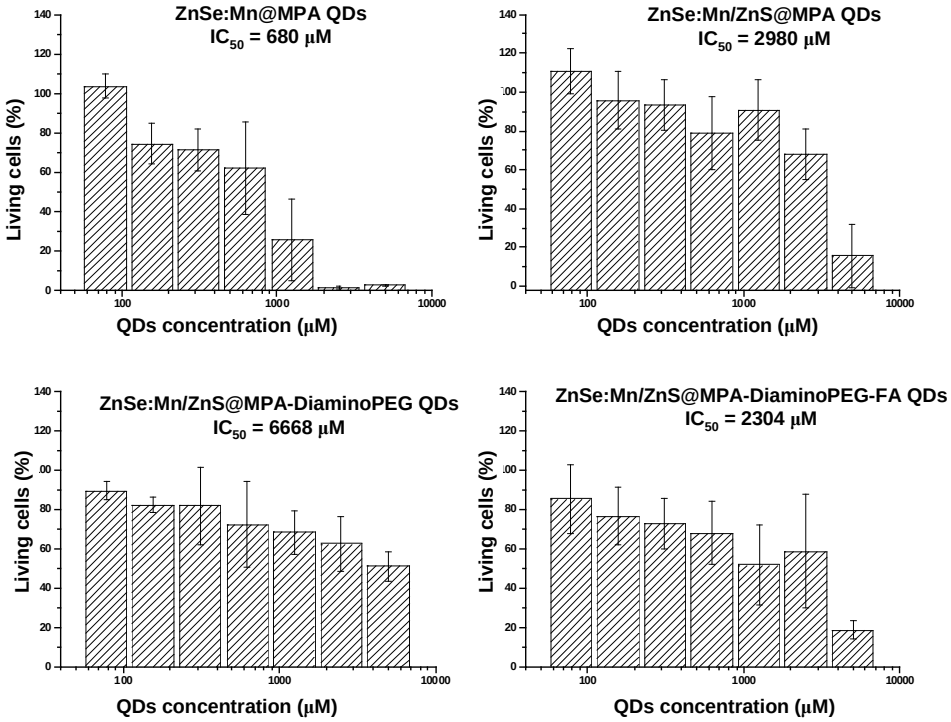

Figure 111. Cytotoxicity of ZnSe:Mn core QDs toward FR+ T47D cells for 72 h at 37ºC measured by MTT assay. Each value is the average of a series of six experiments.

At concentrations below 100 μM, QDs had little or even no influence on cell growth and development. The IC_{50} values for core, core/shell, PEGamine-linked QDs and FA-conjugated ZnSe:Mn@MPA QDs after 72 h of incubation are 0.680, 2.98, 6.68 and 2.30 mM, respectively. Obtained results confirm the role of ZnS shell in lowering the cytotoxicity and protecting the cells from QDs. These QDs are very toxic at high concentration close to 5 mM causing nearly 80% decrease in cells viability, excluding PEG-modified NCs.

Results obtained with MPA-capped ZnSe:Mn QDs covered by the diaminoPEG ligand differ from the ones obtained with MPA-capped ZnS:Mn QDs (see Figure 109). Contrary to ZnS:Mn QDs, in the case of ZnSe:Mn QDs such modification caused lower toxicity. This decrease of ZnSe:Mn cytotoxicity after modification with DiaminoPEG is surprising. However, it should be taken into account that the elemental composition of the core of these QDs is different and due to this fact the cytotoxic mechanism after PEG-conjugation may differ. Additionally, it should be noticed that after modification with FA, the IC_{50} value for these QDs diminished twice.

4.3.3. Cytotoxicity of TG-capped ZnS:Mn QDs evaluated by MTT, XTT and ferrous oxidation-xylenol orange (FOXO) assay

In the MTT assay, the FR+ T47D cells were grown for up to 72 h with the medium containing core and FA-conjugated Mn-doped ZnS@TG QDs with the final concentration ranging from 0 to 5000 μM (Figure 112).

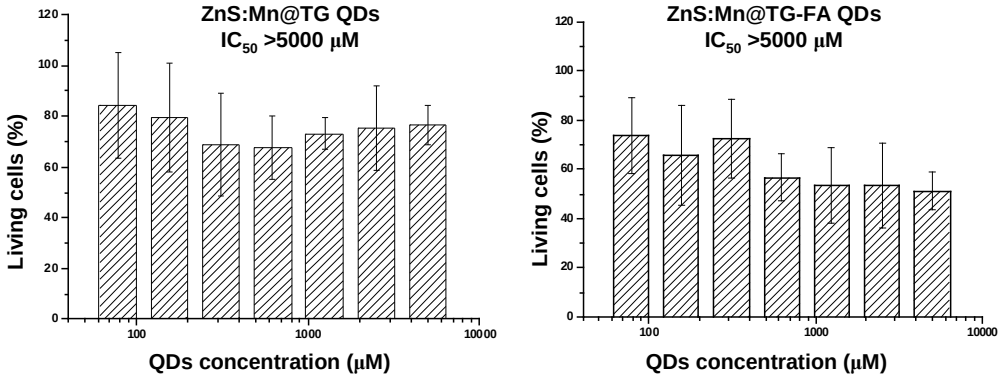

Figure 112. Cytotoxicity of ZnS:Mn@TG QDs toward FR+ T47D cells for 72 h at 37°C measured by MTT assay. Each value is averaged on a series of 6 experiments.

At the wide range of concentrations used, QDs had little influence on cell growth and development. Thus, when used at concentration up to 5 mM, these QDs did not exhibit discernable adverse effects on the targeted cells *in vitro* compared with the same cells not exposed to QDs. IC_{50} values determined for core and FA-conjugated ZnS:Mn@TG QDs after 72 h incubation overcome 5 mM. The obtained results demonstrate than TG-capped ZnS:Mn QDs are the safest NCs and even at high concentration do not cause much changes in cell viability.

To verify these results the cytotoxicity of core and FA–conjugated ZnS:Mn@TG QDs was also checked by use of XTT cell proliferation assay. T47D and PC-3 cells were grown for 24 h and after this time different concentrations (80-1250 mM) of ZnS:Mn@TG and ZnS:Mn@TG-FA QDs were added. Figure 113 demonstrates the results obtained in this assay.

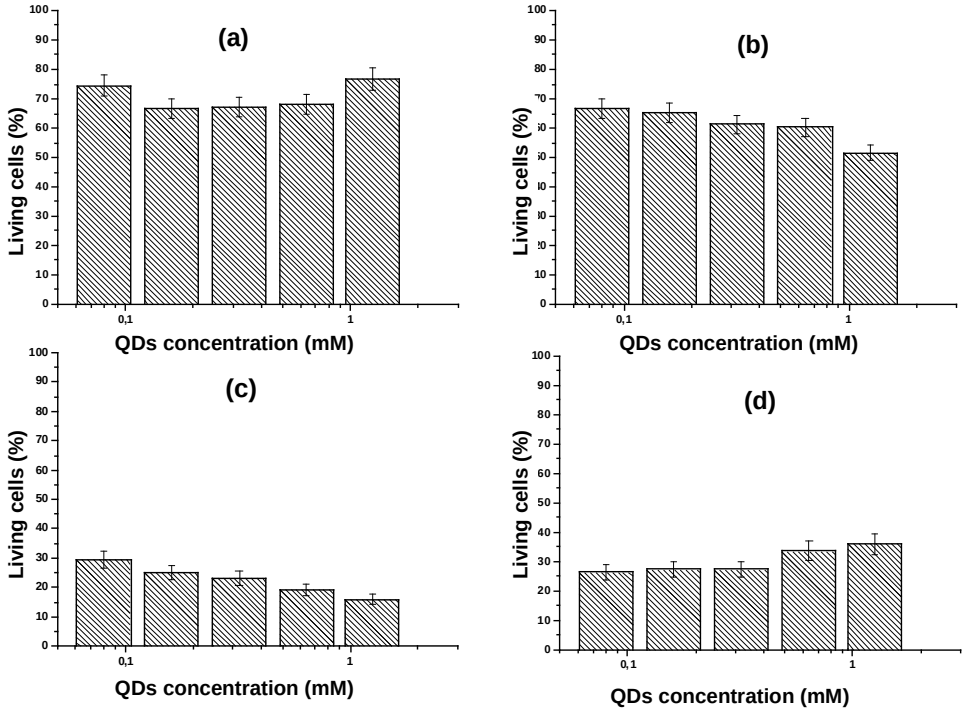

Figure 113. Cytotoxicity of (a, c) ZnS:Mn@TG and (b, d) FA-conjugated ZnS:Mn@TG QDs toward (a, b) T47D and (c, d) PC-3 cells for 72h at 37°C measured by XTT assay. Each value is the average of a series of three experiments.

It can be seen that the response of two different cell lines to the same concentration of bare and FA-functionalized TG-capped QDs is different. The results of the experiment performed on T47D cells correspond to the results obtained in MTT assay (see Figure 112) in which FA-conjugated QDs are a little bit more toxic than non-modified QDs, however general cytotoxicity of both types of these NCs is not marked. Interestingly, the response of PC-3 cells is much more pronounced and even in low concentration such as 80 µM the decrease of cell viability overcoming 70% is observed. It can be noticed that with increasing QDs concentration, TG-capped QDs are slightly more toxic while the cytotoxicity of FA-conjugated QDs slightly decreases.

The last test applied for evaluation of TG-capped QDs cytotoxicity was FOXO assay. T47D cells grown for 24 h were used to measure the concentration of H_2O_2 after exposition to bare and FA -modified ZnS:Mn@TG QDs (0.08-5 mM) in DMEM culture medium over time. The concentration of peroxides was determined using standard peroxide solutions. Standard peroxide solutions (3.125-50 µM) were freshly prepared solution of hydrogen peroxide in the same culture medium that was used to incubate the cells with QDs. The equation of calibration curve obtained was as follows: A= 0.026C - 0.008, where A is the value of absorbance at 570 nm, and C is

the concentration of H_2O_2 (µM). The R^2 value was equal to 0.996. Figure 114 shows the results obtained in ferrous oxidation-xylenol orange assay.

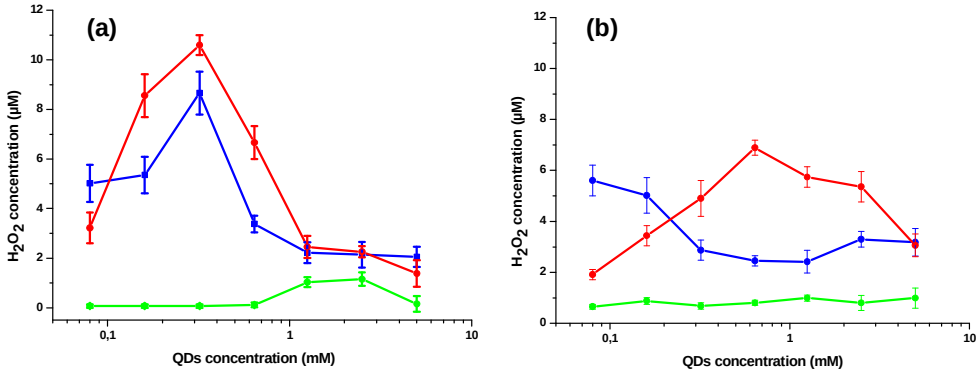

Figure 114. Concentration of H_2O_2 determined in medium of T47D cells after exposition to (a) ZnS:Mn@TG and (b) FA-conjugated ZnS:Mn@TG QDs for 1 h (blue line), 4 h (red) and 24 h (green). Each value is the average of a series of three experiments.

It can be concluded that the production of peroxides in the cell medium is more pronounced in the case of TG-capped ZnS:Mn QDs (max. 11 µM H_2O_2 concentration) in comparison to FA-modified ones (max. 7 µM H_2O_2 concentration). Additionally, it can be noticed that the peroxides presence is much more developed in first hours of exposition to QDs (1-4 h) than after 24 h. In the case of ZnS:Mn@TG QDs the peroxide production is the most extensive for ~300 µM QDs concentration in first few hours, while in case of FA-conjugated QDs at the beginning of exposition to QDs, the peroxides production is intensive at lower concentrations and then, after 4 h of exposition, it is more pronounced at ~700 µM concentration of QDs.

The results of cytotoxicity assays indicate very low toxicity of ZnS:Mn@TG capped QDs in comparison with ZnS:Mn@MPA and ZnSe:Mn@MPA QDs. It can indicated that not only elemental composition of QDs core but also the different surface chemistry can play a crucial role in mechanisms involved in QDs cytotoxicity. It should be noticed that both types of MPA-capped QDs (ZnS and ZnSe core) are less toxic to T47D cells when the core is covered with the ZnS shell. Using the same QDs type (MPA-capped ZnS:Mn QDs) and concentration but two different cell lines, the cytotoxicity assays results differ, which means that also the type of cells plays a role when treated by different NCs. The results of ZnS:Mn@TG cytotoxicity obtained in XTT cell proliferation assay on T47D cells correspond well to the results obtained in MTT test. However, the cytotoxicity of these QDs on PC-3 cells was much higher

even at low QDs concentrations (80 μM). The results obtained in FOXO assay indicate that the production of peroxides in cell culture medium exposed to QDs is higher during the first hours of experiment.

Due to the results obtained in described different cytotoxicity tests, FA-conjugated ZnS:Mn QDs capped by TG and MPA were chosen as the potential labels for cancer cells overexpressing FR on their surface what is the subject of next paragraph.

4.4. Imaging experiments using Mn-doped ZnS nanocrystals

In this paragraph the use of FA-functionalized ZnS core QDs as potential labels for cancer cells is presented. There are two subsections of this paragraph:

- Describing the bioimaging results obtained by use of MPA-capped ZnS:Mn QDs
- Describing studies with TG-capped ZnS:Mn QDs and additional organic fluorophores.

In all performed imaging experiments QDs were excited bifotonically.

4.4.1. MPA-capped ZnS:Mn QDs as fluorescent nanoprobes for bioimaging of T47D and MCF-7 cancer cells

As mentioned in chapter 1, two-photon absorption (TPA) is a process in which two photons are absorbed simultaneously, such that the energy necessary for the molecule excitation is equal to the sum of the energies of the photons [52]. Due to this fact biphotonic excitation may provide markedly increased tissue penetration depth by an accessing of higher-energy excited states using relatively low energy sources [53, 54]. Initial confocal imaging experiments using MPA-capped ZnS:Mn QDs demonstrated that (*i*) the two-photon efficiency for QDs was sufficient enough to use them for two-photon imaging, and that (*ii*) FR+ T47D cells and MCF-7 cells used as control exhibit a very weak autofluorescence in the 550-640 nm spectral range used for the detection. The two-photon emission spectra of ZnS:Mn@MPA and ZnS:Mn/ZnS@MPA QDs are centered around 600 nm (Figure 115) and have the same profile as those recorded under monophotonic excitation.

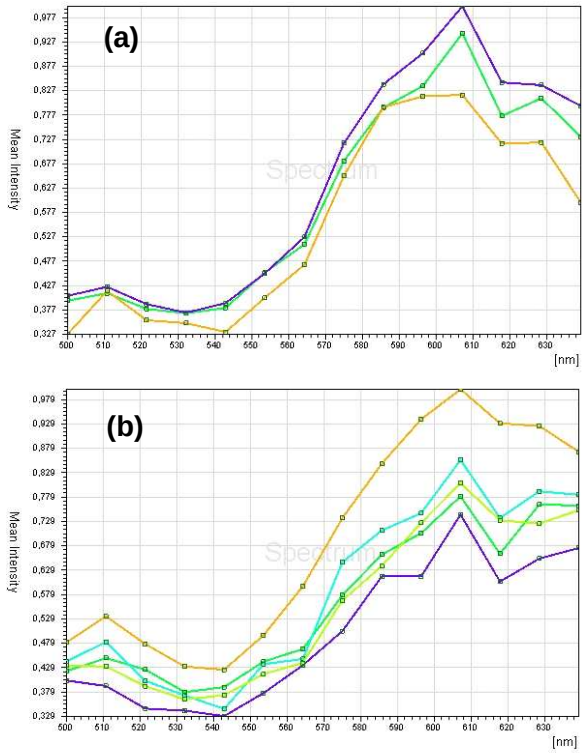

Figure 115. Fluorescence emission spectra of (a) ZnS:Mn@MPA QDs and (b) ZnS:Mn/ZnS@MPA QDs after biphotonic excitation at 720 nm (the samples were scanned from 500 to 640 nm). The points present the values obtained from repeated measurement of the same sample.

The bioimaging experiments were performed using ZnS:Mn@MPA QDs as fluorescent labels of two cancer cell lines, T47D and MCF-7. These cells were cultivated in two media. One of them was FA-defficient medium and second one, the classical Dulbecco's modified Eagle's medium (DMEM). Figures 116 and 117 show the images obtained using ZnS:Mn/ZnS@MPA capped (a-c) and FA-functionalized (d-f) QDs used for imaging of T47D (Figure 116) and MCF-7 (Figure 117) cancer cells cultured in FA-deficient medium.

Confocal images were recorded by excitation at 720 nm and showed a gradual uptake of FA-conjugated QDs over the first 6 h of incubation as observed by a gradual increase of fluorescence intensity within the cells. It is also noteworthy that after 72 h incubation with the cells, the optical properties of QDs were preserved under confocal excitation, thus indicating the good stability of QD probes.

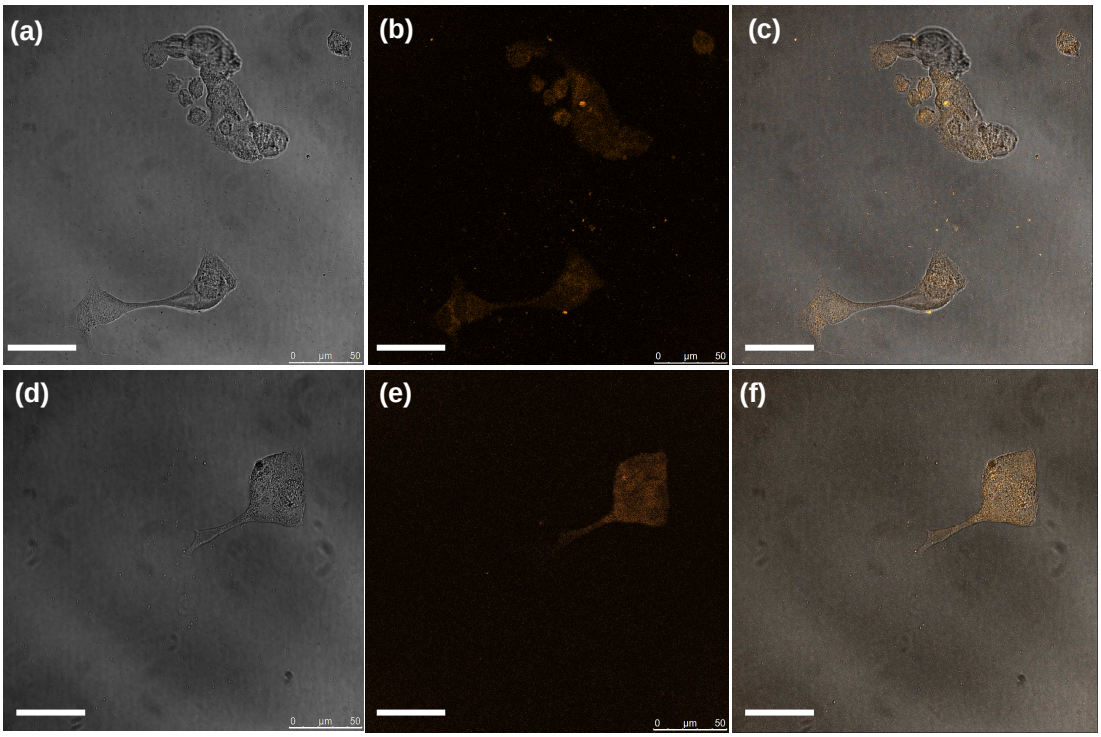

Figure 116. Two-photon confocal microscopic images of T47D cells cultured in folic acid-free medium and treated with (a-c) ZnS:Mn/ZnS QDs, and (d-f) FA-conjugated ZnS:Mn/ZnS QDs. The left boxes correspond to transmission images, the fluorescence images are shown in the middle ones, and the right ones show the overlays of transmission and fluorescence images. Two-photon microscopy images were obtained with laser excitation at 720 nm. Scale bar = 50 μm.

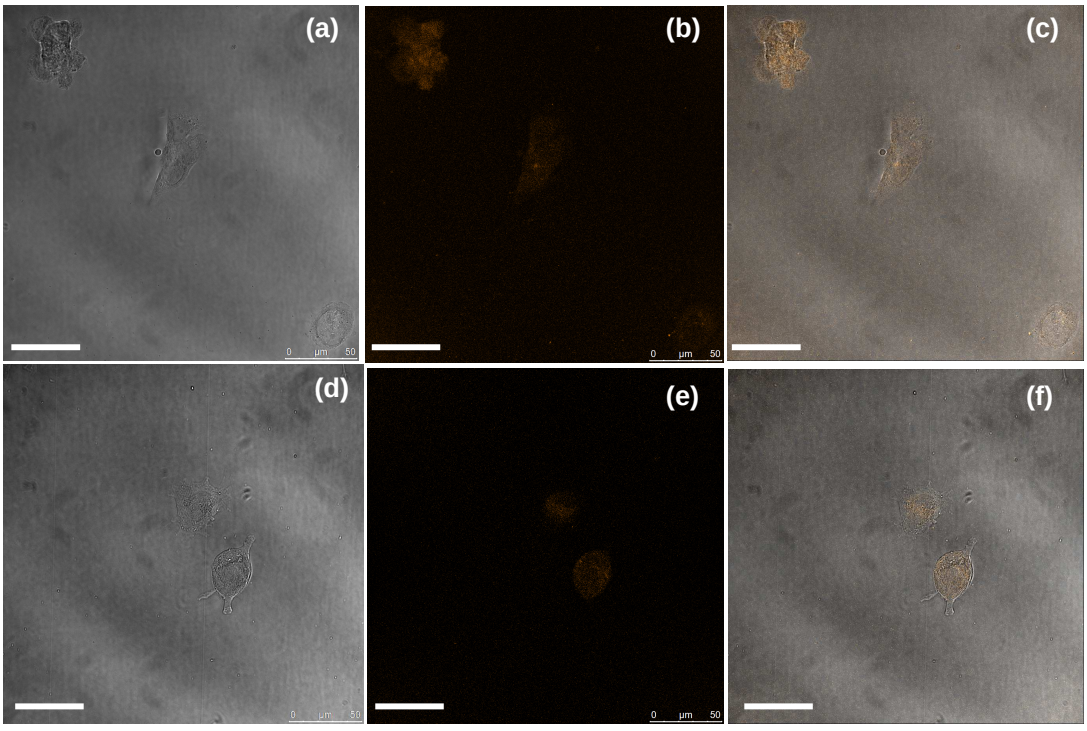

Figure 117. Two-photon confocal microscopic images of MCF-7 cells cultured in folic acid-free medium and treated with (a-c) ZnS:Mn/ZnS QDs, and (d-f) FA-conjugated ZnS:Mn/ZnS QDs. The left boxes correspond to transmission images, the fluorescence images are shown in the middle ones, and the right ones show the overlays of transmission and fluorescence images. Two-photon microscopy images were obtained with laser excitation at 720 nm. Scale bar = 50 μm.

As demonstrated by confocal images obtained with fixed T47D cells cultured in FA-deficient medium depicted on Figure 116d-f, an uptake of FA-linked ZnS:Mn/ZnS QDs was observed and the QDs seem to be distributed throughout the cytoplasm surrounding the nuclei. Using non-modified QDs (Figure 116a-c) the labeling of the cells is also observed, however the QDs dispersion in the cells is not so homogenous. As expected, an uptake of FA-conjugated QDs was observed for MCF-7 cells cultivated in FA-free medium (Figure 117), however QDs uptake is weaker using both FA-conjugated and unmodified QDs.

Figures 118 and 119 show the images obtained using ZnS:Mn/ZnS@MPA capped (a-c) and FA-functionalized (d-f) QDs used for imaging of T47D (Figure 118) and MCF-7 (Figure 119) cancer cells cultured in DMEM medium.

Similarly, the confocal images were recorded by excitation at 720 nm and after 72 h incubation with the cells, the optical properties of QDs were preserved under confocal excitation, thus indicating the good stability of QD probes.

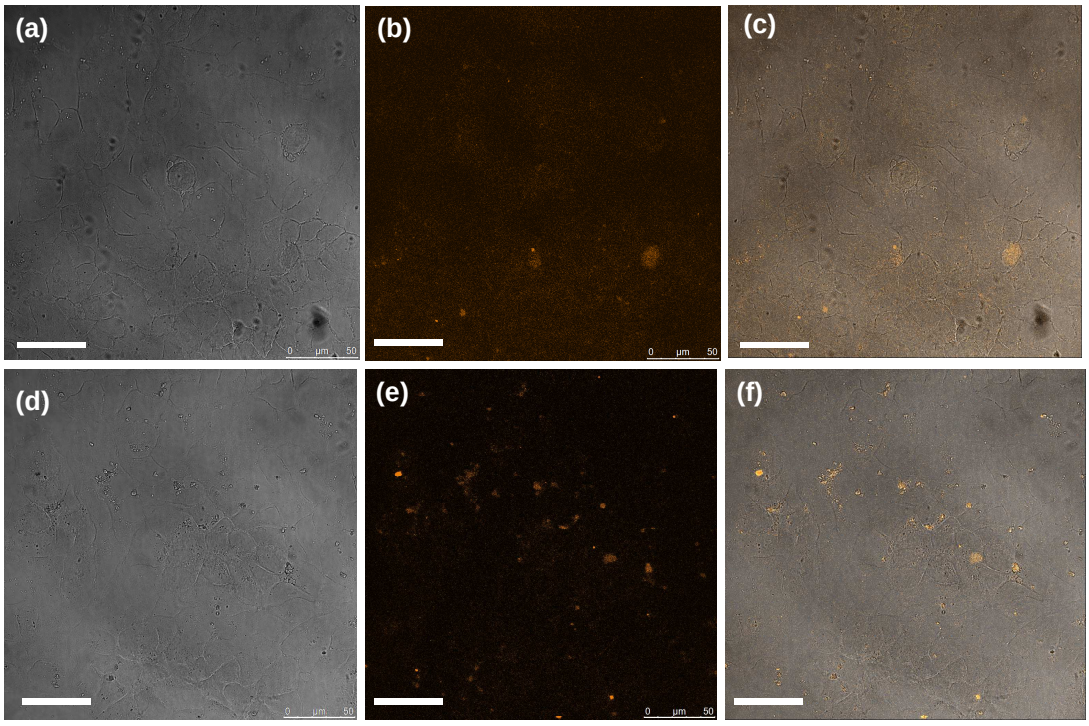

Figure 118. Two-photon confocal microscopic images of T47D cells cultured in DMEM medium and treated with (a-c) ZnS:Mn/ZnS QDs, and (d-f) FA-conjugated ZnS:Mn/ZnS QDs. The left boxes correspond to transmission images, the fluorescence images are shown in the middle ones, and the right ones show the overlays of transmission and fluorescence images. Two-photon microscopy images were obtained with laser excitation at 720 nm. Scale bar = 50 μm.

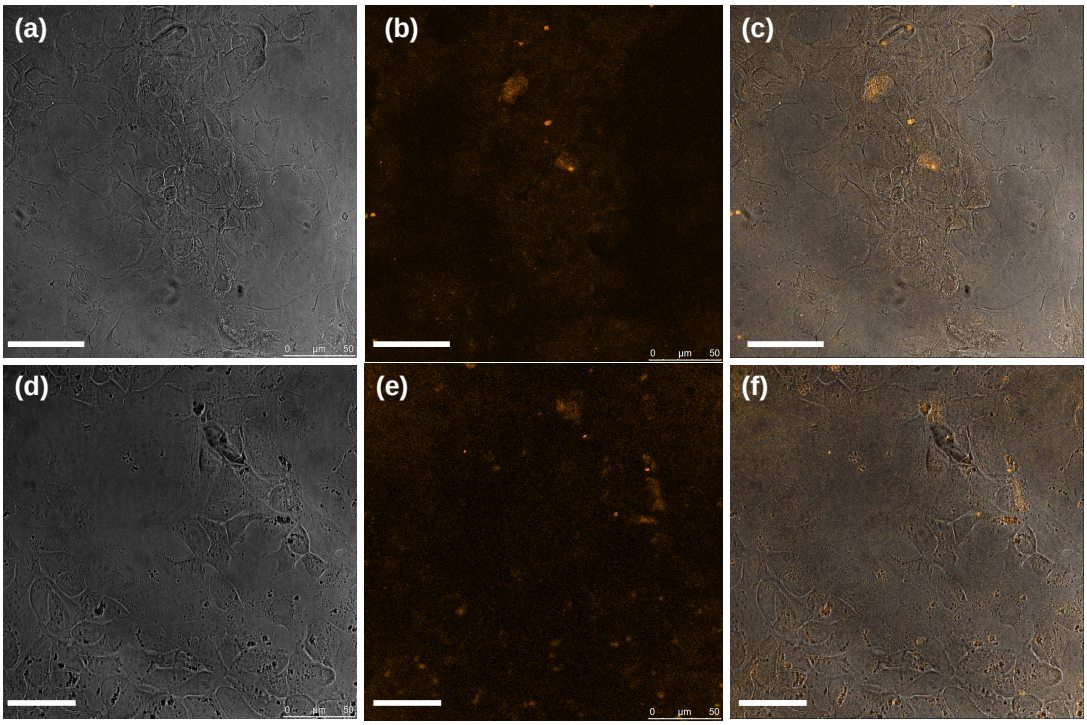

Figure 119. Two-photon confocal microscopic images of MCF-7 cells cultured in DMEM medium and treated with (a-c) ZnS:Mn/ZnS QDs, and (d-f) FA-conjugated ZnS:Mn/ZnS QDs. The left boxes correspond to transmission images, the fluorescence images are shown in the middle ones, and the right ones show the overlays of transmission and fluorescence images. Two-photon microscopy images were obtained with laser excitation at 720 nm. Scale bar = 50 μm.

As demonstrated by confocal images obtained with fixed T47D and MCF-7 cells cultured in DMEM medium depicted on Figure 118 and 119, respectively, an uptake of QDs by the cells was observed, however the QDs seem to be dislocated through all image and to stain the cells in non-homogenous manner.

Figure 120a-c shows the local spectral analysis of the overall cell staining by FA-functionalized QDs, which confirms the origin of the cellular luminescence signal from the QDs. Moreover, no sign of morphological damage to the cells was observed upon treatment with the QDs, thereby further demonstrating their low cytotoxicity. When the membrane FA receptors of T47D cells were saturated with a 3.5 mM free FA solution 30 min before the addition of FA-conjugated QDs (Figure 120d-f) a weak NCs uptake was observed because of specific competition. FA saturation of MCF-7 cells had no significant effect on the FA-conjugated QDs internalization process.

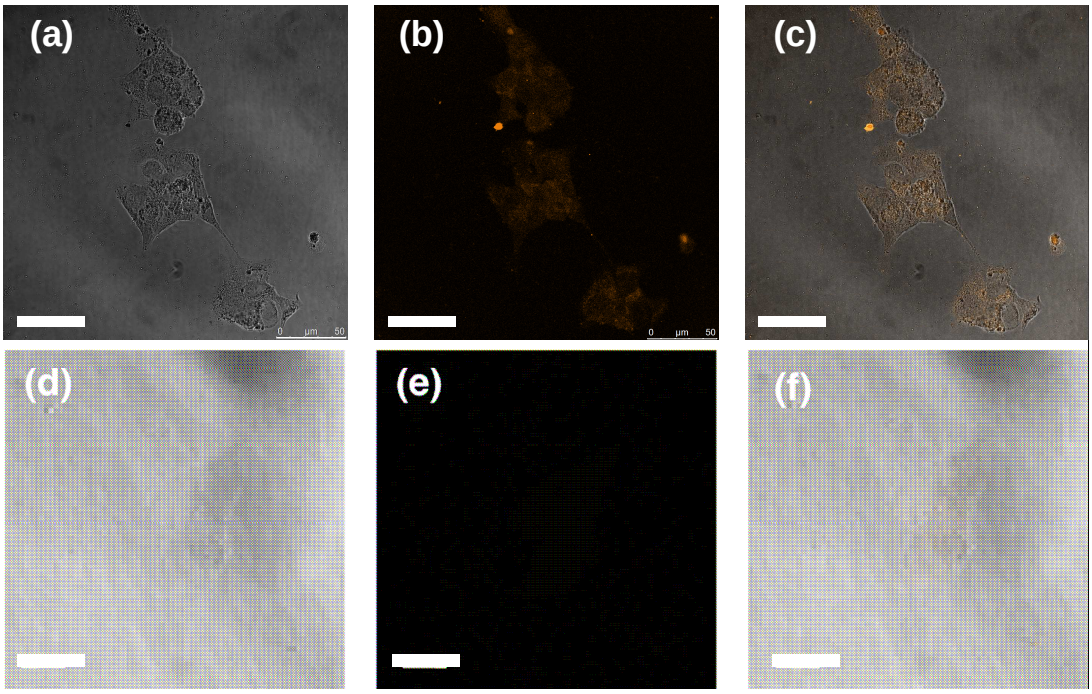

Figure 120. Two-photon confocal microscopic images of T47D cells cultured in folic acid-free medium and treated with (a-c) FA-conjugated ZnS:Mn/ZnS QDs, and (d-f) a 3.5 mM solution of FA before addition of QDs. The left boxes correspond to transmission images, the fluorescence images are shown in the middle ones, and the right ones show the overlays of transmission and fluorescence images. Two-photon microscopy images were obtained with laser excitation at 720 nm. Scale bar = 50 μm.

This result confirms the targeting specificity of FA-linked QDs for FR+ breast cancer cells.

4.4.2. TG-capped ZnS:Mn QDs and organic dyes in bioimaging of T47D and PC-3 cancer cells

In performed bioimaging experiments ZnS:Mn@TG QDs were used together with commercial organic dyes such as Hoechst and JC-1. Hoechst dye is used as DNA stain while Mitochondria Staining Mix containing JC-1 (5,5',6,6'-tetrachloro-1,1',3,3'-tetraethylbenzimidazolocarbocyanine iodide) is used for the detection of changes in mitochondrial inner-membrane electrochemical potential. In this experiment two cell lines, T47D human breast cancer cells and PC-3 human prostate cancer cells were used. Figures 121 and 122 show the images obtained using ZnS:Mn/ZnS@MPA capped (a-d) and FA-functionalized (e-h) QDs used for imaging of T47D (Figure 121) and PC-3 (Figure 122) cells cultured in DMEM medium. From left to right, the boxes correspond to the fluorescence images of the cells stained with JC-1, Hoechst, QDs, and the overlay of these three fluorescence images.

Confocal images were recorded by excitation at 800 nm after 24 h incubation time with QDs and 10 min incubation time with organic dyes. It is also noteworthy that after 24 h incubation with the cells, the optical properties of QDs were preserved under confocal excitation, thus indicating the good stability of QD probes.

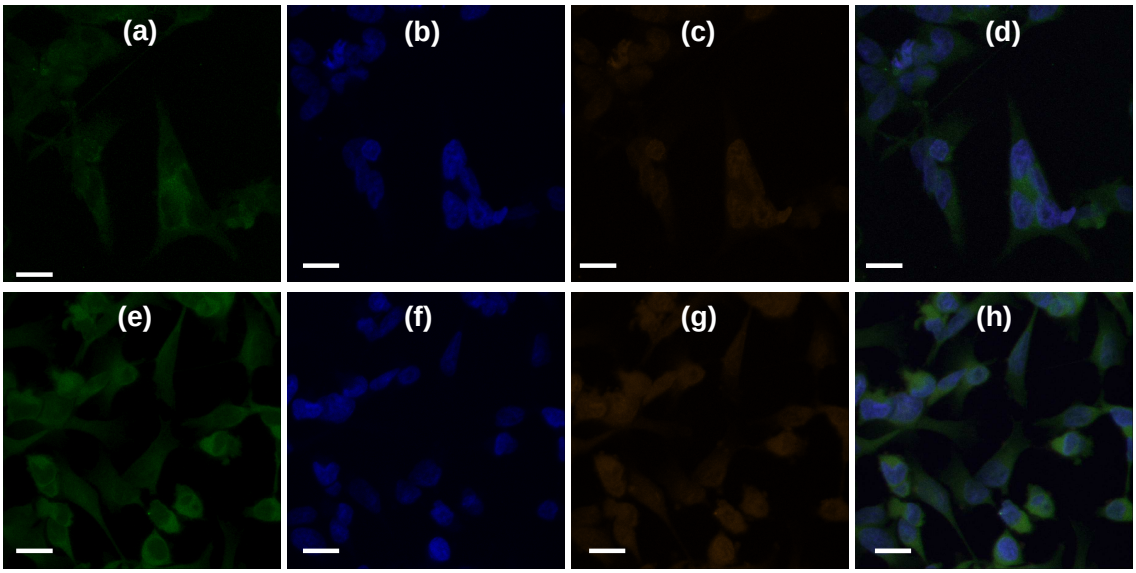

Figure 121. Two-photon confocal microscopic images of T47D cells cultured in DMEM medium and treated with (a-d) ZnS:Mn@TG QDs, and (e-h) FA-conjugated ZnS:Mn@TG QDs. The boxes correspond to the fluorescence images of the cells stained with JC-1, Hoechst, QDs, and the overlay of these three fluorescence images (from left to right). Two-photon microscopy images were obtained with laser excitation at 800 nm. Scale bar = 50 μm.

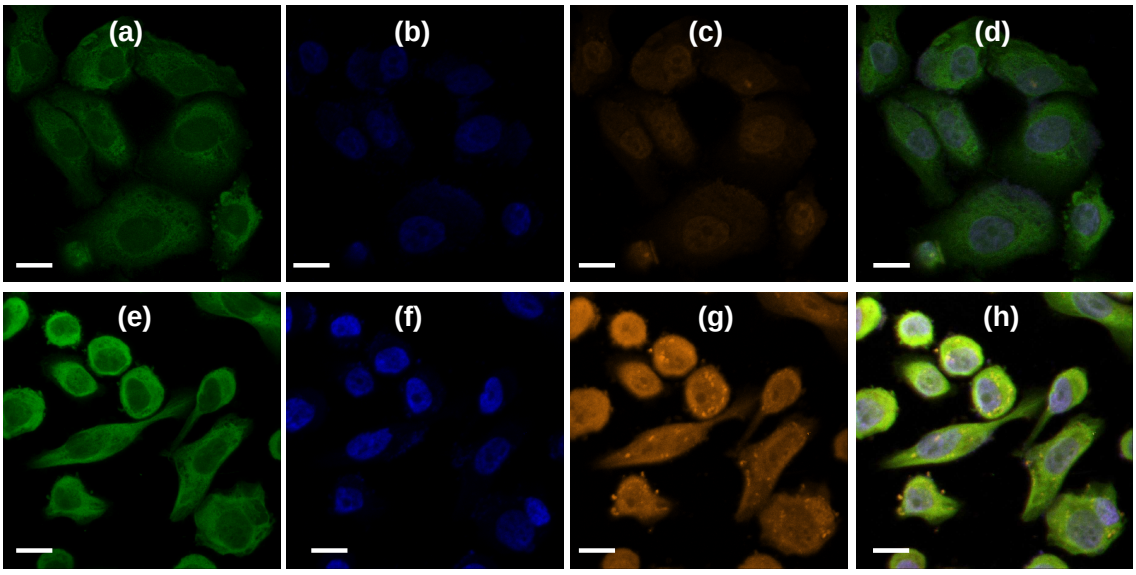

Figure 122. Two-photon confocal microscopic images of PC-3 cells cultured in DMEM medium and treated with (a-d) ZnS:Mn@TG QDs, and (e-h) FA-conjugated ZnS:Mn@TG QDs. The boxes correspond to the fluorescence images of the cells stained with JC-1, Hoechst, QDs, and the overlay of these three fluorescence images (from left to right). Two-photon microscopy images were obtained with laser excitation at 800 nm. Scale bar = 50 μm.

As demonstrated by confocal images obtained with fixed T47D and PC-3 cells cultured in DMEM medium depicted on Figure 121 and 122, an uptake of FA-linked and bare ZnS:Mn/ZnS QDs was observed. The use of organic dyes in the same experiment, namely, Hoechst which label the genetic material and JC-1 which label the mitochondria, allowed me to localize the place of QDs accumulation in the cell. From the Figure 122e-h, which demonstrates the best all fluorescent labels, it could be concluded that QDs labeled both, mitochondria and DNA, however their higher accumulation is observed around the nuclei.

All performed bioimaging experiments indicate that fluorescent QDs can be a potential tool for bioimaging of cancer cells, however the FR-mechanism is not the only one taking place in the uptake of QDs by the cells.

Conclusion

- The developed procedure of the synthesis of fluorescent semiconductor NCs allowed to obtain cadmium-free Mn-doped ZnS QDs stabilized by MPA or TG, Cu-doped QDs stabilized by MPA and Mn-doped ZnSe QDs stabilized by MPA by simple aqueous routes.

- It was proved that:
  - Molar ratio of precursors, dopant concentration, pH value, heating time and the nature of the stabilizer play important roles in final stability and optical properties of synthesized NCs
  - The PL properties are markedly improved by the overcoating of MPA-capped QDs with a ZnS shell
  - All synthesized QDs are monodisperse nanocrystals with diameter smaller than 6 nm

- From the biomedical point of view:
  - ZnS:Mn/ZnS@MPA and ZnS:Mn@TG QDs, due to their good PL properties (PL QY 22 and 11%, respectively, emission wavelength at ca. 590 nm, possibility of biphotonic excitation), and additional low toxicity (results of MTT, XTT and FOXO) can be used in bio-imaging experiments. For example MPA- and TG-capped ZnS:Mn QDs can be efficiently used as fluorescent labels of cancer cells overexpressing folate receptor on their surface
  - ZnSe:Mn/ZnS@MPA and ZnS:Cu/ZnS@MPA (PL QY 9 and 4%, respectively) can be an attractive choice in other biomedical applications e.g. biosensing as their optical properties can be affected by external factors such as pH, temperature and the presence of chemicals or small biomolecules in the surrounding medium.

Abstract

Semiconductor QDs are tiny light-emitting crystals, and are emerging as a new class of fluorescent labels for medicine and biology. Average QDs diameter is in the range of 1-20 nm. These metalloid-crystal structures contain from 200-10,000 atoms. Structurally, QDs consist of a metalloid core and a “cap” or “shell” which covers the core. The core consists of a variety of metal complexes, namely semiconductors, noble metals, and magnetic transition metals. The QDs more often used for biological applications are CdS, CdSe, CdTe, ZnO, ZnS, ZnSe. During the last ten years, and especially for bio-labeling applications, there has been a great interest in cadmium chalcogenide (CdS, CdSe and CdTe) NCs. Because of the ultimate elimination of highly toxic elements like Cd, numerous researches are currently conducted to develop QDs without any heavy metal. Due to the light emitting properties of QDs, which include increased photostability and narrow and symmetric emission spectra, these NCs have been increasingly used as an alternative to organic dyes for bio-imaging. The folate receptor (FR) represents a target for intracellular NPs delivery because it is overexpressed in many cancer cell lines.

Considering the above, the aim of this work was to develop a new class of non-toxic QDs probes with essential attributes such as water dispersibility, photostability, biocompatibility, high luminescence and possible excitation with low-energy visible light, using simple processing method. Such nanoprobes could be used for bio-imaging of cancer cells. In my studies, folic acid (FA) was used to facilitate the FR-mediated targeting of malignant cells. In the performed studies, I focused on ZnS and ZnSe QDs as they are cadmium-free and might be excited biphotonically.

Firstly, the synthesis protocols of zinc sulfide (ZnS) and zinc selenide (ZnSe) QDs doped with two ions such as manganese (Mn) or copper (Cu) and stabilized by 3-mercaptopropionic acid (MPA) or 1-thioglycerol (TG) were established, followed by NCs characterization (diameter, surface charge, photophysical properties, …) using analytical techniques such as spectrophotometry UV-vis, fluorimetry, X-ray diffraction (XRD), X-ray photoelectron spectroscopy (XPS), transmission electron microscopy (TEM), dynamic light scattering (DLS), infra-red analysis (FT-IR), thin layer chromatography (TLC) and electron paramagnetic resonance (EPR).

The optimal concentration of doped metal (Mn or Cu), providing desired PL properties, was established to be of 4% for Mn-doped QDs and of 3% for Cu-doped QDs in comparison to the concentration of zinc precursor used. Effective passivation of MPA-capped QDs and elimination of surface defects of the core was evident from the higher quantum efficiency (22, 9 and 4%) of the core/shell QDs compared to starting QDs (2.7; 5, 3.4%) for ZnS:Mn@MPA, ZnSe:Mn@MPA and ZnCu@MPA QDs, respectively. The PL QY of TG-capped ZnS:Mn QDs was 10.8%. Green-blue fluorescent ZnS:Cu/ZnS@MPA and orange-fluorescent ZnS:Mn/ZnS@MPA QDs in the size range of 3.2 nm and 4.4 nm, respectively, showed specific fluorescence sensitivity towards folic acid (FA).

The same orange-fluorescent monodisperse MPA-capped ZnS:Mn/ZnS as well as ZnSe:Mn/ZnS@MPA QDs and TG-caped ZnS:Mn QDs (average diameter of 4.4; 4.3; 3.9 nm) were conjugated to the cancer targeting ligand, FA, using a PEGamine as a linker in case of MPA-capped QDs what was the subject of the second part of the experimental chapter.

Thirdly, the cytotoxicity of synthesized bare and conjugated NPs was evaluated on cancer cell lines. MTT, XTT and ferrous oxidation-xylenol orange (FOXO) assay were performed towards T47D and MCF-7 breast cancer cells and PC-3 prostate cancer cells. Obtained results indicated the lowest cytotoxicity of TG-capped ZnS:Mn QDs in comparison with MPA-capped ZnS and ZnSe manganese-doped QDs. However, the cytotoxicity of both types of MPA-capped QDs causing 50% decrease in cells viability was observed nearly in all cases only for QDs concentration exceeding 1mM.

Finally, chosen well fluorescent and weakly toxic types of as-prepared and characterized QDs were used for bio-imaging of cancer cells. In these experiments, FA-functionalized NCs were excited biphotonically (excitation wl > 700 nm). The receptor-mediated uptake of MPA- and TG-capped ZnS:Mn QDs in T47D, MCF-7 and PC-3 cancer cells was demonstrated. The experiments using TG-capped QDs were accompanied by organic dyes labeling which enables better localisation of QDs in the cell. The performed experiments showed the potential of QDs as cancer cells fluorescent markers and that they accumulate around the cell nuclei.

Fluorescent semiconductor QDs, owing to their excellent photophysical properties have proven to be an attractive choice in bio-imaging of cancer cells. Due to their low cytotoxicity and fair stability, these QDs should play an important role in a variety of NC-based biomedical applications in a near future.

References

1. Efros A.L. and Efros A.L., *Interband absorption of light in a semiconductor sphere.* Sov. Phys. Semicond., **1982**, 16: 772-775.
2. Bruchez M., Moronne M., Gin P., Weiss S., and Alivisatos A.P., *Semiconductor nanocrystals as fluorescent biological labels.* Science, **1998**, 281: 2013-2016.
3. Chan W.C.W. and Nie S., *Quantum dots bioconjugates for ultrasensitive nonisotopic detection.* Science, **1998**, 281: 2016-2018.
4. Smith A.M., Gao X., and Nie S., *Quantum dot nanocrystals for In vivo Molecular and Cellular Imaging.* Photochem. Photobiol., **2004**, 80: 337-385.
5. Medintz I.L., Uyeda H.T., Goldman R.E., and Mattoussi H., *Quantum dot bioconjugates for imaging, labelling and sensing.* Nature Mater., **2005**, 4: 435-446.
6. Casals E., Vázquez-Campos S., Bastùs N.G., and Puntes V., *Distribution and potential toxicity of engineered inorganic nanoparticles and carbon nanostructures in biological systems.* Trends Anal. Chem., **2008**, 27: 672-683.
7. Smith A.M., Duan H., Mohs A.M., and Nie S., *Bioconjugated quantum dots for in vivo molecular and cellular imaging.* Adv. Drug Deliv. Rev., **2008**, 60: 1226-1240.
8. Pelley J.L., Daar A.S., and Saner M.A., *State of Academic Knowledge on Toxicity and Biological Fate of Quantum Dots.* Toxicol. Sci., **2009**, 112: 276-296.
9. Aldana J., Wang Y.A., and Peng X., *Photochemical instability of CdSe nanocrystals coated by hydrophilic thiols.* J. Am. Chem. Soc., **2001**, 123: 8844-8850.
10. Lommens P., Smet P.F., Donega C.M., Meijerink A., Piraux L., Michotte S., Mátéfi-Tempfli S., Poelman D., and Hens Z., *Photoluminescence properties of Co^{2+}-doped ZnO nanocrystals.* J. Lumin., **2006**, 118: 245-250.
11. Lommens P., Loncke F., Smet P.F., Callens F., Poelman D., Vrielinck H., and Hens Z., *Dopant Incorporation in Colloidal Quantum Dots: A Case study on Co^{2+} Doped ZnO.* Chem. Mater., **2007**, 19: 5576-5583.
12. Rzigalinski B.A. and Strobl J.S., *Cadmium-containing nanoparticles: Perspectives on pharmacology and toxicology of quantum dots.* Toxicol. Appl. Pharmacol., **2009**, 238: 280-288.
13. Cho S.J., Maysinger D., Jain M., Röder B., Hackbarth S., and Winnik F.M., *Long-Term Exposure to CdTe Quantum Dots Causes Functional Impairments in Live Cells.* Langmuir, **2007**, 23: 1974-1980.
14. Cooper D.R., Dimitrijevic N.M., and Nadeau J.L., *Photosensitization of CdSe/ZnS QDs and reliability of assays for reactive oxygen species production.* Nanoscale, **2010**, 2: 114-121.
15. Li H., Shih W.Y., and Shih W.H., *Synthesis and characterization of aqueous carboxyl-capped CdS quantum dots for bioapplications.* Ind. Eng. Chem. Res., **2007**, 46: 2013-2019.
16. Manzoor K., Johny S., Thomas D., Setua S., Menon D., and Nair S., *Bio-conjugated luminescent quantum dots of doped ZnS: a cyto-friendly system for targeted cancer imaging.* Nanotechnol., **2009**, 20: 065102.
17. Moussodia R.O., Balan L., and Schneider R., *Synthesis and characterization of water-soluble ZnO quantum dots prepared through PEG-siloxane coating.* New J. Chem., **2008**, 32: 1388-1393.
18. Zhang J., Li J., Zhang J., Xie R., and Yang W., *Aqueous Synthesis of ZnSe Nanocrystals by Using Glutathione As Ligand: The pH-Mediated Coordination of Zn^{2+} with Glutathione.* J. Phys. Chem. C, **2010**, 114: 11087-11091.
19. Lucey D.W., MacRae D.J., Furis M., Sahoo Y., Cartwright A.N., and Prasad P.N., *Monodispersed InP quantum dots prepared by colloidal chemistry in a noncoordinating solvent.* Chem. Mater., **2005**, 17: 3754-3762.
20. Battaglia D. and Peng X., *Formation of High Quality InP and InAs Nanocrystals in a Noncoordinating Solvent.* Nano Lett., **2002**, 2: 1027-1030.
21. Malik M.A., O'Brien P., Norager S., and Smith J., *Gallium arsenide nanoparticles: Synthesis and characterization.* J. Mater. Chem., **2003**, 13: 2591-2595.
22. Zhu J., Liao X., Wang J., and Chen H.Y., *Photochemical synthesis and characterization of PbSe nanoparticles.* Mater. Res. Bull., **2001**, 36: 1169-1176.
23. Lifshitz E., Brumer M., Kigel A., Sashchiuk A., Bashouti M., Sirota M., Galun E., Burshtein Z., Quang A.Q.L., Ledoux-Rak I., and Zyss J., *Air-stable PbSe/PbS and PbSe/$PbSe_xS_{1-x}$ Core-Shell nanocrystal quantum dots and their applications.* J. Phys. Chem. B, **2006**, 110: 25356-25365.
24. Murphy J.E., Beard M.C., Norman A.G., Ahrenkiel S.P., Johnson J.C., Yu P., Mićić O.I., Ellingson R.J., and Nozik A.J., *PbTe colloidal nanocrystals: Synthesis, characterization, and multiple exciton generation.* J. Am. Chem. Soc., **2006**, 128: 3241-3247.

25. Green M. and O'Brien P., *A novel mataloorganic route to nanocrystallites of zinc phosphide.* Chem. Mater., **2001**, 13: 4500-4505.
26. Foos E.E., Stroud R.M., and Berry A.D., *Synthesis and Characterization of Nanocrystalline Bismuth Telluride.* Nano Lett., **2001**, 1: 693-695.
27. Jindal Z. and Verma N.K., *Photoluminescent properties of ZnS:Mn nanoparticles with in-built surfactant.* J. Mater. Sci., **2008**, 43: 6539-6545.
28. Hild W.A., Breunig M., and Goepferich A., *Quantum dots- Nano-sized probes for the exploration of cellular and intracellular targeting.* Eur. J. Pharm. Biopharm., **2008**, 68: 153-168.
29. Pathak S., Choi S.-K., Arnheim N., and Thompson M.E., *Hydroxylated Quantum Dots as Luminescent Probes for in Situ Hybridization.* J. Am. Chem. Soc., **2001**, 123: 4103-4104.
30. Santra S., Yang H., Holloway P.H., Stanley J.T., and Mericle R.A., *Synthesis of Water-Dispersible Fluorescent, Radio-Opaque, and Paramagnetic CdS:Mn/ZnS Quantum Dots: A Multifunctional Probe for Bioimaging.* J. Am. Chem. Soc., **2005**, 127: 1656-1657.
31. Quan Z., Wang Z., Yang P., Lin J., and Fang J., *Synthesis and Characterization of High-Quality ZnS, ZnS:Mn^{2+}, and ZnS:Mn^{2+}/ZnS (Core/Shell) Luminescent Nanocrystals.* Inorg. Chem., **2007**, 46: 1354-1360.
32. Jiang D., Cao L., Su G., Qu H., and Sun D., *Luminescence enhancement of Mn doped ZnS nanocrystals passivated with zinc hydroxide.* Appl. Surf. Sci., **2007**, 253: 9330-9335.
33. Brus L.E., *Electron-electron and electron-hole interactions in small semiconductor crystallites- the size dependence of the lowest excited electronic states.* J. Chem. Phys., **1984**, 80: 4403-4409.
34. Reiss P. and Chandezon F., *Nanocristaux semiconducteurs fluorescents*. Techniques de l' Ingénieur. Vol. RE22. 2004. 1-15.
35. Bawendi M.G., Steigerwald M.L., and Brus L.E., *The quantum mechanics of larger semiconductor clusters ("Quantum dots").* Annu. Rev. Phys. Chem, **1990**, 41: 477-496.
36. Brus L.E., *Electronic wave functions in semiconductor clusters: experiment and theory.* J. Phys. Chem., **1986**, 90: 2555-2561.
37. Kittel C., *Physique de l' Etat Solide*, ed. Dunod. 1983, Paris. 593.
38. Bimberg D., *Landolt-Börnstein: Crystal and Solid State Physics- Physics of Group IV Elements and III-V Compounds et Physics of II-VI and I-VII Compounds. O. Madelung. Springer.* **1982**.
39. Chang E., Thekkek N., Yu W.W., Colvin V.L., and Drezek R., *Evaluation of Quantum Dot Cytotoxicity Based on Intracellular Uptake.* Small, **2006**, 2: 1412-1417.
40. Tortiglione C., Quarta A., Tino A., Manna L., Cingolani R., and Pellegrino T., *Synthesis and Biological Assay of GSH Functionalized Fluorescent Quantum Dots for Staining Hydra vulgaris.* Bioconjugate Chem., **2007**, 18: 829-835.
41. Costa-Fernández J.M., Pereiro R., and Sanz-Medel A., *The use of luminescent quantum dots for optical sensing*. Trends Anal. Chem., **2006**, 25: 207-218.
42. Sharma P., Brown S., Walter G., Santra S., and Moudgil B., *Nanoparticles for bioimaging.* Adv. Colloid Interface Sci., **2006**, 123-126: 471-485.
43. Chan W.C.W., Maxwell D.J., Gao X., Bailey R.E., Han M., and Nie S., *Luminescent quantum dots for multiplexed biological detection and imaging.* Curr. Opin. Biotechnol., **2002**, 13: 40-46.
44. Wolcott A., Gerion D., Visconte M., sun J., Schwartzberg A., Chen S., and Zhang J.Z., *Silica-Coated CdTe Quantum Dots Functionalized with Thiols for Bioconjugation to IgG Proteins.* J. Phys. Chem. B, **2006**, 110: 5779-5789.
45. Liao L., Zhang H., and Zhong X., *Facile synthesis of red-to near-infrared-emitting $CdTe_xSe_{1-x}$ alloyed quantum dots via a noninjection one-pot route.* J. Lumin., **2011**, 131: 322-327.
46. Biju V., Itoh T., Anas A., Sujith A., and Ishikawa M., *Semiconductor quantum dots and metal nanoparticles: Synthesis, optical properties, and biological applications.* Anal. Bioanal. Chem., **2008**, 391: 2469-2495.
47. Bailey R.E., Smith A.M., and Nie S., *Quantum Dots in biology and medicine.* Physica E, **2004**, 25: 1-12.
48. Yu W.W., Chang E., Drezek R., and Colvin a.V.L., *Water-soluble quantum dots for biomedical applications.* Biochem. Biophys. Res. Commun., **2006**, 348: 781-786.
49. Biju V., Mundayoor S., Omkumar R.V., Anas A., and Ishikawa M., *Bioconjugated quantum dots for cancer research: Present status, prospects and remaining issues.* Biotechnol. Adv., **2010**, 28: 199-213.
50. Rizvi S.B., Ghaderi S., Keshtgar M., and Seifalian A.M., *Semiconductor quantum dots as fluorescent probes for in vitro and in vivo bio-molecular and cellular imaging.* Nano Reviews, **2010**, 1: 5161.
51. Zhu L., Ang S., and Liu a.W.-T., *Quantum Dots as a Novel Immunofluorescent Detection System for Cryptosporidium parvum and Giardia lamblia.* Appl. Environ. Microbiol., **2004**, 70: 597-598.
52. Pati S.K., Marks T.J., and Ratner M.A., *Conformationally Tuned Large Two-Photon Absorption Cross Section in single Molecular Chromophores.* J. Am. Chem. Soc., **2001**, 123: 7287-7291.

53. Drobizhev M., Karotki A., and Rebane A., *Dendrimer molecules with record large two-photon absorption cross section.* Opt. Lett., **2001**, 16: 1081-1083.
54. Oliveira S.L., Corrêa D.S., Misoguti L., Constantino C.J.L., Aroca R.F., Zilio S.C., and Mendonça C.R., *Perylene Derivatives with Large Two-Photon Cross-Sections for Application in Optical Limiting and Upconversion Lasing.* Adv. Mater., **2005**, 17: 1890-1893.
55. Chatterjee D.K., Fong L.S., and Zhang Y., *Nanoparticles in photodynamic therapy: An emerging paradigm.* Adv. Drug Deliv. Rev., **2008**, 60: 1627-1637.
56. Pecharsky V. and Zavalij P., *Fundamentals of Powder Diffraction and Structural Characterization of Materials*. 2009: Springer. 729.
57. Singh J., *Physics of semiconductors and their heterostructures*. 1993, New York: McGraw-Hill 851.
58. Fedorov V.A., Ganshin V.A., and Korkishko Y.N., *Determination of the point of the zincblende-to-wurtzite structural phase transition in cadmium selenide crystals.* Phys. Status. Solid. A, **1991**, 126: K5-K7.
59. Salavati-Niasari M., Davar F., and Mazaheri M., *Synthesis and characterization of ZnS nanoclusters via hydrothermal processing from [bis(salicylidene)zinc(II)]*. J. Alloys Compd., **2009**, 470: 502-506.
60. Li H., Shih W.Y., and Shih W.-H., *Non-heavy-metal ZnS quantum dots with bright blue photoluminescence by a one-step aqueous synthesis.* Nanotechnol., **2007**, 18: 205604.
61. Rajesh C., Lad A.D., Ghangrekar A., and Mahamuni S., *Exciton recombination dynamics in zinc selenide quantum dots.* Solid State Commun., **2008**, 148: 435-439.
62. Peng L., Wang Y., Dong Q., and Wang Z., *Passivated ZnSe nanocrystals prepared by hydrothermal methods and their optical properties.* Nano-Micro Lett., **2010**, 2: 190-196.
63. Moore D. and Wang Z.L., *Growth of anisotropic one-dimensional ZnS nanostructures.* J. Mater. Chem., **2006**, 16: 3898-3905.
64. Kapitonov A.M., Stupak A.P., Gaponenko S.V., Petrov E.P., Rogach A.L., and Euchmüller A., *Luminescence Properties of Thiol-Stabilized CdTe Nanocrystals.* J. Phys. Chem., **1999**, 103: 10109-10113.
65. Rogach A.L., Nagesha D., Ostrander J.W., Giersig M., and Kotov N.A., *'Raisin bun'-type composites spheres of silica and semiconductor nanocrystals.* Chem. Mater., **2000**, 12: 2676-2685.
66. Bowers M.J., McBride J.R., and Rosenthal S.J., *White-light emission from magic-sized cadmium selenide nanocrystals.* J. Am. Chem. Soc., **2005**, 127: 15378-15379.
67. Lin Y.W., Hsieh M.H., Liu C.P., and Chang H.T., *Photoassisted synthesis of CdSe and core-shell CdSe/CdS quantum dots.* Langmuir, **2005**, 21: 728-734.
68. Qian H., Li L., and Ren J., *One-step and rapid synthesis of high quality alloyed quantum dots (CdSe-CdS) in aqueous phase by microwave irradiation with controllable temperature.* Mater. Res. Bull., **2005**, 40: 1726-1736.
69. Kim M.J., Park C., Choi K., and Yoon T.H., *Implications of "Trap Emission" Observed from Quantum Dot Nanoparticles Accumulated in Toxicity Test Organism, Daphnia magna.* Bull. Korean Chem. Soc., **2008**, 29: 1101-1102.
70. Reiss P., Protière M., and Li L., *Core/shell semiconductor nanocrystals.* Small, **2009**, 5: 154-168.
71. Talapin D.V., Koeppe R., Götzinger S., Kornovski A., Lupton J.M., Rogach A.L., Benson O., Feldmann J., and Weller H., *Highly Emissive Colloidal CdSe/CdS Heterostructures of Mixed Dimensionality.* Nano Lett., **2003**, 3: 1677-1681.
72. Steckel J.S., Zimmer J.P., Coe-Sullivan S., Stott N.E., Bulovic V., and Bawendi M.G., *Blue Luminescence from (CdS)ZnS core-shell nanocrystals.* Angew. Chem. Int. Ed., **2004**, 43: 2154.
73. Kim S., Fisher B., Eisler H.J., and Bawendi M., *Type-II quantum dots: CdTe/CdSe (core/shell) and CdSe/ZnTe (core/shell) heterostructures.* J. Am. Chem. Soc., **2003**, 42: 11466-11467.
74. Xie R., Zhong X., and Basché T., *Synthesis, characterization, and spectroscopy of type-II core/shell semiconductor nanocrystals with ZnTe cores.* Adv. Mater., **2005**, 17: 2741-2744.
75. He Y., Lu H.-T., Sai L.-M., Su Y.-Y., Hu M., Fan C.-H., Huang W., and Wang L.-H., *Microwave Synthesis of Water-Dispersed CdTe/CdS/Zns Core-Shell-Shell Quantum Dots with Excellent Photostability and Biocompatibility.* Adv. Mater., **2008**, 20: 3416-3421.
76. Wuister S.F., Swart I., Driel F.V., Hickey S.G., and Donega C.M., *Highly luminescent water-soluble CdTe quantum dots.* Nano Lett., **2003**, 3: 503-507.
77. Zhong P., Yu Y., Wu J., Long Z., and Liang C., *Synthesis of mercaptoethylamine-coated CdSe/CdS nanocrystals and their use for DNA probe.* Anal. Sci., **2007**, 23: 1085-1089.
78. Liu W., Choi H.S., Zimmer J.P., Tanaka E., Frangioni J.V., and Bawendi M., *Compact cysteine-coated CdSe (ZnCdS) quantum dots for in vivo applications.* J. Am. Chem. Soc., **2007**, 129: 14530-14531.
79. Fuente J.M., Fandel M., Berry C.C., Riehle M., Cronin L., Aitchison G., and Curtis A.S.G., *Quantum Dots Protected with Tiopronin: A New Fluorescence System for Cell-Biology Studies.* Chem. Bio. Chem., **2005**, 6: 985-991.

80. Murcia M.J., Shaw D.L., Long E.C., and Naumann C.A., *Fluorescence correlation spectroscopy of CdSe/ZnS quantum dot optical bioimaging probes with ultra-thin biocompatible coatings.* Optics Commun., **2008**, 281: 1771-1780.
81. Michalet X., Pinaud F.F., Bentolila L.A., Tsay J.M., Doose S., Li J.J., Sundaresan G., Wu A.M., Gambhir S.S., and Weiss a.S., *Quantum Dots for Live Cells, in Vivo Imaging, and Diagnostics.* Science, **2005**, 307: 538-544.
82. Algar W.R. and Krull U.J., *Luminescence and stability of aqueous thioalkyl acid capped CdSe/ZnS quantum dots correlated to ligand ionization.* Chem. Phys. Chem., **2007**, 8: 561-568.
83. Uyeda H.T., Medintz I.L., Jaiswal J.K., Simon S.M., and Mattoussi H., *Synthesis of compact multidentate ligands to prepare stable hydrophilic quantum dot fluorophores.* J. Am. Chem. Soc., **2005**, 127: 3870-3878.
84. Daou T.J., Li L., Reiss P., Josserand V., and Texier I., *Effect of poly (ethylene glycol) length on the in vivo behavior of coated quantum dots.* Langmuir, **2009**, 25(5): 3040-3044.
85. Kim S. and Bawendi M.G., *Oligomeric Ligands for Luminescent and Stable Nanocrystal Quantum Dots.* J. Am. Chem. Soc., **2003**, 125: 14652-14653.
86. Wang Y.A., Li J.J., and Chen H., *Stabilization of inorganic nanocrystals by organic dendrons.* J. Am. Chem. Soc., **2002**, 124: 2293-2298.
87. Guo W., Li J.J., Wang A., and Peng X., *Conjugation chemistry and bioapplications of semiconductor box nanocrystals prepared via dendrimer bridging.* Chem. Mater., **2003**, 15(16): 3125-3133.
88. Pons T., Uyeda H.T., Medintz I.L., and Mattoussi H., *Hydrodynamic dimensions, electrophoretic mobility, and stability of hydrophylic quantum dots.* J. Phys. Chem. B, **2006**, 110: 20308-20316.
89. Dubertret B., Skourides P., Norris D.J., Noireau V., Brivanlou A.H., and Libchaber A., *In vivo imaging of quantum dots encapsulated in phospholipid micelles.* SCIENCE, **2002**, 298: 1759-1762.
90. Li H. and Wang X., *Single quantum dot-micelles coated with gemini surfactant for selective recognition of a cation and an anion in aqueous solution.* Sens. Actuators B, **2008**, 134: 238-244.
91. Li H., Wang W., Gao Z., and He Z., *Gemini surfactant for fluorescent and stable quantum dots in aqueous solution.* Nanotechnol., **2007**, 18: 205603.
92. Roullier V., Grasset F., Boulmedais F., Artzner F., Cador O., and Marchi-Artzner V., *Small Bioactivated Magnetic Quantum Dots Micelles.* Chem. Mater., **2008**, 20: 6657-6665.
93. Boulmedais F., Bauchat P., Brienne M.J., Arnal I., Artzner F., Gacoin T., Dahan M., and Marchi-Artzner V., *Water-soluble pegylated Quantum Dots: from a composite hexagonal phase to isolated micelles.* Chem. Mater., **2006**, 22: 9797-9803.
94. Fan H., Leve E.W., Scullin C., Gabaldon J., Tallant D., Bunge S., Boyle T., Wilson M.C., and Brinker C.J., *Surfactant-assisted synthesis of water-soluble and biocompatible semiconductor quantum dot micelles.* Nano Lett., **2005**, 5(4): 654-648.
95. Mulder W.J.M., Koole R., Brandwijk R.J., Storm G., Chin P.T.K., Strijkers G.J., Donega C.M., Nicolay K., and Griffioen A.W., *Quantum dots with a paramagnetic coating as a bimodal molecular imaging probe.* Nano Lett., **2006**, 6: 1-6.
96. Smith A.M. and Nie S., *Nanocrystal synthesis in an amphibious bath: Spontaneous generation of hydrophilic and hydrophobic surface coatings.* Angew. Chem. Int. Ed., **2008**, 47: 9916-9921.
97. Anderson R.E. and Chan W.W.C., *Systematic investigation of preparing biocompatible, single, and small ZnS-capped CdSe quantum dots with amphiphilic polymers.* ACS Nano, **2008**, 2: 1341-1352.
98. Zhou C., Shen H., Guo Y., Xu L., Niu J., Zhang Z., Du Z., Chen J., and Li L.S., *A versatile method for the preparation of water-soluble amphiphilic oligomer-coated semiconductor quantum dots with high fluorescence and stability.* J. Colloid Interface Sci., **2010**, 344.
99. Wu Z., Zhao Y., Qiu F., Li Y., Wang S., Yang B., Chen L., Sun J., and Wang J., *Forming water-soluble CdSe/ZnS QDs using amphiphilic polymers, stearyl methacrylate/ methacrylate copolymers with different hydrophobic moiety ratios and their optical properties and stability.* Colloid Surf., A: Physicochem. Eng. Aspects, **2009**, 350: 121-129.
100. Zhou X., Chen Z., Huang P., Wang X., and Kasuya A., *Preparation and stability of strongly luminescent CdSe/Cd(OH)$_2$/SiO$_2$ nanocomposite particles in aqueous solution.* Colloid J., **2008**, 70: 734-739.
101. Selvan S.T., Tan T.T., and Ying J.Y., *Robust, Non-Cytotoxic, Silica-Coated CdSe Quantum Dots with Efficient Photoluminescence.* Adv. Mater., **2005**, 17: 1620-1625.
102. Zhou X., Kobayashi Y., Romanyuk V., Ochuchi N., Takeda M., Tsunakawa S., and Kasuya A., *Preparation of silica encapsulated CdSe quantum dots in aqueous solution with the improved optical properties.* Appl. Surf. Sci., **2005**, 242: 281-286.
103. Nann T. and Mulvaney P., *Single Quantum Dots in Spherical Silica Particles.* Angew. Chem. Int. Ed., **2004**, 43: 5393-5396.

104. Slocik J.M., Moore J.T., and Wright D.W., *Monoclonal Antibody Recognition of Histidine-Rich Peptide Encapsulated Nanoclusters.* Nano Lett., **2002**, 2: 169-173.
105. Andrade J.J., Brasil A.G., Farias P.M.A., Fontes A., and Santos B.S., *Synthesis and characterization of blue emitting ZnSe quantum dots.* Microelectron. J., **2009**, 40: 641-643.
106. Norris D.J., Efros A.L., and Erwin S.C., *Doped nanocrystals.* Science, **2008**, 319: 1776-1779.
107. Hu H. and Zhang W., *Synthesis and properties of transition metals and rare-earth metals doped ZnS nanoparticles.* Opt. Mater., **2006**, 28: 536-550.
108. Steitz B., Axmann Y., Hofmann H., and Petri-Fink A., *Optical properties of annealed Mn^{2+}-doped ZnS nanoparticles.* J. Lumin., **2008**, 128: 92-98.
109. Maity R. and Chattopadhyay K.K., *Synthesis and optical characterization of ZnS and ZnS:Mn nanocrystalline thin films by chemical route.* Nanotechnol., **2004**, 15: 812-816.
110. Yang P. and Bredol M., *Surface Passivation and photoluminescence of Mn-doped ZnS nanocrystals.* Res. Lett. Mater. Sci., **2008**: 506065.
111. Li Y., Ding Y., Zhang Y., and Qian Y., *Photophysical properties of ZnS quantum dots.* J. Phys. Chem. Solids, **1999**, 60: 13-15.
112. Kim C.C. and Sivananthan S., *Optical properties of ZnSe and its modeling.* Phys. Rev. B, **1996**, 53: 1475-1484.
113. Yu H., Li J., Loomis R.A., Gibbons P.C., Wang L.W., and Buhro W.E., *Cadmium Selenide Quantum Wires and the Transition from 3D to 2D Confinement.* J. Am. Chem. Soc., **2003**, 125: 16168-16169.
114. Jun Y.W., Koo J.E., and Cheon J., *One-step synthesis of size tuned zinc selenide quantum dots via a temperature controlled molecular precursor approach.* Chem. Commun., **2000**: 1243-1244.
115. Heulings H.R., Huang X.Y., and Li J., *Mn-Substituted Inorganic-Organic Hybrid Materials Based on ZnSe Nanostructures That May Lead to Magnetic Semiconductors with a Strong Quantum Confinement Effect.* Nano Lett., **2001**, 1: 521-525.
116. Huang L. and Han H., *One-step synthesis of water-soluble ZnSe quantum dots via microwave irradiation.* Mater. Lett., **2010**, 64: 1099-1101.
117. Ishizumi A. and Kanemitsu Y., *Luminescence Spectra and Dynamics of Mn-Doped CdS Core/Shell Nanocrystals.* Adv. Mater., **2006**, 18: 1083-1085.
118. Kim J.-U., Kim Y.K., and Yang H., *Reverse micelle-derived Cu-doped $Zn_{1-x}Cd_xS$ quantum dots and their core/shell structure.* J. Colloid Interface Sci., **2010**, 341: 59-63.
119. Bhargava R.N. and Gallagher D., *Optical properties of manganese-doped nanocrystals of ZnS.* Phys. Rev. Lett., **1994**, 72: 416.
120. Sooklal K., Cullum B.S., Angel S.M., and Murphy C.J., *Photophysical Properties of ZnS Nanoclusters with Spatially Localized Mn^{2+}.* J. Phys. Chem., **1996**, 100: 4551.
121. Kennedy T.A., Glaser E.R., Klein P.B., and Bhargava R.N., *Symmetry and electronic structure of the Mn impurity in ZnS nanocrystals.* Phys. Rev. B, **1995**, 52: R14356-R14359.
122. Dong B., Cao L., Su G., Liu W., Qu H., and Jiang D., *Synthesis and characterization of the water-soluble silica-coated ZnS:Mn nanoparticles as fluorescent sensor for Cu^{2+} ions.* J. Colloid Interface Sci., **2009**, 339: 78-82.
123. Cruz A.B., Shen Q., and Toyoda T., *The effect of ultraviolet irradiation on the photothermal, photoluminescence and photoluminescence excitation spectra of Mn-doped ZnS nanoparticles.* Thin Solid Films, **2006**, 499: 104-109.
124. Beaulac R., Archer P.I., and Gamelin D.R., *Luminescence in colloidal Mn^{2+}-doped semiconductor nanocrystals.* J. Solid State Chem., **2008**, 181: 1582-1589.
125. Xiao Q. and Xiao C., *Synthesis and photoluminescence of water-soluble Mn:ZnS/ZnS core/shell quantum dots using nucleation-doping strategy.* Opt. Mater., **2008**, 31: 455-460.
126. Sun L., Liu C., Liao C., and Yan C., *ZnS nanoparticles doped with Cu(I) by controlling coordiantion and precipitation in aqueous solution.* J. Mater. Chem., **1999**, 9: 1655-1657.
127. Kim D., Min K.-D., Lee J., Park J.H., and Chun J.H., *Influences of surface capping on particle size and optical characteristics of ZnS:Cu nanocrystals.* Mater. Sci. Eng. B, **2006**, 131: 13-17.
128. Jian W., Zhuang J., Zhang D., Dai J., Yang W., and Bai Y., *Synthesis of highly luminescent and photostable ZnS:Ag nanocrystals under microwave irradiation.* Mater. Chem. Phys., **2006**, 99: 494-497.
129. Qu S.C., Zhou W.H., Liu F.Q., Chen N.F., Wang Z.G., Pan H.Y., and Yu D.P., *Photoluminescence properties of Eu^{3+} -doped ZnS nanocrystals prepared in a water/methanol solution.* Appl. Phys. Lett., **2002**, 80: 3605-3607.
130. Tiseanu C., Mehra R.K., Kho R., and Kumke M., *Comparative Study of Time-Resolved Photoluminescence Properties of Terbium-Doped Thiosalicylic-Capped CdS and ZnS Nanocrystals.* J. Phys. Chem. B, **2003**, 107: 12153-12160.
131. Kushida T., Kurita A., Watanabe M., Kanematsu Y., Hirata K., Okubo N., and Kanemitsu Y., *Optical properties of Sm-doped ZnS nanocrystals.* J. Lumin., **2000**, 87-89: 466-468.

132. Jiang D., Cao L., Su G., Liu W., Qu H., Sun Y., and Dong B., *Shell thickness dependence of luminescence intensity in core/shell ZnS:Mn/ZnS nanoparticles.* Mater. Chem. Phys., **2009**, 115: 795-798.
133. Pradhan N., Battaglia D.M., Liu Y., and Peng X., *Efficient, stable, small, and water-soluble doped ZnSe nanocrystal emitters as non-cadmium biomedical labels.* Nano Lett., **2007**, 7: 312-317.
134. Emin S.M., Sogoshi N., Nakabayashi S., Fujihara T., and Dushkin C.D., *Kinetics of Photochromic Induced Energy Transfer between Manganese-Doped Zinc-Selenide Quantum Dots and Spiropyrans.* J. Phys. Chem. C, **2009**, 113: 3998-4007.
135. Nazerdeylami S., Saievar-Iranizad E., Dehghani Z., and Molaei M., *Synthesis and photoluminescent and nonlinear optical properties of manganese doped ZnS nanoparticles.* Physica B, **2011**, 406: 108-111.
136. Pradhan N., Goorskey D., Thessing J., and Peng X., *An alternative of CdSe nanocrystal emitters: Pure and tunable impurity emissions in ZnSe nanocrystals.* J. Am. Chem. Soc., **2005**, 127: 17586-17587.
137. Srivastava B.B., Jana S., and Pradhan N., *Doping Cu in Semiconductor Nanocrystals: Some Old and Some New Physical Insights.* J. Am. Chem. Soc., **2011**, 133: 1007-1015.
138. Isarov A.V. and Chrysochoos J., *Optical and Photochemical Properties of Nonstoichiometric Cadmium Sulfide Nanoparticles: Surface Modification with Copper (II) Ions.* Langmuir, **1997**, 13: 3142-3149.
139. Jian W., Zhuang J., Yang W., and Bai Y., *Improved photoluminescence of ZnS:Mn nanocrystals by microwave assisted growth of ZnS shell.* J. Lumin., **2007**, 126: 735-740.
140. Porambo M.W. and Marsh A.L., *Synthesis and photoluminescent properties of doped ZnS nanocrystals capped by poly(vinylpyrrolidone).* Opt. Mater., **2009**, 31: 1631-1635.
141. Peng W.Q., Cong G.W., Qu S.C., and Wang Z.G., *Synthesis and photoluminescence of ZnS:Cu nanoparticles.* Opt. Mater., **2006**, 29: 313-317.
142. Wang M., Sun L., Fu X., Liao C., and Yan C., *Synthesis and optical properties of ZnS:Cu(II) nanoparticles.* Solid State Commun., **2000**, 115: 493-496.
143. Cao L., Zhang J., Ren S., and Huang S., *Luminescence enhancement of core-shell ZnS:Mn/ZnS nanoparticles.* Appl. Phys. Lett., **2002**, 80: 4300-4302.
144. Song K.K. and Lee S., *Highly luminescent (ZnSe/ZnS) core-shell quantum dots for blue to UV emission: synthesis and characterization.* Curr. Appl. Phys., **2001**, 1: 169-173.
145. Lamer V.K. and Dinegar R.H., *Theory, production and mechanism of formation of monodisperse hydrosols.* J. Am. Chem. Soc., **1950**, 72: 4847-4854.
146. Murray C.B., Kagan C.R., and Bawendi M.G., *Synthesis and characterization of monodisperse nanocrystals and close-packed nanocrystal assemblies.* Annu. Rev. Mater. Sci., **2000**, 30: 545-610.
147. Voorhees P.W., *The theory of Ostwald ripening.* J. Stat. Phys., **1985**, 38: 231-252.
148. Ehlert O., Bücking W., Riegler J., Merkulov A., and Nann T., *Organometallic synthesis and electrophoretic characterization of high-quality ZnS:Mn/ZnS core/shell nanoparticles for bioanalytical applications.* Microchim. Acta, **2008**, 160: 351-356.
149. Chen H.-S., Lo B., Hwang J.-Y., Chang G.-Y., Chen C.-M., Tasi S.-J., and Wang S.-J.J., *Colloidal ZnSe, ZnSe/ZnS, and ZnSe/ZnSeS Quantum Dots Synthesized from ZnO.* J. Phys. Chem. B, **2004**, 108: 17119-17123.
150. Nemchinov A., Kirsanova M., Hewa-Kasakarage N.N., and Zamkov M., *Synthesis and characterization of Type II ZnSe/CdS Core/Shell Nanocrystals.* J. Phys. Chem. C, **2008**, 112: 9301-9307.
151. Choy W.C.H., Xiong S., and Sun Y., *A facile synthesis of zinc blende ZnSe nanocrystals.* J. Appl. Phys. D: Appl. Phys., **2009**, 42: art. no. 125410.
152. Hines M.A. and Guyot-Sionnest P., *Bright UV-blue luminescent colloidal ZnSe nanocrystals.* J. Phys. Chem. B, **1998**, 102: X-3657.
153. Reiss P., Quemard G., Carayon S., Bleuse J., Chandezon F., and Pron A., *Luminescent ZnSe nanocrystals of high color purity.* Mater. Chem. Phys., **2004**, 84: 10-13.
154. Reiss P., *ZnSe based colloidal nanocrystals: Synthesis, shape control, core/shell, alloy and doped systems.* New J. Chem., **2007**, 31: 1843-1852.
155. Zu L., Norris D.J., Kennedy T.A., Erwin S.C., and Efros A.L., *Impact of ripening on manganese-doped ZnSe nanocrystals.* Nano Lett., **2006**, 6: 334-340.
156. Pradhan N. and Peng X., *Efficient and color-tunable Mn-doped ZnSe nanocrystal emitters: control of optical performance via greener synthetic chemistry.* J. Am. Chem. Soc., **2007**, 129: 3339-3347.
157. Thakar R., Chen Y., and Snee P.T., *Efficient emission from core/(Doped) shell nanoparticles: Applications for chemical sensing.* Nano Lett., **2007**, 7: 3429-3432.
158. Shen H., Wang H., Li X., Niu J.Z., Wang H., Chen X., and Li L.S., *Phosphine-free synthesis of high quality ZnSe, ZnSe/ZnS, and Cu-, Mn-doped ZnSe nanocrystals.* Dalton Trans., **2009**: 10534.
159. Zeng R., Rutherford M., Xie R., Zou B., and Peng X., *Synthesis of highly emissive Mn-Doped ZnSe nanocrystals without pyrophoric reagents.* Chem. Mater., **2010**, 22: 2107-2113.

160. Acharya S., Sarma D.D., Jana N.R., and Pradhan N.J., *An alternate route to high-quality ZnSe and Mn-doped ZnSe nanocrystals.* Phys. Chem. Lett., **2010**, 1: 485-488.
161. Norris D.J., Yao N., Charnock F.T., and Kennedy T.A., *High-Quality Manganese-Doped ZnSe Nanocrystals.* Nano Lett., **2001**, 1: 3-7.
162. More D., Rajesh C., Lad A.D., Kumar G.R., and Mahamuni S., *Two photon absorption in Mn^{2+}-doped ZnSe quantum dots.* Opt. Commun., **2010**, 283: 2150-2154.
163. Mahamuni S., Lad A.D., and Patole S., *Photoluminescence Properties of Manganese-Doped Zinc Selenide Quantum Dots.* J. Phys. Chem. C, **2008**, 112: 2271-2277.
164. Zhang Y., Gan C., Muhammad J., Battaglia D., Peng X., and Xiao M., *Enhanced Fluorescence Intermittency in Mn-Doped Single ZnSe Quantum Dots.* J. Phys. Chem. C, **2008**, 112: 20200-20205.
165. Rogach A.L., Katsikas L., Kornovski A., Su D., Euchmüller A., and Weller H., *Synthesis and Characterization of Thiol-Stabilized CdTe Nanocrystals.* Ber. Bunsen-Ges. Phys. Chem., **1996**, 100: 1772-1778.
166. Mao J., Yao J.N., Wang L.N., and Liu W.S., *Easily-prepared high-quantum-yield CdS quantum dots in water using hyperbranched polyethylenimine as modifier.* J. Colloid Interface Sci., **2008**, 319: 353-356.
167. Rogach A.L., Kornovski A., Gao M., Eychmüller A., and Weller H., *Synthesis and characterization of a size series of extremely small thiol-stabilized CdSe nanocrystals.* J. Phys. Chem. B, **1999**, 103: 3065-3069.
168. Zhang H., Wang L., Xiong H., Hu L., Yang B., and Li W., *Hydrothermal Synthesis for High-Quality CdTe Nanocrystals.* Adv. Mater., **2003**, 15: 1712-1715.
169. Li H., Shih W.Y., and Shih W.H., *Highly photoluminescent and stable aqueous ZnS quantum dots.* Ind. Eng. Chem. Res., **2010**, 49: 578-582.
170. Harrison M.T., Kershaw S.V., Burt M.G., Rogach A.L., Kornowski A., Eychmüller A., and Weller H., *Strong photoluminescence in the near-infrared from colloidally-prepared HgTe nanocrystals.* Mater. Res. Symp. Proc., **1999**, 536: 217-222.
171. Chatterjee A., Priyam A., Bhattacharya S.C., and Saha A., *Differential growth and photoluminescence of ZnS nanocrystals with variation of surfactant molecules.* Colloids Surf. A: Physicochem. Eng. Aspects, **2007**, 297: 258-266.
172. Vacassy R., Scholz S.M., Dutta J., Plummer C.J.G., Houriet R., and Hofmann H., *Synthesis of Controlled Spherical Zinc Sulfide Particles by Precipitation from Homogenous Solutions.* J. Am. Ceram. Soc., **1998**, 81: 2699-2705.
173. Yang P., Lü M., Xü D., Yuan D., and Zhou G., *Synthesis and photoluminescence characteristics of doped ZnS nanoparticles.* Appl. Phys. A, **2001**, 73: 455-458.
174. Lee S., Song D., Kim D., Lee J., Kim S., Park I.Y., and Choi Y.D., *Effects of synthesis temperature on particle size/shape and photoluminescence characteristics of ZnS:Cu nanocrystals.* Mater. Lett., **2004**, 58: 342-346.
175. Becker W.G. and Bard A.J., *Photoluminescence and Photoinduced Oxygen Adsorption of Colloidal Zinc Sulfide Dispersions.* J. Phys. Chem., **1983**, 87: 4888-4893.
176. Zhang B.-H., Wu F.-Y., Wu Y.-M., and Zhan X.-S., *Fluorescent Method for the Determination of Sulfide Anion with ZnS:Mn Quantum Dots.* J. Fluoresc., **2010**, 20: 243-250.
177. Koneswaran M. and Narayanaswamy R., *L-cysteine-capped ZnS quantum dots based fluorescence sensor for Cu^{2+} ion.* Sens. Actuators B, **2009**, 139: 104-109.
178. Yang P., Song C., Lü M., Zhou G., Yang Z., Xu D., and Yuan D., *Photoluminescence of Cu^{+}-doped and Cu^{2+}-doped ZnS nanocrystallites.* J. Phys. Chem. Solids, **2002**, 63: 639-643.
179. Ren Z., Yang H., Shen L., and Han S.D., *Hydrothermal preparation and properties of nanocrystalline ZnS:Mn.* J. Mater. Sci.: Mater. Electron., **2008**, 19: 1-4.
180. Rashad M.M., Rayan D.A., and El-Barawy K., *Hydrothermal synthesis and magnetic properties of Mn doped ZnS nanoparticles.* J. Phys. : Conf. Ser. , **2010**, 200: 072077.
181. Lan G.Y., Lin Y.W., Huang Y.F., and H T Chang J. Mater. Chem. 2007, 2661., *Photo-assisted synthesis of highly fluorescent ZnSe(S) quantum dots in aqueous solution.* J. Mater. Chem., **2007**, 17: 2661-2666.
182. Zheng Y., Yang Z., and Ying J.Y., *Aqueous synthesis of glutathione-capped ZnSe and $Zn_{1-x}Cd_xSe$ alloyed quantum dots.* Adv. Mater., **2007**, 19: 1475-1479.
183. Gong H., Lin Z., Zhai G., Liu K., Wang Z., Huo X., Li J., Huang H., and Wang M., *Preparation of mercaptoacetic acid-capped ZnSe core-shell nanocrystals by hydrothermal method.* Ceramics Int., **2008**, 34: 1085-1087.
184. Deng Z., Lie F.L., Shen S., Ghosh I., Mansuripur M., and Muscat A.J., *Water-based route to ligand-selective synthesis of ZnSe and Cd-doped ZnSe quantum dots with tunable ultraviolet A to blue photoluminescence.* Langmuir, **2009**, 25: 434-442.

185. Fang Z., Li Y., Zhang H., Zhong X., and Zhu L., *Facile synthesis of highly luminescent UV-blue-emitting ZnSe/ZnS Core/Shell nanocrystals in aqueous media.* J. Phys. Chem. C, **2009**, 113: q14145-14150.
186. Qian H., Qiu X., Li L., and Ren J., *Microwave-assisted aqueous synthesis: A rapid approach to prepare highly luminescent ZnSe(S) alloyed quantum dots.* J. Phys. Chem. B, **2006**, 110: 9034-9040.
187. Wang C., Gao X., Ma Q., and Su X., *Aqueous synthesis of mercaptopropionic acid capped Mn^{2+}-doped ZnSe quantum dots.* J. Mater. Chem., **2009**, 19: 7016-7022.
188. Fang Z., Wu P., Zhong X., and Yang Y.-J., *Synthesis of highly luminescent Mn:ZnSe/ZnS nanocrystals in aqueous media.* Nanotechnol., **2010**, 21: 305604.
189. Shao P., Zhang Q., Li Y., and Wang H., *Aqueous synthesis of color-tunable and stable Mn^{2+}-doped ZnSe quantum dots.* J. Mater. Chem., **2011**, 21: 151-156.
190. Algar W.R., Tavares A.J., and Krull U., *Beyond labels: A review of the application of quantum dots as integrated components of assays, bioprobes, and biosensors utilizing optical transduction.* Anal. Chim. Acta, **2010**, 673: 1-25.
191. Clapp A.R., Goldman E.R., and Mattoussi H., *Capping of CdSe-ZnS quantum dots with DHLA and subsequent conjugation with the improved optical properties.* Nature Protocol., **2006**, 1: 1258-1266.
192. Goldman E.R., Anderson G.P., Tran P.T., Mattoussi H., Charles P.T., and Mauro J.M., *Conjugation of luminescent quantum dots with antibodies using an engineered adaptor protein to provide new reagents for fluoroimmunoassays.* Anal. Chem., **2002**, 74: 841-847.
193. Pinaud F., King D., Moore H.P., and Weiss S., *Bioactivation and Cell Targeting of Semiconductor CdSe/ZnS Nanocrystals with Phytochelatin-Related Peptides.* J. Am. Chem. Soc., **2004**, 126: 6115-6123.
194. Shang Q., Wang H., Yu H., Shan G., and Yan R., *Effect of phenylalanine on photoluminescence and stability of CdTe nanocrystals capped with thioglycolic acid.* Colloids Surf. A, **2007**, 294: 86-91.
195. Xing Y., Chaudry Q., Shen C., Kong K.Y., Zhau H.E., Chung L.W., Petros J.A., O'Regan R.M., Yezhhelyev M.V., Simons J.W., and Wang M.D., *Bioconjugated quantum dots for multiplexed and quantitative immunohistochemistry.* Nature Protocol., **2007**, 2: 1152-1165.
196. Pereira M. and Lai E.P.C., *Capillary electrophoresis for the characterization of quantum dots after non-selective or selective bioconjugation with antibodies for immunoassay.* J. Nanobiotech., **2008**, 6: 10.
197. Li K.G., Chen J.T., Bai S.S., Wen X., Song S.Y., Yu Q., Li J., and Wang Y.Q., *Intracellular oxidative stress and cadmium ions release induce cytotoxicity of unmodified cadmium sulfide quantum dots.* Toxicol. in Vitro, **2009**, 23: 1007-1013.
198. Lovrić J., Cho S.J., Winnik F.M., and Maysinger D., *Unmodified Cadmium Telluride Quantum Dots Induce Reactive Oxygen Species Formation Leading to Multiple Organelle Damage and Cell Death.* Chem. Biol., **2005**, 12: 1227-1234.
199. Oberdörster G., Oberdörster E., and Oberdörster J., *Nanotoxicology: an emerging discipline evolving from studies of ultrafine particles.* Env. Health Perspect., **2005**, 113: 823-839.
200. Kirchner C., Liedl T., Kudera S., Pellegrino T., Javier A.M., Gaub A.H., Stizle S., Fertig N., and Parak W.J., *Cytotoxicity of colloidal CdSe and CdSe/ZnS nanoparticles.* Nano Lett., **2005**, 5: 331-338.
201. Male K.B., Lachance B., Hrapovic S., Sunahara G., and Luong J.H.T., *Assessment of Cytotoxicity of Quantum Dots and Gold Nanoparticles Using Cell-Based Impedance Spectroscopy.* Anal. Chem., **2008**, 80: 5487-5493.
202. Ryman-Rasmussen J., Riviere J.E., and Monteiro-Riviere N.A., *Surface coatings determine cytotoxicity and irritation potential of quantum dot nanoparticles in epidermal keratinocytes.* J. Invest. Dermatol., **2007**, 127: 143-153.
203. Derfus A.M., Chan W.C.W., and Bhatia S.N., *Probing the Cytotoxicity of Semiconductor Quantum Dots.* Nano Lett., **2004**, 4: 11-18.
204. Maysinger D., Lovrić J., Eisenberg A., and Savić R., *Fate of micelles and quantum dots in cells.* Eur. J. Pharm. Biopharm., **2007**, 65: 270-281.
205. Lidke D.S., Nagy P., Heintzmann R., Arndt-Jovin D.J., Post J.N., Grecco H.E., Jares-Erijman E.A., and Jovin T.M., *Quantum dot ligands provide new insights into erbB/HER receptor-mediated signal transduction.* Nat. Biotechnol., **2004**, 22: 198-203.
206. Hardman R., *A Toxicologic Review of Quantum Dots: Toxicity Depends on Physicochemical and Environmental Factors.* Environ. Health Perspect., **2006**, 114: 165-172.
207. Lovrić J., Bazzi H.S., Cuie Y., Fortin G.R.A., Winnik F.M., and Maysinger D., *Differences in subcellular distribution and toxicity of green and red emitting CdTe quantum dots.* J. Mol. Med., **2005**, 83: 377-385.
208. Dobrovolskaia M.A. and Mcneil S.E., *Immunological properties of engineered nanomaterials.* Nat. Nanotech., **2007**, 2: 469-478.

209. Yang R.H., Chang L.W., Wu J.P., Tsai M.H., Wang H.J., Kuo Y.C., Yeh T.K., Yang C.S., and Lin P., *Persistent tissue kinetics and redistribution of nanoparticles, quantum dot 705, in mice: ICP-MS quantitative assessment.* Env. Health Perspect., **2007**, 115: 1339-1343.
210. Samia A.C.S., Chen X., and Burda C., *Semiconductor Quantum Dots for Photodynamic Therapy* J. Am. Chem. Soc., **2003**, 125: 15736-15737.
211. Wang L., Nagesha D.K., Selvarasah S., Dokmeci M.R., and Carrier R.L., *Toxicity of CdSe Nanoparticles in Caco-2 Cell Cultures.* J Nanobiotechnol., **2008**, 6: 11.
212. Tang M., Xing T., Zeng J., Wang H., Li C., Yin S., Yan D., Deng H., Liu J., Wang M., Chen J., and Ruan D.-Y., *Unmodified CdSe Quantum Dots Induce Elevation of Cytoplasmic Calcium Levels and Impairment of Functional Properties of Sodium Channels in Rat Primary Cultured Hippocampal Neurons.* Env. Health Perspect., **2008**, 116: 915-922.
213. Letayová L., Vlčková V., and Brozmanová J., *Selenium: From cancer prevention to DNA damage.* Toxicol., **2006**, 227: 1-14.
214. Moldovan L. and Moldovan N.I., *Oxygen free radicals and redox biology of organelles.* Histochem. Cell. Biol., **2004**, 122: 395-412.
215. Stern S.T., Zolnik B.S., McLeland C.B., Clogston J., Zheng J., and McNeil S.E., *Induction of autophagy in porcine kidney cells by quantum dots: a common cellular response to nanomaterials?* Toxicol. Sci., **2008**, 106: 140-152.
216. Shibata T., Lio K., Kawai Y., Shibata N., Kawaguchi M., Toi S., Kobayashi M., Yamamoto K., and Uchida K., *Identification of a lipid peroxidation product as a potential trigger of the p53 pathway.* J. Biol. Chem., **2006**, 281: 1196-1204.
217. Choi A.O., Cho S.J., Desbarats J., Lovrić J., and Maysinger D., *Quantum dot-induced cell death involves Fas upregulation and lipid peroxidation in human neuroblastoma cells.* J. Nanobiotech., **2007**, 5: 1.
218. Choi A.O., Brown S.E., Sysf M., and Maysinger D., *Quantum dot-induced epigenetic and genotoxic changes in human breast cancer cells.* J. Mol. Med., **2008**, 86: 291-302.
219. Voura E.B., Jaiswal J.K., Mattoussi H., and Simon S.M., *Tracking metastatic tumor cell extravasation with quantum dot nanocrystals and fluorescence emission-scanning microscopy.* Nat. Med., **2004**, 10: 993-998.
220. Juzenas P., Generalov R., Juzeniene A., and Moan J., *Generation of Nitrogen Oxide and Oxygen Radicals by Quantum Dots.* J. Biomed. Nanotechnol., **2008**, 4: 450-456.
221. Jamieson T., Bakhshi R., Petrova D., Pocock R., Imani M., and Seifalian A.M., *Biological applications of quantum dots.* Biomaterials, **2007**, 28: 4717-4732.
222. Fischer H., Liu L., Pang K.S., and Chan W., *Pharmacokinetics of nanoscale quantum dots: in vivo distribution, sequestration, and clearance in the rat.* Adv. Funct. Mater., **2006**, 16: 1299-1305.
223. Delehanty J.B., Boeneman K., Bradburne C.E., Robertson K., and Medinz I.L., *Quantum Dots: a powerful tool for understanding the intricacies of nanoparticle-mediated drug delivery.* Expert Opin. Drug Deliv., **2009**, 6: 1091-1112.
224. Schroeder J.E., Shweky I., Shmeeda H., Baniin U., and Gabizon A., *Folate-mediated tumor cell uptake of quantum dots entrapped in lipid nanoparticles.* J. Controlled Release, **2007**, 124: 28-34.
225. Clift M.J.D., Rothen-Rutishauser B., Brown D.M., R R.D., Donaldson K., Proudfoot L., Guy K., and Stone V., *The impact of different nanoparticle surface chemistry and size on uptake and toxicity in a murine macrophage cell line.* Toxicol. Appl Pharmacol., **2008**, 232: 418-427.
226. Larson D.R., Zipfel W.R., Williams R.M., Clark S.W., Bruchez M.P., Wise F.W., and Webb W.W., *Water-Soluble Quantum Dots for Multiphoton Fluorescence Imaging in Vivo.* Science, **2003**, 300: 1434.
227. Meng H., Chen J.-Y., Mi L., Wang P.-N., Ge M.-Y., Yue Y., and Dai N., *Conjugates of folic acids with BSA-coated quantum dots for cancer cell targeting and imaging by single-photon and two-photon excitation.* J. Biol. Inorg. Chem., **2011**, 16: 117-123.
228. Quarta A., Ragusa A., Deka S., Tortiglione C., Tino A., Cingolani R., and Pellegrino T., *Bioconjugation of Rod-Shaped Fluorescent Nanocrystals for Efficient Targeted Cell Labeling.* Langmuir, **2009**, 25: 12614-12622.
229. Yuan Q., Hein S., and Misra R.D.K., *New generation of chitosan-encapsulated ZnO quantum dots loaded with drug: Synthesis, characterization and in vitro drug delivery response.* Acta Biomater., **2010**, 6: 2732-2739.
230. Sun L., Zang Y., Sun M., Wang H., Zhu X., Xu S., Yang Q., Li Y., and Shan Y., *Synthesis of magnetic and fluorescent multifunctional hollow silica nanocomposites for live cell imaging.* J. Colloid Interface Sci., **2010**, 350: 90-98.
231. Bharali D.J., Lucey D.W., Jayakumar H., Pudavar H.E., and Prasad P.N., *Folate-Receptor-Mediated Delivery of InP Quantum Dots for Bioimaging Using Confocal and Two-Photon Microscopy.* J. Am. Chem. Soc., **2005**, 127: 11364-11371.

232. Han R., Yu M., Zheng Q., Wang L., Hong Y., and Sha Y., *A Facile Synthesis of Small-Sized, Highly Photoluminescent, and Monodisperse CdSeS QD/SiO_2 for Live Cell Imaging.* Langmuir, **2009**, 25: 12250-12255.
233. Shi C., Zhu Y., Cerwinka W.H., Zhau H.E., Marshall F.F., Simons J.W., Nie S., and Chung L.W.K., *Seminar article Quantum Dots: Emerging applications in urologic oncology.* Urol. Oncol. Semin. Origin. Invest., **2008**, 26: 86-92.
234. Mathew M.E., Mohan J.C., Manzoor K., Nair S.V., Tamura H., and Jayakumar R., *Folate conjugated carboxymethyl chitosan-manganese doped zinc sulphide nanoparticles for targeted drug delivery and imaging of cancer cells.* Carbohydr. Polym., **2010**, 80: 442-448.
235. Chakravarthy K.V., Davidson B.A., Helinski J.D., Ding H., Law W.-C., Yong K.-T., Prasad P.N., and Knight P.R., *Doxorubicin conjugated quantum dots to target alveolar macrophages/inflammation.* Nanomedicine, **2010**, doi:10.1016/j.nano.2010.09.001.
236. Jhaveri M.S., Rait A.S., Chung K.-N., Trepel J.B., and Chang E.H., *Antisense oligonucleotides targeted to the human α folate receptor inhibit breast cancer cell growth and sensitize the cells to doxorubicin treatment.* Mol. Cancer Ther., **2004**, 3: 1505-1512.
237. Gabizon A., Horowitz A.T., Goren D., Tzemach D., Mandelbaum-Shavit F., Qazen M.M., and Zalipsky S., *Targeting Folate Receptor with Folate Linked to Extremities of Poly(ethylene glycol)-Grafted Liposomes: In Vitro Studies.* Bioconjugate Chem., **1999**, 10: 289-298.
238. Ciofani G., Raffa V., Menciassi A., and Cuschieri A., *Folate Functionalized Boron Nitride Nanotubes and their Selective Uptake by Glioblastoma Multiforme Cells: Implications for their Use as Boron Carriers in Clinical Boron Neutron Capture Therapy.* Nanoscale Res. Lett., **2009**, 4: 113-121.
239. Talwar G.P. and Srivastava L.M., *Textbook of Biochemistry and Human Biology*. 2006: Eastern Economy Edition. 1290.
240. Mohanty S.P. and Kougianos E., *Biosensors: A Tutorial Review.* IEEE Potentials, **2006**, 25: 35-40.
241. Sapsford K.E., Pons T., Medintz I.L., and Mattoussi H., *Biosensing with Luminescent Semiconductor Quantum Dots.* Sensors, **2006**, 6: 925-953.
242. Wang Y., Zheng J., Zhang Z., Yuan C., and Fu D., *CdTe nanocrystals as luminescent probes for detecting ATP, folic acid and L-cysteine in aqueous solution.* Colloid Surf., A: Physicochem. Eng. Aspects, **2009**, 342: 102-106.
243. Liang J., Huang S., Zeng D., He Z., Ji X., Ai X., and Yang H., *CdSe quantum dots as luminescent probes for spironolactone determination.* Talanta, **2006**, 69: 126-130.
244. Ji X., Zheng J., Xu J., Rastogi V.K., Cheng T.-C., DeFrank J.J., and Leblanc R.M., *(CdSe)ZnS Quantum Dots and Organophosphorous Hydrolase Bioconjugate as Biosensors for Detection of Paraoxon.* J. Phys. Chem. B, **2005**, 109: 3793-3799.
245. Chen Y. and Rosenzweig Z., *Luminescent CdS Quantum Dots as Selective Ion Probes.* Anal. Chem., **2002**, 74: 5132-5138.
246. Chen J.-L. and Zhu C.-Q., *Functionalized cadmium sulfide quantum dots as fluorescence probe for silver ion determination.* Anal. Chim. Acta, **2005**, 546: 147-153.
247. Li X., Zhou Y., Zheng Z., Yue X., Dai Z., Liu S., and Tang Z., *Glucose Biosensor Based on Nanocomposite Films of CdTe Quantum Dots and Glucose Oxidase.* Langmuir, **2009**, 25: 6580-6586.
248. Frasco M.F. and Chaniotakis N., *Bioconjugated quantum dots as fluorescent probes for bioanalytical applications.* Anal. Bioanal. Chem., **2010**, 396: 229-240.
249. Freeman R., Bahshi L., Finder T., Gill R., and Willner J., *Competitive analysis of saccharides or dopamine by boronic acid-functionalized CdSe-ZnS quantum dots.* Chem. Commun., **2009**: 764-766.
250. Medintz I.L., Clapp A.R., Mattoussi H., Goldman E.R., Fisher B., and Mauro J.M., *Self-assembled nanoscale biosensors based on quantum dot FRET donors.* Nat. Mater., **2003**, 2: 630-638.
251. So M.K., Xu C., Loening A.M., Gambhir S.S., and Rao J., *Self-illuminating quantum dot conjugates for in vivo imaging.* Nat. Biotechnol., **2006**, 24: 339-343.
252. Yao H., Zhang Y., Xiao F., Xia Z., and Rao J., *Quantum Dot/Bioluminescence Resonance Energy Transfer Based Highly Sensitive Detection of Proteases.* Agnew. Chem. Int. Ed., **2007**, 46: 4346-4349.
253. Huang X., Li L., Qian H., Dong C., and Ren J., *A Resonance Energy Transfer between Chemiluminescent Donors and Luminescent Quantum-Dots as Acceptors (CRET).* Angew. Chem., **2006**, 118: 5264-5267.
254. Li Z., Wang Y., Zhang G., Xu W., and Han Y., *Chemiluminescence resonance energy transfer in the luminol-CdTe quantum dots conjugates.* J. Lumin., **2010**, 130: 995-999.
255. Sharman M.W., Allen C.M., and Lier J.E.V., *Photodynamic therapeutics: Basic principles and clinical applications.* Drug Discov. Today, **1999**, 4: 507-517.
256. MacDonald I.J. and Dougherty T.J., *Basic Principles of Photodynamic Therapy.* J. Porphyr. Phthalocya., **2001**, 5: 105-129.

257. Narband N., Mubarak M., Ready D., Parkin I.P., Nair S.P., Green M.A., Beeby A., and Wilson M., *Quantum dots as enhancers of the efficacy of bacterial lethal photosensitization.* Nanotechnol., **2008**, 19: 445102.
258. Lukšienė Ž., *Photodynamic therapy: mechanism of action and ways to improve the efficiency of treatment.* Medicina, **2003**, 39: 1137-1150.
259. Solban N., Rizvi I., and Hasan T., *Targeted photodynamic therapy.* Laser Surg. Med., **2006**, 38: 522-531.
260. Kübler A.C., *Photodynamic therapy.* Medical Laser Application, **2005**, 20: 37-45.
261. Sukhanova A., Devy J., Venteo L., Kaplan H., Artemyev M., Oleinikov V., Klinov D., Pluot M., Cohen J.H.M., and Nabiev I., *Biocompatible fluorescent nanocrystals for immunolabeling of membrane proteins and cells.* Anal. Biochem., **2004**, 324: 60-67.
262. Talapin D., Mekis I., Götzinger S., Kornowski A., Benson O., and Weller H., *CdSe/CdS/ZnS and CdSe/ZnSe/ZnS core-shell-shell nanocrystals.* J. Phys. Chem. B, **2004**, 108: 18826-18831.
263. He Y., Sai L.M., Lu H.T., Hu M., Lai W.Y., Fan Q.L., Wang L.H., and Huang W., *Microwave-assisted synthesis of water-dispersed CdTe nanocrystals with high luminescent efficiency and narrow size distribution.* Chem. Mater., **2007**, 19: 359-365.
264. Anas A., Akita H., Harashima H., Ishikawa M., and Biju V., *Photosensitized breakage and damage of DNA by CdSe-ZnS quantum dots.* J. Phys. Chem. B, **2008**, 112: 10005-10011.
265. Liang J., He Z., Huang S., Ai X., Yang H., and Han H., *Study on DNA damage induced by CdSe quantum dots using nucleic acid molecular "light switches" as probe.* Talanta, **2007**, 71: 1675-1678.
266. Fischer M. and Georges J., *Fluorescence quantum yield of rhodamine 6G in ethanol as a function of concentration using thermal lens spectrometry.* Chem. Phys. Lett., **1996**, 260: 115-118.
267. Zhuang J., Zhang X., Wang G., Li D., Yang W., and Li T., *Synthesis of water-soluble ZnS:Mn^{2+} nanocrystals by using mercaptopropionic acid as stabilizer.* J. Mater. Chem., **2006**, 13: 1853-1857.
268. Zheng J., Yuan X., Ikezawa M., Jing P., Liu X., Zheng Z., Kong X., Zhao J., and Masumoto Y., *Efficient photoluminescence of Mn^{2+} ions in MnS/ZnS core/shell quantum dots.* J. Phys. Chem. C, **2009**, 113: 16969-16974.
269. Corrado C., Hawker M., Livingston G., Medling S., Bridges F., and Zhang J.Z., *Enhanced Cu emission in ZnS:Cu, Cl/ZnS core-shell nanocrystals.* Nanoscale, **2010**, 2: 1213-1221.
270. Klayman D.L. and Griffin T.S., *Reaction of selenium with sodium borohydride in protic solvents. A facile method for introduction of selenium into organic molecules.* J. Am. Chem. Soc., **1973**, 95: 197-199.
271. Berridge M.V., Herst P.M., and Tan A.S., *Tetrazolium dyes as tools in cell biology: new insights into their cellular reduction.* Biotechnol. Rev., **2005**, 11: 127-152.
272. Jiang Z.J., Woolard A.C.S., and Wolff S.P., *Hydrogen Peroxide production during experimental protein glycation.* FEBS Lett., **1990**, 268: 69-71.
273. Dringen R., Kussmaul L., and Hamprecht B., *Detoxification of exogenous hydrogen peroxide and organic hyperoxides by cultured astroglial cells assesed by microtiter plate assay.* Brain Res. Protoc., **1998**, 2: 223-228.
274. Gülden M., Jess A., Kammann J., Maser E., and Seibert H., *Cytotoxic potency of H_2O_2 in cell cultures: Impact of cell concentration and exposure time.* Free Radical Biol. Med., **2010**, 49: 1298-1305.
275. Aboulaich A., Geszke M., Balan L., Ghanbaja J., Medjahdi G., and Schneider R., *Water-Based Route to Colloidal Mn-Doped ZnSe and Core/Shell ZnSe/ZnS Quantum Dots.* Inorg. Chem., **2010**, 49: 10940-10948.
276. Geszke M., Murias M., Balan L., Medjahdi G., Korczynski J., Moritz M., Lulek J., and Schneider R., *Folic acid-conjugated core/shell ZnS:Mn/ZnS quantum dots as targeted probes for two-photon fluorescence imaging of cancer cells.* Acta Biomater., **2011**, 7: 1327-1338.
277. Martinez-Castanon G.A., Martinez-Mendoza J.R., Ruiz F., and Gonzalez-Hernandez J., *Synthesis and optical characterization of ZnS, ZnS:Mn and (ZnS:Mn)_CdS core–shell nanoparticles.* Inorg. Chem. Commun., **2007**, 10: 531-534.
278. Jiang D., Cao L., Liu W., Su G., Qu H., Sun Y., and Dong B., *Synthesis and luminescence properties of core/shell ZnS:Mn/ZnO nanoparticles.* Nanoscale Res. Lett., **2009**, 4: 78-83.
279. Ethiraj A.S., Hebalkar N., Kulkarni S.K., Pasrisha R., Urban J., Dem C., Schmitt M., Kiefer W., Weinhardt L., Joshi S., Fink R., Heske C., Kumpf C., and Umbach E., *Enhancement of photoluminescence in manganese-doped ZnS nanoparticles due to a silica shell.* J. Chem. Phys., **2003**, 118: 8945-8953.
280. Sun J., Zhang J., Guan S., and Yang W.J., *Synthesis of robust water-soluble ZnS:Mn/SiO2 core/shell nanoparticles.* Nanopart. Res., **2008**, 10: 653-658.
281. Liu X., Ni X., Wang J., and Yu X., *A novel route to photoluminescent, water-soluble Mn-doped ZnS quantum dots via photopolymerization initiated by the quantum dots.* Nanotechnol., **2008**, 19: 485602.

282. Chen W., Sammynaiken R., and Huang Y., *Luminescence enhancement of ZnS:Mn nanoclusters in zeolit.* J. Appl. Phys., **2000**, 88: 5188-5193.
283. Chen W., Sammynaiken R., Huang Y., Malm J.O., Wallenberg R., Bovin J.O., Zwiller V., and Kotov N.A., *Crystal field, phonon coupling and emission shift of Mn^{2+} in ZnS:Mn nanoparticles.* J. Appl. Phys., **2001**, 89: 1120-1129.
284. Visschere P.D. and Neyts K., *Concentration quenching and luminescent decay in AC thin-film ZnS:Mn electroluminescent devices.* J. Lumin., **1992**, 52: 313-323.
285. Khosravi A.A., Kundu M., Kuruvilla B.A., Shekhawat G.S., Gupta R.P., Sharma A.K., Vyas P.D., and Kulkarni S.K., *Manganese doped zinc sulphide nanoparticles by aqueous method.* Appl. Phys. Lett., **1995**, 67: 2506-2508.
286. Peng W.Q., Qu S.C., Cong G.W., and Wang Z.G., *Concentration effect of Mn^{2+} on the photoluminescence of ZnS:Mn nanocrystals.* J. Crystal Growth, **2005**, 279: 454-460.
287. Aldeek F., Balan L., Lambert J., and Schneider R., *The influence of capping thioalkyl acid on the growth and photoluminescence efficiency of CdTe and CdSe quantum dots.* Nanotechnol., **2008**, 19: 475401.
288. Shannon R.D., *Revised effective ionic radii and systematic studies of interatomic distances in halides and chalgogenides.* Acta Cryst. Section A, **1976**, 32: 751-767.
289. Yang H. and Holloway P.H., *Enhanced photoluminescence from CdS:Mn/ZnS core/shell quantum dots.* Appl. Phys. Lett., **2003**, 82: 1965-1967.
290. Yang H. and Holloway P.H., *Efficient and photostable ZnS-passivated CdS:Mn luminescent nanocrystals.* Adv. Func. Mater., **2004**, 14: 152-156.
291. Zhang Z.H., Chin W.S., and Vittal J.J., *Water-Soluble CdS Quantum Dots Prepared from a Refluxing Single Precursor in Aqueous Solution.* J. Phys. Chem. B, **2004**, 108: 18569-18574.
292. Artemyev M.V., Woggon U., Jaschinski H., Gurinovich L.I., and Gaponenko S.V., *Spectroscopic Study of Electronic States in an Ensemble of Close-Packed CdSe Nanocrystals.* J. Phys. Chem. B, **2000**, 104: 11617-11621.
293. Kripal R. and Gupta A.K., *EPR and optical studies of ZnS:Mn nanoparticles* Chalcog. Lett., **2010**, 7: 203-209.
294. Ge J.P., Xu S., Zhuang J., Wang X., Peng Q., and Li Y.D., *Synthesis of CdSe, ZnSe, and $Zn_xCd_{1-x}Se$ Nanocrystals and Their Silica Sheathed Core/Shell Structures.* Inorg. Chem., **2006**, 45: 4922-4927.
295. Peng W.Q., Qu S.C., Cong G.W., Zheng X.Q., and Wang Z.G., *Optical and magnetic properties of ZnS nanoparticles doped with Mn^{2+}.* J. Crystal Growth, **2005**, 282: 179-185.
296. Barthon C., Benoit J., Bennaloul P., and Morell A., *Mn^{2+} concentration effect on the optical properties of Zn_2SiO_4:Mn phosphors.* J. Electrochem. Soc., **1994**, 141: 524-528.
297. Ronda C.R. and Amrein T., *Evidence for exchange-induced luminescence in Zn_2SiO_4 :Mn.* J. Lumin., **1996**, 69: 245-248.
298. Bol A.A. and Meijerink A., *Luminescence quantum efficiency of nanocrystalline ZnS:Mn^{2+}:1. Surface passivation and Mn^{2+} concentration.* J. Phys. Chem. B, **2001**, 105: 10197-10202.
299. Hwang C.S. and Cho I.H., *Characterization of the ZnSe/ZnS core shell quantum dots synthesized at various temperature conditions and the water soluble ZnSe/ZnS quantum dots.* Bull. Korean Chem. Soc., **2005**, 26: 1776-1782.
300. Ali M. and Sarma D.D., *Synthesis of ZnSe quantum dots and ZnSe-ZnS core/shell nanostructures.* J. Nanosci. Nanotech., **2007**, 7(6): 1960-1964.
301. Lad A.D. and Mahamuni S., *Effect of ZnS shell formation on the confined energy levels of ZnSe quantum dots.* Phys. Rev. B, **2008**, 78: 125421.
302. Matylitsky V.V., Shavel A., Gaponik N., ller A.E., and Wachtveitl J., *Ultrafast interfacial charge carrier dynamics in ZnSe and ZnSe/ZnS core/shell nanoparticles: Influence of shell formation.* J. Phys. Chem. C, **2008**, 112: 2703-2710.
303. Xing G., Ji W., Zheng Y., and Ying J.Y., *High efficiency and nearly cubic power dependence of below-band-edge photoluminescence in water-soluble, copper-doped ZnZe/ZnS quantum dots.* Opt. Express, **2008**, 16: 5710-5715.
304. Gan C., Zhang Y., Battaglia D., Peng X., and Xiao M., *Fluorescence lifetime of Mn-doped ZnSe quantum dots with size dependence.* Appl. Phys. Lett., **2008**, 92: 241111.
305. Smith B.A., Zhang J.Z., Joly A., and Liu J., *Luminescence decay kinetics of Mn^{2+}-doped ZnS nanoclusters grown in reverse micelles.* Phys. Rev. B, **2000**, 62: 2021-2028.
306. Bol A.A. and Meijerink A., *Long-lived Mn^{2+} emission in nanocrystalline ZnS:Mn^{2+}.* Phys. Rev. B, **1998**, 58: R15997-R16000.
307. Stewart M.H., Susumu K., Mei B.C., Medintz I.L., Delehanty J.B., Blanco-Canosa J.B., Dawson P.E., and Mattoussi H., *Multidentate Poly (ethylene glycol) Ligands Provide Colloidal Stability to*

Semiconductor and Metallic Nanocrystals in Extreme Conditions. J. Am. Chem. Soc., **2010**, 132: 9804-9813.
308. Valeur B., *Molecular Fluorescence: Principles and Applications.* Wiley-VCH, Weinheim, **2001**: 72-86.
309. Tyagi A. and Penzkofer A., *Fluorescence spectroscopic behaviour of folic acid.* Chem. Phys. , **2010**, 367: 83-92.
310. Ciuchi F., Nicola G.D., Franz H., Giovanni G., Marioni P., Bossi M.G.P., and Spada G.P., *Self-recognition and Self-Assembly of Folic Acid Salts: Columnar Liquid Crystalline Polymorphism and the Column Growth Process.* J. Am. Chem. Soc., **1994**, 116: 7064-7071.
311. Liang L. and Subirade M., *Beta-Lactoglobulin/Folic Acid Complexes Formation, Characterization, and Biological Implications.* J Phys Chem B, **2010**, 114: 6707-6712.
312. Xu C. and Bakker E., *Multicolor Quantum-dot Encoding for Polymeric Particle-Based Optical Sensors.* Anal. Chem., **2007**, 79: 3716-3723.
313. Jin W.J., Fernandez-Arguelles M.T., Costa-Fernandez J.M., Pereiro R., and Sanz-Medel A., *Photoactivated luminescent CdSe quantum dots as sensitive cyanide probes in aqueous solutions.* Chem. Commun., **2005**: 883-885.
314. Williams A. and Ibrahim I.T., *Carbodiimide chemistry: recent advances.* Chem. Rev., **1981**, 81: 589-636.
315. Templeton A.C., Cliffel D.E., and Murray R.W., *Redox and fluorophore functionalization of water-soluble, tiopronin-protected gold clusters.* J. Am. Chem. Soc., **1999**, 121: 7081-7089.
316. Sivakumaron S., Zhang J., Kelley K.M., Gonit M., Hao H., and Ratnam M., *Androgen activation of the folate receptor α gene through partial tethering of the androgen receptor by C/EBP α* J Steroid Biochem Mol Biol, **2010**, 122: 333-340.
317. Chen H., Ahn R., Bossche J.V.d., Thompson D.H., and O'Hallovan T.V., *Folate-mediated intracellular drug delivery increases the anti-cancer efficacy of nanoparticulate formulation of arsenic trioxide.* Mol. Cancer Ther., **2009**, 8: 1955-1963.
318. Hattori H. and Maitani Y., *Folate-linked lipid-based nanoparticle for targeted gene delivery.* Curr. Drug Deliv., **2005**, 2: 243-252.
319. Hoshino A., Fujioka K., Oku T., Suga M., Sasaki Y.F., Ohta T., Yasuhara M., Suzuki K., and Yamamoto K., *Physicochemical properties and cellular toxicity of nanocrystal quantum dots depend on their surface modification.* Nano Lett., **2004**, 4: 2163-2169.
320. Setua S., Menon D., Asok A., Nair S., and Koyakutty M., *Folate receptor targeted, rare-earth oxide nanocrystals for bi-modal fluorescence and magnetic imaging of cancer cells.* Biomaterials, **2010**, 31: 714-729.

Abstract in French

INSTITUT NATIONAL POLYTECHNIQUE DE LORRAINE

ÉCOLE DOCTORALE: RP2E
(Sciences et Ingénierie des Ressources, Procédés, Produits, Environment)
Laboratoire Réaction et Génie des Procédés (LRGP)

POZNAN UNIVERSITY OF MEDICAL SCIENCES

Département de Technologie Pharmaceutique

THÈSE

Présentée et soutenue publiquement le 28/10/2011
Pour l'obtention du grade de Docteur de l'INPL
(Spécialité : Génie des Procédés et des Produits)
et du grade de Docteur de Pharmacie
(Spécialité : Technologie Pharmaceutique)

Par

Małgorzata GESZKE-MORITZ

Synthèse de quantum dots stables et sans cadmium conjugués à l'acide folique pour l'imagerie de fluorescence de cellules cancéreuses

Directeurs de thèse:	Raphaël SCHNEIDER	Professeur (Nancy)
	Janina LULEK	Professeur (Poznań)

Composition du jury :

Président du jury : Professeur Edmund GRZEŚKOWIAK (Poznan)
Rapporteurs : Professeur Jean-Jacques GAUMET (Metz), Profeseur Jerzy Aleksander PAŁKA (Bialystok)
Membre invité : Docteur Lavinia BALAN (Mulhouse)

Poznan, Octobre 2011

Mots clés : quantum dots, nanocristaux, semi-conducteurs, nanotechnologie, fluorescence, sulfure de zinc, séléniure de zinc, quantum dots dopés par le manganèse ou le cuivre, acide folique, cancer, cytotoxicité, imagerie de fluorescence cellulaire, bio-sensing

Les Quantum Dots (QDs) sont des particules cristallines de semi-conducteur ou du métal de forme sphérique et de dimension nanométrique, le diamètre pouvant varier de 1 à 20 nm. Cela correspond à quelques centaines voire dizaine de milliers d'atomes. Beaucoup de ces atomes se trouvent à la surface des nanoparticules. Les QDs sont constitués d'un noyau inorganique de semi-conducteur (cœur) et d'un revêtement extérieur de molécules organiques (ligand). Le ligand permet de stabiliser les particules et empêche leur agrégation. Le cœur lui-même peut être recouvert d'une ou plusieurs coquilles d'autres matériaux semi-conducteurs. Ces coquilles permettent de protéger le cœur photoactif et d'améliorer ses propriétés photophysiques.

Les QDs les plus couramment utilisés, notamment pour les applications biologiques, proviennent du groupe II-VI des éléments du tableau périodique (CdS, CdSe, CdTe, ZnO, ZnS, ZnSe). D'autres QDs appartenant à d'autres familles ont également été synthétisés et étudiés. On peut citer les nanocristaux du groupe III-V (InP, InAs, GaN, GaP, GaAs), IV-VI (PbS, PbSe, PbTe), I-VII (CuCl), V-VI (Bi_2Te_3) et II-V (Cd_3As, Zn_3P_2, Zn_3As_2).

Les QDs de chalcogénures de cadmium (CdS, CdSe, CdTe) possèdent des propriétés physico-chimiques et photophysiques directement dépendantes de leur dimension. La propriété qui a le plus interessée la communauté scientifique au cours des dernières années est la possibilité de changer la largeur de bande d'énergie interdite (énergie de gap : *Eg*) par un simple changement du diamètre de la nanoparticule. Comme mentionné précédemment, les propriétés photophysiques des QDs dépendent de leurs dimensions et plus précisément du confinement quantique. L'absorption d'un photon par le QD a lieu si son l'énergie est supérieure au gap. En raison du confinement quantique, l'énergie du « band gap » est inversement proportionnelle à la longueur d'onde d'absorption du premier exciton. Une diminution du diamètre du nanocristal entraîne un déplacement hypsochrome (c'est-à-dire

vers des énergies plus élevées et donc des longueurs d'onde plus faibles du seuil d'absorption) (Figure 1).

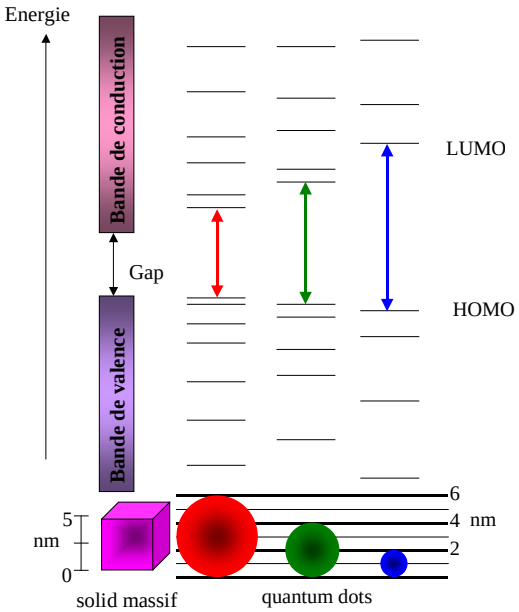

Figure 1. Evolution de la structure électronique entre le solide massif et des QDs de tailles décroissantes.

Lors d'une excitation lumineuse, le QD absorbe un photon conduisant à la formation d'un exciton (paire électron-trou). Via une recombinaison radiative électron-trou, l'électron peut retourner à son état fondamental (bande de valence) générant ainsi de la fluorescence. Le spectre de photoluminescence (PL) présente une raie fine et symétrique qui se déplace selon le diamètre des QDs. En théorie, la fluorescence correspond à l'émission d'un photon d'énergie égale au gap *Eg*. En fait, la raie de PL est déplacée de quelques nm vers les grandes longueurs d'onde par rapport au pic excitonique dans le spectre d'absorption. Ce décalage appelé décalage de Stokes (Stokes shift) trouve son origine dans la structure particulière des niveaux énergétiques des QDs.

La largeur à mi-hauteur (FWHM : *full width at half maximum*) des spectres de fluorescence des QDs est influencée par la polydispersité de l'échantillon. Par exemple, pour une population monodisperse, la largeur à mi-hauteur des spectres de fluorescence est

d’environ 20 à 30 nm. Si les QDs sont plus polydispersés en taille, la largeur à mi-hauteur du spectre de fluorescence peut atteindre 50-60 nm.

Souvent, la surface des nanocristaux contient des imperfections et des défauts comme des liaisons réactives ou des sites vacants dans la maille cristalline. Ces imperfections constituent des pièges à électrons, diminuent les performances optiques du QD, et altèrent notamment le rendement quantique de fluorescence. Si le cœur du QD n’est pas passivé, la désexcitation via des chemins non radiatifs peut devenir plus probable que la recombinaison radiative et, par conséquent, le rendement quantique de fluorescence diminue considérablement. L’apparition de bandes de fluorescence de faibles énergies à des longueurs d’onde élevées (« trap emissions ») est également observée. Afin d’éliminer ces défauts, une coquille inorganique d’un autre semi-conducteur, généralement de band gap plus large, est introduite sur le cœur pour corriger les défauts de surface.

Il existe principalement deux méthodes de synthèse des quantums dots de chalcogénure de cadmium (CdSe et CdTe). La première est appelée « synthèse organométallique » et la seconde est dite « synthèse hydrothermale ». Le principe de la synthèse est la séparation temporelle des processus de nucléation et de croissance (Figure 2).

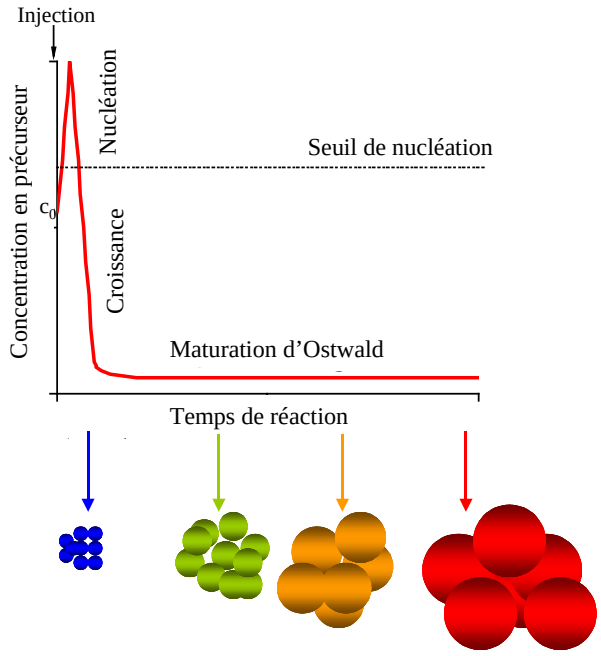

Figure 2. Les différentes étapes de la synthèse de QDs : nucléation homogène par l'injection rapide des précurseurs, croissance des germes par consommation des précurseurs en solution, suivie de la dissolution des germes plus petits au profit des plus gros.

La synthèse organométallique nécessite généralement l'utilisation de solvants toxiques, de coût élevé, ainsi qu'une technologie (boite à gants) qui n'est pas accessible pour tous les laboratoires. Les QDs ainsi préparés sont stabilisés par des ligands hydrophobes qui n'ont aucune affinité avec les milieux aqueux. Leur utilisation pour toute bio-application nécessitera une étape supplémentaire pour les disperser en milieu aqueux. Les synthèses dites hydrothermales constituent des alternatives de préparation de QDs solubles en milieu aqueux dès leur préparation.

La synthèse des QDs en milieux aqueux est une méthode qui permet d'accéder directement à des QDs biocompatibles et hydrodispersables. Ce procédé a, de plus, l'avantage d'être moins onéreux et d'utiliser des précurseurs moins toxiques que ceux employés dans les synthèses organométalliques. La synthèse en milieu aqueux à forte pression et haute température est appelée synthèse hydrothermale. Cette technique permet d'accélérer la phase de croissance des nanoparticules et d'améliorer leurs propriétés photophysiques.

Il existe plusieurs stratégies pour rendre hydrodispersables les QDs issus de la synthèse organométallique : échange de ligand à la surface des QDs, interactions des QDs hydrophobes avec des molécules amphiphiles ou incorporation des QDs dans des nanosphères de silice.

L'échange de ligand à la surface des QDs consiste au déplacement des ligands hydrophobes présent à la surface des QDs par des molécules hydrophiles. Dans le procédé d'interactions de QDs hydrophobes avec des molécules amphiphiles, le ligand hydrophobe reste lié à la surface du QD. La méthode consiste à ajouter des molécules amphiphiles pour disperser les QDs en milieu aqueux. Les chaînes alkyle du composé amphiphile interagissent par liaison de Van der Walls avec les groupements *n*-octyle de la tri-*n*-octylphosphine (TOP) et/ou d'oxyde de tri-*n*-octylphosphine (TOPO). Les extrémités hydrophiles des molécules amphiphiles permettent de disperser l'assemblage en milieu aqueux. Les composés amphiphiles peuvent encapsuler les QDs stabilisés par le TOPO et former des micelles par interaction hydrophobe/hydrophobe ou les QDs peuvent être encapsulés par des polymères amphiphiles. Dans la méthode d'incorporation des QDs dans des nanosphères de silice, les QDs sont mis au contact de tétraéthyl orthosilicate (TEOS). Ce dernier est hydrolysé dans des conditions douces et contrôlées pour former des nanosphères de silice qui enrobent les QDs.

La modification de la surface des QDs est une étape clé pour leur hydrodispersion. Une seconde fonctionnalisation est cependant nécessaire pour que ces sondes fluorescentes interagissent sélectivement avec une cible cellulaire donnée. Les stratégies de conjugaison avec les biomolécules (peptides, protéines, anticorps ou petites molécules) exigent que les biomolécules soient liées aux QDs sans altérer leur activité et/ou leur reconnaissance par certaines cibles cellulaires. Il existe deux grands procédés d'ancrage de biomolécules à la surface de QDs.

Les QDs peuvent être conjugués à des biomolécules chargées via des stratégies non covalentes impliquant des interactions électrostatiques. Dans ce cas, les QDs sont synthétisés

de manière à porter une charge complémentaire de celle de la biomolécule. Les deux entités sont simplement mélangées et s'auto-associent. Cette approche simple a été utilisée avec succès pour la préparation des QDs fonctionnalisés avec des protéines et des anticorps via l'interaction biotine/streptavidine. La conjugaison peut également mettre en jeu une interaction des biomolécules avec le métal (Zn, Cd, …) présent à la surface des QDs. Les protéines ou peptides possèdent des séquences d'acides aminés qui ont une affinité pour les métaux ou les cations métalliques.

L'ancrage des biomolécules par des liaisons covalentes est le plus souvent basé sur la réaction entre une fonction amine de la biomolécule et un acide carboxylique (ou carboxylate) appartenant au ligand du QD. Ce couplage se fait habituellement à l'aide d'un carbodiimide jouant le rôle d'agent de couplage tel que le chlorhydrate du *N*-(3-diméthylaminopropyl)-*N*-éthylcarbodiimide (EDC) et d'un activant tel que le *N*-hydroxysuccinimide (NHS). La conjugaison entre le ligand à la surface des QDs et la biomolécule désirée conduit à la formation d'une liaison amide.

L'intérêt majeur des QDs réside dans leur grande adaptabilité à de nombreuses applications biologiques. C'est en 1998 que deux équipes ont, pour la première fois, réussi à disperser des quantums dots en milieu aqueux.

Les QDs ont des propriétés optiques hors du commun qui offrent beaucoup d'avantages comparés aux fluorophores organiques (Fluorescéine, Rhodamine,...) pour l'imagerie de fluorescence de systèmes biologiques. On peut notamment citer :

- un large spectre d'absorption dans l'UV et le visible et un spectre d'émission étroit et symétrique (la majorité des fluorophores organiques ont un spectre d'absorption étroit et un spectre d'émission large). Un recouvrement des spectres d'absorption et d'émission est généralement observé pour les fluorochromes classiques tels que la

Rhodamine 6G, alors que pour les QDs, ce recouvrement peut être évité grâce à leur large *Stokes shift*,

- sur un même échantillon biologique, il est possible de visualiser simultanément plusieurs QDs émettant à des longueurs d'onde différentes via une excitation unique,
- une excellente photostabilité (résistance au photoblanchiment de plusieurs heures voire plusieurs jours),
- une très bonne résistance aux dégradations chimiques, de bons rendements quantiques de fluorescence (jusqu'à 85%).

A ce jour, relativement peu d'informations concernant la toxicité de ces nanoparticules existent et il demeure très difficile de connaitre tous les impacts de ces particules sur les cellules. Dans la littérature, beaucoup de données sur la toxicité de ces QDs commencent à émerger. Avant 2005, seul le relarguage des métaux lourd du cœur de la nanoparticule était mentionné comme principale cause de cytotoxicité. Depuis, d'autres mécanismes ont été décrits, comme par exemple un phénomène d'agrégation des nanoparticules à la surface de la cellule. Quand les QDs sont des donneurs d'énergies, ils transfèrent également de l'énergie aux molécules d'oxygène voisines et ainsi génèrent la production d'espèces réactives d'oxygène (EROs).

Il convient également d'étudier la toxicité des QDs ainsi que le traitement « pharmacologique » utilisé tel que la libération, l'absorption, la distribution, le métabolisme et leur élimination (LADME). A la différence des traitements médicamenteux, le confinement quantique dans les QDs nécessite d'adapter les paramètres pharmacologiques à la structure de ces nanoparticules. Dans le cas des QDs, il est nécessaire de caractériser à la fois la taille, la composition atomique, la pureté, l'encapsulation et la nature du ligand de la nanoparticule.

Les QDs les plus utilisés en bio-imagerie sont les chalcogénures de cadmium (semi-conducteurs du groupes II-VI), en particulier les cœurs CdSe et CdTe. Les QDs contenant du cadmium peuvent augmenter le taux d'EROS par trois mécanismes : (i) par excitation, la formation de la paire électron-trou engendre un transfert d'électron du QDs vers l'oxygène (génération de H_2O_2, $OH^{\cdot}$, $O_2^{\cdot-}$) (Figure 3), (ii) le système intracellulaire antioxydant peut être directement endommagé par interaction avec le QD et finalement, (iii) par interaction avec les ions Cd^{2+} relargués dans le milieu induisant l'augmentation d'EROS.

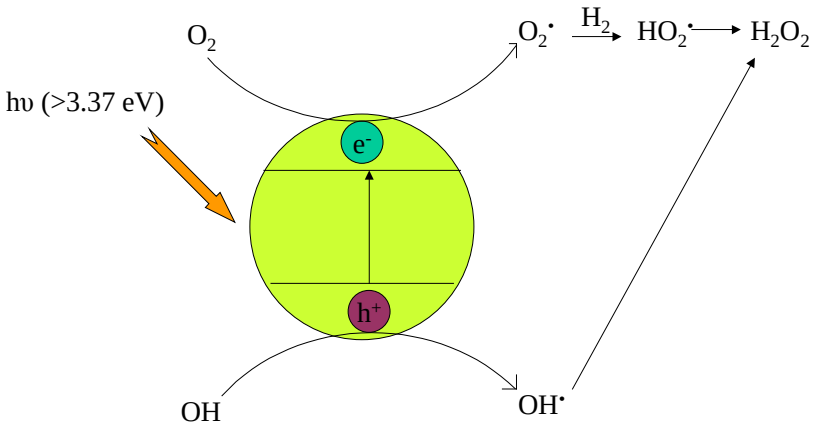

Figure 3. Mécanismes de transfert d'énergie.

La toxicité des QDs peut être utilisée comme un avantage biomédical, particulièrement dans le ciblage des cellules tumorales. Sous irradiation lumineuse, le QD est excité, l'électron produit est transféré à une molécule d'oxygène voisine et initie ainsi une chaine radicalaire qui va générer la mort des cellules. C'est le principe de la thérapie photo-dynamique (PDT).

Du fait de leur similarité dimensionnel avec les molécules biologiques (acides nucléiques, protéines et peptides par exemple), les QDs ont un intérêt majeur comme outils potentiels dans les applications biologiques. Des applications en chimie et physique ont été récemment développées pour permettre notamment la détection de différents états des systèmes biologique, à la fois électrique, optique et magnétique. En effet, les QDs possèdent des qualités attractives pour les applications dans le diagnostique et la thérapie. Ces NPs peuvent

être utilisées comme outils pour l'investigation et la compréhension des procédés moléculaires dans les cellules vivantes. Grâce aux propriétés photophysiques remarquables des QDs (grande photo stabilité, spectres d'émission fins et ajustables), ces nanocristaux sont utilisées comme des alternatives aux fluorophores organiques dans la bio-imagerie. La large bande d'absorption des QDs permet notamment de sélectionner la longueur d'onde d'émission souhaitée (dans le proche infra-rouge (NIR)) notamment par excitation à 2 ou multi-photonique. Grâce à ces sondes, le signal pénétre plus loin dans les tissus biologiques. Les QDs sont également des sondes idéales pour améliorer la détection de fluorescence en temps réel dans les cellules et les animaux vivants. L'avantage principal des QDs pour l'imagerie des cellules vivantes est la possibilité de faire varier la longueur d'onde d'émission du visible au proche IR par un choix judicieux de la taille et de la composition de la nanoparticule. Pour pouvoir utiliser les QDs dans un milieu biologique (aqueux), il faut rendre solubles les QDs (initialement hydrophobes) en fonctionnalisant la surface des QDs. Il a été montré dans la littérature que les QDs peuvent etre conjugués avec de nombreuses molécules biologiques (peptides, acides nucléiques, anticorps et des petites molécules ligands) afin de faire du ciblage. Ce ciblage, largement utilisé, est réalisé en conjugant un faisant un échange de ligand avec un ligand de plus haute affinité pour la nanoparticule. A la surface des cellules tumorales, on trouve un récepteur qui est sur-exprimé, celui-ci est la cible idéale. Le ciblage des cellules tumorale dans le but d'une application thérapeutique se restreint à quelques ligands. L'un d'eux est le récepteur de l'acide folique (FA) qui est reconnu comme le marqueur de nombreux cancers.

Les QDs participant à la création d'une nouvelle génération de biocapteurs fluorescentes ont récemment été développés. Dans le domaine des biocapteurs, les QDs sont particulièrement attractifs puisqu'ils permettent d'obtenir une photostabilité à long terme permettant une surveillance continue et en temps réel. La fluorescence des QDs est très sensible aux états de

surface et des interactions peuvent avoir lieu avec les espèces chimiques à la surface des QDs. Il en résulte un changement de la longueur d'onde d'émission des QDs. Avec ces « QD-based sensor », on mesure un signal de fluorescence qui augmente ou diminue. La composition chimique de la surface doit cependant toujours être parfaitement maitrisée pour augmenter les propriétés d'émission et la sélectivité de la sonde.

Les nanocristaux les plus utilisés pour imager les différents types de cellules sont à base de cadmium, un métal lourd, et leur toxicité doit être considérée. Dans le but de s'affranchir de ces problèmes liés à la toxicité, j'ai choisi, durant ma thèse, de travailler sur des nanoparticules sans métaux lourds de type ZnS et ZnSe.

Le but de mon travail était de développer une nouvelle classe de QDs de faible toxicité afin de les utiliser pour la bio-imagerie des cellules cancéreuses. Pour cela, il est nécessaire de préparer des sondes hydrosolubles, photostables, biocompatibles, de luminescence élevée et possédant une faible toxicité. Lors de ma thèse, j'ai greffé l'acide folique à la surface des QDs afin de faciliter le ciblage des cellules cancéreuses.

Dans une première partie, la synthèse des cœurs de type ZnS and ZnSe dopés au manganèse ou au cuivre et stabilisés par l'acide 3-mercaptopropionique (MPA) ou par le 1-thioglycérol (TG) a été réalisée par la voie hydrothermale. 4 types de nanocristaux ont été étudiés: ZnS:Mn/ZnS@MPA, ZnS:Mn@TG, ZnS:Cu/ZnS@MPA et ZnSe:Mn/ZnS@MPA. L'optimisation de paramètres tels que le pourcentage de dopant, le temps et la température de réaction, le type de ligand stabilisant, le ratio des précurseurs a été réalisée. Les techniques analytiques de caractérisation utilisées sont la spectroscopie UV-visible, la spectroscopie de fluorescence, la diffraction des rayons X (XRD), la spectroscopie photoélectronique de rayon X (XPS), la microscopie électronique à transmission (TEM), la diffusion dynamique de la lumière DLS, la spectroscopie infra-rouge (IR), et la résonance paraélectronique (RPE). La

fonctionnalisation de surface des QDs dopés au manganèse par l'acide folique jouant la rôle d'agent de ciblage a tout d'abord été mise au point. La toxicité des QDs a été déterminée sur des cellules cancéreuses telles que MCF-7, T47D, PC-3 et différents test de cytotoxicité [MTT, XTT et ferrous oxidation-xylenol orange (FOXO)] ont été réalisés. Finalement, les QDs de type ZnS:Mn conjugués à l'acide folique ont été utilisés pour la bio-imagerie des cellules cancéreuses par le biais d'une excitation biphotonique.

Le premier type de nanocristaux synthétisés est de type cœur/coquille ZnS:Mn/ZnS. Ces nanocristaux sont préparés en solution aqueuse en faisant réagir $ZnSO_4$ et $Mn(OAc)_2$ avec Na_2S en présence de MPA. La coquille de ZnS est ensuite introduite par croissance épitaxiale par décomposition du complexe Zn^{2+}-MPA à pH = 10.3. Cette opération permet d'augmenter le rendement quantique de fluorescence de 2.7 à 22%. La concentration optimale de manganèse est de 4%. Le spectre d'émission est exclusivement du à la transition d-d du manganèse. On a évalué l'effet de différents ligands (acide thioglycolique (TGA), acide mercaptopropionique (MPA), acide mercaptohexonique (MHA) et L-cystéine) sur les propriétés optiques des QDs. La meilleure fluorescence a été mesurée pour les QDs stabilisés par le MPA. La structure blende des cœurs ZnS a été confirmée par des études de DRX. La structure sphérique des nanocristaux et le diamètre (4.4 ± 0.7 nm pour ZnS:Mn/ZnS@MPA) ont été obtenus par le MET. La composition des nanocristaux (Zn, S, Mn, O, C et Na) a été obtenue par XPS.

Un deuxième type de QD a été préparé, des nanoparticules ZnS:Mn stabilisées par le thioglycerol (TG). La synthèse est identique à celle des QDs ZnS:Mn@MPA décrite précédemment. La concentration optimale des ions Mn^{2+} est de 4% et correspond à un rendement quantique de fluorescence de 10.8%. Ces QDs émettent à 590 nm. On a étudié les propriétés de photoluminescence avec différentes source de zinc (sulfate, acétate et nitrate de zinc). C'est l'acétate de zinc qui a donné les meilleures propriétés de photoluminescence. Le

diamètre de ces QDs ZnS:Mn (3.9 ± 0.5 nm) a été déterminé par MET. L'analyse XRD a confirmé la nature cristalline des QDs. On a mesuré la photostabilité de ces QDs à différents pH. Les meilleures conditions d'utilisation de ces QDs se trouvent en milieu basique (8-10). L'analyse XPS montre la présence des éléments Zn, S, O, C et Na. Le spectre FT-IR confirme la présence de TG à la surface des QDs et les analyses EPR montrent la présence de manganèse dans la maille cristalline des QDs.

Un troisième type de QDs a été synthétisé, cœur/coquille ZnS:Cu/ZnS stabilisés par le MPA obtenu par réaction de $Zn(NO_3)_2$, de $CuSO_4$ avec Na_2S en présence de MPA. Le rapport molaire optimal $Zn^{2+}/S^{2-}/Cu^{2+}$/MPA déterminé expérimentalement est de 1/0.52/0.003/2.27. La concentration optimale en cuivre est de 3%. Le meilleur rendement quantique de fluorescence (3.4%) a été obtenu en utilisant le ligand MPA pour une longueur d'onde d'émission de 510 nm. L'ajout de la coquille ZnS a permis d'augmenter le rendement quantique de fluorescence de 0.5%. Les spectres XRD confirment la nature cristalline des QDs cœur/coquille ZnS:Cu/ZnS@MPA. Leur diamètre est de 3.2 nm (diamètre hydrodynamique de 11.7 nm). L'analyse XPS confirme la présence de Zn, S, Cu, O, C et Na. Il a été observé qu'en augmentant la concentration des QDs dans le tampon borate, la longueur d'onde d'émission et le rendement quantique de fluorescence augmentaient linéairement et qu'il n'y avait pas de photoblanchiement. On a étudié l'influence de la température et du pH sur le rendement quantique de fluorescence. Un pH légèrement basique (8-10) et une température de 10 à 40°C sont les conditions optimales de ces sondes fluorescentes.

Le dernier type de nanocristaux synthétisés est de type ZnSe:Mn/ZnS stabilisés par le MPA. Leur synthèse est réalisée en milieu aqueux, en utilisant les précurseurs $ZnSO_4$, $Mn(OAc)_2$ et NaHSe en présence de MPA. Le meilleur rendement quantique a été obtenu en utilisant 4% de manganèse et un rapport Zn^{2+}/Se^{2-}/MPA de 1/0.9/20 à pH = 10.3. Après 24 h de réaction, des

QDs stables ont été obtenus avec un rendement quantique de fluorescence de 12.5% qui émettent à 590 nm. L'influence de différents ligands a été étudiée (TGA, MHA, acide mercaptosuccinique et L-cystéine). Avec les ligands TGA, MHA, MSA et Cys, les QDs ZnSe:Mn QDs montrent la transition $^4T_1 \rightarrow {}^6A_1$ de Mn^{2+} à 595 nm mais la bande d'émission est plus large que pour les QDs stabilisés par le MPA. Les résultats DRX confirment la structure cubique zinc blende et le diamètre des nanocristaux est de 3.5 nm. Par DLS, on mesure un diamètre hydrodynamique de 7.6 nm. Dans le spectre FT-IR, la fonction acide du MPA est observée et l'absence de vibration d'élongation des fonctions thiols SH confirme le greffage du ligand MPA à la surface des QDs ZnSe:Mn. L'analyse EDS montre une composition atomique des QDs similaire au ratio de précurseurs utilisé. Une fois la coquille introduite, le diamètre des QDs obtenu par MET est de 4.3 ± 0.5 nm (diamètre hydrodynamique de 8.0 nm). L'introduction de la coquille est confirmée par des mesures de photoluminescence résolue en temps avant et après la modification de la surface. On a également observé une variation de l'intensité de fluorecence des QDs en fonction du pH, les QDs ont une meilleure photostabilité à pH 12.

Une fois la synthèse des QDs réalisée, on s'intéresse à leur fonctionnalisation de surface en réalisant le couplage avec l'acide folique.

L'influence de l'acide folique sur les propriétés de photoluminescence a été réalisée sur quatre types de QDs (ZnS:Mn@MPA, ZnS:Cu@MPA, ZnS:Mn@TG et ZnSe:Mn@MPA). La dépendance des intensités de photoluminescence versus la concentration en acide folique a répond à la relation de Stern-Volmer. La diminution de la photoluminescence des QDs ZnS:Mn et ZnS:Cu QDs stabilisés par MPA dépend de la concentration en acide folique. On conserve cependant la même longueur d'onde d'émission et la forme du pic n'est pas altérée. Les mécanismes de cette diminution ont été étudiés.

Dans le cas de QDs dopés au manganèse, la diminution de photoluminescence corrèle relativement mal à la loi de Stern-Volmer. Le model de Perrin est plus adapté et prend en compte qu'un QD réagit avec plusieurs molécules d'acide folique. L'interférence de l'acide folique avec les QDs ZnS:Cu est d'environ 30% moindre qu'avec les QDs ZnS:Mn. Ces expériences ont permis d'établir le ratio de QD/FA optimal pour le couplage.

Le couplage covalent de l'acide folique sur les QDs ZnS:Mn/ZnS@MPA a été réalisé avec le 2,2'-(ethylenedioxy)-*bis*-ethylamine jouant le rôle d'espaceur. Les agents de couplage utilisés sont le 1-éthyl-3-(3-diméthylaminopropyl)carbodiimide (EDC) et le *N*-hydroxisuccinimide (NHS). Les groupements amine à la surface des QDs permettent de coupler l'acide folique par formation d'une liaison amide en utilisant l'EDC. On a préparé de la même manière des QDs cœur/coquille ZnSe:Mn/ZnS@MPA conjugués à l'acide folique. Le couplage covalent de l'acide folique à la surface des QDs ZnS:Mn@TG sont obtenus en réalisant le couplage entre les QDs et l'acide folique en présence d'EDC et de NHS. Les QDs ZnS:Mn ont conservé de bonnes propriétés de photoluminescence, un bon rendement quantique, et une structure cristalline. Les diamètres des QDs conjugués à l'acide folique ont été mesurés : 5.2 ± 1.0 nm pour les QDs ZnS:Mn/ZnS@MPA et 4.2 ± 0.7 nm pour les QDs ZnS:Mn stabilisés par TG. L'analyse XPS confirme la présence d'un atome d'azote N dans la structure de QDs fonctionnalisés par l'acide folique et la chromatographie (TLC) valide le couplage avec l'acide folique.

Dans le but d'utiliser les QDs comme sonde pour la bio-imagerie, nous avons étudié la cytotoxicité des QDs ZnS:Mn/ZnS@MPA, ZnS:Mn@TG et ZnSe:Mn/ZnS@MPA. Pour les tests, nous avons utilisé deux types de cellules : les cellules humaines cancéreuses surexprimant le récepteur folate (FR) (T47D) et MCF-7 et PC- 3 T47D étant les références. A noter que les cellules T47D sont les cellules responsables du cancer du sein et PC-3 sont les cellules responsables du cancer de la prostate. La toxicité des QDs a été mesurée, par une

exposition chronique, à des concentrations inférieures et supérieures de la concentration optimale pour la microscopie confocale (500 µM). Trois tests ont été utilisés pour évaluer la cytotoxicité des QDs : MTT, XTT et FOXO. Le test MTT est un test colorimétrique basé sur la réduction par les mitochondries du sel de tétrazolium (3-(4,5-diméthylthizaol-2-yl)-2,5-diphenyltétrazolium bromide (MTT) (jaune et hydrosoluble) en formazan (bleu et sous forme de cristaux insolubles). Récemment, des alternatives au test MTT ont été développées, comme par exemple, l'introduction de groupes chargés positivement et négativement sur la chaîne phényle du sel de tetrazolium. Dans le test XTT, la molécule de XTT (2-méthoxy-4-nitro-5-sulfophényl)-5-[(phenylamino)-carbonyl]-2H-tetrazolium hydroxide) est utilisée et offre une plus grande sensibilité de réponse. Nous avons choisi de travailler avec le test « FOXO », dans lequel on mesure la concentration en H_2O_2 dans le milieu cellulaire exposé aux QDs. La concentration en peroxyde d'hydrogène est déterminée par la l'oxydation du Fe^{+2} en Fe^{+3}) (mesure FOXO).

Les tests montrent une très faible toxicité des QDs ZnS:Mn@TG par rapport aux QDs ZnS:Mn@MPA et ZnSe@MPA. On constate que la composition du cœur et le ligand de surface jouent un rôle important dans la toxicité des nanoparticules. Il faut noter que les deux types de QDs stabilisés par le MPA (ZnS:Mn et ZnSe:Mn) sont moins toxiques sur les cellules T47D lorsque le coeur est passivé par la coquille de ZnS. En utilisant le même QD, à la même concentration mais sur les deux lignées de cellules, les résultats diffèrent. Les résultats obtenus avec le test XTT sur les cellules T47D correspondent à ceux obtenus avec le test MTT. En revanche, la cytotoxicité de ces QD sur les cellules PC-3 est beaucoup plus forte, même avec de faibles concentrations. Les résultats obtenus avec le test FOXO indiquent que la production de peroxyde dans le milieu cellulaire exposé aux QDs est plus forte dans les premières heures de l'expérience.

Au vu des résultats obtenus après les tests de cytotoxicité des différents QDs sur les différentes cellules, nous avons choisi de travailler avec les QDs ZnS:Mn stabilisés par le TG et le MPA comme marqueurs potentiels des cellules cancéreuses sur-exprimant le récepteur folate.

Pour mieux localiser les QDs dans les cellules, nous avons utilisé dans les expériences de bio-imagerie, les QDs MPA-capped ZnS:Mn comme sondes fluorescentes des cellules cancéreuses, et les QDs ZnS:Mn stabilisés par TG avec un fluorophore organique commercial pour mieux localiser l'accumulation des QDs dans les cellules. Dans toutes ces expériences, nous avons utilisé l'excitation biphotonique. Les QDs ZnS:Mn@MPA sont utilisés comme marqueur des deux types de cellules cancéreuses T47D et MCF-7. Les cellules ont été cultivées dans deux milieux de cultures : un milieu pauvre en acide folique et le milieu DMEM (Dulbecco's modified Eagle's medium). Les images confocales obtenues par excitation à 720 nm, après différents temps d'incubation, montrent une accumulation croissante des QDs conjugués à l'acide folique durant les six premières heures d'incubation. Après 72 h d'incubation avec les cellules, les propriétés optiques des QDs sont préservées, preuve de leur grande stabilité. Les photographies des QDs ZnS:Mn/ZnS conjugués à l'acide folique avec les cellules T47D cultivées dans le milieu déficient en acide folique montre une distribution homogène dans le cytoplasme à proximité du noyau. Les QDs non-modifiés ont une distribution plus hétérogène. Similairement, les images confocales obtenues avec les cellules T47D et MCF-7 cultivés dans les milieux DMEM démontrent une interaction des QDs avec les cellules, par contre les QDs marquent les cellules de manière non-homogène. De plus, aucun signe d'endommagement des cellules n'a été observé lorsque l'on utilise ces QDs peu toxiques. Quand la membrane des cellules T47D est saturée par une solution 3.5 mM d'acide folique libre avant l'addition des QDs, très peu de nanocristaux sont incorporés,

ce qui est une preuve d'une compétition spécifique. Ces résultats confirment le ciblage des cellules cancéreuses FR+ par les QDs conjugués à l'acide folique.

En conclusion de ce travail, nous avons préparé des sondes qui sont un outil potentiel pour la détection et la bio-imagerie des cellules. J'ai développé la synthèse en milieu aqueux de QDs sans cadmium, ZnS et ZnSe dopés par Mn, et ZnS dopé par Cu. L'optimisation des paramètres de synthèse et la passivation des cœurs ont été réalisées. Les nanocristaux ont été caractérisés par de nombreuses méthodes afin de déterminer leur taille, leur structure cristalline, la dispersion colloïdale, ainsi que les propriétés de photoluminescence. Les QDs ont ensuite été fonctionnalisé par l'acide folique, ligand permettant le ciblage des cellules cancéreuses. La cytotoxicité des QDs a été évaluée par différents tests : MTT, XTT et FOXO. Une faible cytotoxicité a été observée pour les QDs ZnS:Mn stabilisés par TG, les QDs ZnS:Mn et ZnSe:Mn stabilisés par le MPA étant un peu plus toxiques. Le ciblage récepteur-spécifique des QDs a été démontré par microscopie confocale à deux photons. Ces expériences ont également montré que les QDs s'accumulaient près du noyau des cellules.
La faible cytotoxicité de ces sondes fluorescentes, leur grande stabilité, ainsi que les excellentes propriétés photophysiques en font des outils de choix pour des applications biomédicales.

Abstract in Polish

POLITECHNIKA LOTARYŃSKA
(Institut National Polytechnique de Lorraine- INPL)

SZKOŁA DOKTORANCKA: RP2E
Laboratorium Reakcji i Inżynierii Chemicznej
(Laboratoire Réaction et Génie des Procédés- LRGP)

UNIWERSYTET MEDYCZNY IM. K. MARCINKOWSKIEGO W POZNANIU

Katedra i Zakład Technologii Postaci Leku

ROZPRAWA DOKTORSKA

prezentowana 28/10/2011
w celu uzyskania stopnia doktora INPL
(Specjalność: Inżynieria Procesu i Produktu)
(Génie des Procédés et des Produits)
i stopnia doktora farmacji (Specjalność: Technologia Postaci Leku)

przez

Małgorzatę GESZKE-MORITZ

Synteza stabilnych i niezawierających kadmu kropek kwantowych skoniugowanych z kwasem foliowym w celu obrazowania komórek nowotworowych

Promotorzy:	Raphaël SCHNEIDER	Profesor (Nancy)
	Janina LULEK	Profesor (Poznań)

Komisja:

Przewodniczący komisji: Professor Edmund GRZEŚKOWIAK (Poznań)
Recenzenci: Professor Jean-Jacques GAUMET (Metz), Professor Jerzy Aleksander PAŁKA (Białystok)
Zaproszony członek komisji: Doktor Lavinia BALAN (Mulhouse)

Poznań, październik 2011

Słowa kluczowe: kropki kwantowe- quantum dots (QDs), nanokryształy, półprzewodniki, nanotechnologia, fluorescencja, QDs nie zawierające kadmu, siarczek cynku, selenek cynku, QDs domieszkowane manganem i miedzią, kwas foliowy, nowotwór, cytotoksyczność, obrazowanie komórkowe, biosensorowanie

Kropki kwantowe (quantum dots- QDs) są krystalicznymi nanocząstkami zbudowanymi z materiałów półprzewodnikowych lub metalicznych. Mogą one mieć kształt kulisty, ich średnica mieści się w zakresie 1-20 nm, a w ich skład wchodzi 200- 10,000 atomów. Wiele z tych atomów znajduje się na powierzchni nanocząstek. Kropki kwantowe składają się z nieorganicznego rdzenia (materiał półprzewodnikowy) i otaczających go organicznych cząsteczek, zwanych ligandami. Ligandy stabilizują nanocząstki i zapobiegają ich agregacji. Rdzeń może być również otoczony powłoką/powłokami zbudowanymi z innych materiałów półprzewodnikowych. Te powłoki chronią fotoaktywny rdzeń i polepszają właściwości fotofizyczne kropek kwantowych.

Kropki kwantowe zwykle stosowane w naukach biologicznych zawierają w swym składzie pierwiastki należące do grup II-VI układu okresowego (CdS, CdSe, CdTe, ZnO, ZnS, ZnSe). Istnieją również kropki kwantowe zawierające pierwiastki z innych grup jak np. III-V (InP, InAs, GaN, GaP, GaAs), IV-VI (PbS, PbSe, PbTe), I-VII (CuCl), V-VI (Bi_2Te_3) i II-V (Cd_3As, Zn_3P_2, Zn_3As_2).

Kropki kwantowe zawierające kadm (CdS, CdSe, CdTe) posiadają właściwości fizyko-chemiczne i fotofizyczne bezpośrednio zależne od ich wymiarów. Najbardziej interesującą właściwością kropek kwantowych jest to, że istnieje możliwość zmiany wielkości energii ich pasma zabronionego (*Eg*) poprzez zmianę średnicy nanocząstki. Jak wspomniano, właściwości fotofizyczne kropek kwantowych zależą od ich wymiarów, a dokładniej od tzw. ograniczenia kwantowego (kwantowy efekt rozmiarowy). Absorpcja fotonu przez kropkę kwantową ma miejsce jeśli jego energia jest większa niż energia przerwy zabronionej. W wyniku ograniczenia kwantowego, energia pasma zabronionego jest odwrotnie

proporcjonalna do długości fali adsorpcji pierwszego ekscytonu (para: elektron-dziura elektronowa). Zmniejszenie średnicy nanokryształu pociąga za sobą przesunięcie hipsochromowe (to znaczy przesunięcie maksimum absorpcji w kierunku krótszych długości fali) (Rycina 1).

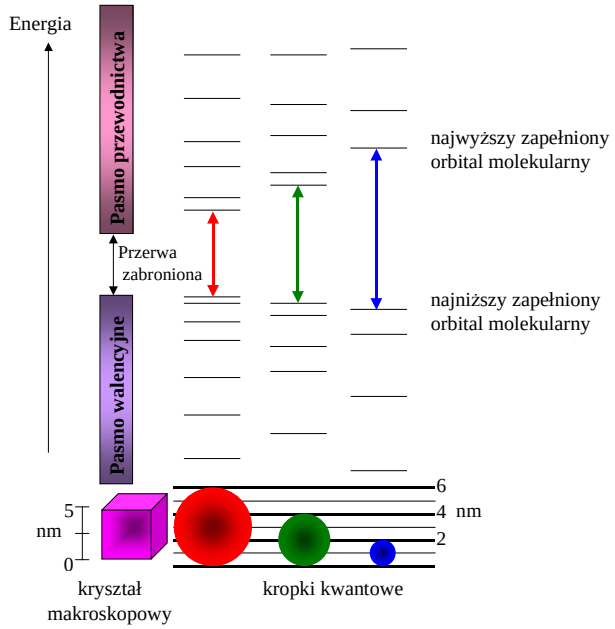

Rycina 1. Ewolucja struktury elektronowej od makrokryształu do kropek kwantowych o zmniejszającej się średnicy.

Podczas wzbudzenia promieniowaniem świetlnym kropka kwantowa absorbuje foton i powstaje ekscyton. Podczas przejścia promienistego elektron- dziura elektronowa, elektron może powrócić na swój poziom podstawowy (pasmo walencyjne) emitując fluorescencję. Widmo fluorescencji jest wąskie, symetryczne i zmienia położenie w zależności od średnicy kropek kwantowych. Teoretycznie, fluorescencja koresponduje z emisją fotonu o energii równej energii pasma zabronionego. W rzeczywistości, widmo fluorescencji jest przesunięte o kilka nm w kierunku fal dłuższych w stosunku do piku ekscytonowego w widmie absorpcji. To przesunięcie nazywa się przesunięciem Stokes'a i znajduje ono swoje wyjaśnienie w szczególnej strukturze poziomów energetycznych kropek kwantowych.

Na szerokość piku w połowie jego wysokości (FWHM : *full width at half maximum*) w widmie fluorescencji kropek kwantowych ma wpływ różnorodność próbki. W przypadku populacji jednorodnych kropek kwantowych, ta szerokość mieści się w granicach od 20 do 30 nm. Jeśli kropki kwantowe są mniej jednorodne, wówczas FWHM w widmie fluorescencji może wynosić od 50 do 60 nm.

Często powierzchnia nanokryształów zawiera defekty wynikające między innymi z nieobsadzonych niektórych węzłów w sieci krystalicznej. Tworzą one pułapki elektronowe, zmniejszając zdolności optyczne kropki kwantowej oraz wydajność kwantową fluorescencji. Jeśli rdzeń kropki kwantowej nie jest pokryty otoczką, możliwość przejść bezpromienistych staje się bardziej prawdopodobna i w konsekwencji, wydajność kwantowa fluorescencji znacznie się obniża. Obecność pasma fluorescencji przy niższych wartościach energetycznych, a przy dłuższych długościach fali jest równocześnie obserwowana (« trap emissions »). W celu eliminacji w/w defektów, na rdzeń kropki wprowadzana jest powłoka nieorganiczna z innego półprzewodnika, zwykle o większej przerwie zabronionej.

Istnieją dwie główne metody syntezy kropek kwantowych zawierających kadm (CdSe i CdTe). Pierwsza nazywana jest syntezą organometaliczną, a druga syntezą hydrotermalną. Zasadą syntezy jest odzielenie w czasie procesu zarodkowania od procesu wzrostu (Rycina 2).

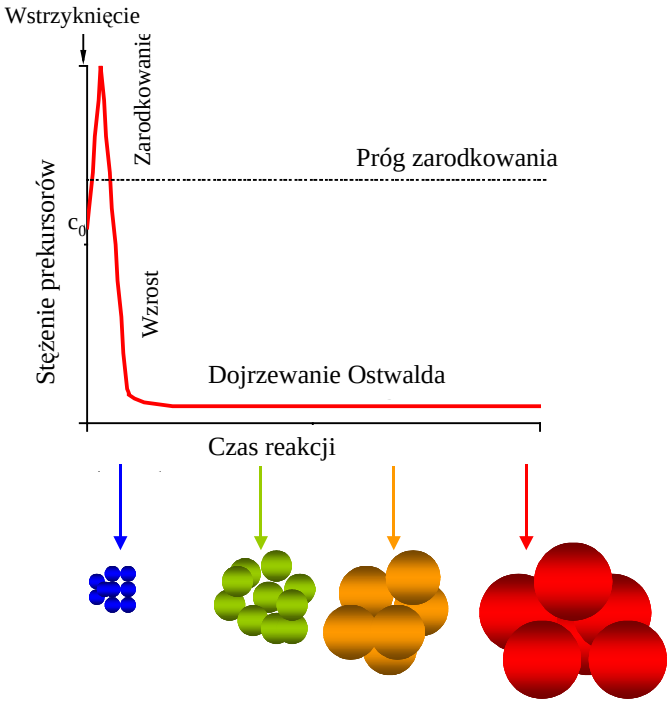

Rycina 2. Poszczególne etapy syntezy kropek: homogeniczne zarodkowanie poprzez szybkie wstrzyknięcie prekursorów, wzrost zarodków poprzez konsumpcję prekursorów z roztworu, a następnie rozpuszczenie mniejszych zarodków na korzyść tych większych.

Synteza organometaliczna wymaga zwykle użycia toksycznych i drogich rozpuszczalników, jak również specjalnych rozwiązań technologicznych (np. komora rękawicowa), które nie zawsze są dostępne we wszystkich laboratoriach. Przygotowane tą drogą kropki kwantowe są stabilizowane przez ligandy hydrofobowe, nie wykazujące powinowactwa do środowiska wodnego. Użycie kropek kwantowych w różnych bionaukach wymaga dodatkowego etapu zapewniającego ich rozpraszanie w roztworach wodnych.

Synteza kropek kwantowych w środowisku wodnym jest metodą pozwalającą na bezpośrednie otrzymanie biokompatybilnych kropek kwantowych rozpraszalnych w wodzie. Dodatkową zaletą tej metody jest użycie mniej toksycznych prekursorów w porównaniu z wykorzystywanymi w syntezie organometalicznej. Prowadzenie syntezy kropek kwantowych w wodnym środowisku pod zwiększonym ciśnieniem w wysokiej temperaturze pozwala na przyspieszenie fazy wzrostu nanocząstek i polepszenie ich właściwości fotofizycznych.

Istenieje kilka sposobów pozwalających na rozpraszanie w wodzie kropek kwantowych otrzymanych na drodze syntezy organometalicznej. Należą do nich: wymiana ligandu na powierzchni kropek, interakcje hydrofobowych kropek w cząsteczkami amfifilowymi lub inkorporowanie kropek kwantowych w nanocząstki silikonowe.

Wymiana ligandu na powierzchni kropek polega na zastąpieniu ligandów hydrofobowych ligandami hydrofilowymi.

W procesie interakcji kropek hydrofobowych z cząsteczkami amfifilowymi, ligand hydrofobowy pozostaje związany z powierzchnią kropek. Metoda ta polega na dodaniu cząsteczek amfifilowych z celu rozproszenia kropek kwantowych w środowisku wodnym. Łańcuchy alkilowe komponentu amfifilowego łączą się poprzez wiązania Van der Waalsa z grupami n-oktylowymi TOP (*n*-trioktylofosfina) i/lub TOPO (tlenek *n*-trioktylofosfiny). Reszty hydrofilowe cząsteczek amfifilowych umożliwiają rozpraszanie powstałej struktury w środowisku wodnym. Kropki kwantowe stabilizowane przez TOPO mogą być enkapsułowane przez komponenty amfifilowe formując micelle na drodze interakcji hydrofobowo/hydrofobowych lub przez amfifilowe polimery.

W metodzie inkorporacji kropek kwantowych w silikonowe nanosfery, kropki kwantowe są wystawione na kontakt z tetraetoksyortokrzemianem (TEOS). Ten ostatni jest hydrolizowany w łagodnych i kontrolowanych warunkach w celu sformułowania nanosfer silikonowych, które otaczają kropki kwantowe.

Modyfikacja powierzchni kropek kwantowych jest etapem kluczowym dla nadania im zdolności do rozpraszania w wodzie. Drugi rodzaj funkcjonalizacji jest niezbędny, aby sondy fluorescencyjne reagowały selektywnie z danym celem komórkowym. Aby to osiągnąć koniugacja kropek kwantowych z biomolekułami (peptydy, białka, przeciwciała, małe cząsteczki) nie może prowadzić do zmiany ich aktywności i/lub zdolności ich rozpoznawania przez określone cele komórkowe.

Istnieją dwie główne procedury koniugowania biomolekuł na powierzchni kropek kwantowych. Kropki kwantowe mogą być skoniugowane z biomolekulami o określonym ładunku poprzez wiązanienie kowalencyjne za sprawą interakcji elektrostatycznych. W tym przypadku kropki kwantowe są syntezowane w taki sposób, że posiadają ładunek komplementarny do tego jaki ma dana biomolekuła. W wyniku mieszania obu podjednostek następuje ich autoasocjacja. Ten prosty sposób był stosowany z sukcesem w przygotowaniu kropek kwantowych funkcjonalizowancyh białkami i przeciwciałami np. podczas interakcji biotyna/streptawidyna. Koniugacja może również zachodzić między biomolekułami a metalami (Cd, Zn,...) obecnymi na powierzchni kropek. Białka lub peptydy posiadają sekwencje aminokwasowe, które maja powinowactwo do metali lub kationów metalicznych.

Koniugowanie z biomolekulami poprzez wiązanie kowalencyjne najczęściej bazuje na reakcji pomiędzy grupą funkcyjną biomolekuly (aminową) i grupą funkcyjną występująca w ligandzie kropki (grupa karboksylowa lub karboksylanowa). Ta koniugacja zwykle dokonuje się przy udziale karbodiimidu pełniącego funkcję czynnika ułatwiającego koniugację takiego jak np. *N*-(3-dimetyloaminopropylo)-*N*-etylokarbodiimid (EDC) i aktywatora takiego *N*-hydroksysukcynimid (NHS). Koniugacja pomiędzy ligandem na powierzchni kropki i pożądaną biomolekułą prowadzi do powstania wiązania amidowego.

Główne zainteresowanie kropkami kwantowymi wynika z możliwości ich szerokiego zastosowania w bionaukach. W 1998 po raz pierwszy dwie niezależne grupy badawcze zdołały rozproszyć kropki kwantowe w środowisku wodnym.

Kropki kwantowe posiadają unikatowe właściwości optyczne oferujące wiele korzyści w porównaniu z tradycyjnymi barwnikami organicznymi (fluoresceina, rodamina,...), m.in.:

- szerokie widmo absorpcji w zakresie UV i światła widzialnego i wąskie i symetryczne widmo emisji (wiekszość fluoroforów organicznych posiada widmo absorpcji wąskie i widmo fluorescencji szerokie). Nakładanie się widm absorpcji i emisji jest zwykle

obserwowane w przypadku klasycznych fluorochromów takich jak rodamina G6 podczas gdy, dzięki przesunięciu Stokes'a, w przypadku kropek kwantowych nakładanie się widm nie ma miejsca

- korzystając z jednego źródła wzbudzenia w tej samej próbce biologicznej jest możliwa jednoczesna wizualizacja kilku rodzajów kropek kwantowych emitujących przy różnej długości fali
- doskonała fotostabilność (odporność na fotowybielanie od kilku godzin do kilku dni)
- bardzo dobra odporność na degradację chemiczną, dobra wydajność kwantowa fluorescencji (do 85%).

Na obecną chwilę mało jest informacji dotyczących toksyczności nanocząstek i niełatwym zadaniem wydaje się poznanie wszystkich wpływów jaki wywierają nanocząstki na komórkę. Dane literaturowe zaczynają jednak być coraz bogatsze. Do 2005, cytotoksyczność kropek kwantowych była przypisywana głównie obecności metali ciężkich w ich rdzeniu. Później zaczęły być opisywane inne mechanizmy toksyczności m.in. agregacja nanocząstek na powierzchni komórek. W związku z tym, że kropki kwantowe są donorami energii, mogą one przenosić energię również na sąsiadujące atomy tlenu i generować powstawanie wolnych rodników.

Rozważając toksyczność kropek kwantowych należy również zwrócić uwagę na ich parametry farmakologiczne takie jak uwalnianie, absorpcja, dystrybucja, metabolizm i wydalanie. Efekt ograniczenia kwantowego wymaga uwzględnienia struktury kropek w rozważaniach w/w parametrów. W odróżnieniu od tradycyjnych cząsteczek leków, w przypadku kropek kwantowych, niezbędne jest dodatkowe równoczesne scharakteryzowanie rozmiaru, składu atomowego, czystości, stopnia enkaspulacji i natury ligandu nanocząstki.

W bioobrazowaniu najczęściej stosuje się nanocząstki zawierające kadm (półprzewodniki grup II-VI), w szczególności o rdzeniu CdSe i CdTe. Takie kropki mogą powodować powstawanie wolnych rodników poprzez trzy mechanizmy: (i) podczas wzbudzenia, tworzenie się pary elektron-dziura elektronowa powoduje przeniesienie elektronu z kropek kwantowych na tlen (powstawanie H_2O_2, $OH^{\cdot}$, $O_2^{\cdot-}$) (Rycina 3), (ii) wewnątrzkomórkowy system antyoksydacyjny może być bezpośrednio uszkodzony poprzez interakcję z kropką kwantową i ostatecznie , (iii) intrakcje z jonami Cd^{2+} mogą indukować w środowisku wzrost wolnych rodników.

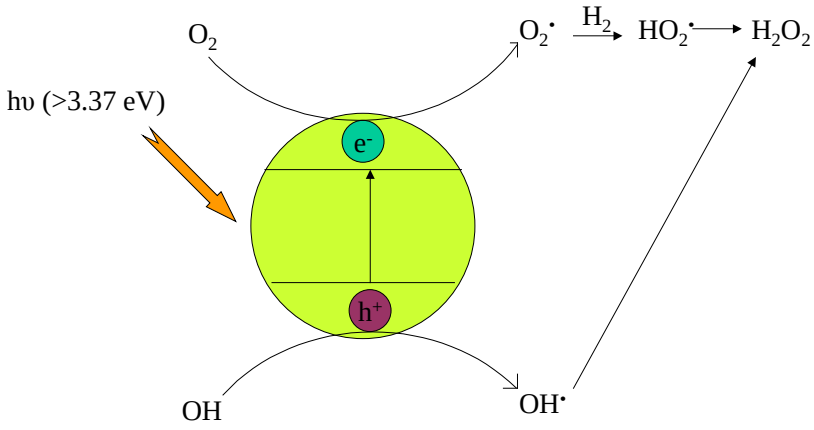

Rycina 3. Mechanizmy przenoszenia energii z udziałem kropek kwantowych w wyniku tworzenia się pary elektron- dziura elektronowa.

Z biomedycznego punktu widzenia toksyczność kropek kwantowych może być cechą korzystną, szczególnie jeżeli celem komórkowym mają być komórki nowotworowe. Pod wpływem naświetlenia, kropka kwantowa jest wzbudzana, elektron jest przenoszony na sąsiadującą cząsteczkę tlenu i inicjuje łańcuch reakcji rodnikowych powodujących śmierć komórki. Opisane zjawisko stanowi podstawę terapii fotodynamicznej.

Ze względu na podobieństwa rozmiarowe z cząsteczkami biologicznymi (kwasy nukleinowe, białka i peptydy), kropki kwantowe cieszą się szerokim zainteresowaniem w potencjalnych zastosowaniach biologicznych. W ostatnim czasie zainteresowanie fizyków i

chemików skupione jest na zastosowaniu kropek kwantowych w celu detekcji różnych stanów systemów biologicznych, wykrywających jednocześnie zmiany elektryczne, optyczne i magnetyczne. W rezultacie, kropki kwantowe posiadają cechy atrakcyjne dla ich użycia zarówno w diagnostyce jak i terapii. Te nanocząstki mogą być użyte jako narzędzia w poszukiwaniu i zrozumieniu procesów molekularnych na poziomie komórkowym. Dzięki pożądanym właściwościom fotofizycznym kropek kwantowych (duża fotostabilność, wąskie i dające się regulować widmo emisji), te nanokryształy są używane jako alternatywa dla fluoroforów organicznych w bioobrazowaniu. Szerokie widmo absorpcji kropek kwantowych pozwala wybrać pożądaną długość fali emisji (w bliskiej podczerwieni) poprzez wzbudzenie dwu lub multi-fotonowe. Dzięki takim sondom fluorescencyjnym, sygnał może penetrować głębiej w tkankę biologiczną. Kropki kwantowe są również idealnymi sondami stosowanymi w celu polepszenia detekcji fluorescencji w czasie rzeczywistym w komórkach żywych zwierząt. Główną korzyścią kropek kwantowych w obrazowaniu żywych komórek jest możliwość zróżnicowania długości fali emisji od zakresu światła widzialnego do bliskiej podczerwienia dzięki odpowiedniemu wyborowi rozmiaru i składu nanocząstek. W celu możliwości użycia kropek kwantowych w środowisku biologicznym (wodnym), hydrofobowe kropki trzeba przeprowadzić w rozpraszalne w wodzie oraz odpowiednio sfunkjonalizować ich powierzchnię. W literaturze znaleźć można przykłady koniugowania kropek kwantowych z licznymi cząsteczkami biologicznymi (peptydy, kwasy nukleinowe, przeciwciała, małe cząsteczki ligandów) w celu zastosowania ich jako sond. W większości przypadków taka funkcjonalizacja jest realizowana poprzez wymianę ligandu na ten o lepszym powinowactwie do nanocząstki. Doskonały cel komórkowy stanowią receptory, które wykazują nadekspresję na powierzchni niektórych komórek nowotworowych. Z terapeutycznego i diagnostycznego punktu widzenia znakowanie komórek nowotworowych ogranicza się do kilku ligandów. Jednym z nich jest kwas foliowy.

Ostatnio przeprowadzone badania przedstawiają kropki kwantowe jako narzędzia uczestniczące w kreowaniu nowej generacji sond fluorescencyjnych. W tej dziedzinie kropki kwantowe są szczególnie atrakcyjne, gdyż pozwalają na uzyskanie długotrwałej fotostabilności pozwalając na śledzenie zjawisk w rzeczywistym czasie. Fluorescencja kropek kwantowych uzależniona jest od stanu ich powierzchni oraz interakcji ze związkami chemicznymi mogącymi mieć miejsce na powierzchni kropek. Może to skutkować zmianą długości fali emisji kropek kwantowych. Dzięki biosensorom bazującym na kropkach kwantowych mierzony jest sygnal fluorescencji, który ulegać może nasileniu bądź osłabieniu. Skład chemiczny powierzchni kropek kwantowych musi być zawsze dobrze znany, aby zapewnić odpowiednie właściwości emisji i selektywność użytych sond.

Jak wspomniano, nanokryształy najczęściej używane do obrazowania różnych celów komórkowych zawierają metal ciężki- kadm. W związku z tym pod uwagę musi być brana ich toksyczność. Stąd też w swoim doktoracie zajęłam sie pracą nad kropkami kwantowymi nie zawierajacymi metali ciężkich typu ZnS i ZnSe

Celem mojej pracy było opracowanie nowej klasy kropek kwantowych o niskiej toksyczności i ich użycie do bioobrazowania komórek nowotworowych.

W pierwszej części pracy została opracowana synteza kropek kwantowych o rdzeniu ZnS i ZnSe domieszkowanych jonami manganu lub miedzi i stabilizowanych przez kwas 3-merkaptopropionowy (MPA) lub przez 1-tioglicerol (TG). Badaniami objęto 4 typy nanokryształów: ZnS:Mn/ZnS@MPA, ZnS:Mn@TG, ZnS:Cu/ZnS@MPA i ZnSe:Mn/ZnS@MPA. Została przeprowadzona optymalizacja parametrów syntezy takich jak procent domieszkowanego składnika, czas i temperatura reakcji, typ ligandu stabilizującego oraz stosunek prekursorów. W celu charakterystyki otrzymanych nanokryształów wykorzystano następujące techniki: spektroskopia Uv-vis, fluorymetria, dyfrakcja promieni

rentgenowskich (XRD), spektroskopia fotoelektronowa z użyciem promieni rentgenowskich (XPS), transmisyjna mikroskopia elektronowa (TEM), dynamiczne rozpraszanie światła (DLS), spektroskopia w podczerwieni (FT-IR), elektronowy rezonans paramagnetyczny (EPR). Po scharakteryzowaniu kropek kwantowych domieszkowanych jonami manganu przeprowadzono funkcjonalizację ich powierzchni przy użyciu kwasu foliowego. Oznaczono toksyczność kropek kwantowych na 3 nowotworowych liniach komórkowych z użyciem 3 testów cytotoksyczności [MTT, XTT i testu utleniania żelaza przy użyciu pomarańczowego ksylenolu (FOXO)]. W końcowym etapie pracy, kropki kwantowe ZnS:Mn skoniugowane z kwasem foliowym zostały wykorzystane do bioobrazowania komórek nowotworowych przy użyciu wzbudzenia dwufotonowego.

Pierwszy typ syntezowanych nanokryształów rdzeń/otoczka stanowiły kropki ZnS:Mn/ZnS. Te nanokryształy były przygotowane w wodnym roztworze w reakcji $ZnSO_4$ i $Mn(OAc)_2$ z Na_2S w obecności MPA. Następnie poprzez epitaksjalny wzrost wynikający z rozkładu kompleksu Zn^{2+}-MPA przy pH =10.3 została wprowadzona otoczka z ZnS. Ta operacja pozwoliła na zwiększenie wydajności fluorescencji z 2.7 do 22%. Optymalne stężenie manganu w mieszaninie reakcyjnej, dające najlepszą wydajność kwantową, wynosiło 4%. Ustalono, że pik emisji ok. 590 nm wynika z tranzycji d-d jonów manganu w miejsce jonów cynku. Zbadano wpływ różnych ligandów (kwas tioglikolowy (TGA), kwas merkaptopropionowy (MPA), kwas merkaptoheksanowy (MHA) i L-cysteina) na właściwości optyczne kropek kwantowych. Najlepszą fluorescencję uzyskano w przypadku kropek kwantowych stabilizowanych przez MPA. Struktura blendy cynkowej rdzenia ZnS została potwierdzona badaniem XRD. Struktura sferyczna rdzenia ZnS i średnica (4.4 ± 0.7 nm kropek ZnS:Mn/ZnS@MPA) została potwierdzona wynikami badań TEM, a skład pierwiastkowy (Zn, S, Mn, O, C et Na) wynikami analizy XPS.

Drugi typ przygotowanych kropek kwantowych stanowiły kropki ZnS:Mn stabilizowane przez tioglicerol (TG). Synteza przebiegała w sposób analogiczny jak kropek ZnS:Mn@MPA opisanych wcześniej. Optymalne stężenie jonów Mn^{2+} było równe 4% i odpowiadało wydajności fluorescencji 10.8%. Te kropki kwantowe emitowały fluorescencję również przy 590 nm. Badano wpływ różnych źródeł cynku na właściwości fotoluminescencji kropek kwantowych (siarczan, octan, azotan cynku). Najlepsze właściwości fotoluminescencyjne wykazywały kropki zsyntezowane z użyciem octanu cynku. Średnica kropek ZnS:Mn oznaczona techniką TEM wynosiła 3.9 ± 0.5 nm. Analiza XRD potwierdziła krystaliczną naturę badanych kropek kwantowych. W kolejnym etapie badań zmierzono wpływ pH na fotostabilność kropek. Najlepszą wydajność fluorescencji kropek stwierdzono w pH lekko zasadowym (8-10). Analiza XPS wykazała obecność następujących pierwiastków : Zn, S, O, C i Na. Przebieg widma FT-IR potwiedził obecność TG na powierzchni kropek, a analiza EPR wykazała obecność manganu w sieci krystalicznej kropek kwantowych.

Trzeci typ syntezowanych kropek kwantowych stanowiły kropki rdzeń/otoczka ZnS:Cu/ZnS stabilizowane przez MPA. Otrzymano je w reakcji $Zn(NO_3)_2$, $CuSO_4$ z Na_2S w obecności MPA. Stwierdzono eksperymentalnie, że optymalny stosunek molowy $Zn^{2+}/S^{2-}/Cu^{2+}$/MPA, prowadzący do najlepszej wydajności fluorescencji, wynosił 1/0.52/0.003/2.27, a optymalne stężenie miedzi wynosiło 3%. Najwyższą wydajność fluorescencji przy długości fali emisji 510 nm (3.4%) otrzymano używając ligandu MPA. Wprowadzenie otoczki ZnS pozwoliło na zwiększenie wydajności fluorescencji o 0.5%. Analiza XRD potwierdziła krystaliczną naturę kropek rdzeń/otoczka ZnS:Cu/ZnS@MPA. Ich średnica wynosiła 3.2 nm (średnica hydrodynamiczna 11.7 nm). Analiza XPS wykazała obecność Zn, S, Cu, O, C i Na. Zaobserwowano, że wraz ze wzrostem stężenia kropek kwantowych w buforze fosforanowym ich wydajność fluorescencji wzrastały liniowo i nie było fotowybielania. Zbadano wpływ

temperatury i pH na wydajnosć fluorescencji. Najwyższą wydajność fluorescencji badanych kropek kwantowych obserwowano w pH lekko zasadowym (8-10) i temperaturze 10-40°C.

Ostatnim typem syntezowanych nanokryształów były kropki kwantowe ZnSe:Mn/ZnS stabilizowane przez MPA. Ich synteza przebiegała w środowisku wodnym przy użyciu prekursorów takich jak $ZnSO_4$, $Mn(OAc)_2$ i NaHSe w obecności MPA. Najlepszą wydajność fluorescencji otrzymano przy stężeniu manganu wynoszącym 4% i stosunku molowym Zn^{2+}/Se^{2-}/MPA wynoszącym 1/0.9/20 w pH = 10.3. Po 24 h reakcji, zostały otrzymane stabilne kropki kwantowe o wydajności fluorescencji 12.5%, które emitowały fluorescencję przy 590 nm. Zbadano wpływ różnych ligandów [TGA, MHA, kwas 2-sulfanylobutanodiowy (mercaptosuccinic acid- MSA) i L-cysteina] na wydajność fluorescencji. Przy zastosowaniu jako ligandów TGA, MHA, MSA i Cys, kropki kwantowe ZnSe:Mn QDs wykazywały tranzycję $^4T_1$-$^6A_1$ pochodzącą od Mn^{2+} przy 595 nm, a ich pasmo emisji było znacznie szersze niż w przypadku kropek stabilizowanych przez MPA. Wyniki analizy XRD potwierdziły kubiczną strukturę blendy cynkowej i średnicę nanokryształów 3.5 nm. Średnica hydrodynamiczna kropek zmierzona techniką DLS wynosiła 7.6 nm. W widmie FT-IR zaobserwowano obecność grupy kwasowej MPA i zanik drgań wibracyjnych grupy tiolowej SH, potwierdzający przyłączenie MPA na powierzchni kropek ZnSe:Mn. Analiza wyników pomiaru różnicy energii promieniowania X (EDS) wykazała, że skład atomowy kropek odpowiada stosunkowi użytych prekursorów. Po wprowadzeniu otoczki, średnice kropek otrzymanych z analizy TEM wynosiły 4.3 ± 0.5 nm (średnica hydrodynamiczna 8.0 nm). Wprowadzenie otoczki ZnS zostało powierdzone przez pomiar fotoluminescencji przed i po modyfikacji powierzchni. Równocześnie zaobserwowano zmianę intensywności fluorescencji kropek jako funcję pH. Kropki charakteryzowaly sie najlepszą fotostabilnością przy pH 12.

Kolejnym etapem pracy była funkcjonalizacja powierzchni zsyntezowanych kropek kwantowych poprzez ich skoniugowanie z kwasem foliowym.

Zbadano wpływ kwasu foliowego na właściwości fotoluminescencyjne 4 typów kropek kwantowych (ZnS:Mn@MPA, ZnS:Cu@MPA, ZnS:Mn@TG i ZnSe:Mn@MPA). Stwierdzono, że zależność intensywności fotoluminescencji kropek od stężenia kwasu foliowego może być opisana funkcją Stern-Volmer'a. Obniżenie fotoluminescencji kropek ZnS:Mn i ZnS:Cu QDs stabilizowanych przez MPA zależało od stężenia kwasu foliowego, pomimo że długość ich fali emisji i kształt piku fluorescencji nie uległy zmianie.

W przypadku kropek kwantowych domieszkowanych manganem, obniżenie fotoluminescencji słabo korelowało z równaniem Stern-Volmer'a. Lepszą korelację danych doświadczalnych uzyskano stosując model Perrin'a, zakładający że kropka kwantowa reaguje z kilkoma cząsteczkami kwasu foliowego. Interferencja kwasu foliowego z kropkami kwantowymi była ok. 30% słabsza w przypadku kropek ZnS:Cu w porównaniu z kropkami ZnS:Mn. Przeprowadzone badania pozwoliły ustalić optymalny stosunek QD/FA w procesie koniugacji.

Kowalencyjne wiązanie kwasu foliowego z kropkami kwantowymi ZnS:Mn/ZnS@MPA zachodziło z wykorzystaniem jako łącznika 2,2'-(etylenodioksy)-*bis*-etylaminy. Czynnikami aktywującymi koniugację były EDC i NHS. Grupy aminowe obecne na powierzchni kropek pozwoliły na dołączenie grupy karboksylowej kwasu foliowego poprzez wiązanie amidowe w obecności EDC. Analogicznie przygotowano kropki rdzeń/otoczka ZnSe:Mn/ZnS@MPA skoniugowane z kwasem foliowym. Kowalencyjne koniugowanie kwasu foliowego na powierzchni kropek kwantowych ZnS:Mn@TG zachodziło poprzez połączenie grupy karboksylowej kwasu foliowego z grupą wodorotlenową tioglicerolu w obecnści EDC i NHS. Po procesie koniugacji kropki kwantowe ZnS:Mn zachowały dobre właściwości fotoluminescencyjne, dobrą wydajność fluorescencji oraz strukturę krystaliczną. Średnice kropek kwantowych skoniugowanych z kwasem foliowym wynosily: 5.2 ± 1.0 nm dla kropek ZnS:Mn/ZnS@MPA i 4.2 ± 0.7 nm dla kropek ZnS:Mn stabilizowancyh przez TG. Obecność

atomów azotu w strukturze kropek kwantowych sfunkcjonalizowanych kwasem foliowym została potwierdzona za pomocą analizy XPS, a sama obecność kwasu foliowego metodą chromatografii cienkowarstwowej.

Przed zastosowaniem kropek kwantowych jako sond w bioobrazowaniu konieczna była wiedza na temat ich cytotoksyczności. W związku z tym w kolejnym etapie badań oceniono cytotoksyczność kropek ZnS:Mn/ZnS@MPA, ZnS:Mn@TG i ZnSe:Mn/ZnS@MPA. W testach wykorzystano linie komórkowe T47D (komórki raka piersi) wykazujące nadekspresję receptora foliowego oraz 2 linie komórek referencyjnych tj. MCF-7 (komórki raka piersi) i PC-3 (komórki raka prostaty). Toksyczność kropek została oszacowana przy ciagłym narażeniu komórek na kropki kwantowe w stężeniu poniżej i powyżej używanego w prezentowanych badaniach w konfokalnej mikroskopii (500 µM). W badaniach zastosowano 3 testy: MTT, XTT i FOXO. Test MTT jest testem kolorymetrycznym opartym na redukcji przez mitochondria rozpuszaczalnej w wodzie soli tetrazolowej- bromku (3-(4,5-dimetylo-2-ilo)-2,5-difenylotetrazolu (MTT) do niebieskich, nierozpuszczalnych w wodzie kryształów formazanu i oznaczeniu kolorymetrycznym roztworu DMSO tego związku. W ocenie cytotoksyczności kropek kwantowych zastosowano róznież test XTT. Charakteryzuje się on większą czułością niż MTT, wynikającą z wprowadzenia do łańcucha fenylowego soli tetrazolowej dodatkowych grup obdarzonych ładunkiem. W teście XTT, jest stosowana cząsteczka XTT (2,2'-wodorotlenek 2,3-*bis*(2-metoksy-4-nitro-5-sulfofenyl)-5-[(fenylamino)-karbonyl]-2H-tetrazolu) zapewniająca wiekszą czułość odpowiedzi komórkowej. W celu określenia zdolności kropek kwantowych do generowania wolnych rodników przeprowadzono test FOXO, w którym mierzono stężenie H_2O_2 w medium komórkowym po ekspozycji na kropki kwantowe. Mierzone stężenie nadtlenku wodoru było wynikiem reakcji utleniania Fe^{+2} do Fe^{+3}.

Przeprowadzone testy wskazały na niską toksyczność kropek ZnS:Mn@TG w porównaniu z kropkami ZnS:Mn@MPA i ZnSe@MPA. Stwierdzono, że skład rdzenia jak i ligandy pełnią istotną rolę w tokyczności tych nanocząstek. Należy zwrócić uwagę, że oba typy kropek kwantowych stabilizowanych przez MPA (ZnS:Mn i ZnSe:Mn) są mniej toksyczne dla komórek T47D w przypadku gdy rdzeń jest pokryty otoczką z ZnS. W przypadku użycia tych samych kropek kwantowych stwierdzono różnice w wynikach przeprowadzonych testów na różnych liniach komórkowych. Wyniki testu XTT korespondują z uzyskanymi w teście MTT. Zauważono, że cytotoksyczność kropek kwantowych w odniesieniu do komórek PC-3 nawet przy niskich stężeniach kropek jest dużo mniejsza. Wyniki testu FOXO wskazują na większą produkcję nadtlenku wodoru w medium komórkowym komórek narażonych na działanie kropek w ciągu pierwszych godzin eksperymentu.

Mając na uwadze wyniki testów cytotoksyczności różnych kropek na różnych liniach komórkowych, jako potencjalne znaczniki komórek nowotworowych mających nadekspresję receptora foliowego wybrano kropki ZnS:Mn stabilizowane TG i MPA.

W eksperymencie bioobrazowania jako fluorescencyjne sondy dla komórek nowotworowych zostały wykorzystane kropki ZnS:Mn stabilizowane MPA, a kropki ZnS:Mn stabilizowane TG razem z komercyjnymi fluoroforami organicznymi zostały użyte w celu lepszej lokalizacji miejsca gromadzenia kropek kwantowych w komórce. We wszystkich eksperymentach wykorzystano technikę mikroskopii konfokalnej o dwufotonowym wzbudzeniu. Kropki ZnS:Mn@MPA zostały wykorzystane jako znaczniki dwóch rodzajów komórek nowotworowych, T47D i MCF-7. Komórki były hodowane w dwóch różnych mediach: jednym pozbawionym kwasu foliowego i drugim DMEM (Dulbecco’s modified Eagle’s medium). Obrazy konfokalne uzyskane po wzbudzeniu światłem o długości fali 720 nm, po różnym czasie inkubacji, wskazywały na wzrost gromadzenia kropek skoniugowanych z kwasem foliowym podczas pierwszych 6 h inkubacji. Na dobrą stabilność kropek

kwantowych wskazywał fakt, że po 72 h inkubacji z komórkami właściwości optyczne kropek zostały utrzymane. Fotografie kropek ZnS:Mn/ZnS skoniugowanych z kwasem foliowym w przypadku komórek T47D hodowanych w medium ubogim w kwas foliowy wskazują na jednorodne rozmieszczenie kropek w cytoplazmie w pobliżu jądra komórkowego. Kropki niezmodyfikowane wykazywały mniej jednorodne rozmieszczenie. Podobnie, obrazy konfokalne otrzymane dla komórek T47D i MCF- 7 hodowane w DMEM wskazują na interakcje kropek z komórkami, ale barwienie jest niejednorodne. Ponadto, nie zaobserwowano żadnego znaku uszkodzenia komórek po interkacji z kropkami kwantowymi wskazując na ich niską toksyczność. Kiedy błona komórkowa komórek T47D została wysycona 3.5 mM roztworem kwasu foliowego przed dodaniem kropek, bardzo mało nanokryształów zostało inkorporowanych, co jest wynikiem inhibicji kompetycyjnej. Otrzymane wyniki potwierdziły znakowanie komórek nowotworowych wykazujących nadekspresję receptora foliowego przez kropki kwantowe skoniugowane z kwasem foliowym. Użycie do bioobrazowania skoniugowanych z kwasem foliowym kropek ZnS:Mn stabilizowanych TG wraz z barwnikami organicznymi wskazało na większe gromadzenie się kropek w komórce w okolicach jądra komórkowego.

Opracowana procedura syntezy półprzewodnikowych nanokryształów pozwoliła na otrzymanie niezawierających kadmu kropek kwantowych na drodze prostej syntezy przebiegającej w środowisku wodnym. W wyniku przeprowadzonych badań otrzymano sondy fluorescencyjne stanowiące potencjalne narzędzie w bioobrazowaniu komórek. Niska cytotoksyczność fluorescencyjnych nanokryształów, ich duża stabilność i doskonałe właściwości fotofizyczne sprawiają, że kropki kwantowe mogą stać się atrakcyjnym narzędziem w naukach biomedycznych.